UNIVERSITAT DE BARCELONA

YAP1 modulates hormonal response in Breast Cancer cells via a Non-canonical pathway involving the pioneer factor FOXA1

Rosario Teresa Sanz Perez

YAP1 modulates hormonal response in Breast Cancer cells via a Non-canonical pathway involving the pioneer factor FOXA1

Rosario Sanz Perez

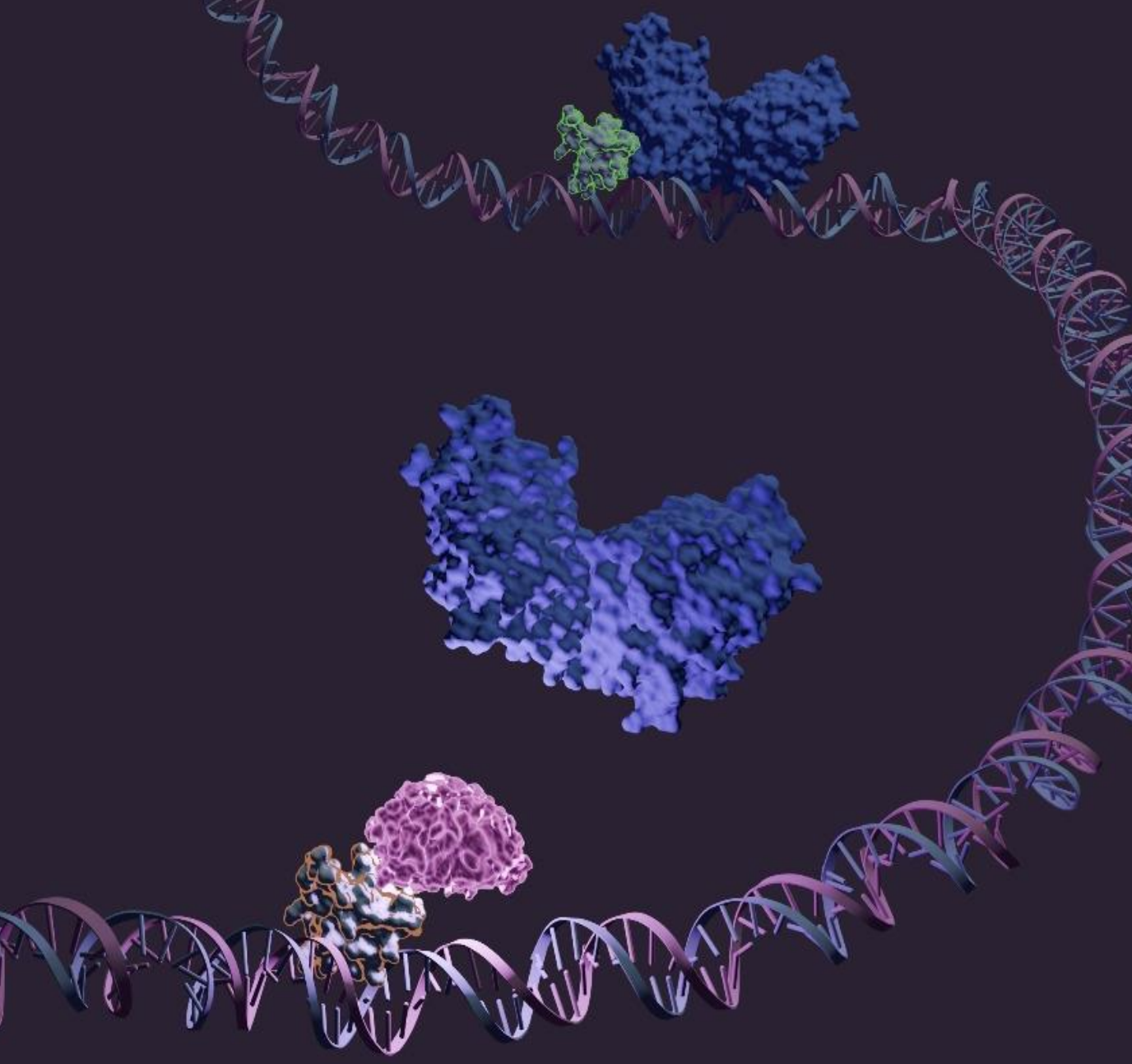

Barcelona, 2025

UNIVERSITAT DE BARCELONA

FACULTAT DE FARMÀCIA I CIÈNCIES DE L'ALIMENTACIÓ

PROGRAMA DE DOCTORAT

YAP1 modulates hormonal response in Breast Cancer cells via a Non-canonical pathway involving the pioneer factor FOXA1

YAP1 modula la resposta hormonal en càncer de mama a través d'una via no canònica que involucra el factor pioner FOXA1

YAP1 modula la respuesta hormonal en cáncer de mama a través de una vía no canónica que involucra el factor pionero FOXA1

Memòria presentada per Rosario Teresa Sanz Perez per optar al títol de doctor per la Universitat de Barcelona

Director: Guillermo Vicent Martinez

Tutora: Veronica Noe Mata

Rosario Teresa Sanz Perez

Acknowledgments

En primer lugar, me gustaría agradecer a mi director Guille porque si no fuese porque en el 2020 me propusiste empezar el doctorado hoy no estaría escribiendo mi tesis. Me quedo con alguna de tus frases célebres como la de que “ningún mar en calma hizo experto a un marinero”.

Silvina, durante el trabajo de final de máster me enseñaste mucho de lo que he tenido que aplicar durante el doctorado. Y durante, siempre has estado pendiente para enseñarme o ayudarme con cualquier protocolo. No podría olvidarme de Julieta, Flopy, Belen, Ada y Diego, quienes me han ayudado con los esferoides y los condensados.

Judith, has sido una buenísima compañera. Siempre recordaré lo mucho que nos hemos reído haciendo virus juntas en cultivos y explicando las historias del laboratorio a las personas que llegaban. Estoy segura de que te irá genial durante tu etapa de doctorado. Esther y Juliana, espero que disfrutéis mucho del inicio de vuestra etapa en investigación.

Martita, no sé en qué karaoke de cultivos pasamos a ser amigas. En el lab hemos pasado muchos momentos juntas, algunos de ellos inexplicables como los viales saltones, y estoy segura de que fuera pasaremos muchos más. Gracias por ser un gran apoyo en todo, por los buenos momentos y nuestros desayunos entre experimentos.

Des de l’inici, compartir al lab amb vosaltres ha estat més divertit. Jordi, Albert i Monica, gràcies pel suport aquests anys. Quan vam començar en el laboratori i estava sola a l’últim passadís era una alegria poder xerrar de tot amb vosaltres pel laboratori.

Paula Bujosa, des de l’inici vaig veure la gran científica i persona que ets, sempre disposada a ajudar. Gràcies per sempre donar-me tant bons consells i escoltar-me sempre que ho he necessitat.

Juan, un gracias se quedaría corto. Me llevo un buen amigo en quien poder confiar y con quien compartir momentos, recomendaciones de series, películas y más. Voy a echar mucho de menos tenerte al lado trabajando, la tesis ha sido más fácil sabiendo que tú estabas a mi lado.

Durante estos años, el laboratorio ha cambiado mucho, y más desde que llegasteis las Vicky's y las Irene's. Yoli, Carla y Alberto le habéis dado un giro completo al laboratorio. Me alegra mucho haber podido compartir un año con vosotras. Elliot, Laura, Maria Helena, Irene y Mar, estoy segura de que también os irá genial en este lab tan peculiar.

Gracias a estar en el IBMB también he podido conocer a personas de otros grupos y otros centros. Laura y Paula, vau ser les primeres persones que vaig conèixer i m'han agradat molts els dinars a la terrassa que hem pogut fer. Núria, te tengo que agradecer especialmente tu ayuda con los análisis. Iván, Guillem y Adrián, durante estos años hemos jugado en dos equipos, de futbol y de ordenador, y pese a no ganar mucho en ninguno de ellos me lo hemos pasado muy bien.

Nos conocimos en la carrera y desde entonces supe que por muchos años que pasaran Aigue iba seguir igual. Ivan, Paula, Jordi, Quim, Armand y Marc hemos cogido caminos diferentes, pero poder apoyarnos y escucharnos estos años le ha dado una perspectiva diferente al doctorado. Por que continúen nuestras tradiciones y cada vez nos perdamos menos en nuestras rutas improvisadas.

Siguiendo con amigos de ciencia, gracias NBT por acogerme tan bien. Sois un grupo de 10 y siempre me lo he pasado genial. La lista es muy larga pero todos deberíais estar, Tuti, Alvi, Eric, Mireia, Hector, Naroa, Eloi, Aida, Carlos, Jara, Mel, Josevi, Marianna, Sara, Ugutz y Ari.

Granollerins, me lo he pasado genial en todos los planes que hemos hecho durante estos años como las cenas temáticas o el wipeout. Eudald, Raul, Antonio, Cat, Laia, Derry y Berta gracias porque estos años

nuestras quedadas me han hecho desconectar, reírme mucho y aprender de muchos temas gracias a lo diverso que es nuestro grupo.

Y por supuesto no me olvido de mis amigas de Mollet. Paula, sé que eres una amiga con la que siempre voy a poder contar. Gracias por escucharme todos estos años. Nuria, sempre m'has demostrat ser una amiga de veritat. Gràcies per recolzar-me sempre que ho he necessitat.

Mari y Toni, gracias por el apoyo que siempre me habéis dado. Siempre recuerdo los ensayos que escuchasteis del TFG y como me decíais que lo iba a hacer genial, siempre habéis creído en mi. Raquel, Riki, Montse, Nuri, Miguel y Owen, gracias también por apoyarme y poder hablar y debatir siempre sobre cualquier tema. Daniel y Alex, solo con sonreír, con vuestro cariño y jugar a cualquier cosa ya me alegrais el día.

Mama y Paquito, siempre habéis creído en que podía con cualquier cosa así que si hoy estoy aquí acabando de redactar mi tesis es en gran parte gracias a vosotros. Estos años os he hablado mucho del laboratorio, gracias por siempre escucharme cuando lo he necesitado y animarme a seguir. Tete, gracias también por apoyarme siempre en lo que quiero hacer, sé que en cada paso y en cada logro, igual que la Alicia y la Valentina, siempre vais a estar a mi lado. Valentina, tu energía sin límites me alegra el día, siempre me tendrás para todo.

Y finalmente Roger, tú has sido la persona que más ha estado todos estos años en cualquier aspecto. Ha sido una suerte tenerte al lado para aconsejarme, apoyarme y sobre todo compartir juntos esta etapa. Saber que por muy complicado que pareciese podía contar contigo, que en días malos al llegar estarías tú esperándome para hacerme reír, me ha ayudado a acabar escribiendo estos capítulos. Mi mejor forma de agradecértelo es apoyándote igual, no podré hacerte una portada tan bonita como la que me has hecho pero estoy convencida de que lo harás perfecto viendo las cosas que has ido haciendo todos estos años.

Abstract

Hormone receptors play a critical role in breast cancer (BC) progression and treatment response. While the function of estrogen receptor (ERα) has been well determined, the role of progesterone receptor (PR) remains controversial. PR has been shown to exert context-dependent functions while the mechanisms regulating the specificity and magnitude of these responses have not been explored in depth.

In this study, we uncover a modulation of PR by YAP1, the effector of the Hippo signaling pathway, which regulates both the magnitude and the specificity of PR response. Depletion of YAP1 increased the PR-induced dedifferentiation capacity, its proliferative response, the progestin-dependent gene expression and the PR binding to DNA without altering chromatin accessibility.

Mechanistically, through genome-wide analysis, we identified around 6,000 DNA binding regions where YAP1 and PR colocalized, either in chromatin-bound YAP1 regions under untreated conditions (~3,000 YAP-bound) or after hormone stimulation (~ 3,000 Co-recruited regions). Notably, FOXA1 emerged as the transcription factor anchoring YAP1 to DNA through a TEAD-independent mechanism. We did not detect a physical interaction between YAP1 and PR, suggesting that they could be competing for FOXA1 binding.

Consistent results were observed in 3D cultures, where extracellular matrix (ECM)-induced LATS1 kinase activity increased YAP1 phosphorylation and reduced nuclear YAP1 levels. PR and FOXA1 binding increased in 3D cultured cells, with PR exhibiting a more pronounced enhancement than FOXA1. Additionally, YAP1 and PR colocalized extensively in nuclear foci, and the repression of YAP1 to PR and FOXA1 was confirmed as, upon YAP1 depletion, the foci density of both proteins was increased.

Finally, we extended our analysis to ERα. In YAP1-depleted conditions, estrogen-dependent gene expression was affected and ERα binding was increased. We observed a similar pattern although much research should be performed to clarify the role of YAP1 on ERα modulation and confirm if the observed mechanism could be relevant to other steroid hormone receptors.

Our findings uncover a novel regulatory role of YAP1 in modulating PR function and binding dynamics through a possible competition between YAP1 and PR for its binding to the pioneer factor FOXA1 (in a TEAD-independent mechanism), with potential implications for understanding hormone receptor specificity in BC.

Keywords: Breast cancer, PR, YAP1, FOXA1, specificity, magnitude, 3D culture, ERα.

Resum

Els receptors hormonals tenen un paper crític en la progressió del càncer de mama i en la resposta al tractament. Tot i que la funció del receptor d'estròg ens (ERα) ha estat ben determinada, el paper del receptor de progesterona (PR) continua sent controvertit. S'ha demostrat que la funció del PR depèn del context, però els mecanismes que regulen l'especificitat i la magnitud d'aquestes respostes no s'han explorat en profunditat.

En aquest estudi, revelem una modulació del PR per part de YAP1, l'efector de la via de senyalització Hippo, que regula tant la magnitud com l'especificitat de la resposta del PR. La degradació de YAP1 va augmentar la capacitat de desdiferenciació induïda per PR, la seva resposta proliferativa depenent de progesterona, l'expressió gènica dependent de progesterona i la unió del PR al ADN sense alterar l'accessibilitat de la cromatina.

A nivell mecanístic, mitjançant una anàlisi a escala genòmica, vam identificar al voltant de 6,000 regions de l'ADN on YAP1 i PR es colocalitzen, ja sigui en regions on YAP1 es troba unit a la cromatina sense tractament (~3.000 YAP-unides) o després de l'estimulació hormonal (~3.000 regions Co-reclutades). Sobtadament, FOXA1 va emergir com el factor de transcripció que ancora YAP1 a l'ADN mitjançant un mecanisme independent de TEAD. No vam detectar cap interacció física entre YAP1 i PR, suggerint que podrien competir per la unió a FOXA1.

Es van observar resultats consistents en cultius 3D, on l'activitat de la quinasa LATS1 induïda per la matriu extracel·lular va augmentar la fosforilació de YAP1 i va reduir els nivells nuclears de YAP1. La unió de PR i FOXA1 va augmentar en cèl·lules cultivades en 3D, amb una millora més pronunciada del PR en comparació amb FOXA1. A més, YAP1 i PR

es van co-localitzar àmpliament en condensats nuclears, i es va confirmar la repressió de YAP1 a PR i FOXA1, ja que, després de la seva degradació, va augmentar la densitat dels condensats de tots dos.

Finalment, vam estendre la nostra anàlisi a ERα. En condicions de falta de YAP1, l'expressió gènica dependent d'estròg ens es va veure afectada i la unió d'ERα al DNA va augmentar. Es va observar un patró similar, tot i que caldria fer molta més recerca per aclarir el paper de YAP1 en la modulació d'ERα i confirmar si el mecanisme observat podria ser rellevant per a altres receptors hormonals esteroides.

Les nostres troballes revelen un nou paper regulador de YAP1 en la modulació de la funció del PR i la seva dinàmica d'unió al ADN, mitjançant una possible competència entre YAP1 i PR per unir-se al factor pioner FOXA1 (en un mecanisme independent de TEAD), amb possibles implicacions per entendre l'especificitat dels receptors hormonals en el càncer de mama.

Paraules clau: Càncer de mama, PR, YAP1, FOXA1, especificitat, magnitud, cultiu 3D, ERα.

Resumen

Los receptores hormonales desempeñan un papel fundamental en la progresión del cáncer de mama y en la respuesta al tratamiento. Mientras que la función del receptor de estrógeno (ERα) ha sido bien establecida, el papel del receptor de progesterona (PR) sigue siendo controvertido. Se ha demostrado que la función del PR depende del contexto, pero los mecanismos que regulan la especificidad y magnitud de estas respuestas no se han explorado en profundidad.

En este estudio, revelamos una modulación del PR por parte de YAP1, efector de la vía de señalización Hippo, que regula tanto la magnitud como la especificidad de la respuesta del PR. La eliminación de YAP1 aumentó la capacidad de desdiferenciación inducida por PR, su respuesta proliferativa dependiente de progesterona, la expresión génica dependiente de progesterona y la unión del PR al ADN sin alterar la accesibilidad de la cromatina.

A nivel mecanístico, mediante un análisis genómico global, identificamos unas 6,000 regiones de unión al ADN donde YAP1 y PR colocalizan, ya sea en regiones con YAP1 unido a la cromatina sin tratamiento (~3,000) o tras estimulación hormonal (~3,000 regiones Coreclutadas). De forma destacada, FOXA1 emergió como el factor de transcripción que ancla YAP1 al ADN a través de un mecanismo independiente de TEAD. No detectamos una interacción física entre YAP1 y PR, lo que sugiere que podrían estar compitiendo por unirse a FOXA1.

Se observaron resultados consistentes en cultivos 3D, donde la actividad de la quinasa LATS1 inducida por la matriz extracelular aumentó la fosforilación de YAP1 y redujo sus niveles nucleares. La unión de PR y FOXA1 aumentó en células cultivadas en 3D, con un aumento más marcado en el PR en comparación con FOXA1. Además, YAP1 y PR se colocalizaron ampliamente en condensados nucleares, y

se confirmó la represión de YAP1 sobre PR y FOXA1, ya que, tras su eliminación, se incrementó la densidad de condensados de ambas proteínas.

Finalmente, extendimos nuestro análisis al ERα. En condiciones de falta de YAP1, la expresión génica dependiente de estrógenos se vio afectada y la unión de ERα al ADN se incrementó. Se observó un patrón similar, aunque será necesario realizar más investigaciones para esclarecer el papel de YAP1 en la modulación de ERα y confirmar si el mecanismo observado puede ser relevante para otros receptores hormonales esteroides.

Nuestros hallazgos revelan un nuevo papel regulador de YAP1 en la modulación de la función del PR y su dinámica de unión al ADN, mediante una posible competencia entre YAP1 y PR por su unión al factor pionero FOXA1 (en un mecanismo independiente de TEAD), con posibles implicaciones para entender la especificidad de los receptores hormonales en cáncer de mama.

Palabras clave: Cáncer de mama, PR, YAP1, FOXA1, especificidad, magnitud, cultivo 3D, ERα.

TABLE OF CONTENTS

LIST OF FIGURES

LIST OF TABLES

ABBREVIATIONS

2D	Two-dimensional
3D	Three-dimensional
AR	Androgen receptor
ATAC-seq	Assay for transposase-accessible chromatin sequencing
ATP	Adenosine triphosphate
BC	Breast cancer
BSA	Bovine serum albumin
CaCl2	Calcium chloride
CD24 / CD 44	Cluster of differentiation 24 / 44
CHD	Chromodomain helicase DNA binding
ChIP-seq	Chromatin immunoprecipitation – sequencing
Co-IP	Coimmunoprecipitation
CSCs	Cancer stem cells
DCC/FBS	Dextran-coated charcoal-treated fetal bovine serum
DOX	Doxycycline
DNA	Deoxyribonucleic acid
DMSO	Dimethyl sulfoxide
ECM	Extracellular matrix
EMT	Epithelial to mesenchymal transition
ER	Estrogen receptor
EREs	Estrogen-responsive elements
FBS	Fetal bovine serum
FH	Forkhead
FKHD	Forkhead DNA binding domain
FOXA1	Forkhead box protein A1
GFP	Green fluorescent protein
GO	Gene Ontology

GR	Glucocorticoid receptor
H3K27ac	Histone H3 lysine 27 acetylation
HATs	Histone acetyltransferases
HDAC	Histone deacetylase
HER2	Human epidermal growth factor 2
HMT	Histone methyltransferase
HNF α	Hepatocyte nuclear factor
HRE	Hormone responsive elements
HSP90	Heat shock protein 90
HSP70	Heat shock protein 70
IDR	Intrinsically disordered region
IGV	Integrative genomics viewer
JAK/STAT	Janus kinases / signal transducer and activator of transcription proteins
KD	Knockdown
LATS1/2	Large tumor suppressor kinase 1/2
MOB1	MOB kinase activator 1A
mPR	Membrane-associated progesterone receptor
MR	Mineralocorticoid receptor
MsigDB	Molecular signatures database
MST1/2	Mammalian STE20-like kinase 1/2
N-CoR	Nuclear receptor corepressor
NaCl	Sodium chloride
NuRD	Nucleosome remodeling and deacetylase
NR	Nuclear receptor
O/N	Overnight
PBS	Phosphate-buffered saline
PDX	Patient-derived xenografts
PI3K	
PIC	Protein inhibitor cocktail
PR	Progesterone receptor
PTM	Post-translational modification

R5020	Progestin analogue (synthetic progesterone)
RNA	Ribonucleic acid
RNAse	Ribonuclease
RT	Room temperature
SAV1	Salvador homologue 1
SDS-PAGE	Sodium Dodecyl Sulfate Polyacrylamide Gel Electrophoresis
SHR	Steroid hormone receptor
siRNA	Small interfering RNA
SMRT	Silencing mediator of retinoid and thyroid hormone receptor
SWI/SNF	switch/sucrose non-fermentable
T-TBS	Tris-buffered saline with tween
TAZ	WW-domain-containing transcription regulator 1
TEAD	Transcriptional enhanced associated domain
Tris	Tris (Hydroxymethyl)aminomethane Hydrochloride
UV response	Ultraviolet response
YAP1	Yes-associated protein 1

Introduction

Introduction

1. Breast cancer

Breast cancer (BC) is the leading cause of cancer-related death in women worldwide (Bray et al., 2024). In Europe, approximately 580,000 new cases and 160,000 deaths were reported in 2022. This high mortality underscores the aggressiveness of certain tumor subtypes and the limitations of current therapeutic approaches in effectively treating BC (Yu et al., 2024).

BC progression shares molecular similarities with normal development, as both rely on tightly regulated signaling pathways governing cell communication, proliferation, survival, and migration (Ercan et al., 2011). However, in cancer, both genetic and epigenetic alterations - arising from diverse origins- disrupt these pathways, ultimately contributing to uncontrolled cell growth. Consequently, a great degree of heterogeneity is observed within each tumor, as each subtype is characterized by a distinct molecular profile, morphology, and expression pattern of specific biomarkers (Byler et al., 2014), which will be discussed in the following section.

1.1. BC subtypes and their associated signaling pathways

As previously mentioned, BC is a heterogeneous disease with distinct biological and clinical characteristics. One of the most important factors in classifying BC subtypes is the presence of hormone receptors, including estrogen receptor alpha (ERα), progesterone receptor (PR), and the human epidermal growth factor receptor 2 (HER2). Based on these markers, BC can be categorized into different molecular subtypes (depicted in Table 1) (Harbeck et al., 2019 ; Feng et al., 2018). A description of each subtype is presented below:

Luminal tumors are the most common, representing approximately 80% of all BC diagnosed. Luminal tumors are further divided into two subtypes: Luminal A, characterized by ERα and PR expression and the absence of HER2 and, luminal B, which are ERα and HER2 positive and, can be either positive or negative for PR. Those are primarily treated with endocrine therapies that target ERα and PR-mediated pathways.

HER2 positive (HER2^{+}) tumors account for 15-20% of BC cases and are characterized by HER2 overexpression and the absence of PR and ERα. These tumors are primarily treated with targeted therapies- such as trastuzumab or pertuzumab, which block HER2 receptor- and chemotherapeutic agents, including taxanes or vinorelbine.

Triple negative (also called basal-like) tumors are the least prevalent subtype and did not express any of the three biomarkers (ERα, PR, HER2). Those tumors are among the most aggressive and difficult to treat, often requiring chemotherapy -such as nab-paclitaxel combined with ateozolizumab- or targeted inhibitors, including PARP, PI3K/mTOR or EGFR inhibirors.

Table 1. BC classification (adapted from Feng et al., 2018).

Molecular subtypes		***Luminal A***	***Luminal B***		***HER2+***	***Triple negative***
			HER2 -	**HER2 +**		
Receptors	**ERα**	+	+	+	-	-
	PR	+	-	-/+	-	-
	HER2	-	-	+	+	-
Frequency (%)		50	20-30		15-20	10-20
Response to therapies		Endocrine	Endocrine Chemotherapy	Endocrine Chemotherapy Target Therapy	Target Therapy Chemotherapy	Chemotherapy PARP inhibitors

According to BC classification, the expression and dysregulation of ERα, HER2, and PR play critical roles in driving tumor progression and influencing treatment responses for most cases. The main characteristics of these three signaling pathways are summarized below:

ERα signaling: ER signaling is crucial in BC initiation and progression. The two major ER isoforms, ERα and ERβ, function as nuclear hormone receptors that regulate gene expression upon estrogen binding. ERα, encoded by the ESR1 gene, drives tumor growth by interacting with cyclin D1, which promotes cell cycle progression from G1 to S phase (Musgrove, EA. & Sutherland RL., 1994). On the other hand, ERβ, encoded by ESR2, is emerging as a potential tumor suppressor. Its expression declines as tumors progress, and recent studies suggest that it may counteract ERα-driven tumorigenesis (Shen et al., 2023).

PR signaling: PR exists in two isoforms, PR_B, a full length 114 kDa protein, and PR_A, that is truncated in the N-terminal region which decreases its molecular weight to 94 kDa. Despite its similar structure, functional assays have suggested the balance between PR_A and PR_B expression to be critical in determining PR signaling outcomes, as an altered PR_A/PR_B ratio has been observed in BC and it has been associated with disease progression (Khan et al., 2012 ; Richer et al., 1998). In this context, PR_B functions primarily as a transcriptional activator, while PR_A can act as a dominant inhibitor of PR_B in certain contexts. Although the mechanistic insights are not yet fully understood, emerging evidence suggests that PR activation can either enhance or suppress tumor growth, depending on the cellular context, ligand availability, and interactions with specific co-regulators (Tian et al., 2018; C. C. Chen et al., 2011). A better understanding of the modulation mechanisms by which progestins drive tumor progression could facilitate the development of more effective therapeutic strategies.

HER2 signaling: HER2, a member of the epidermal growth factor receptor (EGFR) family, functions as a receptor tyrosine kinase that plays a crucial role in BC biology, particularly in HER2-positive cases (Feng et al., 2018). HER2 overexpression is strongly associated with aggressive tumor behavior and poorer prognosis. However, targeted therapies have significantly improved outcomes for HER2-positive patients

(Mercogliano et al., 2023). HER2 testing is essential for guiding treatment decisions, as only patients with confirmed HER2 overexpression or amplification are likely to benefit from targeted therapies -such trastuzumab or pertuzumab- which block the HER2 receptor (Harbeck et al., 2019).

1.2. Advances in BC Treatment: Targeting Molecular Pathways

Early detection and prevention remain the most effective strategies to improve patient outcomes, as the exact etiology of BC is not yet fully understood. Additionally, treatment approaches vary depending on the tumor subtype and may include surgery, radiation therapy, chemotherapy, or endocrine therapy (ET), either alone or in combination. A detailed analysis of ET and combined treatments are presented below:

Endocrine therapy (ET):

As previously mentioned, approximately 80% of breast cancers are hormone-dependent and express ERα and/or PR, making them potentially responsive to targeted therapies directed at these pathways.

ET is a treatment that blocks or modulates the growth of hormone-sensitive BC tumors. For ER^+ BC management, Selective ERα Modulators (SERMs, e.g., tamoxifen), Aromatase Inhibitors (AIs, e.g., anastrozole, letrozole, exemestane), and Selective ERα Degraders (SERDs, e.g., fulvestrant) are used (Patel et al., 2023). Despite their efficacy in BC treatment, resistance to these therapies is sometimes generated due to ERα mutations, gene duplications or the interaction of other signaling pathways with hormone receptors (Martin et al., 2017 ; Merenbakh-Lamin et al., 2013 ; Jeselsohn et al., 2016).

A new generation of anti-estrogen therapies, including SERMs different than tamoxifen, novel orally administered SERDs, and emerging agents like Complete ERα ANtagonists (CERANs), Selective ERα Covalent Antagonists (SERCAs), and PRoteolysis TArgeting Chimeric (PROTACs) are being developed to overcome ET resistance (Patel et al., 2023). In Figure I1, the mechanisms of the different compounds used in ET are depicted.

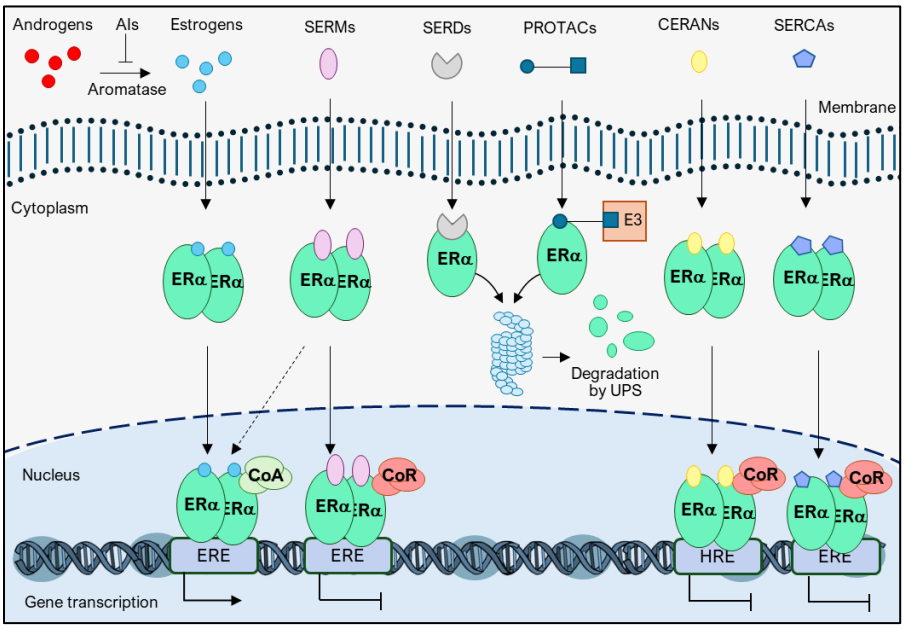

Figure I1. Mechanism of action of ETs. Estrogen activation of ERα triggers its translocation to the nucleus, where it binds to EREs and promotes estrogen-dependent gene expression. AIs inhibit the aromatase enzyme, thereby suppressing estrogen production from androgen. SERMs compete with estrogens for ERα binding and, in BC, are associated with co-repressors. SERDs and PROTACs, which bind ERα and the E3 ubiquitin ligase, facilitate ERα degradation. Additionally, CERAs and SERCAs inactivate ERα by recruiting co-repressors blocking transactivation domains and the cysteine residue (C530), respectively (Adapted from Patel et al., 2023).

In this context, large-scale cancer genome studies have identified numerous mutated genes (Cha et al., 2021; Pereira et al., 2016). Many of these mutations are concentrated within critical pathways such as PI3K/AKT/mTOR, RAS, and MAPK, highlighting the therapeutic potential of targeting entire signaling networks rather than individual genes.

Combined therapies

Advancements in cancer research have led to the development of targeted therapies that offer high therapeutic efficacy with minimal side effects by selectively targeting tumor-specific molecular pathways. To enhance the efficacy of ET, combination strategies have been developed, particularly with cyclin-dependent kinase 4/6 (CDK4/6) inhibitors. These agents, including palbociclib, ribociclib, and abemaciclib, have significantly improved response rates and survival in ER^+ BC when used in combination with ET (Sheikh & Satti, 2021). Beyond CDK4/6 inhibition, inhibitors of the PI3K-AKT-mTOR pathway are used to improve treatment efficacy in patients with PI3K-mutated ER^+ BC (L. Liu et al., 2025). These combinations aim to overcome resistance mechanisms and enhance long-term disease control.

As previously mentioned, an in-depth study of the signaling pathways involved in estrogen and progesterone activation is essential for guiding future treatments (Demir Cetinkaya & Biray Avci, 2022). To achieve this, robust experimental models are essential for studying targeted signaling pathways and assessing their interactions with hormone receptors.

1.3. Patient-derived xenografts and BC cell lines, including 3D models: two complementary approaches to study the role of hormone receptors in BC

In this section we will discuss the experimental models commonly used in BC research, highlighting their advantages and disadvantages:

Patient-derived xenografts (PDXs) are tumor tissues taken directly from BC patients and implanted into immunocompromised mice to evaluate the effectiveness of potential treatments (Y. Liu et al., 2023).

PDX models offer several advantages, such as preservation of the genetic landscape and recapitulation of morphology and the interactions between the tumor and the immune system. Additionally, they maintain tumor heterogeneity, making them valuable for studying cancer complexity and the response to drugs observed in patients, offering clinically relevant insights (Y. Liu et al., 2023). However, while PDX models are valuable for identifying suitable therapies for that tumor, their heterogeneity presents challenges in understanding the dysregulation driving tumor growth. Over time, the tumor stroma in PDX models tends to be replaced by murine-derived extracellular matrix (ECM) and stromal cells, which hinders immune cell activation and limits human cytokine secretion (Evans et al., 2017) (Y. Liu et al., 2023) (Figure I2).

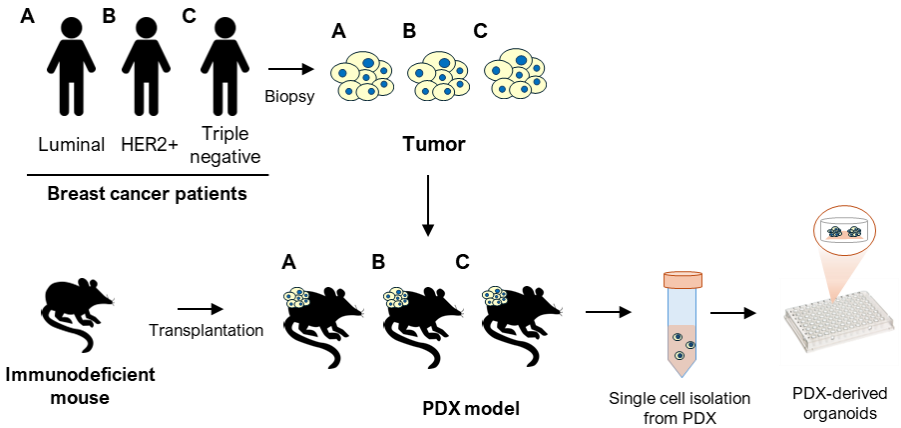

Figure I2. Procedure for generating PDXs. Tumor tissue is collected from patients via biopsy and implanted into immunodeficient mice for research purposes. For in vitro experiments, PDXs are cut into pieces and cultured as organoids in matrigel, providing cell-to-cell contact and extracellular matrix (ECM) support (adapted from Murayama & Gotoh, 2019).

BC cell lines: To explore the mechanisms underlying hormone functions, cell lines with varying receptor levels serve as valuable tools for studying interactions between different signaling pathways and providing insights applicable to PDX models. In this context, several cell models have been established to investigate the role of PR and ERα and their crosstalk with other signaling pathways involved in BC (Dai et al., 2017). Notably, the MCF-7 cell line, a luminal A model with high ERα expression, is widely used to study estrogen function (G. J. Cheng et al., 2022 ; Broome et al., 2021), while T47D cells, a luminal A model with high PR expression, are particularly suited for assessing the effects of progestins (Yu et al., 2017) (Figure I3).

Three-dimensional (3D) cultures: The 3D system is particularly effective for studying hormonal regulation, as it better replicates the cellular microenvironment compared to 2D cultures. By enhancing cell-to-cell and cell-extracellular matrix (ECM) interactions, 3D cultures create more complex systems that closely resemble tissue conditions in vivo (Ramírez-Cuéllar et al., 2024). This ability to integrate and transmit external signals between cells grown in 3D is crucial for investigating hormonal regulation in diseases like BC.

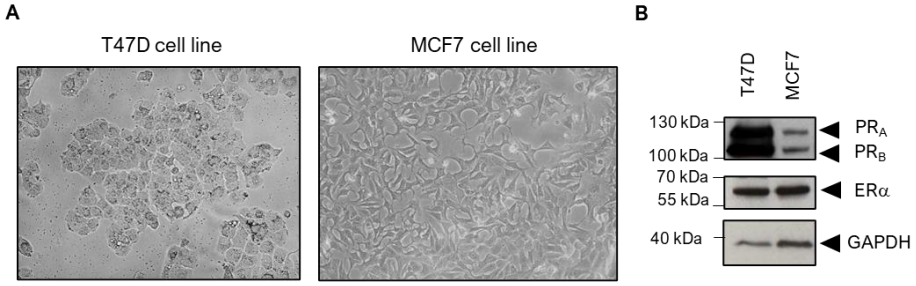

Figure I3. Cell lines used in this study. (A) T47D cells, which express higher levels of PR than ERα, are a suitable model for assessing the effects of progestins (left panel). MCF-7 cells, which express more ERα than PR, provide an ideal system for studying the effects of estrogens (right panel). (B): ERα and PR levels in MCF-7 and T47D cell lines, as determined by Western blot. GAPDH is used as a loading control.

2. Steroid hormone action

As mentioned, the expression of ERα and PR serve as key biomarkers in BC therapy to guide therapeutic decisions. This section will focus on understanding their mechanisms of action and exploring related receptors with similar or antagonistic functions.

Steroid hormones are crucial for regulating a variety of biological functions, including reproduction, inflammation, immune responses and cholesterol distribution (Weikum et al., 2018). These effects are mediated by Steroid Hormone Receptors (SHRs), which include receptors for estrogens (ER), progestins (PR), androgens (AR), glucocorticoids (GR) and mineralocorticoids (MR). While all SHRs share a common structural organization (Figure I4), their binding to specific genomic regions varies due to differences in their quaternary structure and interactions with other regulators (Pecci et al., 2022).

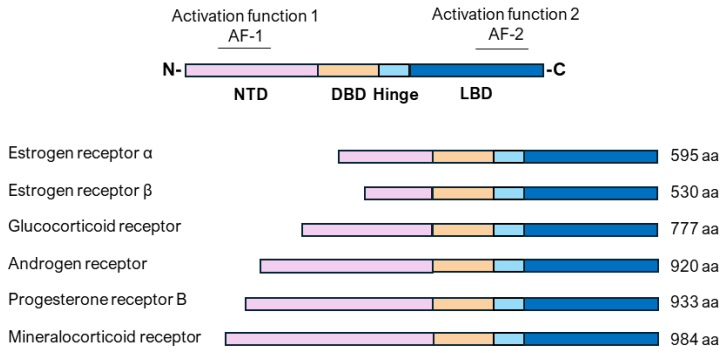

Figure I4. Structural organization of SHRs. The N-terminal domain (NTD) of SHRs contains the transcriptional activation function-1 (AF-1) while the DNA binding domain (DBD) recognizes the palindromic DNA binding site. In addition, the C-terminal domain includes the ligand binding domain (LBD), which allows ligand binding and contains the AF-2 that interacts with specific residues present in specific coregulators. Differences between the size in the N-terminus domain are shown for ER (α and β), GR, AR, PR and MR highlighting its importance in SHRs specificity (adapted from Pecci et al., 2022).

In their inactive state, SHRs are localized either in the cytoplasm or in the nucleus, depending on the specific receptor subtype. These receptors are stabilized by chaperone proteins such as HSP90, HSP70 and immunophilins (Pratt & Toft, 1997), which help to maintain their correct 3D structure and ensure that they are in a high-affinity state for specific ligand binding (Cheung & Smith, 2000 ; Norman et al., 2004) (Figure I5).

The hormone signaling pathway starts when steroid hormones circulating in the bloodstream diffuse across the lipid membrane and bind to their respective receptors. This binding induces conformational changes that lead to chaperone dissociation, promoting receptor dimerization (Figure I5). This conformational change activates a cascade of molecular events that initiate rapid and long-term effects on cellular function, which will be discuss in the next section (Ellmann et al., 2009).

2.1. Genomic signaling

As previously mentioned, SHRs are ligand-activated transcription factors which regulate cellular processes by inducing genomic events. In the case of PR, once dimerized, the receptor translocates to the nucleus and binds to specific DNA sequences (5′-AGAACAnnnTGTTCT-3′), known as Hormone Responsive Elements (HREs) (Payvar et al., 1983 ; A. C. Cato et al., 1988) (Figure I5). Hormone receptors typically bind to promoter or enhancer regions, which are regulatory DNA sequences that modulate gene expression either in close proximity (promoters) or over long distances (enhancers) from their target genes (Severson et al., 2018). Receptor binding is highly dependent on chromatin accessibility, as chromatin acts as a ‘landing platform’ and exists in dynamic states with varying degrees of compaction (Wiench et al., 2011).

A genome-wide analysis of PR binding using Chromatin Immunoprecipitated followed by sequencing (ChIP-seq) revealed that functional PR binding sites (PRbs) accumulate in the proximity of progesterone-induced genes, primarily in enhancers. Most of these sites exhibit high nucleosome occupancy (Ballaré et al., 2013). Progestin stimulation leads to remodeling of these nucleosomes, with displacement of histones H1 and H2A/H2B dimers, strongly suggesting that nucleosomes play a crucial role in PR binding and hormonal gene regulation. Moreover, enriched PR binding regions contain not only HRE motifs but also motifs for the pioneer factor FOXA1, supporting its role in facilitating receptor binding to target sites in the genome.

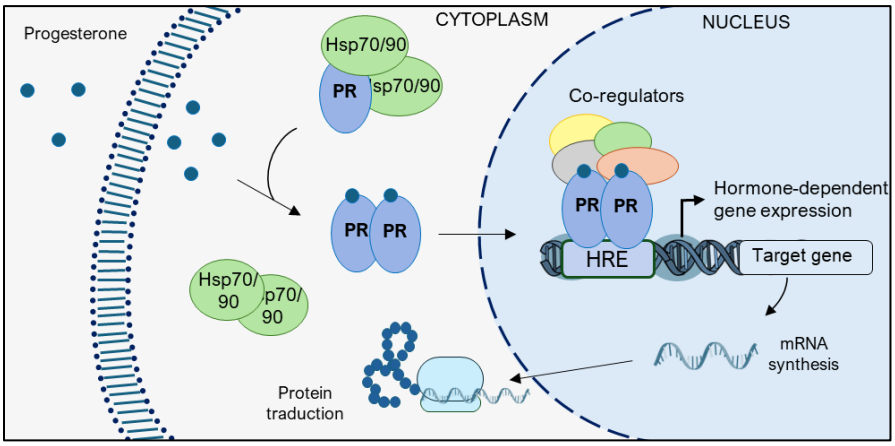

Figure I5. PR genomic signaling pathway. In the absence of a ligand, PR remains bound to HSP90 and chaperones. Upon progesterone binding, PR dissociates from HSP90/chaperones, dimerizes, and translocates to the nucleus, where it binds to HREs to regulate the expression of progestin-responsive target genes (adapted from Pedroza et al., 2020 & Saha et al., 2021).

2.1.1. Pioneer factors in hormone-dependent gene regulation

It is well established that the specificity and magnitude of hormonal responses in BC are closely linked to the strength of receptor binding to specific genomic regions. For ERα and PR, canonical DNA motifs (EREs

and HREs, respectively) are critical but insufficient to explain the complexity of receptor binding patterns. Interactions with other co-factors such as FOXA1, GATA3, and AP-1 are known to modulate receptor binding pattern (Kong et al., 2011).

GATA3 and FOXA1 are recognized as pioneer transcription factors, capable of binding to chromatin in its closed conformation. By facilitating chromatin opening, they enable the recruitment of transcription factors, chromatin remodelers, and histone modifiers, ultimately enhancing gene expression (Takaku et al., 2020). Consequently, it is important to understand their structural and functional features:

FOXA1 (formerly named as hepatocyte nuclear factor, HNF3α) has been found to reprogram the binding of SHRs, including ERα and AR, to control gene expression (Robinson & Carroll, 2012 ; Augello et al., 2011). FOXA1 consists of three functional regions: a central Forkhead (FH) DNA-binding domain and two flanking N- and C-terminal regions (Figure I6). The FH domain adopts a 'winged helix' structure, similar to linker histones, enabling stable binding to its target DNA sequence as monomer forming stable nucleosome complexes and displacing linker histone H1 (Zhou et al., 2024). This activity facilitates chromatin accessibility, allowing other transcription factors to bind and enhance transcription (Augello et al., 2011) (Figure I6). In addition to histone H1 displacement, FOXA1 also recruits ATP-dependent and no-dependent chromatin remodelers that maintain chromatin accessibility and enhance nuclear receptor binding (Fournier et al., 2016).

Despite these findings, the overall mechanism by which pioneer transcription factors like FOXA1 decondense chromatin remains unclear, although this process likely involves interactions with additional proteins (Barral & Zaret, 2024).

Thus, FOXA1 plays a critical role in facilitating receptor binding to these genomic target sites by maintaining chromatin in an open conformation (Augello et al., 2011). Once SHRs bind to chromatin, a variety of co-regulators are recruited to either enhance or silence target gene expression.

GATA3 is characterized by its ability to bind DNA at GATA motifs. It plays an important role in mammary development while it has also been implicated in hormone-dependent BC (Takaku et al., 2015). Importantly, GATA3 and FOXA1 have been found to cooperate in modulating ERα response as many ERα binding regions have been reported to be co-occupied by both pioneer factors. Furthermore, a different role for GATA3 has also been reported, as it mediates ERα binding to chromatin that is depleted of active histone modifications, highlighting its importance as a structural pioneer factor (Theodorou et al., 2013).

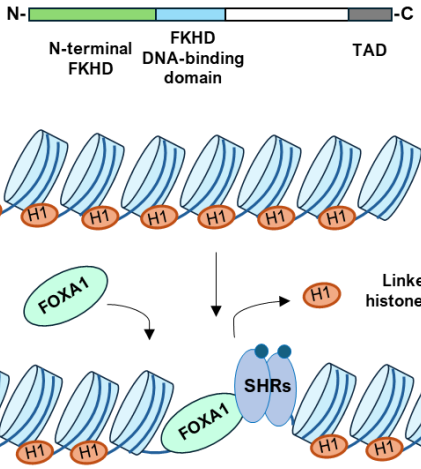

Figure I6. FOXA1 structure and mechanism of chromatin opening. FOXA1 structure is composed of the N-terminal FKHD, the DNA-binding domain and the transactivator domain (TAD). In one of the proposed mechanisms of action, FOXA1 binding to chromatin promotes linker histone H1 displacement while enables SHRs binding to modulate gene expression (adapted from Hirai et al., 2010 ; Adams et al., 2019).

Role of FOXA1 on ERα and PR binding

The role of pioneer factors may differ between ERα and PR, influencing their specific gene expression programs in a context-dependent manner. In BC, FOXA1 is often upregulated, and its binding to chromatin at ERα binding sites can enhance the transcriptional activity and promote the growth of ER-positive BC cells (Manavathi et al., 2014). In endocrine-resistant BC models, elevated FOXA1 levels, driven by gene amplification and overexpression, have been associated with resistance to endocrine therapy and increased invasiveness through reprogramming the ER-dependent transcriptome (X. Fu et al., 2016). Clinical studies report FOXA1 genetic aberrations, including gene amplifications and activating mutations, in approximately 6% of primary and 10% of metastatic ER+ BC cases (Ciriello et al., 2016).

While the importance of FOXA1 in ERα-driven transcription is well documented, its role in PR signaling remains less well defined. However, our group found that prior to hormone exposure, FOXA1 was significantly enriched at the PRbs that mediate hormonal repression. Knockdown of FOXA1 impacted a larger proportion of both hormone-dependent downregulated and upregulated genes (68.5% vs. 48%, respectively) (Nacht et al., 2016 ; Nacht et al., 2019). In fact, in the presence of progestins, an increase in FOXA1 is detected at the sites where PR binds to the genome, suggesting an active role for FOXA1 in the hormonal response of BC cells (Ballaré et al., 2013).

Historically considered undruggable due to a lack of small molecule binding sites, FOXA1 represents a significant challenge in BC therapy. Its role in both ERα and PR signaling further highlights its importance in the regulation of hormone-driven BC.

2.1.2. SHRs and their Co-regulators: orchestrators of the hormonal transcription response

SHRs function rely on the recruitment of a diverse set of co-regulators, including co-activators and co-repressors. Co-activators generally facilitate transcription by enhancing chromatin accessibility and promoting the assembly of the transcriptional machinery, while co-repressors repress gene expression through chromatin compaction and inhibition of transcriptional initiation (Talukdar & Chatterji, 2023). Together, co-regulators integrate signals from hormone pathways and promote a cell-specific transcriptional program.

SHR co-regulators are classified as ATP-dependent or ATP-independent, based on their mechanism of action:

ATP-dependent co-regulators use ATP hydrolysis to modify chromatin structure by altering the DNA accessibility by repositioning or modifying nucleosomes. Eukaryotic cells contain four families of chromatin remodelers, categorized on the basis of similarities and differences in the ATPase subunits: switch/sucrose non-fermentable (SWI/SNF), imitation switch (ISWI), chromodomain helicase DNA-binding (CHD) and INOsitol requiring 80 (INO80 family) (J. Chen et al., 2006 ; Vignali et al., 2000 ; Hargreaves & Crabtree, 2011 ; Stallcup & Poulard, 2020).

ATP-independent co-regulators remodel chromatin through histone modifications, including acetylation, methylation, and phosphorylation, mediated by enzymes such as histone acetyltransferases (HATs), deacetylases (HDACs), methyltransferases (HMTs), demethylases (HDMs) and kinases.

Co-regulators are essential for modulating gene expression in response to hormonal signals by exerting enzymatic activity and promoting the recruitment of additional regulatory factors (Talukdar et al., 2023). As previously mentioned, co-regulators can be broadly classified into two

main groups based on their function: coactivators, which promote gene expression by interacting with agonist-bound SHRs, and corepressors, which repress gene expression by associating with unliganded or antagonist-bound SHRs (Dasgupta et al., 2014). Below, we briefly describe the main characteristics of each group:

Coactivators play a crucial role in hormone-dependent transcription by interacting with SHRs in a ligand-dependent manner. Key coactivators include the SRC family (SRC-1, SRC-2 and SRC-3), as well as transcriptional adaptors as p300/CBP and p/CAF. SRCs facilitate transcription by bridging SHRs with the basal transcription machinery and recruiting HATs like CBP/p300 to chromatin (Figure I7, left panel). These HATs acetylate lysine residues on histones, such as H4K16ac, H3K9ac, H3K14ac, H3K18ac and H3K27ac among others, neutralizing their positive charge and weakening histone-DNA interactions. This chromatin relaxation enhances transcription factor accessibility, allowing RNA polymerase II to bind and activate gene transcription (Talukdar et al., 2023). The interaction between SHRs and coactivators is often mediated by the conserved LXXLL motif, also known as the nuclear receptor box (Savkur & Burris, 2004).

In contrast, SHRs **corepressors** repress gene expression by association with both liganded and unliganded SHRs. Key corepressors include nuclear receptor corepressor (N-CoR), silencing mediator of retinoid and thyroid hormone receptor (SMRT), histone deacetylases (HDACs) and other regulatory factors (Leonard & O'Malley, 2012; Stallcup & Poulard, 2020). Additional corepressors, such as thyroid hormone receptor uncoupling protein (TRUP) (Burris et al., 1995), BRCA1, and the nucleosome remodeling and deacetylase (NuRD) complex, further contribute to transcriptional repression (Dobrzycka et al., 2003).

Structurally, N-CoR and SMRT share significant similarities, particularly in their N-terminal repression domains, which mediate interactions with

HDAC-containing complexes and other chromatin-modifying proteins (Varlakhanova et al., 2010). The corepressors bind SHRs at defined sites, supporting a model in which a single corepressor associates with a DNA-bound SHR dimer (Lonard & O'Mallev, 2012).

Mechanistically, HDACs catalyze the removal of acetyl groups from histones, facilitating chromatin condensation and transcriptional repression (De Ruijter et al., 2003). Similarly, histone methyltransferases (HMTs) contribute to gene silencing by adding methyl groups to specific histone residues (Figure I7, right panel). For instance, SUV39H1 methylates histone H3 at lysine 9 (H3K9me3), while EZH2 targets lysine 27 (H3K27me3), both of which promote chromatin compaction and restrict access to the transcriptional machinery (Romagnolo et al., 2014).

Therefore, in the genomic signaling SHRs bind to co-regulators that act as chromatin modifiers. When recruited with the receptor, these co-regulators alter the target chromatin thereby influencing gene activity. This is a highly dynamic process, marked by ongoing cycles of binding and release. The outcome -whether the receptor-co-regulator complex activates or represses a given regulatory region- depends on a multifaceted interplay, where the chromatin environment encountered by these complexes plays a key role.

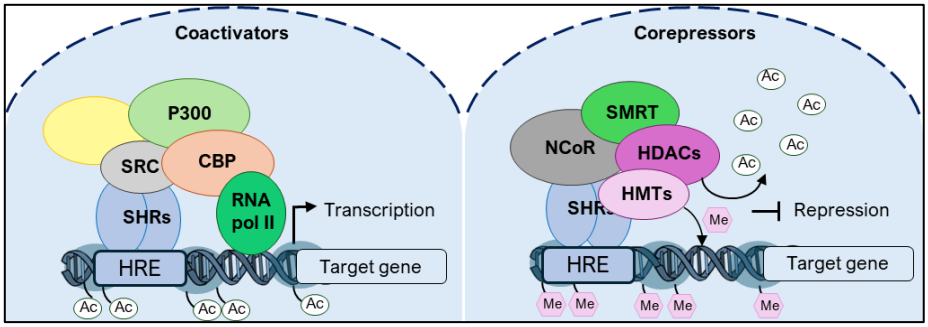

Figure I7. SHRs co-activators and co-repressors. SHRs coactivators include proteins such as SRCs, CBP, and P300, which enhance gene transcription by acetylating histones and stabilizing the RNA polymerase II transcriptional complex (left panel). In contrast, corepressors like HDACs and HMTs deacetylate and methylate histones, respectively, leading to the repression of gene expression (adapted from Tetel et al., 2009).

2.2. The so-called non-genomic signaling

Beyond their well-known genomic signaling, ERα and PR also mediate rapid effects that were previously assumed to not require direct receptor binding to target regions in the genome. These so-called non-genomic signaling events are initiated at the cell membrane and activate various intracellular cascades in the cytoplasm, including kinases and second messenger pathways (A. Migliaccio et al., 1996).

For instance, the Src/RAS/Erk and PI3K kinase signaling pathways can be activated by the direct interaction of membrane-associated PR (mPRs, attached via cysteine palmitoylation) with the SH3 domain of c-Src (Pedram et al., 2007 ; Boonyaratanakornkit et al., 2001) or through interaction with ERα which activates c-Src and PI3K (Antimo Migliaccio et al., 1998 ; Vicent et al., 2010) (Figure I8). These events are essential for hormone-driven genomic activity, as extracellular signal-regulated kinase (Erk) phosphorylates the mitogen- and stress-activated protein kinase (Msk) and PR at serine 294 (pPR S294), thereby enhancing its

transcriptional activity (Antimo Migliaccio et al., 1998) (Zaurin et al., 2021).

The PR signaling network is not limited to Erk1/2/Msk1; it is more complex, as PR also interacts with other pathways, such as CyclinA/Cdk2 (Narayanan et al., 2005), JAK/STAT (Richer et al., 1998) and EGF receptors (A. C. B. Cato, 1991) (Figure I8).

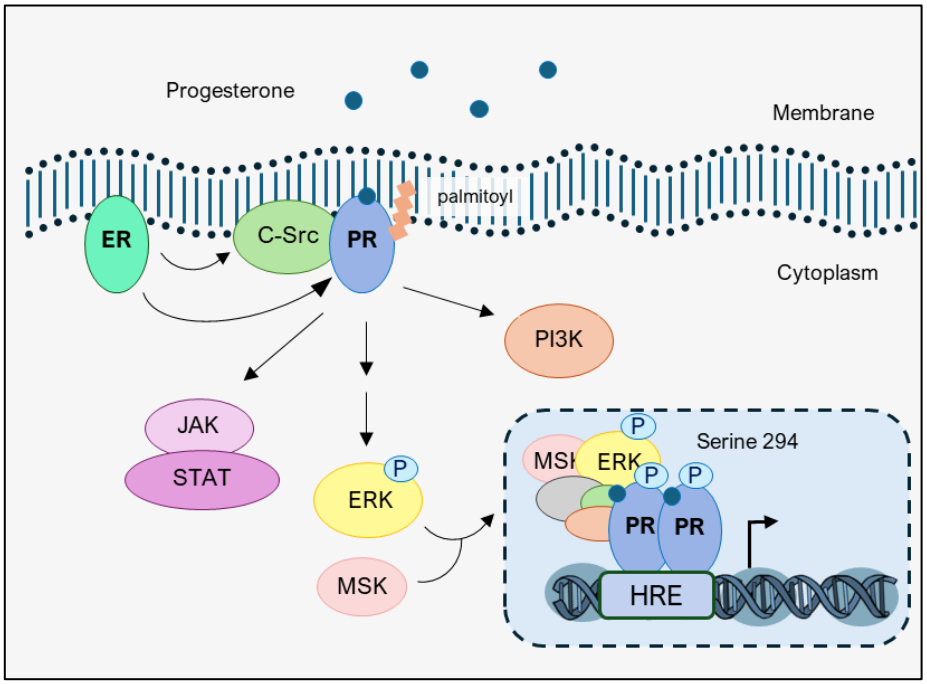

Figure I8. Activation of mPR and signaling pathway modulation. Progestins activate mPR, which is bound to c-Src (also activated by ERα), triggering several signaling pathways, including JAK/STAT, PI3K and the Src/Ras/Erk pathway. Upon progestin binding, nuclear accumulation of activated ERK phosphorylates PR at serine 294 and MSK, forming a PR/ERK/MSK ternary complex. This complex is then recruited to HREs, where it modulates gene expression (adapted from Vicent et al., 2006 ; Vicent et al., 2008).

2.3. Convergence of genomic and non-genomic pathways

For decades, genomic and rapid (so-called non-genomic) effects mediated by SHRs were considered relatively independent signaling pathways. Genomic signaling, which involves direct modulation of gene transcription in the nucleus, was traditionally viewed as the primary pathway responsible for the long-term effects of steroid hormones (Hurst C Lawrence, 1976). Conversely, non-genomic signaling, characterized by rapid cellular responses independent of direct gene transcription, was seen as a faster, secondary, yet complementary mechanism (A. Migliaccio et al., 1996).

However, some years ago, our laboratory reported that these pathways are not mutually exclusive but instead function in a coordinated and simultaneous manner at the chromatin level, allowing cells to integrate rapid responses with long-term transcriptional changes (Vicent et al., 2006 *;* Vicent et al., 2008). The integration of genomic and nongenomic signaling pathways is mediated by post-translational modifications of SHRs and their associated co-regulators (Agbana & McIlroy, 2024). In the case of PR, within 5 minutes of hormone exposure, PR forms a ternary complex with the kinases Erk1/2 and Msk1. Activated Erk1/2 phosphorylate PR at S294, while Msk1 phosphorylate histone H3 at serine 10 displacing a repressor complex containing HP1γ and initiating PR-dependent gene activation (Vicent et al., 2006). Thus, genomic and non-genomic pathways converge on chromatin, as the activation of cytoplasmic signaling cascades is essential for chromatin remodeling and transcriptional activation of steroid hormone target genes (Vicent et al., 2010).

2.4. The relevance of studying the crosstalk between SHRs and novel signaling pathways

In BC, the identification and the interplay between hormone regulated signaling pathways alongside other cellular pathways represents a challenge in the treatment of breast tumors. While luminal tumors are typically treated with ET to limit hormone-dependent tumor progression, constitutive activation of other signaling pathways plays a crucial role in resistance to these therapies, allowing tumors to evade anti-hormonal treatments (Montaser & Coley, 2018 ; Araki & Miyoshi, 2018 ; Kato et al., 1995).

Despite extensive research, the crosstalk between hormonal receptors and other signaling pathways remains only partially understood, largely due to BC heterogeneity. Consequently, a deeper understanding of how these signaling pathways interact with SHRs could represent a significant breakthrough in the development of combined therapies for BC.

In this context, the Hippo signaling pathway is of particular interest as is a key regulator of cell proliferation, apoptosis and tissue homeostasis (M. Fu et al., 2022). Importantly, the dysregulated expression of its nuclear effectors has been associated with tumor progression in several cancers (Dong et al., 2007 ; Tapon et al., 2002), highlighting Hippo as a highly interesting pathway that deserves further study.

3. Hippo signaling pathway

The Hippo signaling pathway was initially identified through tumor suppressor screening studies in Drosophila melanogaster (Xu et al., 1995). Mice with a mutation in the Hippo nuclear effector YAP1 developed liver overgrowth due to increased aberrant proliferation, suggesting that this pathway plays a key role in tumor progression (Dong et al., 2007). Later, it was discovered to be highly conserved in mammals (Lai et al., 2005 ; Justice et al., 1995 ; Tao et al., 1999) and its involvement in human cancer was subsequently confirmed (Dong et al., 2007 ; Camargo et al., 2007).

3.1. Core components

The Hippo signaling pathway consists of several components, including the intermediate kinases: mammalian STE20-like kinase 1/2 (MST1/2), protein Salvador homologue 1 (SAV1), MOBKL1A/B (MOB1A/B) and large tumor suppressor kinase 1/2 (LATS1/2), and the nuclear effectors: Yes-associated protein 1 (YAP1), WW-domain-containing transcription regulator 1 (TAZ), and the transcriptional enhanced associated domain (TEAD) family (M. Fu et al., 2022).

Notably, the Hippo pathway acts as a negative regulator of the nuclear effectors YAP/TAZ (Figure I9). Both proteins are negatively regulated by phosphorylation at specific residues by LATS1/2 kinases, which are activated by MST1/2. For YAP1, key phosphorylation sites include S127 and S381 (Bae et al., 2017), while TAZ is phosphorylated at S89 and S311 (Y. W. Li et al., 2015). Phosphorylation of YAP1 and TAZ results in their cytoplasmic retention through binding to the 14-3-3 protein and subsequent degradation via the proteasomal pathway by the SCF complex (Figure I9) (Koo & Guan, 2018), allowing the TEAD-binding competitor VGLL4 to access and occupy TEAD-enriched regions (Zhao et al., 2010). SAV1 serves as a mediator, facilitating the proximity of

MST1/2 and LATS1/2 to promote phosphorylation, while MOB1A and MOB1B act as adaptor molecules that enhance LATS1/2 kinase activity.

In contrast, when the Hippo pathway is OFF, the unphosphorylated forms of YAP1 and TAZ translocate to the nucleus where they exert their functions by interacting with TEAD transcription factors (Figure I9). Because YAP1 and TAZ lack a DNA-binding domain, they are unable to bind directly to DNA. Instead, they modulate specific genes through their interaction with TEAD transcription factors (M. Fu et al., 2022).

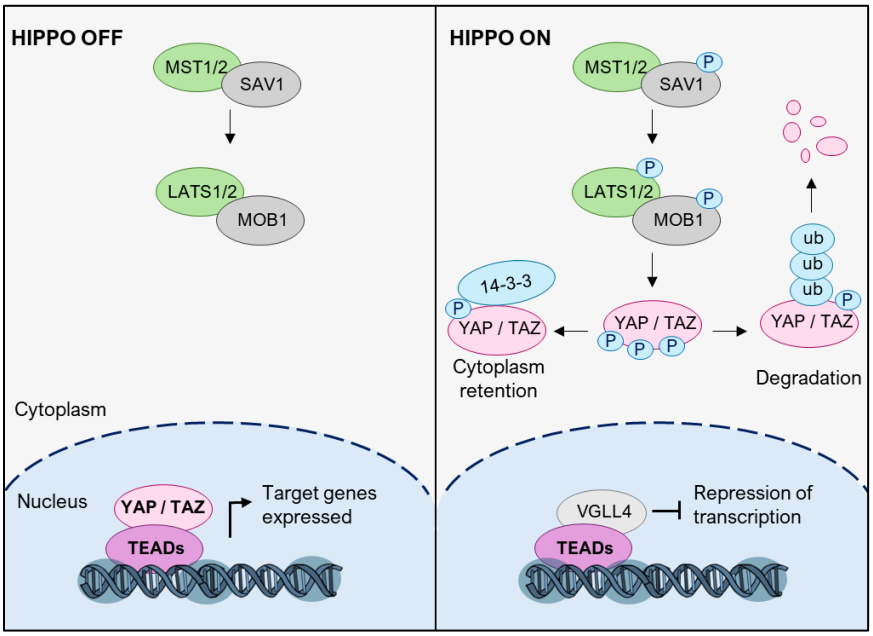

Figure I9. Overview of the components, activation, and subcellular dynamics of the Hippo signaling pathway. When the Hippo pathway is OFF (left panel), the intermediate cytoplasmic kinases remain unphosphorylated, allowing YAP/TAZ to translocate into the nucleus and exert their transcriptional functions through interaction with TEAD transcription factors. In contrast, when the Hippo pathway is ON (right panel), the intermediate kinases become phosphorylated, leading to phosphorylation of YAP/TAZ by LATS1/2. As a result, YAP/TAZ are sequestered in the cytoplasm by 14-3-3 proteins or targeted for degradation via ubiquitination, allowing VGLL4 to bind TEAD proteins (adapted from Juan & Hong, 2016).

3.2. Role of the Hippo pathway in gene regulation

YAP/TAZ/TEAD regulate the expression of numerous target genes involved in cell proliferation, survival and tissue regeneration. Among the genes controlled by the Hippo pathway, CTGF (Connective Tissue Growth Factor) and CYR61 (Cysteine-Rich Angiogenic Inducer 61) are key mediators of cell adhesion and migration. Others, such as AMOT (angiomotin), contribute to cell polarity and migration, while BIRC5 (survivin) and Cdk1 play crucial roles in preventing apoptosis and promoting cancer cell survival. Additionally, the Hippo pathway also regulates the oncogene MYC, that governs cell cycle progression and metabolism (Ramesh Kumar & Hong, 2024). Through the regulation of these genes, the Hippo pathway controls organ size, tissue repair, stem cell function, and tumor suppression. Dysregulation of this pathway has been linked to various diseases, including cancer and developmental disorders.

3.3. Regulation of the Hippo pathway

The Hippo pathway is regulated by several upstream signals, with the mechanical environment of the cell playing a key role. High cell density and increased cell-to-cell contact activate the pathway, leading to YAP1 retention in the cytoplasm and inhibiting the expression of proliferative genes (Saadh et al., 2025). Similarly, the ECM influences the activation of the pathway by activating focal adhesions and the RAP2 GTPase, which modulates actin polymerization and serves as an important regulator of LATS1 activity (Hippo-dependent). Additionally, the ECM can activate Ajuba proteins, which inhibit SRC proteins and modulate YAP/TAZ translocation to the nucleus (Hippo-independent) (Figure I10) (Luo & Li, 2022).

Moreover, the effect of the cellular environment on YAP's subcellular localization was recently studied in depth, revealing that force-induced

nuclear flattening leads to increased YAP import. The proposed model suggests that on soft substrates, nuclear import and export of YAP are balanced, while on stiff substrates, mechanical forces enhance YAP import by distorting nuclear pores (Elosegui-Artola et al., 2017). In this context, our laboratory observed differences in YAP1 localization between cells grown as monolayers on culture plates (2D) and those grown as 3D spheroids, where ECM function is preserved. In 2D cultures, YAP1 was predominantly localized in the nucleus. In contrast, in 3D cultures, the presence of ECM and enhanced cell–cell interactions activated LATS1 kinase, leading to increased YAP1 phosphorylation and its subsequent retention in the cytoplasm (Ramírez-Cuéllar et al., 2024).

Cellular and metabolic stress also regulate the Hippo pathway, with factors such as hypoxia or glucose levels influencing the subcellular localization of YAP1/TAZ. High glucose levels activate the O-GlcNAc transferase (OGT), which disrupts YAP/LATS interaction, thereby activating YAP1 transcriptional activity. Conversely, low glucose levels activate AMPK, which promotes AMOTL1-mediated activation of LATS1 (Hippo-dependent) or directly phosphorylates YAP1 at Ser94, disrupting YAP1-TEAD interaction (Hippo-independent). In hypoxia conditions, which are common in solid tumors, the Hippo pathway is altered to promote tumor cell growth. The E3 ubiquitin ligase SIAH2 facilitates the degradation of LATS2, reducing YAP1 phosphorylation and increasing its activity in the nucleus (Hippo-dependent modulation). In parallel, a Hippo-independent mechanism has been described, where HIF1 directly interacts with TAZ, promoting the transcription of genes involved in cell proliferation and migration (Figure I10) (Luo & Li, 2022).

Furthermore, the Hippo pathway can be modulated through crosstalk with other signaling pathways, including TGF-β (Varelas et al., 2008), Notch (Rayon et al., 2014), Wnt (N. Li et al., 2019) and PI3K/Akt (Qian et al., 2021). Thus, the Hippo pathway integrates various environmental cues, including mechanical forces, ECM stiffness, cell-cell interactions,

and cellular and metabolic stress, making it a key pathway for maintaining proper cellular function.

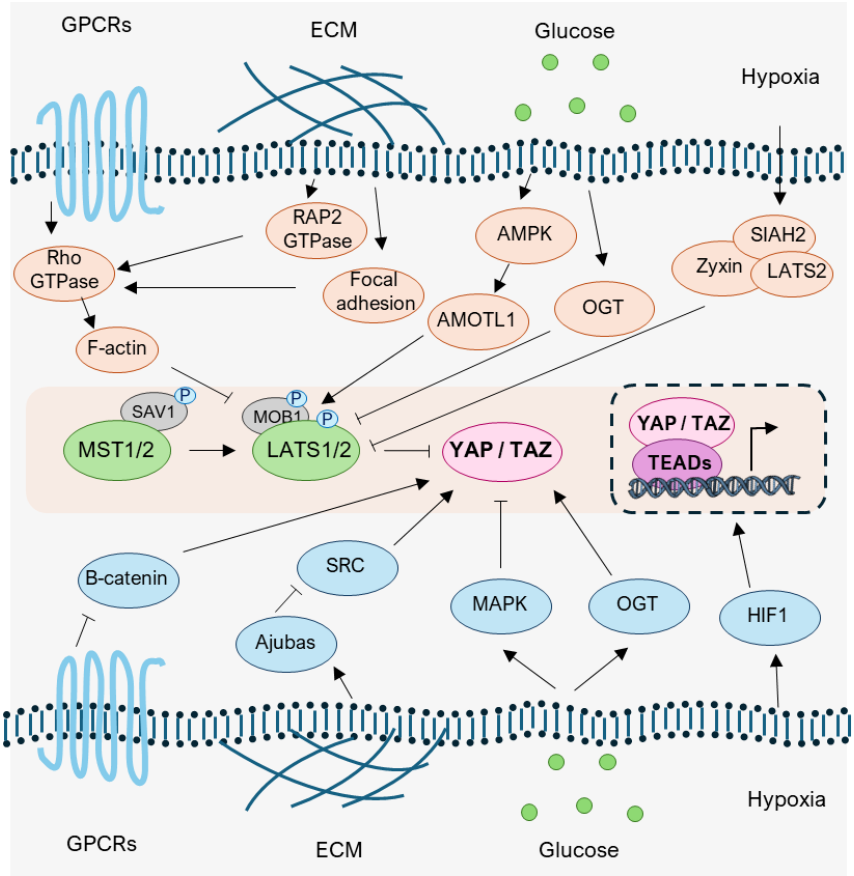

Figure I10. Complex modulation of Hippo signaling by external cues. The Hippo pathway is regulated by a variety of external signals -including GPCRs, the extracellular matrix (ECM), glucose availability, and hypoxia- through both Hippo-dependent and Hippo-independent mechanisms (adapted from Luo & Li, 2022).

3.4. Dysregulation of the Hippo pathway in breast tumor progression and resistance

In breast tissue, the Hippo pathway is critical for normal mammary gland development, stem cell function, and epithelial integrity (Saadh et al., 2025). Dysregulation of this pathway is associated to BC progression, metastasis and resistance to therapy (Kyriazoglou et al., 2021).

Hippo-dependent tumor progression is typically driven by two mechanisms: overexpression of YAP/TAZ proteins in the nucleus (K. H. Chen et al., 2014), or a reduction in the levels of LATS1/2 and MST1, accompanied by decreased kinase phosphorylation activity (Kern et al., 2022 ; Kima et al., 2020). These alterations result in enhanced transcriptional activity of YAP/TAZ, driving oncogenic gene expression, uncontrolled proliferation, and resistance to apoptosis. However, we also identified a non-canonical modulation of LATS1 on PR function that does not involve changes in LATS1 expression levels. In 3D-cultured cells, we observed that LATS1 not only phosphorylates YAP1 but also CTCF, affecting its binding to chromatin and influencing genome architecture. This modulation enhances PR binding, hormone-dependent gene expression and cell proliferation (Ramírez-Cuéllar et al., 2024). In this context, the absence of nuclear YAP1 is linked to an enhanced hormonal response, suggesting that YAP1 plays a negative role in the growth and hormonal responsiveness of BC cells.

In addition, dysregulation of the Hippo pathway is associated with BC resistance to therapy. Overexpression of YAP1 and TAZ has been associated with resistance to chemotherapeutic agents and CDK4/6 inhibitors (Li et al., 2018). Similarly, downregulation of MST1 and LATS1/2, key negative regulators of YAP/TAZ, has been associated with chemotherapy resistance (Zeng & Dong, 2021). The significant and diverse roles of various components of this pathway highlight its complexity in BC progression.

4. Role of YAP1 in hormone action

In recent years, emerging evidence has revealed context-dependent roles for YAP1. While it has traditionally been considered as a tumor promoter (Thompson, 2020 ; Zanconato et al., 2016). Recent studies suggest it may also act as a tumor suppressor in certain types of cancer (F. L. Li & Guan, 2022). However, the cellular factors that determine whether YAP1 functions as an oncogene or a tumor suppressor remain poorly understood. Additionally, YAP1 has been shown to modulate hormonal signaling pathways in a non-canonical, TEAD-dependent manner, through interactions with other transcription factors.

Regarding the modulation of hormonal signaling by YAP1/TEAD4, an initial study described a direct interaction of YAP1, TEAD4 and ERα. It was proposed that both YAP1 and TEAD4 act as coactivators of ERα, but exclusively at active enhancers. Their positive modulation of ERα activity contributes to the induction of estrogen-dependent target genes, thereby promoting tumor progression and cell growth. The mechanism involves YAP1 and TEAD4 recruiting MED1, a key component of the enhancer activation machinery. Interestingly, while TEAD4 is typically recognized as a transcription factor that binds directly to DNA, it was suggested that it could also function as a co-activator of ERα independent of its DNA-binding activity (Figure I11A) (Zhu et al., 2019).

However, an alternative role for YAP1 in relation to ERα has been proposed. In this model, YAP1 functions as a negative regulator, whereas TEAD4 remains an active co-regulator of ERα. Specifically, TEAD4 promotes ERα activity, while YAP1 interferes with the ERα-TEAD4 interaction, thereby attenuating the transcriptional response (Figure I11B) (Xu Li et al., 2022).

In prostate cancer (PC), YAP1 has been shown to negatively regulate the androgen receptor (AR) through a non-canonical mechanism that

disrupts the AR-TEAD4 complex, which is essential for AR-driven gene expression. This antagonistic interaction results in reduced PC cell proliferation and tumor growth, suggesting that YAP1 acts as a tumor suppressor in PC by modulating AR signaling (Figure I11C) (Xu Li et al., 2023).

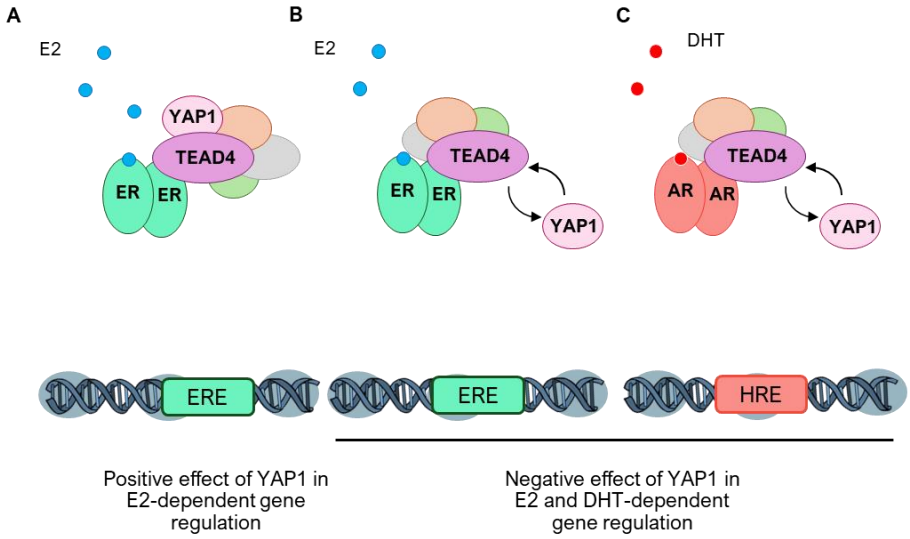

Figure I11. YAP1 crosstalk with hormonal signaling pathways. (A) Positive modulation of ERα by YAP1 and TEAD4 in BC. (B) Competition between YAP1 and TEAD4 for ERα binding in BC. (C) Competition between YAP1 and TEAD4 for AR binding in PC. (adapted from Zhu et al., 2019 ; Xu Li et al., 2022 ; Xu Li et al., 2023).

Several studies provide examples where YAP1 functions independently of TEAD proteins. In these cases, YAP1 may exert its effects through interactions with other transcription factors. For example, JunB (a member of the AP-1 family) and STAT3 have been shown to interact with YAP1 and modulate the expression of genes involved in tumor progression (He et al., 2021). Additionally, YAP1 and FOXA1 were found to interact in MCF-7 cell lines through BioID mass spectrometry assays,

suggesting a potential association within a complex that also includes ERα and TEAD proteins (Zhu et al., 2019).

Despite extensive research, the mechanisms underlying the specificity and magnitude of hormone receptor responses -particularly under physiological conditions, where receptors can be simultaneously activated by their cognate ligands- remain incompletely understood. Studies conducted so far have shown that TEAD and YAP1 primarily function as co-regulators of hormone receptors, acting as scaffolds in the regulation of hormone responses (Figure I11) (Zhu et al., 2019 ; Xu Li et al., 2022 ; Xu Li et al., 2023). However, the role of YAP1 as a positive or negative regulator in the cell nucleus remains unclear. Notably, YAP1 has been linked to cancer resistance, highlighting the need to better understand its role in BC and its impact on disease progression and treatment responses

Objectives

Objectives

The main objective of this thesis was to elucidate the interplay between hormonal and Hippo signaling pathways in BC cells. The specific aims were:

1. To assess how YAP1 modulates the PR response in T47D cells by investigating its role in cell proliferation, dedifferentiation, gene expression, PR binding and chromatin accessibility.

2. To determine if there is a direct link between YAP1 and PR by defining YAP1-PR overlapping genomic regions.

3. To evaluate whether the role of YAP1 in PR function is mediated by the canonical Hippo pathway via TEAD proteins.

4. Investigate the proposed crosstalk in more physiological contexts, including transcriptional condensate formation in living cells, 3D spheroid cultures, and PDXs.

5. Determine whether the proposed mechanism for PR also applies to ERα by analyzing estrogen-dependent gene expression and ERα binding to chromatin.

Materials and Methods

Materials

1. Chemicals and reagents

Table 2. Chemicals and reagents

Name	*Reference*	*Supplier*
B-glycerophosphate	G5422	Merck Life Sciences
B-mercaptoethanol	-	-
Absolute Ethanol	20821.321	VWR
Agarose, ultra-pure	16500	Life technologies
Bradford Bio-rad 5X	5000006	Bio-rad laboratories
Braun water	387874	B. Braun medical
Bovin Serum Albumin (BSA)	A7906	Merck Life Sciences
ChIP Buffer 5X	K02390001	Diagenode
coIP Beads (G protein / A protein) agarose beads	IP05	Merck Life Sciences
Complete EDTA-free (PIC)	45148300	Merck Life Sciences
DMEM	41965-062	Life technologies
DMEM W/O phenol red	31053-028	Life technologies
Dimethyl sulfoxide (DMSO)	D2650	Merck Life Sciences
DTBP	20665	Merck Life Sciences
EDTA	03677-100G	Merck Life Sciences
EGTA	324626	Merck Life Sciences
Fetal Bovine Serum (FBS)	A5256701	Life technologies
Formaldehyde 37%	F8775	Merck Life Sciences
Glycine	G7126	Merck Life Sciences
Insulin	-	-
IGEPAL (NP40)	I8896	Merck Life Sciences

Isopropanol	1.096.341.000	Merck Life Sciences
L-glutamine	25030-024	Life technologies
Lipofectamine 2000	11668027	Life technologies
Loading buffer	K929	Quimivita
Methanol	309001	Sudelab
OPTIMEM	31985-047	Life technologies
Ortovanadate	S6508	Merck Life Sciences
PageRuler protein ladder	26616	Life technologies
PBS	P4417	Merck Life Sciences
Penicillin / Streptavidin (Pen/Strep)	15140-122	Life technologies
Phenylmethanesulfonyl fluoride (PMSF)	78830	Merck Life Sciences
Phenol/Chloroform	P2069	Merck Life Sciences
Propidium iodide	P4864	Merck Life Sciences
RPMI	42401-042	Life technologies
RPMI W/O phenol red	32404-014	Life technologies
Sodium n-dodecyl sulfate (SDS)	428023	Merck Life Sciences
Skim Milk	70166	Merck Life Sciences
Sodium orthovanadate	S6508	Merck Life Sciences
Sodium pyruvate	11360-039	Life technologies
Triton	T8787	Merck Life Sciences
Tris	1.083.821.000	Merck Life Sciences
Trypsin	25200-072	Life technologies
Water RNAse, DNAse free	AM9939	Life technologies

2. Buffers and solutions

Table 3. Composition of buffers, solutions and culture media used in this study.

Buffer	*Preparation*
A solution	Sodium citrate (38 mM) + propidium iodide (500 ug/mL in water)
B solution	RNAse A (10 mg/ mL in PBS)
DMEM medium	500 mL DMEM + 10% FBS + 5 ml Pen/Strep + 5 ml L-glutamine + 5 ml Sodium Pyruvate + 100 µl Insulin
Elution Buffer	1 % SDS + 100 mM $NaHCO_3$ (Volume adjusted with Braun water)
FACS Buffer	PBS + 3% CD/FBS
HBS Buffer (2X)	281 mM NaCl + 100 mM HEPES + 1,5 mM NA_2HPO_4
Lysis Buffer I (ChIP)	5 mM Pipes pH=8 + 85 mM KCl + 0,5% NP40 + 1 mM PMSF + 1 ug/mL B-Glycerophophate + 1X PIC + 1 µg/mL Na_3VO_4 (Volume adjusted with Braun water)
Lysis Buffer II (ChIP)	1% SDS + 10 mM EDTA pH=8 + 50 mM Tris pH=8 + 1 mM PMSF + 1 µg/mL B-Glycerophophate + 1X PIC + 1 µg/mL Na_3VO_4 (Volume adjusted with Braun water)
Lysis buffer for co-immunoprecipitation	50 mM Tris-HCl pH 7.5 + 130 mM NaCl + 1 mM EDTA + 1 mM EGTA + 5 mM MgCl2 + 1% Triton + 0,2 mg/mL BSA + B-Glycerophophate + PIC + PMSF + Na_3VO_4 (Volume adjusted with Braun water)
PBS + inhibitors	9,3 mL PBS + 0,4 mL PIC + 0,2 mL B-Glycerophophate + 0,05 mL PMSF + 0,05 mL Na3VO4
Protein digestion buffer	For every ChIP -> 16 µL 1 M Tris pH= 6.5 + 8 µL 0.5 M EDTA PH= 8 + 0,8 µL proteinase K (20 mg/mL)
Protein extraction buffer	5 mM Tris-HCl pH7.5 + 1% SDS + 1 mM EDTA + 1 mM EGTA + B-Glycerophosphate + PIC + PMSF + Na_3VO_4 (Volume adjusted with Braun water)
RBS (ATAC)	10 mM Tris-HCl pH 7.5 + 10 mM NaCl + 3 mM $MgCl_2$ + 0.1% Igepal

RPMI medium	500 ml RPMI + 10% FBS + 5 ml Pen/Strep + 5 ml L-glutamine + 100 µl Insulin
RPMI white medium	500 mL RPMI + 10% FBS charcoal + 5 ml Pen / Strep + 5 ml L-glutamine + 100 µl Insulin
TE Buffer	10 mM Tris-HCl pH=8 + 1 mM EDTA
Working solution	For each 1 mL: 940 µL PBS + 30 µL A solution + 30 µL B solution

3. Antibodies

3.1. Western Blot antibodies

Table 4. Antibodies used in this study for Western Blot analysis

Antibody	*Host*	*Dilution*	*Reference*	*Company*	*MW*	*Type*
PR F4	M	1/1000	sc166169	Santa Cruz	81 and 116	Monoclonal
PR H-190	Rb	1/1000	sc7208	Santa Cruz	81 and 116	Polyclonal
FOXA1	Rb	1/1000	ab170933	Abcam	49	Monoclonal
YAP1	M	1/1000	sc101199	Santa Cruz	65	Monoclonal
GAPDH	M	1/5000	sc32233	Santa Cruz	37	Monoclonal
BRG1	Rb	1/5000	ab110641	Abcam	185	Monoclonal
α-tubulin	M	1/4000	2144	Cell signaling	52	Polyclonal
pRP Ser 294	Rb	1/1000	61785	Abcam	81 and 116	Polyclonal
pPR Ser 400	Rb	1/1000	60954	Abcam	81 and 116	Polyclonal
pYAP	Rb	1/1000	4911	Cell signaling	65-78	Polyclonal

3.2. ChIP antibodies

Table 5. Antibodies used in this study for chromatin immunoprecipitation (ChIP) experiments.

Antibody	*Reference*	*Host*	*Type*
PR H-190	sc7208	Rabbit	Polyclonal
FOXA1	ab5089	Goat	Polyclonal
YAP1	ab52771	Rabbit	Polyclonal
TEAD4	sc101184	Mouse	Monoclonal
H3K27Ac	4729	Rabbit	Polyclonal

3.3. Co-immunoprecipitation antibodies

Table 6. Antibodies used in this study for co-immunoprecipitation (co-IP) experiments.

Antibody	*Reference*	*Host*	*Type*
YAP	ab52771	Rabbit	Polyclonal
PR H-190	Sc7208	Rabbit	Polyclonal
PR F4	sc166169	Mouse	Monoclonal
FOXA1	ab170933	Rabbit	Monoclonal

4. Secondary antibodies

Table 7. Secondary antibodies used in this study for Western Blot analysis.

	Reference	*Supplier*
Rabbit	NA934	VWR
Mouse	NA931	VWR

5. shRNA vector and siRNAs

Table 8. shRNAs and siRNAs used in this study.

	Reference	*Supplier*
shYAP1	TRCN0000019894	MISSION (Merck)
siControl	1027310	QIAGEN
siYAP1	J-012200-07-0020	Dharmacon
siFOXA1	L-010319-00-0020	Dharmacon

6. Commercial kits

Table 9. Commercial kits used in this study.

Name	*Reference*
NZY Total RNA isolation kit	MB13402
Qiagen MinElute PCR Purification Kit	28004

Methods

1. Cell culture and hormonal treatments

T47D BC cells were cultured in RPMI 1640 medium supplemented with 10% Fetal Bovine Serum (FBS), 2 mM L-glutamine, 100 U/mL penicillin, 100 µg/mL streptomycin, and insulin. Cells were maintained at 37°C in a humidified atmosphere with 5% CO_2. For hormone-dependent experiments, cells were plated in RPMI medium without phenol red, supplemented with 10% dextran-coated charcoal-treated FBS (DCC/FBS). After 48 hours, the medium was replaced with fresh medium and incubated for an additional 24 hours. The next day, cells were treated with 10 nM R5020 at 37ºC for 30 minutes for ChIP-seq and coIP experiments or 6 hours for RNA-seq experiments.

MCF-7 BC cells were cultured in DMEM medium supplemented with 10% FBS, L-glutamine, sodium pyruvate, penicillin/streptomycin and insulin. For hormone-dependent experiments, cells were plated in DMEM medium without phenol red, supplemented with 5% DCC/FBS (as in 10% DCC/FBS cells are not enough starved and some ERα can remain activated). After 48 hours, the medium was replaced with fresh medium and incubated for an additional 24 hours. The next day, cells were treated with 10 nM estradiol (E2) at 37°C for 30 minutes for ERα ChIP-seq or 6 hours for RNA-seq.

For long-term storage, cells were frozen under controlled conditions. A P-150 plate was trypsinized, and approximately 8×10^6 cells were pelleted by centrifugation at 1,000 rpm for 5 minutes at room temperature (RT). The cell pellet was washed with PBS, centrifuged again, and resuspended in FBS containing 10% DMSO. Aliquots of 1.5 mL of the cell suspension were transferred into cryovials. To ensure a gradual cooling rate of approximately -1°C per minute, the vials were

placed in a Frosty container (Merck) filled with 100% isopropyl alcohol before being transferred to liquid nitrogen storage.

2. 3D cell culture on matrigel

Matrigel was thawed overnight at 4 °C on ice. The seeding procedure took place on ice. Prechilled p60 plates were coated with 600 µL Matrigel and spread carefully on the plate area without touching the walls of the dish. Plates were then incubated for 20–30 minutes at 37 °C to allow matrigel polymerization. Trypsinized cells were resuspended to obtain a single cell suspension of 200,00 cells diluted in 4 mL of medium. Cells were plated on top of the matrigel and they were maintained in the incubator for 10 days changing medium every 2-3 days.

For hormonal induction, T47D cells were plated on top of phenol red-free Matrigel and after 7 days of culture the cells were deprived of phenol-red by changing the medium to RPMI white medium supplemented with dextran-coated charcoal treated FBS for 48 hours. After that, the medium was replaced with fresh medium and incubated for an additional 24 hours. The next day, cells were treated with 10 nM R5020 at 37°C for 30 minutes for PR and FOXA1 ChIP-seq.

3. RNA interference experiments

T47D or MCF-7 cells were seeded in red medium at approximately 70% confluence. After 24 hours, the medium was replaced with white medium, followed by siRNA transfection into cells using Lipofectamine 2000. For example, $1{,}8 \times 10^6$ cells were plated in a P-100 dish. The next day, the siRNA was diluted in OPTI-MEM medium (32,5 µL siRNA (650 pmols) in 717,5 µL OPTI-MEM) in one tube, while the corresponding volume of Lipofectamine (42 µL in 708 µL OPTI-MEM) was diluted separately and incubated for 5 minutes. The siRNA solution was then combined with the Lipofectamine solution and incubated for 20 minutes.

The resulting siRNA-lipofectamine complex was added dropwise to the cells. After 48 hours, the medium was replaced with fresh medium. Sixteen hours later, cells were incubated at 37°C for either 30 minutes for ChIP assays or 6 hours for RNA-seq experiments with 10 nM R5020, 10 nM estradiol or vehicle (ethanol).

4. Lentiviral infection assays

T47D shControl, T47D YAP knockdown (shYAP) and inducible YAP1 (rTTA YAP) cell lines were generated from T47D cells (Sancho et al., 2008). To achieve YAP1 knockdown, a lentiviral infection protocol was used.

For each shRNA, 1,5 million HEK293T cells were seeded in a P-100 dish containing 8 mL of DMEM supplemented with 10% FBS, 100 U/mL penicillin, 100 µg/mL streptomycin. The next day, transfection reactions were prepared. In one tube, 500 µL of 2× HBS buffer (Table 3) was thawed. In a separate tube, a plasmid mixture was prepared, consisting of 5 µg VSVG (G glycoproteins of the vesicular stomatitis virus), 8 µg H8.91, 7 µg of the shRNA-encoding plasmid, and 62,5 µL of 2 M $CaCl_2$, in a final volume of 500 µL. The VSVG plasmid encodes the G glycoprotein, that forms part of the envelope of the virus to enhance its infectivity (Okimoto et al., 2001) while the H8.91 encodes for the gag, pol and rev viral proteins necessary for lentiviral packaging (Carnell et al., 2017).

The plasmid mixture was gradually added to the HBS buffer with gentle mixing. After 35 minutes at room temperature, the transfection solution was added to the HEK293T cells. After 24 hours, the medium was replaced with RPMI and T47D cells were seeded for infection the next day.

After 24 hours, virus-containing media was collected, filtered, and added to the cultured T47D cells. This step was repeated the following day to

increase infection efficiency. Infected cells were then selected using puromycin resistance.

5. Cell proliferation assay

T47D wild type and T47D rTTA YAP1 cells were plated in duplicate in P60 plates at a density of 500,000 cells per well in RPMI white medium with DCC/FBS. After 24 hours, cells were treated with 10 nM R5020 for 18 hours. In the inducible YAP1 cell line (rTTA YAP), doxycycline (dox) was added 3 hours before hormone treatment.

Cells were trypsinised, washed with PBS and resuspended in 300 µL PBS. Fixation was carried out by the gradual addition of 700 µL of ethanol to a final concentration of 70%, followed by incubation at 4°C for 24 hours before staining.

The fixed cell suspension was pelleted by centrifugation at 5,000 rpm at 4ºC, stained with 250 µL working solution (940 µL PBS + 30 µL solution A containing propidium iodide + 30 µL solution B). Stained samples were kept at 4°C for at least 24 hours before analysis. A total of 10,000 cells per sample were analyzed using a Gallios flow cytometer (Beckman Coulter) (University of Barcelona, CCiTUB).

6. Dedifferentiation assay

T47D wild-type cells transfected with either siControl or siYAP1, and T47D rTTA YAP1 cells were seeded in duplicate in 6-well plates at a density of 250,000 cells per well, using RPMI white medium supplemented with 10% charcoal-stripped FBS. After 16 hours, the medium was changed and DOX was added when required. Six hours later, the cells were treated with 10 nM R5020 or left untreated, then incubated for an additional 24 hours.

The next day, the cells were trypsinized and viable cells were counted. For each condition, 100,000 cells (in duplicate) were resuspended in separate tubes. Antibodies were added sequentially: first the CD24-PE (4 µL), followed by CD44-APC (4 µL). For controls, two replicates of unstained cells and single stained controls (CD24 or CD44) were prepared. Cells were stained for 15 minutes at room temperature (RT), washed with 1 mL FACS Buffer, centrifuged 1,000 rpm for 5 minutes and resuspended in 250 µL FACS Buffer. Samples were analyzed using a Gallios flow cytometer analyzer (University of Barcelona, CCiTUB).

7. Protein extraction

Cell pellets were collected by centrifugation 5 minutes at 1,000 rpm, washed with PBS, and lysed in protein extraction buffer (Table 3). The lysates were then incubated at 95°C for 10 minutes. For Western blot analysis, samples were centrifuged at 13,000 rpm for 10 minutes, quantified using the Bradford method (Bio-Rad), and loaded onto acrylamide gels for electrophoresis.

8. Western Blotting

Western blotting was used to compare protein levels between samples. A total of 20 µg of protein extract was loaded on a 10% polyacrylamide gel and subjected to electrophoresis at 120 V for 1.5 h. Proteins were then transferred to a Trans-Blot Pure nitrocellulose membrane (Bio-Rad) at 80 V for 90 minutes at 4°C.

Membranes were blocked with 5% milk for 1 hour at room temperature and then incubated overnight at 4°C with the primary antibody at the appropriate dilution in T-TBS 2.5% milk.

The next day, the membranes were washed three times with T-TBS and incubated with the secondary antibody for 1 hour at room temperature.

Protein bands were detected using ECL solution and visualized using the iBright imaging system (Roche).

9. RNA extraction

RNA extraction was performed using the NZY Total RNA isolation kit (NZYtech, MB13402) according to the manufacturer's instructions. Briefly, cells were lysed directly in the plate with RLT buffer, then scraped and transferred to an NZYSpin homogenisation column. After centrifugation, the flow-through was mixed with 70% ethanol and transferred to an NZYSpin binding column for further centrifugation at 1,000g for 30 seconds.

The RNA bound to the column was washed with buffer NI, centrifuged and treated with DNase I for 15 minutes. The column was then washed once with NWR1, twice with NWR2 and dried. Finally, RNA was eluted by adding 50 µL of RNase-free water to the column followed by centrifugation. The RNA yield was quantified using a Biochrom spectrophotometer.

10. RNA-seq

RNA was extracted from T47D cells (siControl, siYAP1, siTEAD4, siTEAD1) and MCF-7 cells (siControl, siYAP1) cells untreated or treated with R5020 or estradiol for 6 hours, using the Qiagen kit following the manufacturer's instructions.
RNA was submitted to the CRG Genomics Facility, where it was quantified, subjected to quality control analysis, and prepared for massive sequencing using the Next-seq 2000 (Illumina). Details on RNA-seq data analysis are provided in the Bioinformatics Analysis section

11. ChIP-sequencing (ChIP-seq)

a. Chromatin preparation

Chromatin immunoprecipitation followed by sequencing (ChIP-seq) assays were performed as described (Strutt & Paro, 1999). T47D or MCF-7 cells were treated with progestins or estradiol and cross-linked with 1% formaldehyde for 10 minutes at 37ºC. For YAP1 ChIP-seq, protein–protein crosslinking was performed by adding 2 mM DSG for 30 minutes at room temperature prior to formaldehyde crosslinking. Crosslinking was stopped by adding 125 mM glycine and the solution was incubated for 5 minutes at RT. The cells were washed twice with PBS and collected by scraping in 2 mL PBS + inhibitors (Table 3). Then, cells were centrifuged at 4,000 rpm for 5 minutes at 4ºC. For 3D spheroids, after crosslinking solution the matrigel is dissolved and cells are collected in a 5 mL Eppendorf tube and washed twice with PBS + 5 mM EDTA + 1X PIC.

b. Cell lysis, sonication and size selection

The cell pellet was resuspended in 2,5 mL of Lysis Buffer I (Table 3) and incubated on ice for 10 minutes, followed by centrifugation at 4,000 rpm for 5 minutes. The nuclei were then resuspended in Lysis Buffer II (Table 3) and incubated for 10 minutes on ice. Next, sonication was performed to shear the chromatin into DNA fragments ranging from 200 to 500 base pairs, which are optimal for detection and specificity. Sonication was typically carried out with 7 cycles of 30 seconds ON / 30 seconds OFF using the Bioruptor Next Gen (Diagenode).

The size of the sonicated chromatin was checked by taking a 10 µL aliquot, which was then decrosslinked overnight in LB1 buffer containing proteinase K (20 mg/ml) at 65ºC. DNA was purified by phenol/chloroform extraction and resolved in 1,2% GelRed-stained agarose gel. For phenol/chloroform purification an equal volume of equilibrated

phenol:chloroform was added to phase lock gel tubes, mixed by inversion, and centrifuged at 13,000 rpm for 5 minutes.

The aqueous phase was transferred to a fresh tube containing 1.3 µL of Glycoblue, 40 µL of NaCl 5M and 2.5 volumes of 100% ethanol. After mixing by inversion, the DNA was precipitated at -80ºC for 30 minutes, followed by centrifugation at 13,000 rpm at 4ºC for 20 minutes. The pellet was washed with 1 mL of 70% ethanol and centrifuged at 13,000 rpm for 5 minutes at room temperature. The pellet was air dried and resuspended in 20 µL of 10 mM Tris-HCl, pH 8.

c. Immunoprecipitation

For immunoprecipitation, 25 µg of chromatin were diluted in 1x IP buffer (Diagenode) to a final volume of 1.2 mL. An input sample (50 µL) was taken from each sample before the addition of the corresponding antibody (5 µg/IP). Chromatin was incubated with the antibody overnight at 4ºC with constant rotation. The next day, Protein A-agarose beads (Diagenode, 42 µL beads/IP) were washed and blocked with 5% BSA for 15 minutes at 4ºC. IP samples were incubated with beads on a rotating wheel for 3 hours at 4°C. After incubation, the beads were eluted with 400 µL elution buffer for 25 minutes with rotation at room temperature. Crosslinking of samples and inputs was reversed by incubating with 200 mM NaCl at 65°C overnight in a thermoblock.

d. Precipitation and purification

Samples and inputs were treated with RNase A (10 mg/ml) for 1.5 hours at 37ºC, followed by Proteinase K digestion (20 mg/ml) for 2 hours at 45ºC, DNA was then purified using phenol/chloroform extraction method (see above).

12. Assay for Transposase-Accessible Chromatin sequencing (ATAC-seq)

Assay for Transposase-Accessible Chromatin sequencing (ATAC-seq) experiments were performed as described (Buenrostro et al., 2013).

a. Cell culture conditions

T47D cells were cultured in P60 plates (500.000 cells per condition) in red medium. The following day, the medium was replaced with hormone-deprived RPMI and transfection with siCTRL or siYAP1 was performed as described in the RNA interference experiments section. After 48 hours, the medium was changed, and 18 hours later cells were treated or not with progestins (R5020) for 30 minutes.

b. Preparation of nuclei

Cells were trypsinized, centrifuged at 500g for 5 minutes at 4ºC and gently resuspended in RBS buffer + PIC to prevent protein degradation. The suspension was incubated with RBS buffer + containing NP40 for 10 minutes to disrupt the cell membrane and isolate cell nuclei. The resulting nuclear suspension was then resuspended in RBS buffer and counted using a Neubauer chamber.

c. Transposition reaction

For the transposition reaction, 50,000 nuclei were combined with 25 µL 2X TD buffer and 2.5 µL Tn5 transposase (Illumina) in a final volume of 50 µL. The reaction was incubated for 30 minutes at 37ºC. After transposition, the transposed DNA was purified using the Qiagen MiniElute Kit and eluted in 10 µL of 10 mM Tris, pH 8.0.

d. PCR Amplification

To amplify transposed DNA fragments, 10 µL of DNA was mixed in a PCR tube with 2.5 µL 25 µM Custom Nextera PCR Primer 1, 2.5 µL 25 µM Custom Nextera PCR Primer 2 (Barcoded), 25 µL NEBNext High-Fidelity 2X PCR Master Mix to a final volume of 50 µL. Primer 1 or primer 2 were customized for each sample following Illumina's adaptor combination instructions (Primer 1 i7 and Primer 2 i5 for sequencing adaptors). PCR conditions were as follows: 72 °C for 5 minutes, 98 °C for 30 seconds, followed by 5 cycles of 98 °C for 10 seconds, 63 °C for 30 seconds and 72 °C for 1 minute.

Quantitative PCR (qPCR) was used to determine the optimal number of PCR cycles to minimize GC and size bias and to avoid PCR saturation.

For qPCR assays, 5 µL PCR amplified DNA was mixed with 3,88 µL nuclease-free water, 0,5 µL 25 µM Custom Nextera PCR Primer 1, 0,5 µL 25 µM Custom Nextera PCR Primer 2, 0,12 µL 100x SYBR Green I and 10 µL Next High-Fidelity 2X PCR Master Mix (New England Biolabs) PCR was programmed as follows: 1 cycle of 98ºC for 30 seconds; 20 cycles of 98ºC for 10 seconds, 63ºC for 30 seconds, and 72ºC for 1 minute. The required number of cycles (Y) was determined by plotting linear Rn vs. cycle number and calculating the cycle corresponding to ¼ maximum fluorescent intensity.

Once the number of cycles was determined, the same PCR conditions were applied to all samples: 72ºC for 5 minutes, 98ºC for 30 seconds, Y cycles of 98ºC for 10 seconds, 63ºC for 30 seconds, and 72ºC for 1 minute.

e. Size Selection

To ensure proper library size before sequencing, Ampure beads (Agencourt RNAClean XP Beads, S01307) were equilibrated for 30 minutes at room temperature. The DNA sample volume was adjusted to 50 µL by adding 5 µL of 10 mM Tris, pH 8, and incubated with 25 µL of Ampure beads (0,5X) for 10 minutes at room temperature. The tubes were then placed on a magnetic rack, and the supernatant was transferred to a fresh low-binding tube. Next, 75 µL of Ampure beads (1X) was added to the supernatant and incubated for another 10 minutes at room temperature. The samples were placed back on a magnetic rack and washed twice with 200 µL of freshly prepared 80% ethanol. After air-drying the beads, they were resuspended in 20 µL of 10 mM Tris, pH 8, and placed on the magnetic rack. The supernatant containing the DNA was then transferred to a new tube. Finally, the samples were sent to the CRG Genomics Unit for library quantification, quality control, and sequencing on the NextSeq 2000 (Illumina).

13. Co-immunoprecipitation assay

a. Culture conditions

T47D cells (5x 10^6) were cultured in RPMI white medium. After 48 hours, the medium was refreshed, and 18 hours later, cells were treated or not with 10 nM R5020 for 30 minutes. Both treated and untreated plates were washed with PBS and protein-protein cross-linking was performed using 1 mM DTBP for 30 minutes at 37°C. To stop the reaction, the solution was aspirated and the cells were incubated with 15 mL of ice-cold 100 mM Tris-HCl (pH 7.4) for 5 minutes. Cells were then harvested in 2 mL PBS + inhibitors and centrifuged for 5 minutes at 1000 rpm.

b. Lysis, beads-antibody binding and immunoprecipitation

Cells were resuspended in 400 µL of lysis buffer for coimmunoprecipitation (Table 3) and incubated for 30 minutes in a rotation wheel at 4ºC. After incubation, extracts were sonicated in a Bioruptor (Diagenode) for 3 cycles (10 seconds ON / 30 seconds OFF) and then centrifuged for 20 minutes at 13,000 rpm at 4ºC. The supernatant was collected, and protein concentration was quantified using the Bradford method. Immunoprecipitations were performed using 1 mg of total protein and 45 µL of protein G Plus/ protein A agarose beads (Milipore).

Coupling antibody with the beads: Beads were washed with 1 mL of lysis buffer, centrifuged, and resuspended in 1 mL of lysis buffer. The required amount of antibody (3 µg per mg of protein extract) was added, and the antibody-bead mixture was incubated for 4 hours at 4°C on a rotating wheel. After 4 hours, the bead–antibody mixture was centrifuged, the supernatant was discarded, and 1 mg of protein extract was added to the antibody-coupled beads. The samples were then incubated overnight at 4°C with continuous rotation.

c. Washings and elution

After 24 hours, the beads were washed three times with lysis buffer for coimmunoprecipitation (table 3). To elute proteins bound to the beads, 30 µL of 2X loading buffer were added, and then boiled for 5 minutes. Inputs and immunoprecipitated samples (IPs) were then analyzed by Western blot using specific antibodies.

14. Imaging

Imaging experiments were conducted in collaboration with Dr. Adali Pecci and Dr. Florencia Ogara (Molecular Pharmacology Lab), and Dr. Diego Presman (Transcription Factor Dynamics Lab) at the Instituto de Fisiología, Biología Molecular y Neurociencias (IFIBYNE), University of Buenos Aires. The protocol used to obtain the results presented in this thesis is described below.

Culture conditions and transfections

The experiments involving Imaging were performed in collaboration with Dr Adali Pecci and Dr Florencia Ogara (Molecular Pharmacology Lab) and Dr Diego Presman (Transcription Factor dynamics Lab) from the "Instituto de Fisiología, Biologia Molecular y Neurociencias (IFIBYNE), University of Buenos Aires. The protocol used to obtain the results of this thesis is detailed below. Culture conditions and transfections

T47D cells (4×10^5 cells/plate) were grown on 25 mm coverslips in p-35 plates. Fluorescent protein expression was achieved by transient transfection. Halo-tagged proteins were labelled by incubation with the fluorescent dye JF549 for 40 minutes, followed by three washes before imaging. Cells were incubated with 10 nM R5020 for 0.5-2 hours in DMEM without phenol red supplemented with 10% DCC/FBS prior to imaging. T47D-WT cells were transfected with 1 µg Halo-PR and peGFP-YAP or peGFP-FOXA1 and incubated with vehicle or 10 nM R5020 for at least 1 hour.

Plasmids: FUW-tetO-wtYAP was a gift from Stefano Piccolo (Addgene plasmid # 84009). pEGFP-FOXA1 and pHalo-PR were kindly provided by Gordon Hager (NIH, USA).

a. Microscopy

Images were obtained in a LSM980 confocal laser scanning microscope (ZEISS) with Airyscan. Images were acquired in a Zeiss LSM980 confocal microscope using a Plan-Apochromat 63x oil immersion objective (NA = 1.4). EGFP was excited with a solid diode laser of 488 nm. JF549-labeled Halo was excited using a solid diode laser of 543 nm. Fluorescence was registered with photomultipliers (confocal, EGFP 490-659 nm) or the AiryScan 2 detector using 495-550 nm (EGFP) and 574-720 nm (JF549-labeled Halo) filtering. Two-color images were acquired in sequential mode. Airyscan images were registered with pixel size and dwell time of 43 nm and 16 µs, respectively. Microscopy measurements were run at 37ºC and 5% CO2.

b. Foci analysis

Airyscan images were analyzed using ImageJ software (NIH, USA). The images of the cell's nucleus were binarized through a thresholding procedure to quantify the nuclear mean fluorescence intensity (excluding nucleoli) and area. Foci were defined as bright spots with sizes above the optical resolution (~ 200 nm) within the nuclei. These structures were identified from the nuclei binarized image considering an optimal intensity threshold (i.e. nuclear mean intensity/4) selected based on the analysis of a representative set of images from all conditions. Using the ImageJ plugin "Analyze Particles" (Schindelin et al., 2012), the foci number, area and mean intensity were computed. Foci density was calculated as the ratio of the number of foci to the nuclear area. Relative foci intensity was calculated as the intensity of foci normalized to the mean nuclear intensity of the corresponding channel.

c. Spatial correlation analysis

Colocalization analysis was performed with the ImageJ JACoP plugin (Bolte & Cordelieres, 2006) using the Van Steensel procedure. Briefly, the software enables quantitative cross-correlation analysis for dual color images by shifting (pixel by pixel) the image of one-channel relative to the second-channel along the X-axis direction and calculating the Pearson coefficient (PC) at each iteration. The cross-correlation function (CCF) is determined by the dependence of this coefficient value on the pixel shift (Δx). For all experimental conditions, PR and FOXA1 foci binary images were shift ± 20 pixels (0.86 μm) to compute the CCF averaging the PC obtained for X-Y coordinates. The CCF expected for uncorrelated events were determined by rotating one of the images 90 degrees relative to the other.

d. Statistical analysis

Results were expressed as means ± SEM of at least three replicates. Statistical significance was analyzed using Student’s t-test was performed for mean pairwise comparisons. The experimental design was unpaired. Before statistical analysis, data were tested for normality and homogeneity of variances using Shapiro-wilk's test and Levene's test, respectively. If data distribution were not normality using Man Whitney' test (nonparametric test). If variances were not equal, using unpaired t test with Welch's correction. Statistical analyses were performed with GraphPad Prism version 8.4.2 for Windows, GraphPad Software, Boston, Massachusetts USA, www.graphpad.com. Differences were considered as significant at $P < 0.05$.

15. PDX-derived Organoids (PDXO) experiments

PDXO models were generated from metastatic ER+ BC patients from the Vall d´Hebron University Hospital, following the institutional guidelines. Informed written patient consent, approved by the Ethics Committee for Clinical Research and Animal Research of Vall d'Hebron Hospital (PR(AG)130/2015) was obtained for the use of these patient samples.

Patient-derived cells were isolated from PDX tumors through the combination of mechanic disruption and enzymatic disaggregation (Bruna et al., 2016). Briefly, PDX tumors not bigger than 500 mm3 were freshly collected in DMEM (GIBCO) after surgery resection, minced using sterile scalpels and dissociated for 60 minutes in DMEM (GIBCO), 1mg/ml collagenase (Roche), 100 u/ml, hyaluronidase (Sigma-Aldrich), 5% BSA (Sigma-Aldrich), 5 µg/ml Insulin and 50 µg/ml gentamycin (GIBCO). This was followed by further dissociation using trypsin (GIBCO), dispase 5 mg/ml (StemCell technologies) and DNase 1mg/ml (Sigma-Aldrich). Red blood cell lysis was done by washing the cell pellet with 1X Red Blood Cell (RBC) Lysis Buffer containing ammonium chloride (Invitrogen). Then, cells were resuspended in DMEM (Gibco) supplemented with 2% of heat inactivated fetal bovine serum (Gibco), 10 µM ROCK inhibitor (Sigma-Aldrich), 1X B-27 Supplement (Invitrogen), 3 µg/ml EGF (Peprotech), 5 µg/ml Insulin (Roche), 1 µg/ml Hydrocortisone (Sigma) and Gentamycin (Gibco) (Driehuis et al., 2020).

To test drug antiproliferative responses, cells were seeded on top of collagen-enriched matrix Corning® Matrigel® growth factor reduced (GFR) basement membrane matrix at 3x105 cells in 96-well white flat bottom plates. After 24 hours, patient-derived cells started to form patient-derived organoids (PDXO) and were treated with Truli 10 µM or DMSO and cultured at 37 °C in 5% of CO2. Medium and treatments were refreshed every 2-3 days. Representative bright field pictures of each well were taken at day 7 using DS-Fi2-U3 camera with NIS-Elements

software (Nikon) and spheroid size analysis was performed with Image J (http://rsb.info.nih.gov/ij/). Matrigel® was melted in PBS-EDTA 5mM on ice for 30 minutes and plate readings were performed using Cell Titer Glo® Luminescent Cell Viability Assay (Promega). The mean spheroid area of three technical replicates for each condition was calculated and normalized to DMSO-treated controls. Spheroid areas for every treatment and the ± SEM were plotted.

16. Bioinformatic methods

a. RNA-seq processing and analysis

Paired-end RNA-Seq reads were mapped to the human reference genome (GRCh37/hg19) using HISAT2 v2.2.1 (Kim et al., 2015) with default parameters and specifying strand-specific information (--rna-strandness RF). SAMtools v1.11 (H. Li et al., 2009) was used to sort BAM files and filter for properly paired-end reads (-f 2). Aligned reads were mapped to Ensembl GRCh37.87 gene annotation with TEtranscripts v2.1.4 (--sortByPos --mode multi --stranded reverse) (Jin et al., 2015).

DESeq2 v1.26.0 (Love et al., 2014) was used to identify differentially expressed genes between control and YAP1 KD, TEAD1 KD, or TEAD4 KD cells. Moderated log2 fold change values were calculated by applying the shrinkage method, which is useful for ranking and visualization without the need for arbitrary filters on low count genes. The Benjamini-Hochberg (BH) method was used to correct for multiple testing and control the proportion of false positives or FDR. Gene expression changes were considered significantly different if the absolute value of the FC was higher than 2 and the adjusted P-value was lower than 0.05.

b. ChIP-seq processing and analysis

Single-end reads were aligned to the human hg19 reference genome using Bowtie2 (v2.3.5.1)(Langmead & Salzberg, 2012) with default

options. Unmapped reads, duplicates, and low-quality alignments were filtered out using SAMtools (v1.9) (H. Li et al., 2009) with the flag 3844. The resulting BAM files were sorted, and input-subtracted, counts per million (CPM)-normalized signal tracks were generated in bedGraph and bigWig formats using deepTools (Ramírez et al., 2016) (bamCompare --operation subtract --normalizeUsing CPM --scaleFactorsMethod None). Peak calling was performed with MACS2 v2.1.2 (Zhang et al., 2008) using the --broad argument, as this approach identified a greater number of well-defined peaks. Peaks overlapping with ENCODE Blacklist regions (Amemiya et al., 2019) were excluded from further analysis, and only peaks shared across replicates were retained using BEDTools (Quinlan & Hall, 2010).

Transcription factors binding motifs were identified using the findMotifsGenome.pl function from the HOMER software suite (v4.11.1) (Heinz et al., 2010). BEDTools was also employed to calculate the overlap between different groups of peaks and quantify the ChIP-Seq signal of the samples within specific genomic regions of interest.

c. ATAC-seq processing and analysis

Paired-end reads were aligned to the human hg19 reference genome using Bowtie2 (v2.3.5.1) (Langmead & Salzberg, 2012) with the --very-sensitive-local mode. Low-quality reads were filtered out using SAMtools (v1.9) (H. Li et al., 2009). Additionally, reads mapped to the mitochondrial chromosome and those with a MAPQ score below 20 were excluded. The resulting BAM files were sorted and deepTools was used to generate counts per million (CPM)-normalized signal tracks in bedGraph and bigWig formats (bamCoverage --samFlagInclude 64 --normalizeUsing CPM). ATAC-Seq profiles at meta-peaks were constructed and visualized using the computeMatrix and plotProfile functions from the deepTools software suite (Ramírez et al., 2016).

Results

Results

1. *Chapter I:* YAP1 modulates PR response in T47D cells

1.1. Role of YAP1 in hormone-dependent cell proliferation and dedifferentiation

To test whether the nuclear effector of the Hippo pathway, YAP1, is involved in hormone-dependent response, we chose the BC cell line T47D, which showed high expression of PR (Figure R1A, top panel). In this cell line, PR has been reported to modulate several functional pathways implicated in tumor progression as cell differentiation and proliferation (Cittely et al., 2013; Nacht et al., 2019; Zaurin et al., 2021). To assess the potential role of YAP1 we generated two cellular models for the studies: YAP1 depleted (siYAP1) and YAP1-inducible T47D cells (T47D_YAP1ind).

YAP1 KD cells were generated using transient depletion by transfection of specific YAP1 siRNAs (Materials section, Table 8) accompanied by their siControl (siCTRL) counterpart; whereas T47D_YAP1ind cells were established by lentiviral infection to introduce a doxycycline-inducible YAP1 expression system. Transfection with siRNA successfully reduce around 85% of total YAP1 levels in T47D cells without affecting PR expression (Figure R1A). Inducible YAP1 cells showed strong YAP1 expression following 18 hours of DOX treatment (1 µg/mL) detected by western blot (Figure R1B).

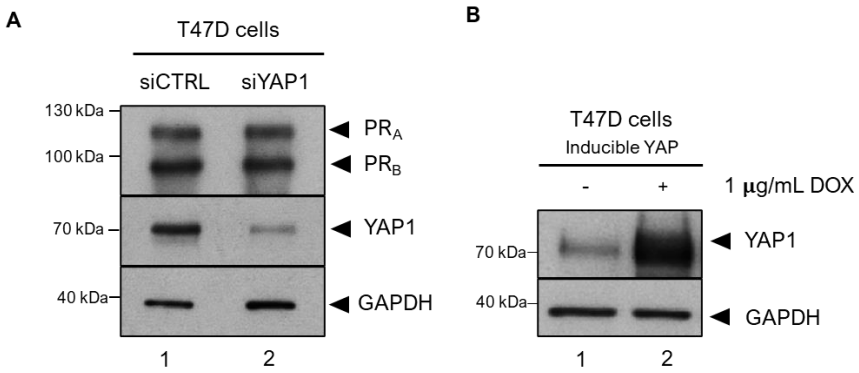

Figure R1. Cellular models used in this study. (A) YAP1 depletion levels achieved after transient transfection with siYAP1, using GAPDH and PR as loading controls. (B) YAP1 induction levels in T47D_YAP1ind cells treated or untreated with DOX for 18 hours, using GAPDH as a loading control.

Cancer stem cells (CSCs) are a subpopulation of cells within a tumor that are believed to contribute to the failure of BC therapy due to their ability to self-renew and differentiate driving tumor growth, metastasis and tumor relapse (Xiaoxian Li et al., 2008 ; Frank et al., 2005). Importantly, even a small population of CSCs can give rise to a tumor when isolated and injected into a suitable mouse model, highlighting their tumorigenic potential. Breast CSCs are characterized by the expression of the cell surface markers CD24 and CD44, both of which are involved in cell adhesion and cell-cell interactions. Notably, in many types of cancer, CSCs exhibit a $CD44^{high}/CD24^{low}$ phenotype (Al-Hajj et al., 2003).

Progestins have been reported to increase the number of murine mammary cells (Asselin-Labat et al., 2010), normal human breast progenitor cells (Graham et al., 2009) and stem-like cells in human breast tumor xenografts (Horwitz et al., 2008). Consequently, we examine whether YAP1 plays a role in modulating the progestin-dependent dedifferentiation capacity of T47D cells by analyzing the percentage of $CD44^{high}/CD24^{low}$ population as previously reported (Citelly et al., 2013).

In siCTRL cells, treatment with the synthetic progestin R5020 for 24 hours resulted in a 7-fold increase in the $CD44^{high}/CD24^{low}$ population, which was further increased by 2-fold in YAP1-depleted cells (Figure R2A). Conversely, in T47D_YAP1ind cells, YAP1 overexpression reduced the progestin-dependent $CD44^{high}/CD24^{low}$ population by 60% compared to the untreated condition (Figure R2B), suggesting that YAP1 may play a negative role in the regulation of PR activity.

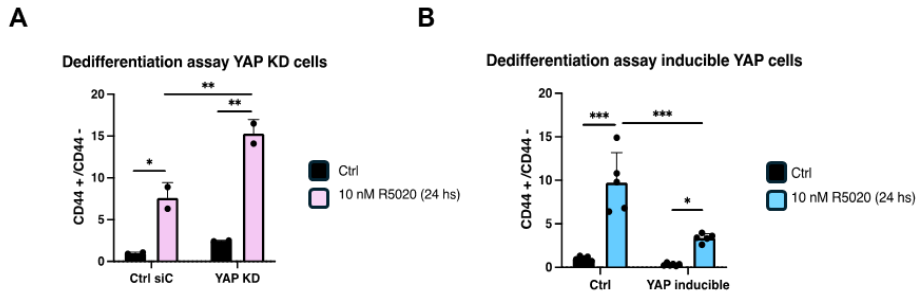

Figure R2. Effect of YAP1 modulation in progestin-dependent cell dedifferentiation in T47D cells. (A) The percentage of $CD44^{high}/CD24^{low}$ cells transfected with siCTRL or siYAP1 treated or not during 24 hours with R5020 is shown. (B) The percentage of $CD44^{high}/CD24^{low}$ T47D_YAP1ind cells induced or not with DOX and treated or untreated with R5020 for 24 hours is presented. CD44 and CD24 levels were measured by flow cytometry as described in Methods section 5. Data are presented as mean ± SD from three different experiments performed in duplicate. * $p<0.05$, ** $p<0.01$ and *** $p<0.001$.

Next, we tested the effect of YAP1 modulation on hormone-dependent cell proliferation measuring the percentage of cells in S phase by flow cytometry (Methods section 4). In the absence of DOX (control conditions), treatment of T47D_YAP1ind cells with R5020 for 18 hours led to a 3-fold increase in cell proliferation. Notably, YAP1 overexpression significantly compromised progestin-dependent cell proliferation (Figure R3).

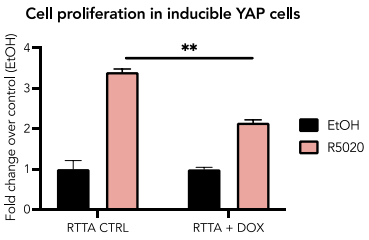

Figure R3. Effect of YAP1 overexpression on progestin-induced S-phase entry. T47D cells were treated with Ethanol or R5020 for 16 hours and subjected to flow cytometric analysis. Data are represented as mean ± SD from three experiments performed in duplicate. * p<0.05, ** p<0.01 and *** p<0.001.

Overall, these assays suggest that YAP1 may act as a modulator of PR function, regulating its activity and preventing uncontrolled PR signaling.

1.2. Impact of YAP1 knockdown on hormone-dependent gene expression

We then decided to investigate whether the effects observed in the functional assays upon YAP1 depletion were reflected in changes in hormone-dependent gene expression. Therefore, T47D cells transfected with either siCTRL or siYAP1 were treated or not with R5020 for 6 hours and subjected to RNA-seq analysis (Methods, Section 9). In siCTRL cells treated with R5020, 1056 genes were upregulated and 480 were downregulated (Figure R4A, upper panels). In contrast, YAP1-depleted cells showed a significant increase in transcriptional changes, with a 61.6% rise in upregulated genes (651 additional genes, Figure R4A, upper panel) and an 82% rise in downregulated genes (394 additional genes, Figure R4B, upper panel) compared to siCTRL cells.

Moreover, genes modulated under both conditions displayed a significant increase in their extent of regulation (Figure R4C). For further analysis, in addition to the newly identified genes that were up-regulated upon YAP1 depletion, we included common regulated genes that showed a 1.8-fold increase in the siYAP1 condition compared to the control. Consequently, we identified a set of 812 up-regulated genes and

438 down-regulated genes, which were combined into a dataset categorized as siYAP1-dependent enhanced genes (1250 genes).

GO term analysis of the 812 enhanced up-regulated genes indicated that YAP1-modulated genes are involved in key processes such as Hypoxia (PKP1, SCD3, AKAP12), Estrogen response early/late (MYC, FOS, CD44, STC2), Epithelial Mesenchymal Transition (PDGFRB, VEGFA, LRRC15, HTRA1) and Apoptosis (BCL2L11, CASP6, FAS). These findings partially support, the functional results described above (Figure R4D, upper panel). The 438 enhanced down-regulated genes showed categories associated to Inflammation response, TNFA signaling and Apoptosis (Figure R1D, lower panel).

Interestingly, in the absence of YAP1, the response to progestins is associated with the activation of both early and late estrogen signaling pathways (Figure R4D). This suggests that YAP1 may regulate the specificity of the hormonal response, ensuring that progestins act as progestins rather than activating estrogen-related pathways more closely associated with cell proliferation.

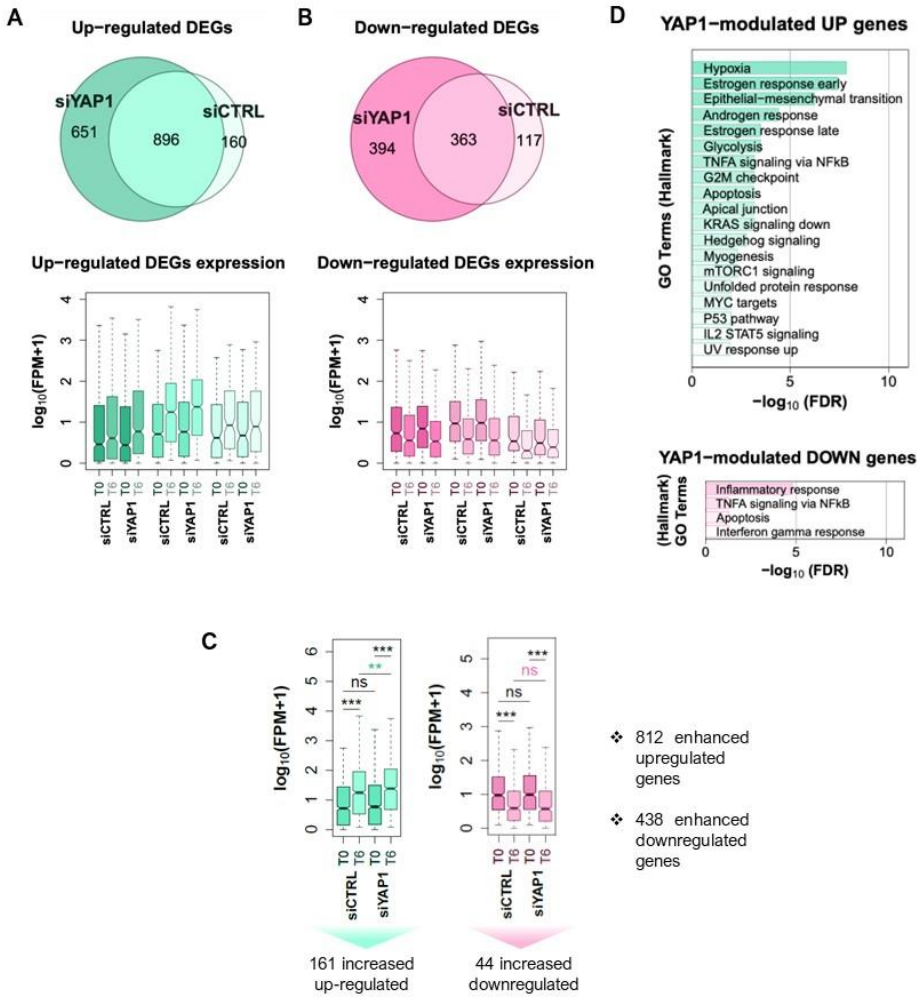

Figure R4. YAP1 modulates progestin-dependent gene regulation in T47D cells (A-B) Venn diagram and boxplot illustrating up (left) and down-regulated genes (right) in control and YAP1 KD condition. (C) Statistical analysis of common up-regulated (left) and down-regulated genes (right). Genes which expression was increased by 1.8 in YAP1 KD condition compared to control were included as differentially regulated. The Wilcoxon signed-rank test was used to statistically support the observed gene expression changes (***) P-value < 0.001; (**) P-value < 0.01. (D) Gene set enrichment analysis showing the MsigDB (Subramanian et al., 2005) Hallmark terms associated with the significantly up- and down-regulated genes identified in Figure R4C.

As an example, we highlight two siYAP1-dependent genes: CD44, a key stem cell marker for assessing the hormone-dependent differentiation capacity of BC cells (Cittelly et al., 2013), and PKP1, which has recently been associated with increased metastatic potential by promoting tumor survival (K. Li et al., 2021) (Figure R5).

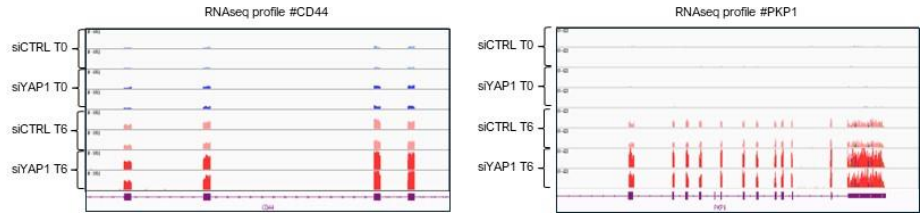

Figure R5. Gene expression analysis of CD44 and PKP1, two genes repressed by YAP1. RNA-seq profile (IGV) of CD44 and PKP1 genes up-regulated in siYAP1 condition in the presence of R5020.

In summary, YAP1-depleted T47D cells showed an enhanced proliferative response to progestins, increased dedifferentiation resulting in a more pronounced stem cell phenotype, and elevated hormone-dependent gene expression, including an unexpected activation of estrogen signaling pathway.

1.3. PR and ERα activation upon YAP1 knockdown

Considering that PR function is enhanced in siYAP1 T47D cells, we decided to investigate whether this translated into changes in the receptor's activation capacity, measured as rapid phosphorylation at S294 dependent on ERK1/2 (Lange et al., 2000). Hormone-dependent PR-S294p levels in extracts from siControl and siYAP cells treated for 0, 5, and 30 minutes were analyzed by western blot using a phospho-PR Serine 294 antibody (Methods, Section 7). The results showed that PR activation at S294 was not affected by YAP1 status (Figure R6) suggesting that enhanced PR activity observed in YAP1 KD condition was not associated with increased phosphorylation at this particular residue.

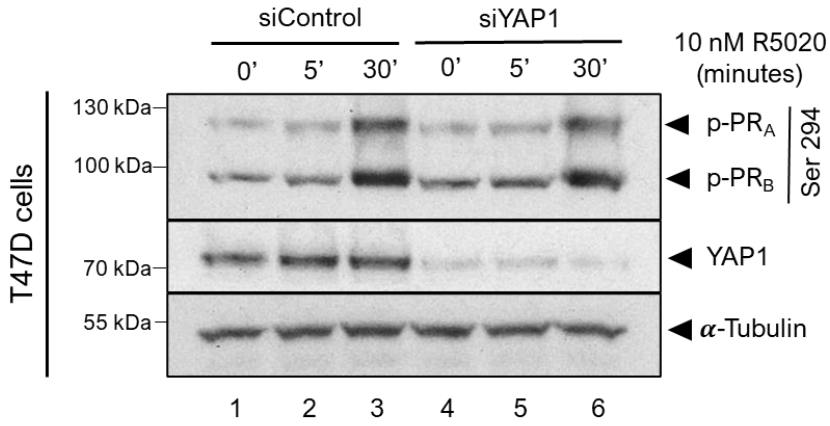

Figure R6. PR activation in YAP1 depleted T47D cells. PR activation was tested in siControl and siYAP1 T47D cells, treated or not with R5020 for 5 and 30 minutes. Western blot analysis was performed to assess the levels of p-PR S294, YAP1, FOXA1, and GAPDH using specific antibodies. Data are representative of two experiments performed in duplicate.

As previously shown, in the absence of YAP1, the gene response to progestins is associated to both early and late estrogen pathways (Figure R4D). Thus, this finding led us to investigate whether ERα activation is influenced by the presence of YAP1. Analysis of ERα-S118 phosphorylation, a marker of active ERα (Cheng et al., 2007), revealed that activation occurred exclusively in response to estrogens and remained comparable between siCTRL and siYAP1 cells (Figure R7, compare lane 5 with lanes 1 and 3). No activation of ERα-S118 phosphorylation is detected in the presence of R5020 independently of the YAP1 abundance (Figure R7, compare lanes 5 and 6 with lanes 7 and 8). These results exclude the activation of ERα under progestin treatment in the absence of YAP1, indicating that PR alone mediates the estrogen-associated profiles observed in gene expression assays.

Furthermore, our findings highlight that YAP1 is important for maintaining PR specificity by activating its distinct gene network. In the

absence of YAP1, PR partially loses its specificity, adopting a more estrogenic response and driving an estrogen-like gene signature.

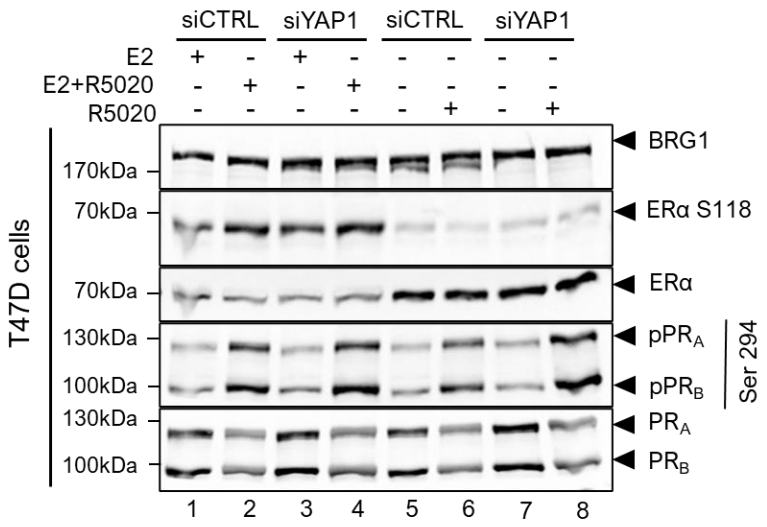

Figure R7. ERα and PR activation in siCTRL and siYAP1 cells. T47D cells transfected with control or YAP1 siRNAs were treated or not with 10 nM R5020 for 30 minutes. Western blotting analysis was performed to assess the levels of S118p-ERα, S294p-PR, ERα, PR, and BRG1 (Control) using specific antibodies. Data are representative of two experiments performed in duplicate.

Next, we asked whether the increased PR activity observed in the absence of YAP1 correlated with enhanced DNA binding upon R5020 stimulation.

1.4. Effect of YAP1 depletion on PR binding and chromatin accessibility

To investigate the role of YAP1 in PR binding to its genomic target regions, we performed ChIP-seq in siCTRL and siYAP1 T47D cells treated or untreated with hormone for 30 minutes (Methods, Section 10). Consistent with the functional and gene expression findings (Figures R2, R3 and R4), our results revealed that siYAP1 cells exhibited 10,800 additional PRbs compared to siCTRL cells. Moreover, the shared PRbs

between both conditions (12,337 regions) displayed stronger PR binding in the absence of YAP1 (Figure R8A, right panel). To fully assess the effect of YAP1, we also focused on 4,608 PRbs that showed a ≥50% increase in PR binding (Figure R8A, right panel). In contrast, only 737 PRbs (3% of the total) were negatively affected by YAP1 knockdown.

DNA motif analysis showed significant enrichment for PR ($p = 10^{-1397}$), FOXA1 ($p = 10^{-370}$), and HSF ($p = 10^{-306}$) motifs in the 10,800 siYAP-dependent PR binding sites (Figure R8B). Interestingly, the TEAD binding motif (5'-GGAATG-3') (Lin et al., 2017) showed low enrichment, ranking 10th in the motif analysis (Figure R8B). Further analysis of the binding motifs in the 4,608 enhanced PRbs revealed that, similar to the siYAP1-dependent sites, the most enriched motif was PR/HRE (p-value: 10^{-642}), followed by FOXA1 (p-value: 10^{-256}), HSF (p-value: 10^{-196}) and AR half site (p-value: 10^{-194}). Notably, the TEAD binding motif was not detected in these regions.

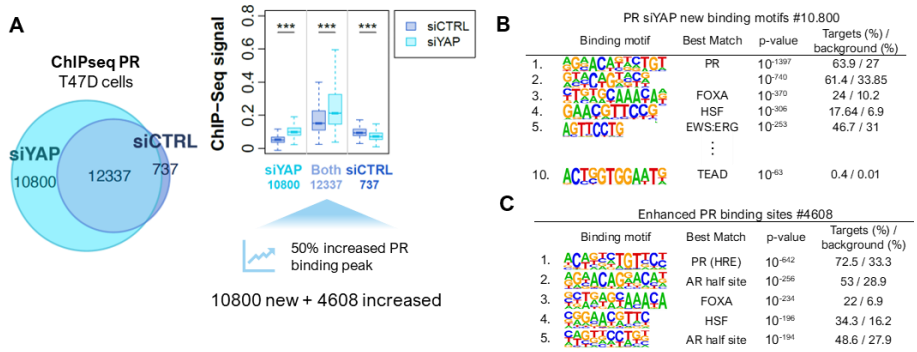

Figure R8. YAP1 modulates progestin-dependent PR binding in T47D cells. (A.) Venn diagram illustrating the overlap of PR ChIP-Seq peaks identified in siCTRL and siYAP1 conditions. Right Panel: Boxplot displaying ChIP-seq signal for the siYAP1-dependent, common, and siCTRL-dependent peaks showed in the left panel. The Wilcoxon signed-rank test was used to statistically assess the PR dynamics in the siCTRL condition compared to siYAP1 condition. (***) P-value < 0.001 (right panel). (B-C) Homer motif analysis associated to the 10800 new and 4608 enhanced PR binding sites identified in siYAP1 condition.

We next examined PR binding at the CD44 and PKP1 genes, which exhibit increased hormone-dependent gene expression upon YAP1 depletion (Figure R5). Consistent with our previous findings, PR binding was significantly increased at these two genes in siYAP1 cells compared to siCTRL (Figure R9).

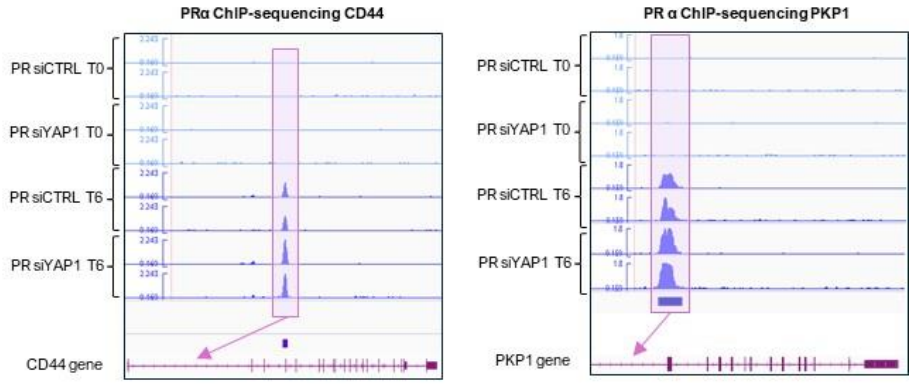

Figure R9. PR binding to CD44 and PKP1 genes. The PR ChIP-seq profile (IGV) of CD44 and PKP1 shows enhanced PR binding in the siYAP1 condition upon R5020 treatment compared to siCTRL.

In conclusion, our PR ChIP-seq results further support that YAP1 negatively regulates PR. Motif analysis suggests that this mechanism is unlikely to involve YAP1 binding to TEAD proteins, as seen in the canonical Hippo pathway (see Introduction). Instead, it points to an alternative cofactor mediating YAP1 recruitment to specific genomic regions.

1.4.1. Role of YAP1 in modulating chromatin accessibility in T47D cells

Given the negative effect of YAP1 on PR binding, we hypothesized that YAP1 may help in maintaining a closed chromatin conformation, thereby controlling PR function. To test this hypothesis, ATAC-seq experiments were performed in control and siYAP1 T47D cells treated or not with R5020 (Methods, section 11).

Overall, our ATAC-seq results revealed a dual role for YAP1 in regulating chromatin accessibility. Under basal conditions, 47,025 accessible regions were identified in siCTRL cells, compared to 43,648 in siYAP1 cells. Among these, YAP1 was required to maintain chromatin accessibility at 12,200 regions (~27% of the total), while it contributed to chromatin compaction at 8,842 regions (~20%) (Figure R10A). Upon hormone stimulation, 54,182 accessible regions were identified in siCTRL cells and 58,050 in siYAP1 cells. YAP1 was required to maintain chromatin accessibility at approximately 23% of these regions, whereas it limited accessibility at 28% of them (Figure R10B).

Next, we focused our analysis on regions where PR binding was enhanced upon YAP1 depletion, specifically the 10,800 new bound regions or the 4,608 regions showing a 50% increase in PR binding (Figure R8A). Both sets of regions exhibited no significant changes in accessibility compared to the control condition (Figure R10C-D).

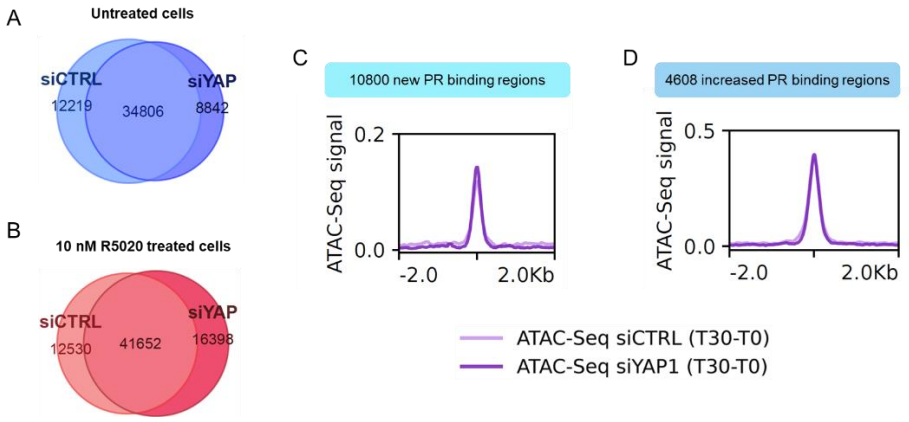

Figure R10. Chromatin accessibility in siCTRL and siYAP1 T47D cells. (A-B) Venn diagram displaying the ATAC-seq signal in siYAP1 compared to siCTRL condition in untreated and after hormone-treated T47D cells. Meta-peak average profiles comparing the ATAC-Seq signal between siCTRL and siYAP1 cells at the 10,800 newly identified (C) and the 4608 enhanced PR peaks (D) (Figure R8A).

In conclusion, our data suggest that the increased PR binding observed after YAP1 knockdown is not directly linked to substantial changes in chromatin accessibility, as shown by ATAC-sequencing under the experimental conditions used.

1.5. Does YAP1 directly mediate the increased PR binding observed following its knockdown?

To address whether the effects observed in siYAP1 are mediated by a direct interaction between YAP1 and PR, we performed YAP1 ChIP-seq experiments in T47D cells treated or not with hormone for 30 minutes (Figure R11A). Our results showed that only 7.5% of the 10,800 new PRbs detected upon siYAP1 overlap with YAP1 at any point (either with or without R5020) (Figure R11B). These findings suggest that YAP1 may influence PR binding in these regions through an indirect mechanism. The potential direct mechanism underlying this effect will be further investigated in the following chapter.

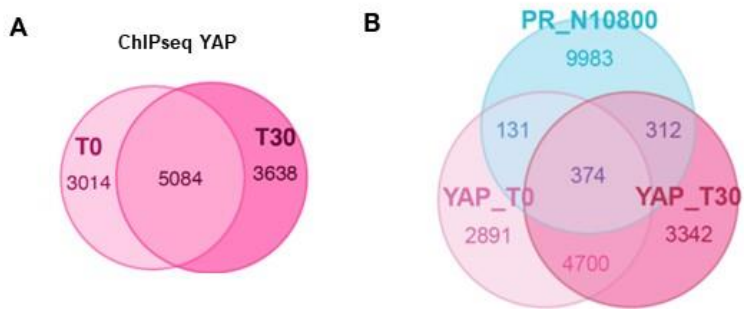

Figure R11. Overlapping between YAP1 and the 10,800 newly identified PRbs. (A) YAP1 ChIP-seq performed in T47D cells treated or not with R5020. (B) Overlapping between YAP1 and the 10,800 new PR binding regions detected upon siYAP1.

In fact, although the relevance of these 10,800 regions gaining PR binding upon YAP1 depletion cannot be ruled out, these sites exhibit much weaker PR binding than the shared regions (Figure R8A, right panel).

2. *Chapter II:* Direct interaction between YAP1 and PR in BC cells

Next, we aimed to investigate whether YAP1 could directly influence PR function. To tackle this, we first compared YAP1 and PR ChIP-seq data, enabling us to identify potential overlapping regions.

2.1. Defining YAP1-PR regions

In the absence of hormone, YAP1 was bound to 8098 genomic regions, 37% of which (3,014 regions) were lost upon R5020 treatment. Therefore, hormone treatment induces a redistribution of YAP1 across the genome (Figure R12A).

Motif analysis of YAP1 binding sites in the absence of hormone identified TEAD4 as the most represented motif (p-value: 10^{-2157}), followed by the DNA binding motif corresponding to the pioneer factor FOXA1 (p-value: 10^{-590}) and TFCP2 (p-value: 10^{-216}) (Figure R12C, upper panel). Upon hormonal treatment, YAP1 redistributed to 3,638 new binding sites, where TEAD4 remained the predominant motif (p-value: 10^{-1952}), followed by a half-site of the androgen receptor (AR)/PR/HRE motif (p-value: 10^{-525}) and FOXA1 (p-value: 10^{-341}) (Figure R12C, lower panel).

In the presence of progestins, PR is bound to 32,464 genomic regions while no PR binding was detected without hormone treatment (Figure R12B). Motif analysis of PR binding sites identified the hormone response element (HRE) as the top motif (p-value: 10^{-4725}), ZBTB32(p-value: 10^{-1814}), TEAD (p-value: 10^{-1234}), SOX4 (p-value: 10^{-1173}), and FOXP3 (p-value: 10^{-1068}) (Figure R12D) confirming previous results from our laboratory (Ballaré et al., 2013 ; Zaurin et al., 2021).

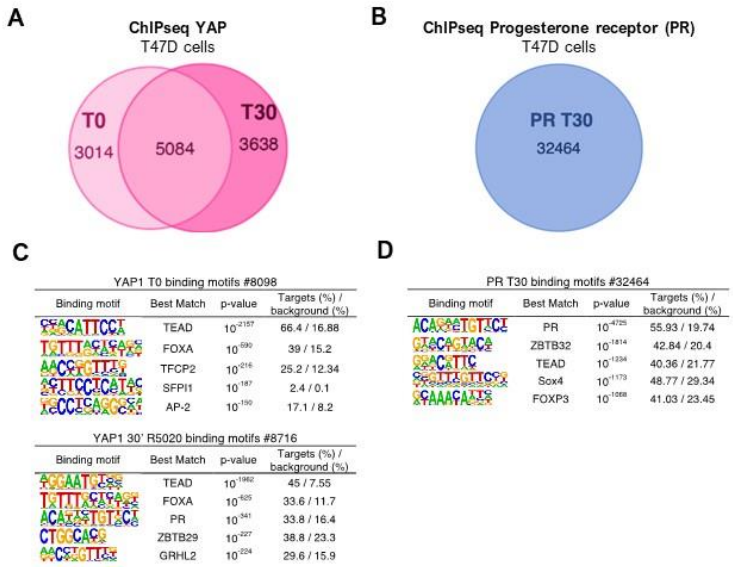

Figure R12. Dynamics of PR and YAP1 binding in T47D cells upon progestin treatment. (A) Venn diagram showing the overlap of YAP1 ChIP-Seq in untreated (T0) cells and treated with R5020 for 30 minutes (T30). (B) Venn diagram showing PR ChIP-seq peaks identified in cells treated with R5020 for 30 minutes (T30); no PR peaks were detected in untreated cells. (C) Homer motif analysis of YAP1 binding sites in the absence (top panel) and presence (bottom panel) of R5020. (D) Homer motif analysis of PR binding sites in cells treated with R5020.

A combined analysis of YAP1 and PR ChIP-seq data from T47D cells, either treated or not with hormone, enabled us to identify two groups of genomic regions where YAP1 and PR overlap genome wide. The first group, termed “YAP-bound,” consists of 2,973 regions where PR is recruited in the presence of hormone, with YAP1 already bound before induction (Figure R13A). We also identified a second group, referred to “Co-recruited,” comprising 3,111 regions where both PR and YAP1 are recruited in response to hormone (Figure R13B).

Interestingly, both the YAP-bound and Co-recruited groups are located in regions where PR binding is enhanced following YAP1 depletion (Figure R13C). These regions are also significantly enriched for

H3K27ac, a hallmark of active enhancers, when compared to an equivalent number of random genomic regions (Figure R13D). Moreover, an integrated analysis of RNA-seq and ChIP-seq data revealed that YAP-bound and Co-recruited regions are closer to genes whose expression increases upon YAP1 knockdown compared to genes that remain unaffected (Figure R13E). This finding reinforces the role of these regions in driving the gene expression changes described above (Figure R4). Motif analysis showed strong similarities between YAP-bound and Co-recruited regions, with PR, TEAD, and FOXA1 emerging as the most enriched motifs (Figure R14A-B). In YAP-bound motifs, TEAD was the most represented (p-value: 10^{-292}), followed by FOXA (p-value: 10^{-188}) and PR/HRE (p-value: 10^{-109}). In contrast, in the Co-recruited regions PR (p-value: 10^{-517}) was the most represented, followed by TEAD (p-value: 10^{-242}) and FOXA (p-value: 10^{-176}).

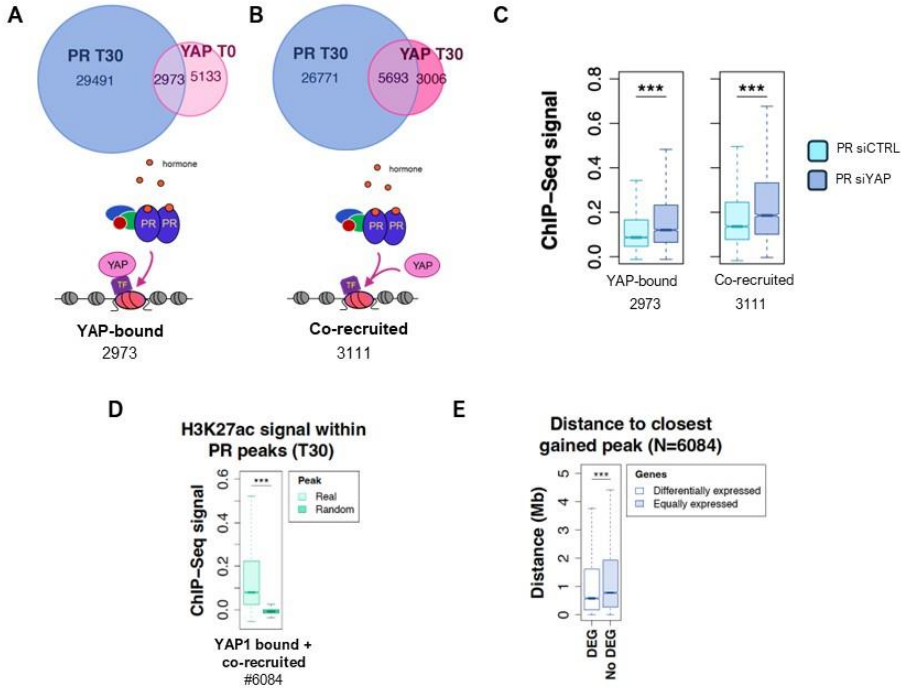

Figure R13. YAP1 influences PR binding to transcriptionally active enhancers upon hormone stimulation. (A) Venn diagram showing the overlap between PR ChIP-Seq peaks (10 nM R5020 for 30 minutes) and YAP1 binding sites prior to hormone induction. (B) Venn diagram showing the overlap between PR ChIP-seq peaks and YAP1 binding sites after R5020 treatment. (C) Boxplot displaying PR ChIP-seq signal of siCTRL and siYAP1 cells at YAP-bound and Co-recruited peaks identified in panels A-B. Statistical significance was assessed using the Wilcoxon signed-rank test (*** P-value < 0.001). (D) Boxplot showing H3K27ac ChIP-seq signal at YAP-bound and Co-recruited peaks (panels A-B) compared to random genomic regions. Statistical significance was determined using the Mann-Whitney U test (*** P-value < 0.001). (E) Boxplot showing the genomic distance (in megabases, Mb) to the closest PR-gained peak for differentially expressed genes (DEGs, N=1,250, Figure R4A-C) compared to non-differentially expressed genes (No DEGs; N = 1,255). PR-gained peaks were defined as PR peaks showing ≥50% increased signal in siYAP1 cells compared to siCTRL (N = 4,608). Statistical differences were evaluated using the Mann–Whitney U test (*** P < 0.001).

Since motif analysis only predicts potential binding sites of transcription factors, we performed ChIP-seq for TEAD4 and FOXA1 to verify their presence at YAP-bound and Co-recruited regions, under both progestin-treated and untreated conditions. FOXA1 was found to be significantly more enriched at YAP-bound and Co-recruited sites compared to TEAD (Figure R14C). Notably, FOXA1 occupied 87.2% of YAP-bound and 53.7% of Co-recruited regions, highlighting a strong association between YAP1 and FOXA1 (Figure R14D).

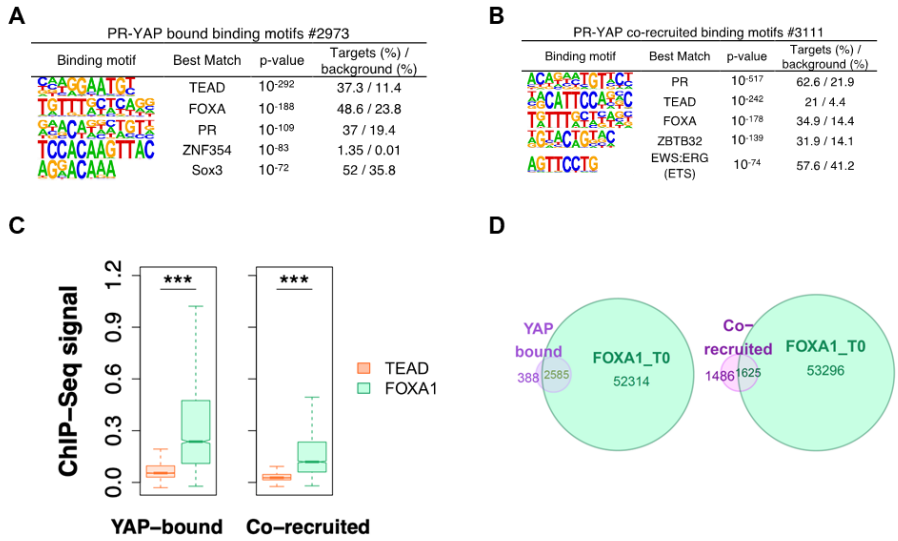

Figure R14. YAP-bound and Co-recruited regions are enriched in FOXA1. (A-B) Homer motif analysis of YAP-bound and Co-recruited regions. (C) Boxplot showing TEAD4 and FOXA1 ChIP-seq signals at YAP-bound and Co-recruited regions. The data represent the average TEAD4 and FOXA1 ChIP-Seq quantification obtained from cells unexposed (T0) and exposed to R5020 for 30 minutes (T30). Statistical significance was assessed using the Mann-Whitney U test (**** P-value < 0.001). (D) Venn diagram illustrating the overlap between FOXA1 ChIP-seq peaks from untreated cells (T0) and YAP-bound and Co-recruited regions identified in Figure R13A-B.

To illustrate the dynamic interaction between YAP1 and FOXA1, we show the genes CD44 and PKP1, both of which exhibit increased activity and enhanced PR binding in the absence of YAP1 (Figures R4 and R8). CD44, located at chromosome 11p13, contains a Co-recruited regulatory region, while PKP1 on chromosome 1q32.1 harbors a YAP-bound region (Figure R15). For these genes, we visualized the intensity of YAP1 and FOXA1 peaks using Integrative Genomics Viewer (IGV). Notably, in the PKP1 gene, both YAP1 and FOXA1 were present even in the absence of R5020 (Figure R15, right panel). In contrast, YAP1 was recruited to the CD44 gene along with FOXA1 upon hormone treatment, suggesting that both proteins may be co-recruited (Figure R15, left panel).

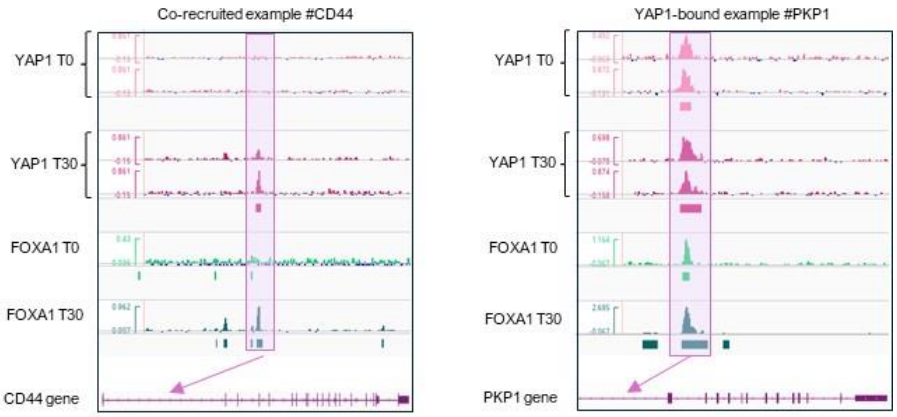

Figure R15. YAP1 and FOXA1 binding to CD44 and PKP1 genes. ChIP-seq profiles of YAP1 and FOXA1 at the CD44 and PKP1 genes (visualized in IGV), obtained from T47D cells treated or not with R5020 for 30 minutes (left and right panels, respectively).

2.2. Exploring the underlying mechanism: chromatin accessibility

Given the negative impact of YAP1 on PR function and its association with FOXA1, we hypothesize that YAP1 may compromise or destabilize FOXA1's pioneer activity, thereby affecting PR binding. If this hypothesis is correct, YAP1 depletion should enhance FOXA1's pioneer activity, thereby increasing chromatin accessibility at its target regions. To test this, we performed ATAC-seq in siCTRL and siYAP1 cells treated or not with R5020, focusing on YAP1-bound and Co-recruited regions.

For the analysis, we selected the top 25% PRbs that exhibited the most significant increase in PR binding upon YAP1 depletion within YAP-bound and Co-recruited regions (Figure R16A). In both cases, the increase in PR binding did not correlate with increased chromatin exposure. In fact, a slight trend toward decreased accessibility in the absence of YAP1 was observed (Figure R16B-C).

Notably, before hormone treatment, the ATAC-seq signal was higher in YAP-bound compared to Co-recruited (see Figure R16, comparing Panel B with Panel C, left). This difference may arise because Co-recruited regions are likely more dependent on PR binding to HREs, followed by chromatin remodeling to activate these sites. In contrast, YAP-bound regions depend more on FOXA1, as demonstrated in Figure R14D.

Overall, no major differences in chromatin accessibility were observed between siCTRL and siYAP1 conditions. Therefore, the mechanism by which YAP1 prevents PR binding to these regions does not involve chromatin compaction (Figure R16B-C).

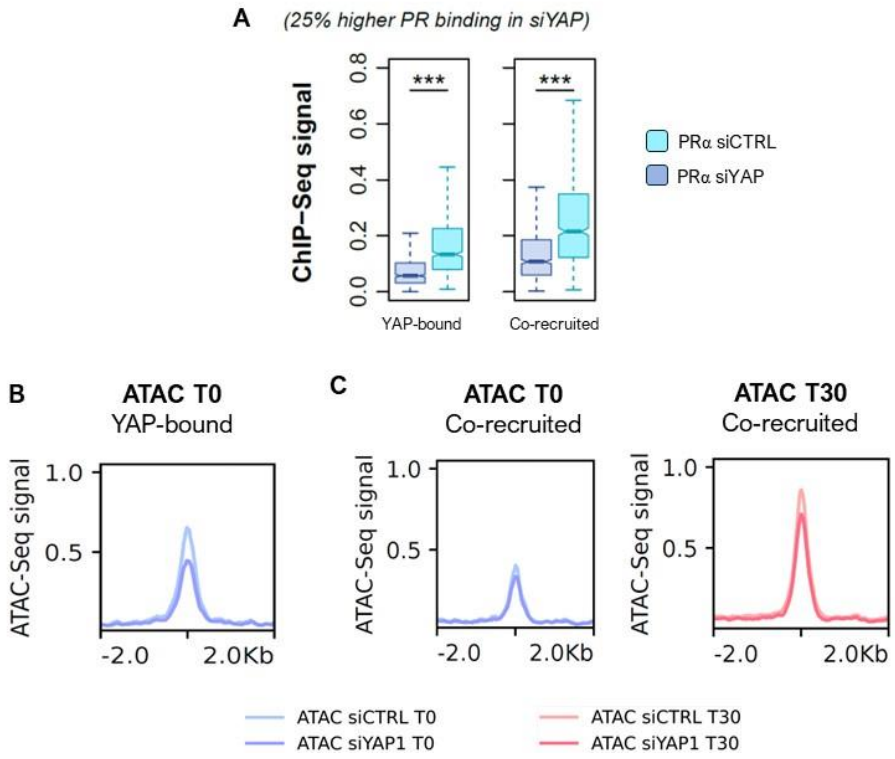

Figure R16. Chromatin accessibility at YAP-bound and Co-recruited regions. (A) Box plots showing the top 25% PRbs in siYAP1 for YAP-bound and Co-recruited sites. The Wilcoxon signed-rank test was used to assess PR enrichment or depletion in siCTRL compared to siYAP1 condition. (***) P-value < 0.001 (right panel). (B) ATAC-seq signal in YAP-bound regions in siCTRL and siYAP1 untreated cells. (C) ATAC-seq signal in Co-recruited regions comparing siCTRL and siYAP1 cells treated with or without R5020 (T30 and T0, respectively).

In conclusion, we have described a negative role for YAP1 on PR function and identified 2973 genomic regions where YAP1 is bound to chromatin prior to hormone treatment and 3,111 regions where both proteins are co-recruited with progestins. These ~6,000 regions are enriched in H3K27ac, a mark of active enhancers, and are closer to YAP1-dependent genes.

In addition, our results suggest that FOXA1 anchors YAP1 to chromatin, compromising PR binding (Figure R14C). We therefore aimed to investigate whether YAP1 and FOXA1 present a broader functional interaction.

2.3. Exploring the functional interaction of YAP1 with the pioneer factor FOXA1

To assess whether the interaction between YAP1 and FOXA1 extends beyond YAP-bound and Co-recruited regions, we analyzed ChIP-seq data for YAP1 and FOXA1 across the entire genome.

Globally, under basal conditions, YAP1 co-localized with FOXA1 in 5,659 regions, representing 70% of the total YAP1 sites identified (Figure R17A, left panel). In the presence of R5020, there was an overlap in 7,762 regions, accounting for 87% of total YAP regions found with R5020 (Figure R17A, right panel). Thus, at a genomic level, there is a significant co-localization between YAP1 and FOXA1 in BC cells.

To further investigate the potential interaction between FOXA1 and YAP1, we conducted co-IP experiments in T47D cells treated or untreated with R5020 (Figure R17B). Using an antibody that efficiently immunoprecipitated YAP1 (Figure R17B, left panel), we detected co-precipitated FOXA1 independent of R5020 treatment (Figure R17B, left panel, compare lanes 3 and 4 with lane 5), supporting the genomic data (Figure R14A). Importantly, no interaction between YAP1 and PR was detected (Figure R17B, right panel). Therefore, YAP1 forms a complex with FOXA1 and plays a role in the PR dynamics, as observed in the YAP-bound and Co-recruited regions.

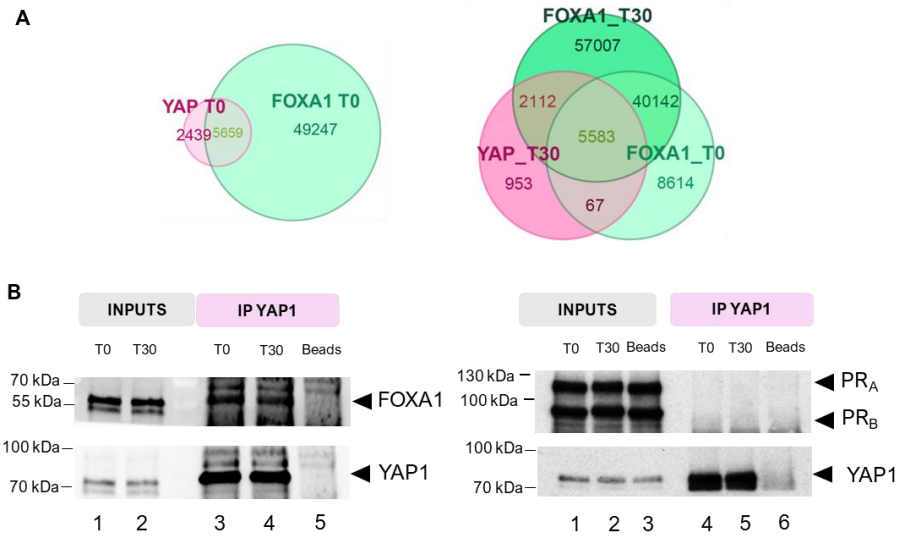

Figure R17. Interaction between YAP1 and FOXA1 in T47D cells. (A) Venn diagram showing the overlap of YAP1 and FOXA1 ChIP-seq peaks in untreated cells (T0) (left panel) and the overlap of FOXA1 peaks in untreated (T0) and R5020-treated cells (T30) with YAP1 peaks at T30 (right panel). (B) T47D cells, either exposed or not to R5020, were lysed and immunoprecipitated with YAP1-specific antibody or beads alone. The IPs were analyzed by Western blotting using specific antibodies for FOXA1, PR and YAP1.

As outlined in the introduction, YAP1 lacks direct DNA-binding ability and relies on other proteins for its recruitment to specific genomic regions where it exerts its nuclear function. In the canonical Hippo pathway, this recruitment is typically mediated by TEAD proteins (Fu et al., 2022). However, our analysis revealed that i) YAP-bound and Co-recruited regions exhibited greater enrichment for FOXA1 than for TEAD (Figure R14C), and ii) we observed evidence supporting a YAP1-FOXA1 physical interaction (Figure R17B). Based on these findings, we hypothesize that FOXA1 may anchor YAP1 to genomic regions via a non-canonical pathway.

To test this hypothesis, we performed YAP1 ChIP-seq in T47D cells transfected with siFOXA1, either treated or untreated with R5020 (Figure R18). We found that the presence of YAP1 was significantly reduced in regions where it overlaps with FOXA1 compared to regions where they do not colocalize (Figure R18B). These findings suggest that, in addition to the canonical TEAD-mediated mechanism, FOXA1 may serve as an anchor for YAP1 binding to target chromatin.

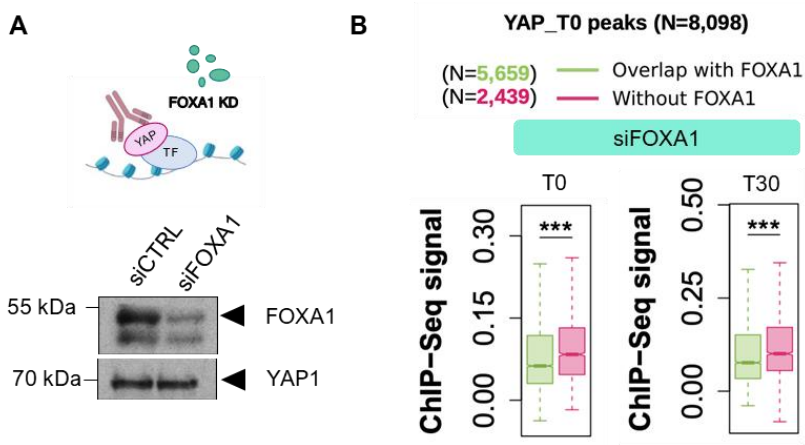

Figure R18. FOXA1 anchors YAP1 to chromatin in T47D cells. (A) FOXA1 depletion levels were assessed by western blot using YAP1 as a loading control. (B) Boxplots displaying YAP1 ChIP-seq signal in YAP1 peaks overlapping or not with FOXA1 peaks in siFOXA1 cells, unexposed (T0) or exposed to R5020 for 30 minutes (T30). Statistical significance was assessed using the Mann-Whitney U test (***) P-value < 0.001 (panel B).

3. *Chapter III:* YAP1 modulates PR through a non-canonical pathway, TEAD-independent mechanism

As mentioned, in the canonical Hippo pathway YAP1 bind to TEAD proteins to regulate gene expression (see Introduction). To determine whether TEAD depletion replicates the effect of siYAP1 on progestin-dependent gene expression, we performed RNA-seq in siTEAD1 and siTEAD4 T47D cells before and after progestin treatment.

The results indicated that depletion of TEAD1 or TEAD4 did not recapitulate the gene expression profile observed after YAP1 knockdown. In particular, TEAD1 appears to be a key factor in the progesterone response, as 85% of hormone-induced and 77% of hormone-repressed genes lost regulation upon TEAD1 depletion (Figure R19A-B).

In fact, these findings suggest that TEAD1 plays a different role from that of YAP1, acting as a positive regulator of PR. Furthermore, analysis of the subset of genes regulated under both conditions (indicated by intermediate color) showed that their regulation was impaired upon TEAD1 depletion, in contrast to the effects observed with YAP1 depletion (compare Figures R4A-B and R19A-B).

Although only 99 genes (9.3% of the total) gained regulation upon TEAD1 KD, we examined the enriched pathways under these conditions to compare them with those affected by siYAP1. GO analysis revealed a significant upregulation of epithelial-mesenchymal transition (e.g. LOX and CALD1) and estrogen response pathways (e.g. CXCL12 and AFF1). Notably, these pathways resemble those activated by siYAP1 (Figure R4F).

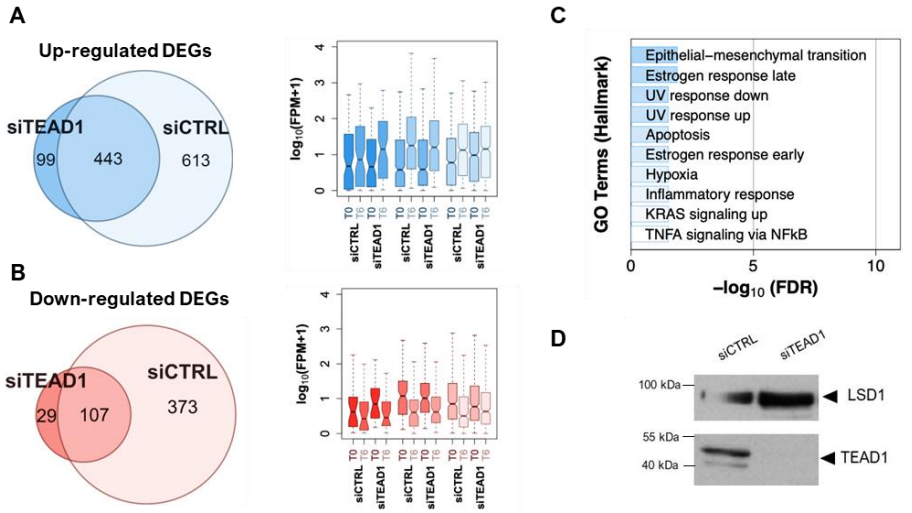

Figure R19. Impact of TEAD1 on progestin-dependent gene regulation in T47D cells. (A-B) Venn diagram showing up- and down-regulated genes comparing siCTRL versus siTEAD1 conditions. (C) Gene set enrichment analysis using the MsigDB Hallmark terms, highlighting pathways associated with significantly up-regulated genes identified in Panel A. No GO terms were associated with significantly downregulated genes. (D) TEAD1 depletion levels, with LSD1 used as loading control. *Genes were considered significantly deregulated if the |FC| > 2 and the adjusted p-value < 0.05 (upper panel).

Next, we investigated the potential role of TEAD4 in progestin-dependent gene regulation. TEAD4 seems to have a dual role in regulating progestin-dependent genes. Approximately 32% of hormone-regulated genes lost regulation upon siTEAD4, while 37% gained regulation. Consistent with siTEAD1 results, genes that were already regulated under control conditions (indicated by intermediate color) showed reduced regulation upon TEAD4 depletion, exhibiting an opposite effect to that seen with YAP1 depletion (Figure R20A-B). Among the down-regulated genes, 60% required TEAD4, while 38% were repressed only upon TEAD4 depletion (Figure R20B).

To further explore the pathways affected by siTEAD4, we conducted pathway enrichment analysis. As shown in the hallmark study, hormonal

signaling pathways, such as estrogen and androgen response, UV response and Hypoxia turned out to be enriched upon TEAD4 depletion.

Notably, several up-regulated genes in these pathways are associated with key cellular functions, for example BIRC3 in inhibiting apoptosis (Frazzi, 2021), IGFBP1 in regulating cell migration and metabolism (Cai et al., 2023), and SAT1 in polyamine acetylation(Ou et al., 2016) (Figure R20C).

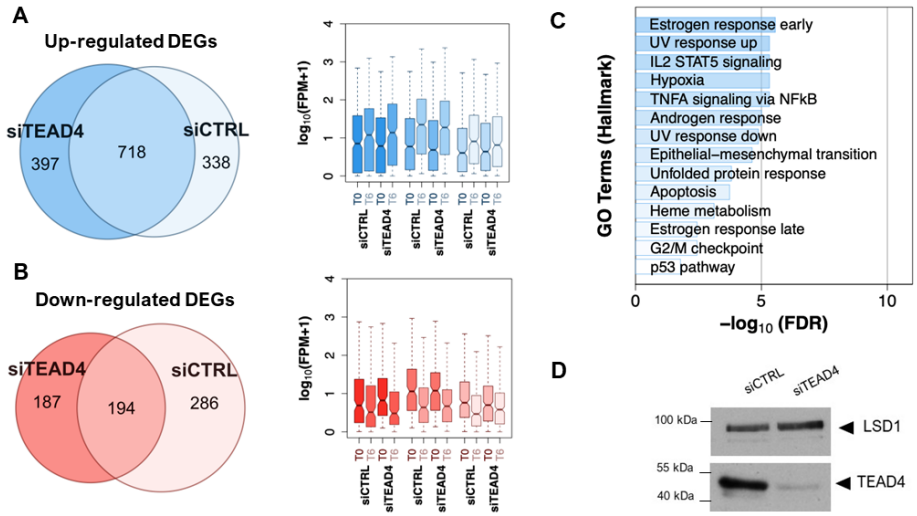

Figure R20. Impact of TEAD4 depletion on progestin-dependent gene regulation in T47D cells. (A-B) Venn diagram depicting up- and down-regulated genes in siCTRL and siTEAD4 conditions. (C) Gene set enrichment analysis showing the MsigDB Hallmark terms associated with the significantly up-regulated genes from Figure 20A. No associated GO terms were found for the significantly down-regulated genes (lower panel). (D) TEAD4 depletion levels, with LSD1 used as a loading control. *Genes were considered significantly deregulated if |FC| > 2 and the adjusted p-value < 0.05 (upper panel).

Although the number of genes that gained regulation upon siTEAD1 and siTEAD4 were smaller compared to the siYAP1 condition, some gene ontology (GO) terms were conserved. The shared GO terms were associated to epithelial-mesenchymal transition, apoptosis, and early

and late estrogen response. Considering these similarities, we performed an intersection analysis of genes that gained regulation (either up- or down-regulated) following YAP1, TEAD1, or TEAD4 depletion (Figure R21A), as well as genes that depend on these factors for progestin-dependent regulation (Figure R21B).

Our results suggest that, although limited in number, genes requiring YAP1 for the progestin response were also affected by the depletion of TEAD1 and TEAD4. This suggests that these genes may be regulated via the canonical nuclear Hippo pathway (Figure R21A). In contrast, genes where YAP1 acts as a repressor and modulates progestin-responsive genes exhibited much less overlap, with only 24% being commonly affected by all three knockdowns. This indicates that the majority of these genes are likely regulated through a non-canonical pathway."(Figure R21A).

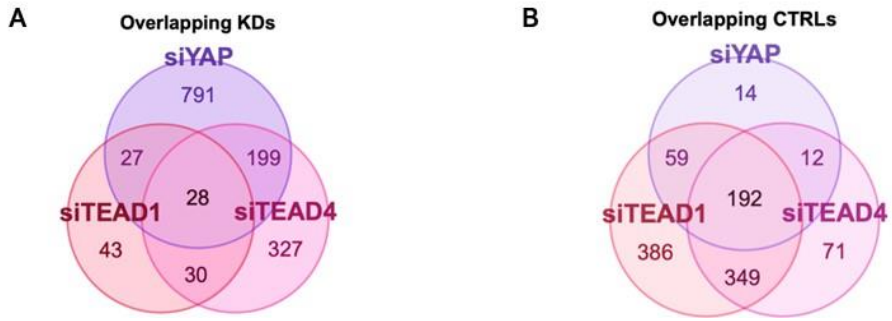

Figure R21. Gene overlap between YAP1, TEAD1 and TEAD4-dependent and repressed genes. (A) Venn diagram showing genes that gained regulation upon YAP1, TEAD1 or TEAD4 knockdown. (B) Overlap of genes for which YAP1, TEAD1 or TEAD4 depletion was required for progestin-dependent gene regulation.

Thus, depletion of TEAD1 and TEAD4 had a significant impact on progestin-dependent gene expression, though the effects differed from those observed with siYAP1. TEAD1 was identified as a key positive regulator of PR function, while TEAD4 displayed a dual regulatory role.

4. Chapter IV: Investigating the impact of YAP1 modulation on 3D cultured models and transcriptional nuclear condensates in living BC cells

To validate our findings under conditions that better mimic BC cells in their physiological context, we studied the effect of YAP1 modulation on cells grown in three dimensions (3D) and during the formation of transcriptional nuclear condensates in living cells.

4.1. 3D environment reduces nuclear YAP1 and increases PR binding

The results presented so far, which suggested a negative role for YAP1 on PR function, were primarily derived from knockdown experiments. Next, we aimed to investigate whether our findings were also applicable in systems where nuclear YAP1 levels can be physiologically tuned.

Our group recently found that in 3D-cultured cells, YAP1 is predominantly cytoplasmic and exhibit increased S127 phosphorylation, compared to cells grown in 2D monolayers (Ramirez-Cuellar et al., 2024; Zanconato et al., 2019). In contrast, under 2D conditions YAP1 primarily localizes in the nucleus. Thus, 3D culture provides a physiologically relevant model to downregulate nuclear YAP1 levels.

With the aim of assessing whether the PR dynamics observed in siYAP1 cells can be replicated in systems where the reduction of nuclear YAP1 is triggered by mechanical stimuli and changes in the cellular environment, we next investigated PR binding in T47D cells cultured under 2D and 3D conditions (Figure R22). Consistent with observations in siYAP1 cells, PR binding was significantly increased at 10,787 regions in 3D-grown cells compared to 2D cells (Figure R22A). This trend was also observed at PRbs shared between 2D and 3D cultures (Figure R22B). We then focused on PR binding at previously identified YAP-bound and Co-recruited regions (Figure R22C-D). Our results showed enhanced PR occupancy in 3D-grown cells compared to monolayer

cultures, further supporting the notion that YAP1 may influence PR binding at these sites.

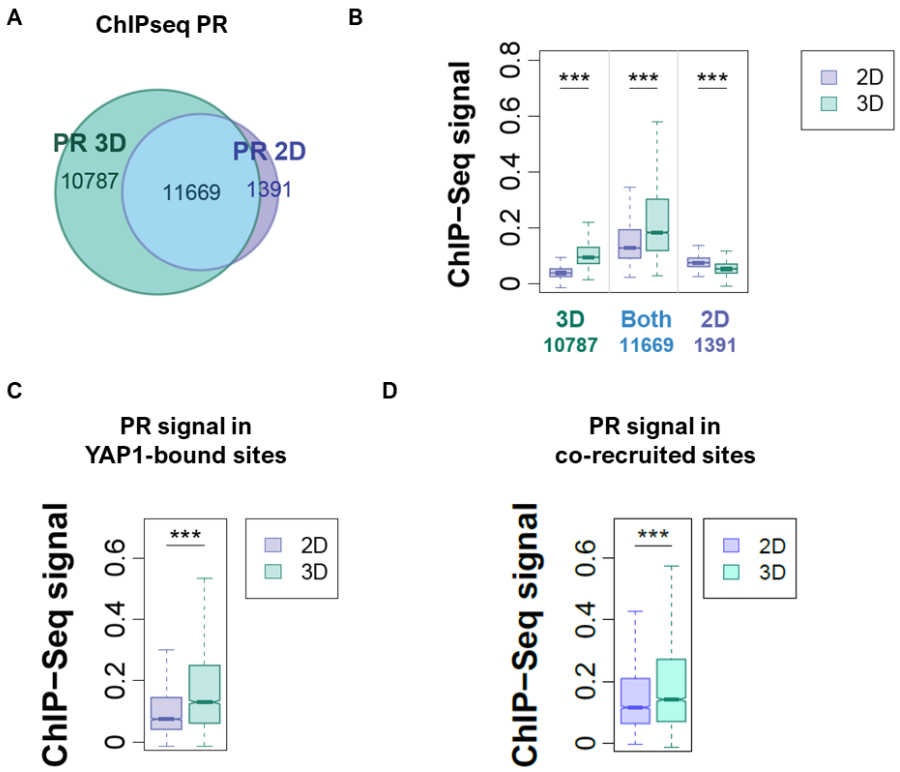

Figure R22. PR binding in 2D and 3D-grown T47D cells. (A) Comparison of progestin-dependent PR binding in cells grown as monolayer (2D) or spheroids (3D) through ChIP-seq analysis. (B) Box plot showing the intensity of samples presented in panel A. (C-D) Boxplot displaying the PR ChIP-seq signal in 2D and 3D cultures for the YAP1-bound and Co-recruited regions identified in Figure R13A-B. Statistical differences in PR signal between 2D and 3D cultured cells were evaluated using the Mann-Whitney U test. (**) P-value < 0.001.

Since FOXA1 was enriched in ~87% of YAP-bound sites and ~53% of Co-recruited regions (Figure R15D), we hypothesized that YAP1 may also influence FOXA1 binding. To test this, we compared FOXA1 distribution in 2D and 3D cultures to determine if the reduced nuclear YAP1 presented in 3D conditions affected FOXA1 binding.

Notably, 3D culture conditions led to a redistribution of FOXA1, causing displacement from sites exclusively bound in 2D cultures, while also promoting binding to 83,595 new regions associated with the 3D environment (Figure R23A). Analysis of FOXA1 occupancy at YAP1-bound and Co-recruited regions (Figure R23C-D) revealed increased FOXA1 binding in 3D cultures compared to 2D, although this increase was less pronounced than the one observed for PR (Figure R22C-D).

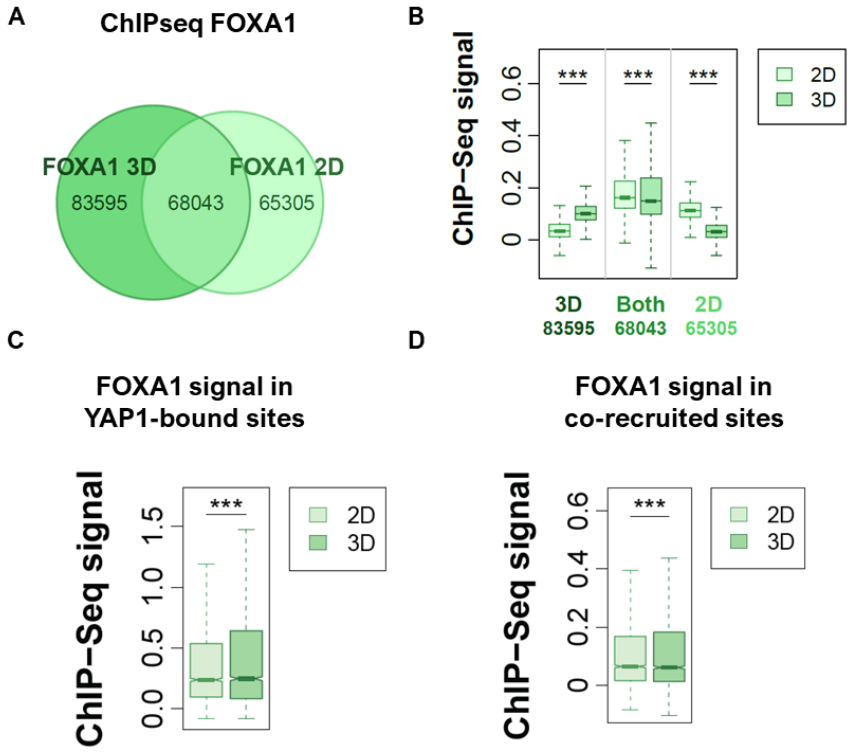

Figure R23. FOXA1 binding in 2D and 3D-grown T47D cells. (A) Comparison of FOXA1 binding in cells cultured as 3D spheroids or monolayers using ChIP-seq analysis. (B) Boxplot comparing FOXA1 binding between the samples presented in panel A. (C-D) Boxplot displaying FOXA1 ChIP-seq signal in 2D and 3D cultured cells, for YAP-bound and Co-recruited regions identified in Figure R13A-B. Statistical differences in FOXA1 ChIP-seq signal between 2D and 3D conditions were evaluated using the Mann-Whitney U test. (***) P-value < 0.001.

Finally, we assessed PR and FOXA1 occupancy at the 10800 novel PR binding regions that gained PR binding upon YAP1 depletion (Figure R8A), under both 2D and 3D culture conditions. Both PR and FOXA1 showed increased binding in 3D condition compared to 2D, with a more pronounced effect towards PR (Figure R24A-B).

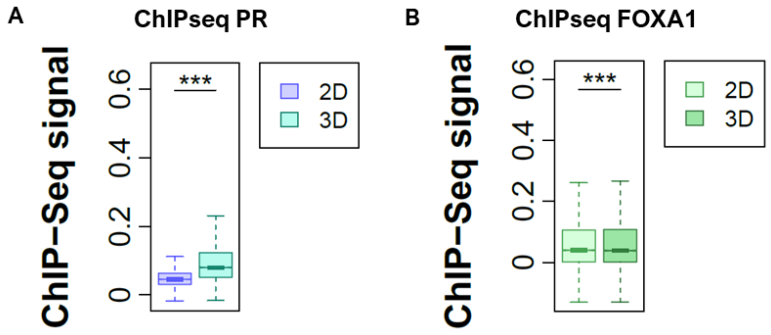

Figure R24. PR and FOXA1 occupancy at siYAP1-dependent PR binding regions under 2D and 3D conditions. (A) PR binding and (B) FOXA1 binding at 10,800 siYAP1-dependent PRbs, comparing 2D and 3D cultured cells. Statistical differences between FOXA1 and PR ChIP-seq signals in 2D and 3D cultured were assessed using the Mann-Whitney U test. (***) P-value < 0.001.

These results from 3D-cultured cells further support and expand our previous findings in YAP1-depleted cells. In 3D conditions, where nuclear YAP1 levels are reduced in response to ECM environment, we observed increased FOXA1 and PR binding at YAP1-bound, Co-recruited regions, as well as at the 10,800 siYAP1-dependent sites where YAP1 negatively regulates PR binding.

4.2. Live-cell imaging analysis of PR, YAP1 and FOXA1 nuclear condensates in native BC cells

To investigate the interplay between PR, YAP1, and FOXA1, we used quantitative live-cell imaging microscopy. This approach enables: i) single-cell resolution, ii) nuclear distribution analysis, and iii) precise quantification of nuclear receptor condensates in native T47D cells (Rayasam et al., 2005) (Bagheri et al., 2022).

Biomolecular condensates are dynamic membraneless assemblies critical for regulating gene expression, signaling, stress responses, and other essential processes (Jeon et al., 2025). The presence of Intrinsically Disordered Regions (IDRs) in proteins is not always required or sufficient for condensate formation but are widely recognized as key contributors to this process.

IDRs are strongly linked to their ability to form liquid-liquid phase-separated condensates (also called liquid droplets) as those proteins present an unstable structure with high flexibility to adopt multiple conformations (Borcherds et al., 2021). Moreover, IDRs flexibility allow proteins to engage in transient interactions with other proteins presenting IDRs enhancing its importance in organization and changes in compaction in the nucleus (Holehouse & Kragelund, 2024). YAP1 is notably enriched in IDRs, which span the entire structure with an average score of 0.7 (Figure R25A). In contrast, PR contains an IDR region in its N-terminal domain, enabling interaction with other molecular partners due to its structural flexibility (Figure R25B) (Raj Kumar et al., 2013).

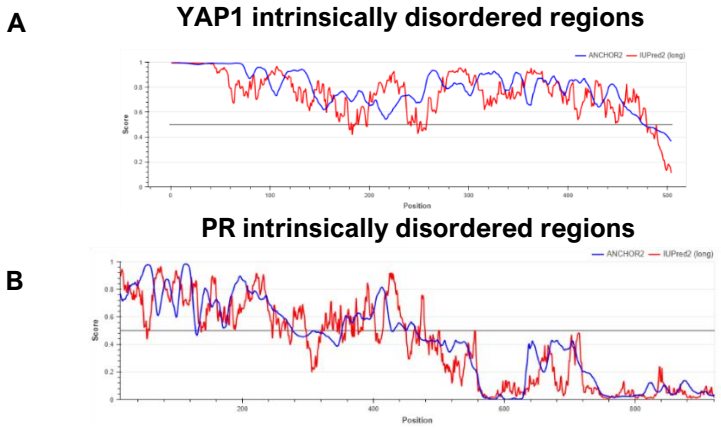

Figure R25. IDRs of YAP1 (A) and PR (B) were analyzed using iupred2a (https://iupred2a.elte.hu/). The results from ANCHOR2 are shown in blue, while those from IUPred2 (long) are displayed in red.

Thus, first, we examined whether YAP1 and PR form condensates in T47D cells, given that both proteins contain IDRs (Figure R26A-B).

The methodology is detailed in Section 13 of the Materials and Methods. Transient transfections of Halo-PR and YAP1-GFP in T47D cells revealed that both proteins form distinct nuclear condensates. Representative images of live cells acquired under control conditions and after PR activation with R5020 for 60 min illustrated the distribution pattern of each protein in both conditions (Figure R26A). In the absence of R5020, neither PR nor YAP1 form visible condensates, even though some cells show nuclear localization for both proteins. Upon R5020 stimulation, both PR and YAP1 concentrate mostly in the nuclear compartment (Figure R26B) and form discrete PR and YAP1 condensates (Figure R26A). Notably, PR condensates are more abundant and display greater intensity, with a higher concentration of PR molecules per condensate, compared to YAP1 (Figure R26C). This is consistent with ChIP-seq data, which reveal a significantly larger number of PR binding events compared to YAP1 (Figure R12A-B), enhancing our understanding that these clusters could represent chromatin binding sites.

To assess whether progestin-induced PR condensates might be associated with YAP1 condensates, we analyzed their colocalization. Overlay images showed qualitative colocalization (Figure R26D), supported by image correlation analysis (Benítez et al., 2024), which revealed a positive spatial cross-correlation function (CCF) centered at zero (Figure R26D, lower left panel). Quantification of the PR condensate area overlapping with YAP1 (fPR) confirmed a significantly higher association than expected for unrelated distributions (Figure R26D, lower right panel). These data indicate that a subpopulation of PR condensates colocalized with YAP1 during the acquisition time window. It is tempting to speculate that some of these condensates correspond to the YAP-bound and Co-recruited regions identified by ChIP-seq (Figure R13A-B).

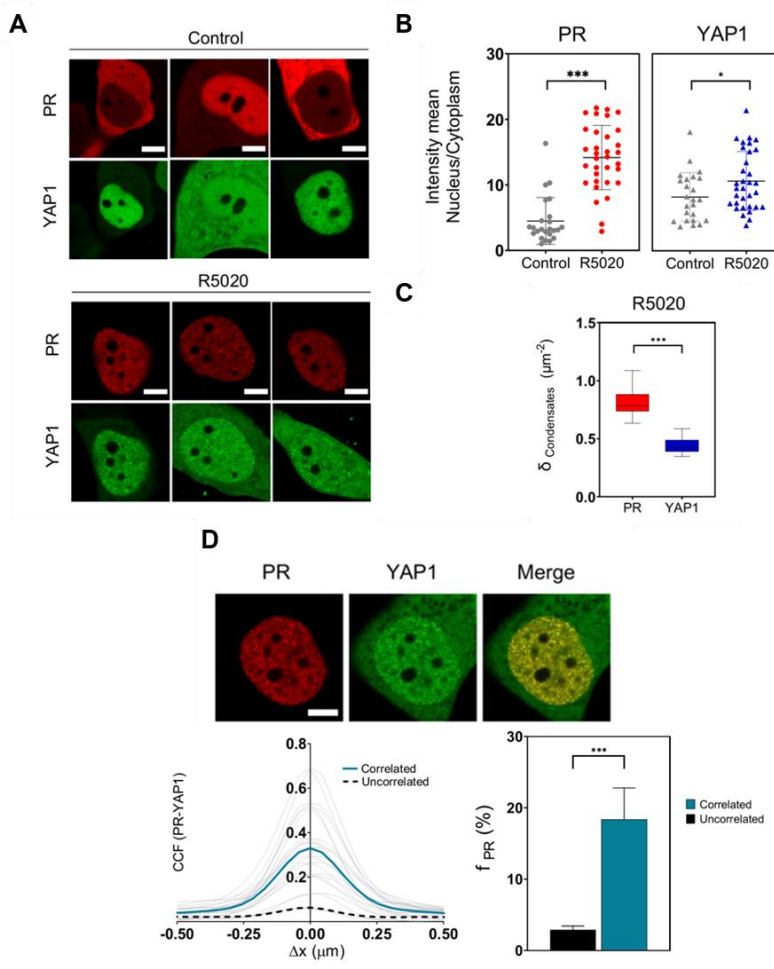

Figure R26. PR and YAP1 condensates colocalize in the presence of progestins. (A) Representative Airyscan images of T47D cells expressing Halo-PR (red) and peGFP-YAP (green) after 1 hour incubation with 10 nM R5020. Images were acquired using a ZEISS LSM980 confocal microscope and analyzed with ImageJ. (B) Comparison of PR and YAP1 foci intensity between R5020-treated and untreated conditions. (C) Density of PR and YAP1 condensates observed in the presence of R5020. (D) Airyscan images showing condensate colocalization of PR and YAP1 (upper panel), with image correlation analysis shown in the bottom panel. Data are representative of ≥3 independent experiments. Statistical analysis: Mann-Whitney test (ns, not significant; * $p < 0.05$; ** $p < 0.01$; * $p < 0.001$).

The pioneer factor FOXA1 forms biomolecular condensates, driven by its C-terminal IDR (Figure R27). This disordered region facilitate FOXA1's ability to bind and unpack condensed chromatin, playing a critical role in regulating BC cell proliferation and migration (Ji et al., 2024). Therefore, we decided to investigate whether FOXA1 could also form condensates in T47D cells and whether progestin treatment influences condensate formation. We hypothesize that FOXA1-formed condensates could mark and maintain a chromatin state favorable for promoting PR binding once the hormone is present.

Figure R27. IDRs of FOXA1 were analyzed using iupred2a (https://iupred2a.elte.hu/). The results from ANCHOR2 are shown in blue, while those from IUPred2 (long) are displayed in red.

To test this hypothesis, we performed transient transfections with GFP-FOXA1 in combination with Halo-PR. Our results showed that FOXA1 was constitutively nuclear and able to form condensates independently of R5020 stimulation (Figure R28A-C). These findings suggest that FOXA1 binding occurs prior to ligand-induced PR chromatin association and transcriptional activation of PR-regulated genes. This is consistent with previous studies indicating that FOXA1 plays a role in chromatin decompaction (Won et al., 2024).

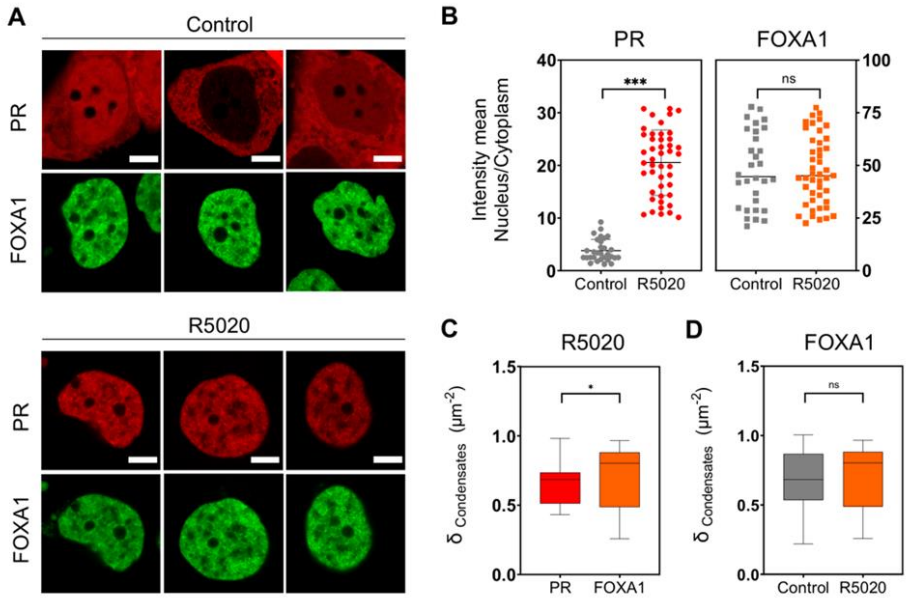

Figure R28. Formation of PR and FOXA1 condensates in T47D cells. (A) Representative Airyscan images of T47D cells expressing Halo-PR (red) and peGFP-FOXA1 (green) after 1 hour incubation with 10 nM R5020. Data are presented as means ± SEM from at least three replicates, with statistical significance determined using Student's t-test. (B) Intensity profiles of PR and FOXA1 in control and R5020-treated condition. (C) Foci density of PR and FOXA1 observed after R5020 treatment (D) Dynamics of FOXA1 foci density in the absence and presence of R5020.

To test whether PR and FOXA1 condensates are affected by YAP1 depletion, we performed similar analysis in shCTRL and shYAP1 cells (T47D cells with stable YAP1 depletion). Interestingly, depletion of YAP1 led to an increased density of both PR and FOXA1 foci (Figure R29B). The formation of new PR condensates supports previous findings, where 10,800 new PRbs were detected upon YAP1 depletion (Figure R8A). In addition, the increased density of FOXA1 foci upon YAP1 depletion suggests that YAP1 may prevent the formation of FOXA1-containing condensates, potentially compromising its role as a stabilizing factor for PR binding (Figure R29D).

Image correlation analysis showed a slight but significant increase in PR/FOXA1 colocalization after YAP1 knockdown (Figure 37D).

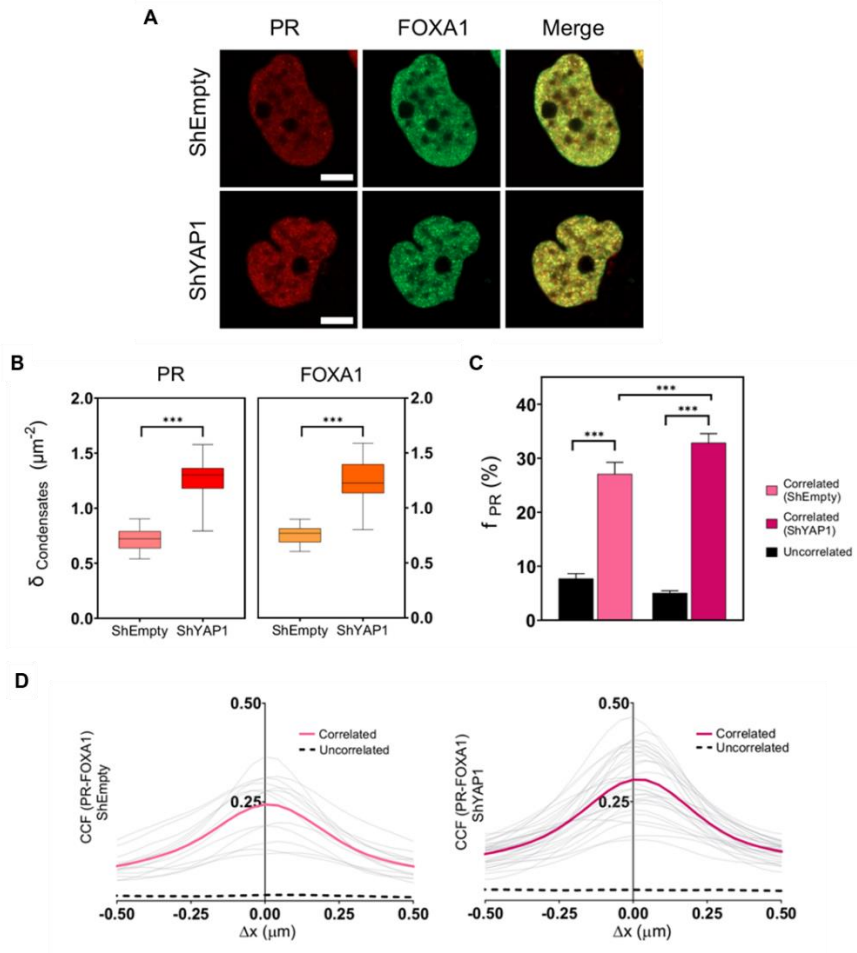

Figure R29. PR and FOXA1 condensates colocalize and their density was increased upon YAP1 depletion in T47D cells. (A) Representative Airyscan images of shCTRL and shYAP T47D cells co-expressing Halo-PR (red) and peGFP-FOXA1 (green) after incubation with 10 nM R5020 for at least 1 hour. (B) Comparison of foci intensity upon R5020 treatment for PR and FOXA1 between shEmpty and shYAP1 conditions. (C-D) Image correlation analysis comparing shEmpty and shYAP1 conditions. Data are presented as means ± SEM from at least three replicates, with statistical significance determined using Student's t-test.

Taken together, our image analysis demonstrates that YAP1 can modulate the intranuclear organization of PR by modulating condensate density and its colocalization with PR partners such as the pioneer factor FOXA1. These results align with the inhibitory role of YAP1 on PR activity and support the hypothesis that biomolecular condensates play a key role in progestin-dependent gene transcription.

4.3. Clinical implications

To investigate the potential clinical implications of our findings, we analyzed the correlation between YAP1 levels and survival in ER+/PR+ BC patients. Using the METABRIC database (Curtis et al., 2012), which includes gene expression data from 2,000 tumors, we found that YAP1 overexpression is associated with improved overall and relapse-free survival (Figure R30A, p-value 0.1 and 0.033, respectively).

To further validate the role of YAP1 in ER+ BC, we employed ER+ patient-derived xenografts (PDXs) as well as MCF-7 cells to assess the effect of the LATS1 inhibitor TRULI, which increases nuclear YAP1 levels by shifting the balance toward its non-phosphorylated form (Kastan et al., 2021). MCF-7 cells as well as two ER+ PDXs, PDX0479 and PDX0244T, were incubated with 10 μM TRULI for 7 days and cell proliferation was measured with a luminescent cell viability assay (Figure R30B). We found that TRULI significantly reduced cell growth compared to control (DMSO-treated) cells (Figure R30B). These findings support the role of nuclear YAP1 in modulating cell proliferation. Notably, both PDX0479 and PDX0244T are metastatic, aggressive tumors resistant to hormone therapies like fulvestrant, highlighting the significance of this new approach in patient treatment. From a therapeutic perspective, these findings represent a first step toward exploring the potential use of nuclear YAP1 regulators in treating ER+ BC.

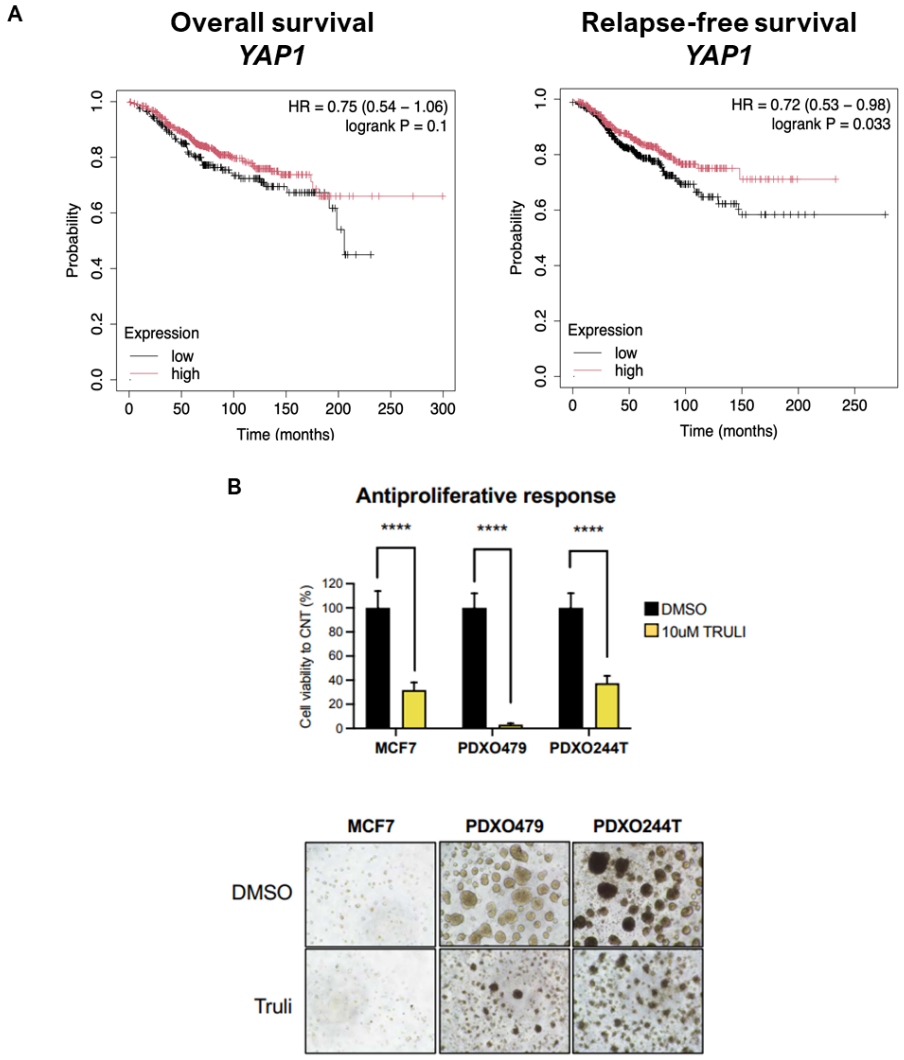

Figure R30. YAP1 as a therapeutic target in ER+ BC. (A) Kaplan–Meier plots showing the association between YAP1 mRNA expression and overall survival (left) and relapse-free survival (right) in ER+/PR+ tumors. The data were obtained from the cBioportal for Cancer genomics containing targeted sequencing of 2509 primary breast tumors with 548 matched normal (Curtis et al., 2012). (B) MCF-7 cells as well as two ER+ PDXs, PDX0479 and PDX0244T, were incubated with 10 μM TRULI for 7 days and cell proliferation was measured using a luminescent cell viability assay. Data are represented as mean ± SD from two different experiments.

5. Chapter V: Exploring the role of YAP1 in modulating ERα function in MCF-7 cells

YAP1 has been previously described to interact with several hormone receptors, including ERα. However, its role as an activator or repressor in this context remains unclear. To investigate whether the repressive effect of YAP1 on PR could be extended to other hormone receptors, we performed RNA-seq and ChIP-seq experiments for ERα in siCTRL and siYAP1 MCF-7 cells, which respond efficiently to estrogens.

Our results revealed that, although to a lesser extent than with progestins, the estrogen response was enhanced in the absence of YAP1, with 127 genes gaining regulation that fall within the Estrogen response late/early GO terms (e.g. ANXA9 and XBP1) (Figure R31A-C).

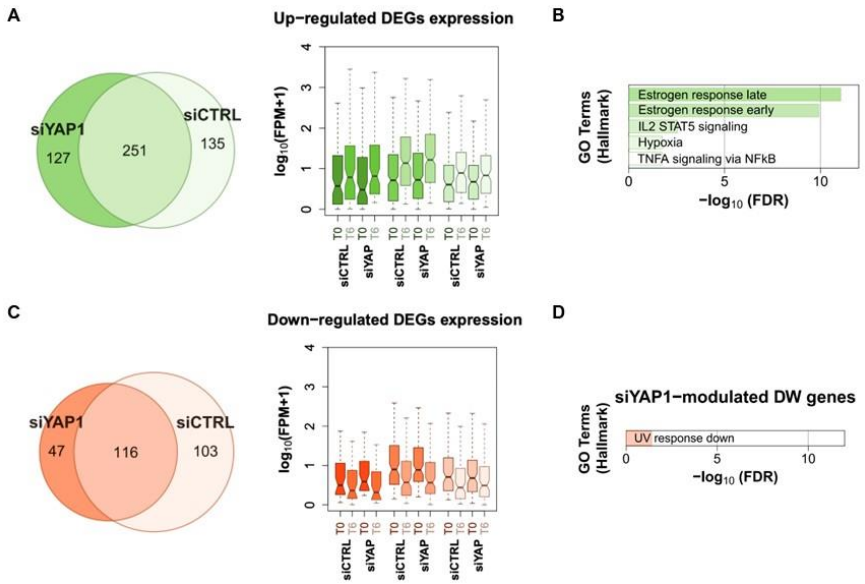

Figure R31. Role of YAP1 in ERα signaling. (A-B) Venn diagram of common up- and down-regulated genes in siCTRL and siYAP1 MCF-7 cells (|FC| > 2, p-value < 0.05). Boxplots of RNA-seq expression at T0 and T6 (6 hours E2). (C-D) GSEA showing Hallmark terms of significantly deregulated genes.

Additionally, similar to PR, ERα binding to genomic target sites increased upon YAP1 depletion (Figure R32A). After siYAP1 treatment, ERα bound to 8,958 new regions, and a general increase in binding intensity was observed at the 33,611 common ERα binding sites. These results suggest that YAP1 depletion not only alters ERα binding patterns but also increases its recruitment to regions where ERα is bound under control conditions. (Figure R32A).

Motif enrichment analysis of gained ERα binding sites upon YAP1 depletion identified the estrogen response element (ERE) motif (p-value: 10^{-1298}) as the most prevalent, followed by motifs for GATA (p-value: 10^{-175}), SIX1 (p-value: 10^{-145}) and FOXA (p-value: 10^{-135}) (Figure R32B).

Thus, in the estrogen pathway -the main regulator of BC cell proliferation-YAP1 functions as a negative regulator of a limited set of genes, mirroring its role in the PR pathway (Figures R4 and R8). In this context, YAP1 primarily modulates the magnitude of the hormonal response.

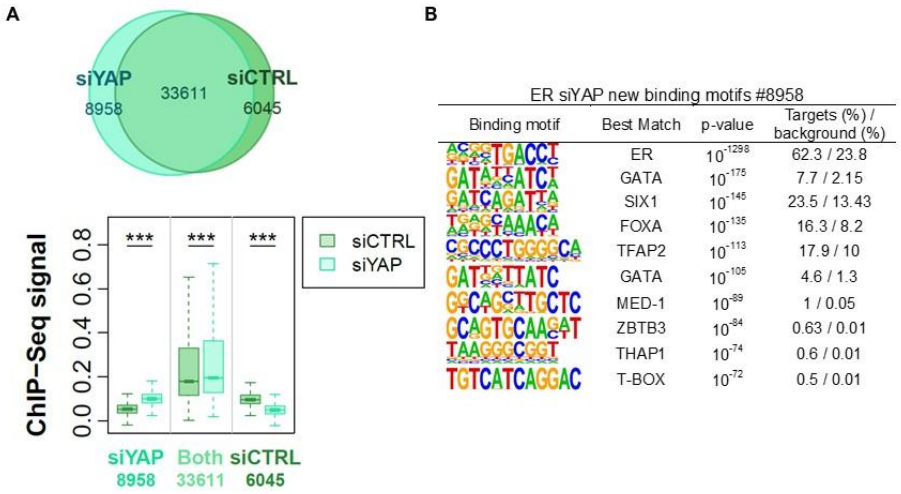

Figure R32. YAP1 modulates estrogen-dependent ERα binding in MCF-7 cells. (A) Venn diagram showing the overlap of ERα ChIP-Seq peaks in control and siYAP1 MCF7 cells (upper panel). Boxplot displaying CPM-normalized, input-subtracted ERα ChIP-seq signals for siYAP1-dependent, common, and siCTRL-dependent peaks (lower panel). Statistical significance was determined using the Wilcoxon signed-rank test (***) P-value < 0.001. (B) Homer motif analysis of siYAP-dependent ERα binding sites, highlighting the most abundant motifs and corresponding P-values

Discussion

Discussion

Hormone receptor function is tightly regulated by multiple signaling pathways (Narayanan et al., 2005) (Richer et al., 1998) (Boonyaratanakornkit et al., 2001). The study of these signaling pathways provides valuable insights into the mechanisms by which nuclear receptors function in the context of cancer, while also contributing to the development of novel therapeutic strategies. A clear example is the Hippo pathway, which plays a key role in regulating cell proliferation and maintaining tissue homeostasis (M. Fu et al., 2022). Notably, its deregulation has been linked to tumor progression and malignancy (Dong et al., 2007 ; Tapon et al., 2002).

To date, studies investigating the connection between SHRs and the Hippo pathway have identified YAP1 and TEAD as co-regulators of ERα and AR (Li et al., 2023; Li et al., 2022; Zhu et al., 2019). These findings, while providing mechanistic understanding, also presented conflicting evidence, making it unclear whether YAP1 functions as a tumor suppressor or promoter in hormone-dependent cancers.

1. A novel role for YAP1 modulating PR function

Our study reveals a novel role for nuclear YAP1, which, independent of TEAD proteins, modulates PR function in BC cells. Specifically, we found that YAP1 acts as a suppressor of PR as depletion of YAP1 increased hormone-dependent dedifferentiation (Figure R2), gene expression (Figure R4) and PR binding to chromatin (Figure R8). Interestingly, when depleting YAP1, PR modified its gene expression pattern by activating new genes involved in estrogen response early and late and EMT, suggesting a novel role for YAP1 in maintaining hormonal specificity.

By using ChIP-seq analysis we identified two sets of regions where YAP1and PR colocalize: YAP-bound regions (2,973 genomic sites), where YAP1 was pre-bound to DNA and, Co-recruited regions (3,111

genomic sites), where YAP1 is dynamically recruited upon hormone stimulation (Figure 1D). These regions, located on active enhancers, shows increased PR binding upon YAP1 depletion and were in proximity to DEGs, highlighting their functional relevance in PR-mediated gene regulation (Figure R13).

DNA binding motif analysis of YAP-bound and Co-recruited regions revealed TEAD1/4 and FOXA1 as the top representative motifs (Figure R14). ChIP-seq experiments confirmed that FOXA1 was indeed the key transcription factor, not only for PR-YAP1 regions but also present in 70% of all YAP1-bound sites identified in untreated cells and 87% of those detected upon hormone treatment. Co-IP experiments validated the interaction between YAP1 and FOXA1; however, no interaction between YAP1 and PR was observed (Figure R17). This finding suggests that YAP1 modulates PR function through its association with FOXA1, rather than by directly interacting with PR.

Interestingly, while YAP1 is typically recruited through TEAD proteins in the canonical Hippo pathway, our results suggest that FOXA1 offers an alternative mechanism for YAP1 binding to chromatin in BC cells. In fact, the depletion of TEAD1 and TEAD4 did not fully recapitulate the effects of YAP1 knockdown in PR-dependent gene expression assays. While TEAD1 was required for progestin-dependent gene activity, TEAD4 played a more complex role, with some genes requiring its presence and others becoming regulated in its absence (Figure R19 and R20). These findings highlight that YAP1's inhibitory role on PR function occurs primarily through a TEAD-independent, non-canonical pathway involving FOXA1. Actually, depletion of FOXA1 by siRNA notably reduced YAP1 binding in regions where YAP1 and FOXA1 overlap (Figure R18).

Notably, the 10,800 regions that gained PR binding upon progestin stimulation in the absence of YAP1 (Figure R8, left panel), exhibited only

a 7.5% overlap with YAP1 (Figure R11). This observation suggests a mechanism in which the squelching of FOXA1 by YAP1 indirectly represses gene transcription, independently of YAP1 loading onto DNA (Figure D1).

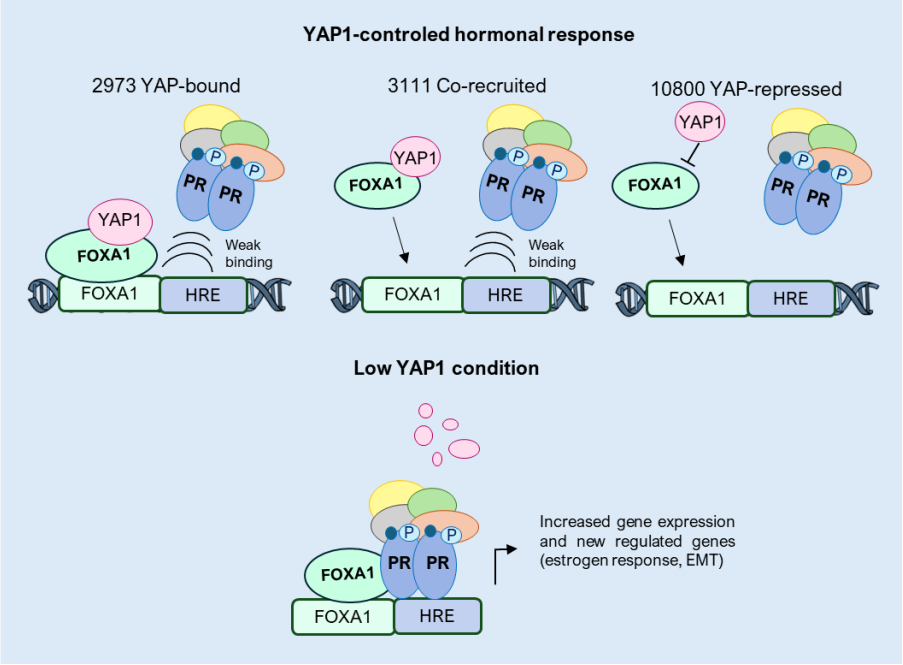

Figure D1. Role of YAP1 in PR binding. A) Schematic representation of the YAP1-regulated hormonal response. YAP1 directly influences PR chromatin binding both prior to progestin stimulation (2,973 YAP1-bound regions) and following R5020 treatment (3,111 co-recruited regions). Additionally, YAP1 indirectly represses PR binding at 10,800 genomic sites, likely through modulation of FOXA1 activity. B) PR binding is enhanced under conditions of reduced YAP1 levels.

2. YAP1 modulates PR binding without affecting chromatin accessibility

While the mechanisms by which hormones act on their target cells have been extensively studied, the precise regulation of the magnitude and

specificity of these responses remains poorly understood. Different factors such as the expression levels of hormone receptors, pioneer factors, specific co-regulators, and the accessibility of regulatory regions (e.g., enhancers) have been suggested to play crucial roles in this process.

Given YAP1's negative effect on PR function and its association with FOXA1, we hypothesized that YAP1 may compromise or destabilize the pioneering activity of FOXA1, thereby affecting PR binding. If this hypothesis is correct, YAP1 depletion should enhance FOXA1’s pioneer activity, increasing chromatin accessibility at target regions.

Interestingly, we did not detect significant changes in chromatin accessibility that could explain the increased PR binding detected in YAP-bound, Co-recruited and siYAP1-dependent regions upon YAP1 depletion (Figure R16A). The ability of YAP1 to enhance PR binding without altering chromatin accessibility points to a different regulatory mechanism.

One possible explanation is that FOXA1, beyond its canonical role as a pioneer factor that opens chromatin regions, may also stabilize receptor binding through protein-protein interactions. This mechanism has been described for the hinge region of AR, specifically the 629-RKLKKL-634 motif (Messner et al., 2020). Although this motif is poorly conserved across other receptors, a similar sequence is preserved in PR at 638-KXKK-641, which has been shown to regulate its function in both normal and pathological contexts (Daniel et al., 2010). Thus, YAP1 may affect the stabilizing function of FOXA1, potentially by competing with PR for interaction with FOXA1 (Figure D1). This competition alters PR binding dynamics by reducing its stabilization at target sites and modulating its transcriptional activity.

3. Interplay between YAP1 and PR in 3D grown cells

Most findings regarding PR function in BC cells, including our own, have been obtained using T47D cells cultured as 2D monolayers. Although this model is widely used, it does not fully capture the complexity of the cellular environment. Notably, YAP1 activity is highly sensitive to contextual cues such as cell-cell contact and interactions with the ECM -conditions that are more accurately recapitulated in 3D cultured systems. On this regard, we recently reported a connection between the activation of the Hippo pathway kinase LATS1 and the hormonal response in cells grown in three-dimensional (3D) cultures (Ramirez-Cuellar et al., 2024).

In 3D-grown cells, LATS1 phosphorylated YAP1, promoting its retention in the cytoplasm. This system, that physiologically downregulates YAP1, revealed an increased hormonal response, characterized by enhanced gene expression, greater PR binding to its target regions, and elevated hormone-dependent cell proliferation (Ramirez-Cuellar et al., 2024). However, the underlying mechanisms linking Hippo activation, YAP1 phosphorylation, and PR function remain unclear.

When analyzing PR binding at the YAP-bound and Co-recruited regions identified in Chapter II (Figure R13A), we observed an increase in PR binding in cells grown in 3D compared to 2D cells (Figure R22). Interestingly, FOXA1 also showed a distinct binding pattern between 2D and 3D, with 55% of its binding sites in 3D being exclusive to that condition. FOXA1 binding at YAP-bound and Co-recruited regions, was also enhanced in 3D compared to 2D cells, although to a lesser extent than PR (Figure R23).

4. YAP1 and PR in nuclear condensates

Recent studies suggest that phase separation, driven by multivalent interactions among transcription factors (TFs), coactivators, and RNA polymerase II, facilitates the assembly of these factors into dynamic clusters or condensates at specific enhancer elements (Shrinivas et al., 2020).

Notably, YAP1, FOXA1, and PR contain intrinsically disordered regions (Figures R25 and R27). Using live cell imaging, we confirmed the presence of PR within condensates alongside YAP1 (Figure R26) and FOXA1 (Figure R28) suggesting a more pronounced colocalization of YAP1 and PR than the observed by ChIP-seq combined analysis. It is important to note that, in these assays, the proteins are overexpressed, which may lead to an overestimation of their colocalization.

Interestingly, YAP1 depletion led to the formation of additional FOXA1 and PR condensates, reinforcing YAP1's role as a negative modulator of PR and supporting its involvement in destabilizing FOXA1 activity (Figure R29). Therefore, while these results support the findings from ChIP-seq experiments, they should be interpreted with caution.

5. Role of YAP1 in estrogen-dependent gene regulation

In the context of estrogen signaling, YAP1 depletion produced detectable but less pronounced effects than those observed with progesterone. This difference may be attributed to the involvement of multiple pioneer factors beyond FOXA, such as GATA3, AP-1, and RUNX (Stender et al., 2010), which collectively facilitate ERα binding. Additionally, YAP1 may influence ERα through mechanisms that depend on TEAD proteins, as previously reported (Li et al., 2023; Li et al., 2022; Zhu et al., 2019). Despite this, YAP1 depletion enables 127 new genes to become estrogen-regulated, which are classified under the Gene

Ontology category of estrogen response (Figure R31), highlighting its key role in modulating the magnitude of the hormonal response.

Regarding ERα binding, we identified ~9000 new binding regions and observed a general increase in the ERα binding sites upon YAP1 depletion, supporting a negative role in ERα modulation (Figure R32). Although a clear increase in ERα binding upon YAP1 knockdown is observed, it does not correlate with a significant upregulation of gene expression beyond the 127 genes identified. Therefore, while the inhibitory effect of YAP1 operates within the ER-dependent pathway, other regulatory factors are likely contributing, adding complexity of the underlying mechanisms.

6. Clinical implication of YAP1 modulation in PDXs

The effect of YAP1 on PR function was studied in T47D cells grown either as monolayers or spheroids. To expand our research, we also tested the role of YAP1 modulation in PDXOs. Our approach was to use TRULI, a LATS1 inhibitor, that increases nuclear YAP1 levels and, in turn, compromises PR and ERα function. Consistent with these findings, TRULI inhibited cell proliferation in both cell lines and PDXs, highlighting its potential as a promising YAP1-based therapeutic approach for BC (Figure R30B). Interestingly, higher nuclear YAP1 levels were associated with improved survival rates in patients with PR+ BC (Figure R30A).

The importance of these results is highlighted by the fact that FOXA1 has been implicated in genetic aberrations, including gene amplification and activating mutations, in approximately 6% of primary and 10% metastatic ERα-positive breast cancer cases (Ciriello et al., 2016). In this respect, FOXA1 overexpression and amplification have been linked to endocrine resistance and increased invasiveness in both endocrine-resistant (X. Fu et al., 2016) and ER+ (X. Fu et al., 2019) BC cells by reprogramming the ERα-dependent transcriptome.

Historically considered undruggable due to the absence of suitable small molecule binding sites, FOXA1 represents a significant challenge in BC therapy. We observed YAP1 interacts and modulates FOXA1 function, thereby regulating the stabilization of downstream transcription factors such as PR and ERα, influencing their genomic binding and activity. Therefore, targeting YAP1 represents an alternative to indirectly influence FOXA1 activity.

Conclusions

Conclusions

1. YAP1 functions as a molecular rheostat for PR, controlling the extent of progestin-dependent dedifferentiation, proliferation, PR binding and gene expression, thereby enforcing PR specificity.

2. YAP1's repressive effect on PR operates independently of its interaction with TEAD proteins, as RNA-seq results from siTEAD1 or TEAD4 treatments differed from those with siYAP1. Instead, TEAD1 is crucial for proper PR function, while TEAD4 plays a dual role in PR modulation.

3. The minor positive influence of YAP1 on PR-dependent gene regulation is primarily mediated through TEAD proteins, following the canonical pathway.

4. YAP1 and PR co-localize at the chromatin level, both in the absence of hormone within 2,973 YAP-bound regions, and after progestin treatment in 3,111 Co-recruited regions. Notably, YAP1 depletion enhances PR binding in these regions.

5. Our findings show that FOXA1 is the key transcription factor anchoring YAP1 in the YAP-bound and Co-recruited regions, with 70% of these regions enriched in FOXA1. Mechanistically, no changes in chromatin accessibility were observed in the siYAP1 condition, suggesting that YAP1 and PR may compete for FOXA1 binding.

6. In 3D-cultured cells, which provide a more physiologically relevant model for studying PR function, YAP1 remains predominantly in the cytoplasm. In these cells, both PR and FOXA1 binding were increased in YAP-bound and Co-recruited regions compared to 2D cultures.

7. YAP1/PR and PR/FOXA1 condensates colocalize upon progestin treatment. In YAP1-depleted cells, the density and intensity of PR and FOXA1 foci increases.

8. In patient-derived xenograft organoids (PDXOs), treatment with the LATS1 inhibitor TRULI (which enhances nuclear YAP1) impairs cell proliferation, highlighting the potential of YAP1 modulation as a therapeutic strategy for certain types of BC.

9. In the MCF-7 cell line, YAP1 played a dual role in estrogen-dependent gene expression: its depletion activated 127 genes, while 135 genes depended on YAP1 for their expression.

10. Similar to what is observed for PR, YAP1 negatively modulates ER binding, as approximately 9,000 ERα binding regions gained binding upon YAP1 depletion.

Bibliography

Bibliography

Adams, E. J., Karthaus, W. R., Hoover, E., Liu, D., Gruet, A., Zhang, Z., Cho, H., DiLoreto, R., Chhangawala, S., Liu, Y., Watson, P. A., Davicioni, E., Sboner, A., Barbieri, C. E., Bose, R., Leslie, C. S., & Sawyers, C. L. (2019). FOXA1 mutations alter pioneering activity, differentiation and prostate cancer phenotypes. Nature, 571(7765), 408–412. https://doi.org/10.1038/s41586-019-1318-9

Agbana, S., & McIlroy, M. (2024). Extra-nuclear and cytoplasmic steroid receptor signalling in hormone dependent cancers. Journal of Steroid Biochemistry and Molecular Biology, 243(May), 106559. https://doi.org/10.1016/j.jsbmb.2024.106559

Al-Hajj, M., Wicha, M. S., Benito-Hernandez, A., Morrison, S. J., & Clarke, M. F. (2003). Prospective identification of tumorigenic breast cancer cells. Proceedings of the National Academy of Sciences of the United States of America, 100(7), 3983–3988. https://doi.org/10.1073/pnas.0530291100

Amemiya, H. M., Kundaje, A., & Boyle, A. P. (2019). The ENCODE Blacklist: Identification of Problematic Regions of the Genome. Scientific Reports, 9(1), 1–5. https://doi.org/10.1038/s41598-019-45839-z

Araki, K., & Miyoshi, Y. (2018). Mechanism of resistance to endocrine therapy in breast cancer: the important role of PI3K/Akt/mTOR in estrogen receptor-positive, HER2-negative breast cancer. Breast Cancer, 25(4), 392–401. https://doi.org/10.1007/s12282-017-0812-x

Asselin-Labat, M. L., Vaillant, F., Sheridan, J. M., Pal, B., Wu, D., Simpson, E. R., Yasuda, H., Smyth, G. K., Martin, T. J., Lindeman, G. J., & Visvader, J. E. (2010). Control of mammary stem cell function by steroid hormone signalling. Nature, 465(7299), 798–802. https://doi.org/10.1038/nature09027

Augello, M. A., Hickey, T. E., & Knudsen, K. E. (2011). FOXA1: Master of steroid receptor function in cancer. EMBO Journal, 30(19), 3885–3894. https://doi.org/10.1038/emboj.2011.340

Bae, J. S., Kim, S. M., & Lee, H. (2017). The Hippo signaling pathway provides novel anti-cancer drug targets. Oncotarget, 8(9), 16084–16098. https://doi.org/10.18632/oncotarget.14306

Bagheri, N., Carpenter, A. E., Lundberg, E., Plant, A. L., & Horwitz, R. (2022). The new era of quantitative cell imaging-challenges and opportunities. Molecular Cell, 82(2), 241–247. https://doi.org/10.1016/j.molcel.2021.12.024

Ballaré, C., Castellano, G., Gaveglia, L., Althammer, S., González-Vallinas, J., Eyras, E., Le Dily, F., Zaurin, R., Soronellas, D., Vicent, G. P., & Beato, M. (2013). Nucleosome-Driven Transcription Factor Binding and Gene Regulation. Molecular Cell, 49(1), 67–79. https://doi.org/10.1016/j.molcel.2012.10.019

Barral, A., & Zaret, K. S. (2024). Pioneer factors: roles and their regulation in development. Trends in Genetics, 40(2), 134–148. https://doi.org/10.1016/j.tig.2023.10.007

Belén Benítez, Martin Stortz, María Cecilia De Rossi, Diego M. Presman, Valeria Levi
bioRxiv 2024.11.14.623561; doi: https://doi.org/10.1101/2024.11.14.623561

Bolte, S. & Cordelières, F. P. (2006). A guided tour into subcellular colocalization analysis in light microscopy. Journal of Microscopy, 224 (December), 213–232.

Boonyaratanakornkit, V., Scott, M. P., Ribon, V., Sherman, L., Anderson, S. M., Maller, J. L., Miller, W. T., & Edwards, D. P. (2001). Progesterone receptor contains a proline-rich motif that directly interacts with SH3 domains and activates c-Src family tyrosine kinases. Molecular Cell, 8(2), 269–280. https://doi.org/10.1016/S1097-2765(01)00304-5

Borcherds W, Bremer A, Borgia MB, Mittag T. How do intrinsically disordered protein regions encode a driving force for liquid-liquid phase separation? Curr Opin Struct Biol. 2021 Apr; 67: 41-50. doi: 10.1016/j.sbi.2020.09.004.

Broome, R., Chernukhin, I., Jamieson, S., Kishore, K., Papachristou, E. K., Mao, S. Q., Tejedo, C. G., Mahtey, A., Theodorou, V., Groen, A. J., D'Santos, C., Balasubramanian, S., Farcas, A. M., Siersbæk, R., & Carroll, J. S. (2021). TET2 is a component of the estrogen receptor complex and controls 5mC to 5hmC conversion at estrogen receptor cis-regulatory regions. Cell Reports, 34(8), 108776. https://doi.org/10.1016/j.celrep.2021.108776

Bruna, A., Rueda, O. M., Greenwood, W., Batra, A. S., Callari, M., Batra, R. N., Pogrebniak, K., Sandoval, J., Cassidy, J. W., Tufegdzic-Vidakovic, A., Sammut, S. J., Jones, L., Provenzano, E., Baird, R., Eirew, P., Hadfield, J., Eldridge, M., McLaren-Douglas, A., Barthorpe, A., … Caldas, C. (2016). A Biobank of Breast Cancer Explants with Preserved Intra-tumor Heterogeneity to Screen Anticancer Compounds. Cell, 167(1), 260-274.e22. https://doi.org/10.1016/j.cell.2016.08.041

Buenrostro, J. D., Giresi, P. G., Zaba, L. C., Chang, H. Y., & Greenleaf, W. J. (2013). Transposition of native chromatin for fast and sensitive epigenomic profiling of open chromatin, DNA-binding proteins and nucleosome position. Nature Methods, 10(12), 1213–1218. https://doi.org/10.1038/nmeth.2688

Burris, T. P., Nawaz, Z., Tsai, M. J., & O'Malley, B. W. (1995). A nuclear hormone receptor-associated protein that inhibits transactivation by the thyroid hormone and retinoic acid receptors. Proceedings of the National Academy of Sciences of the United States of America, 92(21), 9525–9529. https://doi.org/10.1073/pnas.92.21.9525

Byler, S., Goldgar, S., Heerboth, S., Leary, M., Housman, G., Moulton, K., & Sarkar, S. (2014). Genetic and epigenetic aspects of breast cancer progression and therapy. Anticancer Research, 34(3), 1071–1077.

Cai, G., Qi, Y., Wei, P., Gao, H., Xu, C., Zhao, Y., Qu, X., Yao, F., & Yang, W. (2023). IGFBP1 Sustains Cell Survival during Spatially-Confined Migration and Promotes Tumor Metastasis. Advanced Science, 10(21), 1–17. https://doi.org/10.1002/advs.202206540

Camargo, F. D., Gokhale, S., Johnnidis, J. B., Fu, D., Bell, G. W., Jaenisch, R., & Brummelkamp, T. R. (2007). YAP1 Increases Organ Size and Expands Undifferentiated Progenitor Cells. Current Biology, 17(23), 2054–2060. https://doi.org/10.1016/j.cub.2007.10.039

Carnell, G., Grehan, K., Ferrara, F., Molesti, E., & Temperton, N. (2017). An Optimized Method for the Production Using PEI, Titration and Neutralization of SARS-CoV Spike Luciferase Pseudotypes. Bio-Protocol, 7(16), 1–10. https://doi.org/10.21769/bioprotoc.2514

Cato, A. C. B. (1991). Solveigh krusekopf, 1 anne chauchereau, 2 edwin milgrom, 2 david henderson 3. 40(1), 239–245.

Cato, A. C., Skroch, P., Weinmann, J., Butkeraitis, P., & Ponta, H. (1988). DNA sequences outside the receptor-binding sites differently modulate the responsiveness of the mouse mammary tumour virus promoter to various steroid hormones. The EMBO Journal, 7(5), 1403–1410. https://doi.org/10.1002/j.1460-2075.1988.tb02957.x

Cha, S., Lee, E., & Won, H. H. (2021). Comprehensive characterization of distinct genetic alterations in metastatic breast cancer across various metastatic sites. Npj Breast Cancer, 7(1), 1–11. https://doi.org/10.1038/s41523-021-00303-y

Chen, C. C., Hardy, D. B., & Mendelson, C. R. (2011). Progesterone receptor inhibits proliferation of human breast cancer cells via induction of MAPK phosphatase 1 (MKP-1/DUSP1). Journal of Biological Chemistry, 286(50), 43091–43102. https://doi.org/10.1074/jbc.M111.295865

Chen, J., Kinyamu, H. K., & Archer, T. K. (2006). Changes in attitude, changes in latitude: Nuclear receptors remodeling chromatin to regulate transcription. Molecular Endocrinology, 20(1), 1–13. https://doi.org/10.1210/me.2005-0192

Chen, K. H., He, J., Wang, D. L., Cao, J. J., Li, M. C., Zhao, X. M., Sheng, X., Li, W. Bin, & Liu, W. J. (2014). Methylation-associated inactivation of LATS1 and its effect on demethylation or overexpression on YAP and cell biological function in human renal cell carcinoma. International Journal of Oncology, 45(6), 2511–2521. https://doi.org/10.3892/ijo.2014.2687

Cheng, J., Zhang, C., & Shapiro, D. J. (2007). A functional serine 118 phosphorylation site in estrogen receptor-α is required for down-regulation of gene expression by 17β-estradiol and 4-hydroxytamoxifen. Endocrinology, 148(10), 4634–4641. https://doi.org/10.1210/en.2007-0148

Cheung, J., & Smith, D. F. (2000). Molecular chaperone interactions with steroid receptors: An update. Molecular Endocrinology, 14(7), 939–946. https://doi.org/10.1210/mend.14.7.0489

Ciriello, G., Gatza, M. L., Beck, A. H., Wilkerson, M. D., Rhie, K., Pastore, A., Zhang, H., Mclellan, M., Yau, C., Chen, Y., Jensen, K., Johnson, N. B., Oesterreich, S., Gordon, B., Laird, P. W., Hoadley, K. A., & King, T. A. (2016). Cancer. 163(2), 506–519. https://doi.org/10.1016/j.cell.2015.09.033.Comprehensive

Cittelly, D., Finlay-Schultz, J., Howe, E. et al. Progestin suppression of miR-29 potentiates dedifferentiation of breast cancer cells via KLF4. Oncogene 32, 2555–2564 (2013). https://doi.org/10.1038/onc.2012.275

Curtis, C., Shah, S. P., Chin, S. F., Turashvili, G., Rueda, O. M., Dunning, M. J., Speed, D., Lynch, A. G., Samarajiwa, S., Yuan, Y., Gräf, S., Ha, G., Haffari, G., Bashashati, A., Russell, R., McKinney, S., Aparicio, S., Brenton, J. D., Ellis, I., … Caldas, C. (2012). The genomic and transcriptomic architecture of 2,000 breast tumours reveals novel subgroups. Nature, 486(7403), 346–352. https://doi.org/10.1038/nature10983

Daniel, A. R., Gaviglio, A. L., Czaplicki, L. M., Hillard, C. J., Housa, D., & Lange, C. A. (2010). The progesterone receptor hinge region regulates the kinetics of transcriptional responses through acetylation, phosphorylation, and nuclear retention. Molecular Endocrinology, 24(11), 2126–2138. https://doi.org/10.1210/me.2010-0170

Dasgupta, S., Lonard, D. M., & O'Malley, B. W. (2014). Nuclear receptor coactivators: Master regulators of human health and disease. Annual Review of Medicine, 65(3), 279–292. https://doi.org/10.1146/annurev-med-051812-145316

De Ruijter, A. J. M., Van Gennip, A. H., Caron, H. N., Kemp, S., & Van Kuilenburg, A. B. P. (2003). Histone deacetylases (HDACs): Characterization of the classical HDAC family. Biochemical Journal, 370(3), 737–749. https://doi.org/10.1042/BJ20021321

Demir Cetinkaya, B., & Biray Avci, C. (2022). Molecular perspective on targeted therapy in breast cancer: a review of current status. Medical Oncology, 39(10), 1–12. https://doi.org/10.1007/s12032-022-01749-1

Dobrzycka, K. M., Townson, S. M., Jiang, S., & Oesterreich, S. (2003). Estrogen receptor corepressors - A role in human breast cancer? Endocrine-Related Cancer, 10(4), 517–536. https://doi.org/10.1677/erc.0.0100517

Dong, J., Feldmann, G., Huang, J., Wu, S., Zhang, N., Comerford, S. A., Gayyed, M. F. F., Anders, R. A., Maitra, A., & Pan, D. (2007). Elucidation of a Universal Size-Control Mechanism in Drosophila and Mammals. Cell, 130(6), 1120–1133. https://doi.org/10.1016/j.cell.2007.07.019

Driehuis, E., Kretzschmar, K., & Clevers, H. (2020). Establishment of patient-derived cancer organoids for drug-screening applications. Nature Protocols, 15(10), 3380–3409. https://doi.org/10.1038/s41596-020-0379-4

Ellmann, S., Sticht, H., Thiel, F., Beckmann, M. W., Strick, R., & Strissel, P. L. (2009). Estrogen and progesterone receptors: From molecular structures to clinical targets. Cellular and Molecular Life Sciences, 66(15), 2405–2426. https://doi.org/10.1007/s00018-009-0017-3

Elosegui-Artola, A., Andreu, I., Beedle, A. E. M., Lezamiz, A., Uroz, M., Kosmalska, A. J., Oria, R., Kechagia, J. Z., Rico-Lastres, P., Le Roux, A. L., Shanahan, C. M., Trepat, X., Navajas, D., Garcia-Manyes, S., & Roca-Cusachs, P. (2017). Force Triggers YAP Nuclear Entry by Regulating Transport across Nuclear Pores. Cell, 171(6), 1397-1410.e14. https://doi.org/10.1016/j.cell.2017.10.008

Ercan, C., J. van Diest, P., & Vooijs, M. (2011). Mammary Development and Breast Cancer: The Role of Stem Cells. Current Molecular Medicine, 11(4), 270–285. https://doi.org/10.2174/156652411795678007

Evans, K. W., Paez-Arango, N., Akcakanat, A., Yuca, E., & Meric-Bernstam, F. (2017). Modeling breast cancer heterogeneity with patient-derived xenografts. In Patient Derived Tumor Xenograft Models: Promise, Potential and Practice. Elsevier Inc. https://doi.org/10.1016/B978-0-12-804010-2.00018-7

Feng, Y., Spezia, M., Huang, S., Yuan, C., Zeng, Z., Zhang, L., Ji, X., Liu, W., Huang, B., Luo, W., Liu, B., Lei, Y., Du, S., Vuppalapati, A., Luu, H. H., Haydon, R. C., He, T. C., & Ren, G. (2018). Breast cancer development and progression: Risk factors, cancer stem cells, signaling pathways, genomics, and molecular pathogenesis. Genes and Diseases, 5(2), 77–106. https://doi.org/10.1016/j.gendis.2018.05.001

Fournier, M., Bourriquen, G., Lamaze, F. C., Côté, M. C., Fournier, É., Joly-Beauparlant, C., Caron, V., Gobeil, S., Droit, A., & Bilodeau, S. (2016). FOXA and master transcription factors recruit Mediator and Cohesin to the core transcriptional regulatory circuitry of cancer cells. Scientific Reports, 6(October), 1–11. https://doi.org/10.1038/srep34962

Frank, N. Y., Margaryan, A., Huang, Y., Schatton, T., Waaga-Gasser, A. M., Gasser, M., Sayegh, M. H., Sadee, W., & Frank, M. H. (2005). ABCB5-mediated doxorubicin transport and chemoresistance in human malignant melanoma. Cancer Research, 65(10), 4320–4333. https://doi.org/10.1158/0008-5472.CAN-04-3327

Frazzi, R. (2021). BIRC3 and BIRC5: multi-faceted inhibitors in cancer. Cell and Bioscience, 11(1), 1–14. https://doi.org/10.1186/s13578-020-00521-0

Fu, M., Hu, Y., Lan, T., Guan, K. L., Luo, T., & Luo, M. (2022). The Hippo signalling pathway and its implications in human health and diseases. Signal Transduction and Targeted Therapy, 7(1). https://doi.org/10.1038/s41392-022-01191-9

Fu, X., Jeselsohn, R., Pereira, R., Hollingsworth, E. F., Creighton, C. J., Li, F., Shea, M., Nardone, A., De Angelis, C., Heiser, L. M., Anur, P., Wang, N., Grasso, C. S., Spellman, P. T., Griffith, O. L., Tsimelzon, A., Gutierrez, C., Huang, S., Edwards, D. P., … Schiff, R. (2016). FOXA1 overexpression mediates endocrine resistance by altering the ER transcriptome and IL-8 expression in ER-positive breast cancer. Proceedings of the National Academy of Sciences of the United States of America, 113(43), E6600–E6609. https://doi.org/10.1073/pnas.1612835113

Fu, X., Pereira, R., De Angelis, C., Veeraraghavan, J., Nanda, S., Qin, L., Cataldo, M. L., Sethunath, V., Mehravaran, S., Gutierrez, C., Chamness, G. C., Feng, Q., O'Malley, B. W., Selenica, P., Weigelt, B., Reis-Filho, J. S., Cohen, O., Wagle, N., Nardone, A., … Schiff, R. (2019). FOXA1 upregulation promotes enhancer and transcriptional reprogramming in endocrine-resistant breast cancer. Proceedings of the National Academy of Sciences of the United States of America, 116(52), 26823–26834. https://doi.org/10.1073/pnas.1911584116

Graham, J. D., Mote, P. A., Salagame, U., Van Dijk, J. H., Balleine, R. L., Huschtscha, L. I., Reddel, R. R., & Clarke, C. L. (2009). DNA replication licensing and progenitor numbers are increased by progesterone in normal human breast. Endocrinology, 150(7), 3318–3326. https://doi.org/10.1210/en.2008-1630

Harbeck, N., Penault-Llorca, F., Cortes, J., Gnant, M., Houssami, N., Poortmans, P., Ruddy, K., Tsang, J., & Cardoso, F. (2019). Breast cancer. In Nature Reviews Disease Primers (Vol. 5, Issue 1). https://doi.org/10.1038/s41572-019-0111-2

Hargreaves, D. C., & Crabtree, G. R. (2011). ATP-dependent chromatin remodeling: Genetics, genomics and mechanisms. Cell Research, 21(3), 396–420. https://doi.org/10.1038/cr.2011.32

He, L., Pratt, H., Gao, M., Wei, F., Weng, Z., & Struhl, K. (2021). Yap and taz are transcriptional co-activators of ap-1 proteins and stat3 during breast cellular transformation. ELife, 10, 1–26. https://doi.org/10.7554/eLife.67312

Heinz, S., Benner, C., Spann, N., Bertolino, E., Lin, Y. C., Laslo, P., Cheng, J. X., Murre, C., Singh, H., & Glass, C. K. (2010). Simple Combinations of Lineage-Determining Transcription Factors Prime cis-Regulatory Elements Required for Macrophage and B Cell Identities. Molecular Cell, 38(4), 576–589. https://doi.org/10.1016/j.molcel.2010.05.004

Hirai H, Tani T, Kikyo N. Structure and functions of powerful transactivators: VP16, MyoD and FoxA. Int J Dev Biol. 2010; 54 (11-12): 1589-96. doi: 10.1387/ijdb.103194hh.

Holehouse, A. S., & Kragelund, B. B. (2024). The molecular basis for cellular function of intrinsically disordered protein regions. Nature Reviews Molecular Cell Biology, 25(3), 187–211. https://doi.org/10.1038/s41580-023-00673-0

Horwitz, K. B., Dye, W. W., Harrell, J. C., Kabos, P., & Sartorius, C. A. (2008). Rare steroid receptor-negative basal-like tumorigenic cells in luminal subtype human breast cancer xenografts. Proceedings of the National Academy of Sciences of the United States of America, 105(15), 5774–5779. https://doi.org/10.1073/pnas.0706216105

Hurst C Lawrence, B. (1976). Mechanism of Action of the Sex Steroid Hormones (First of Three Parts). New England Journal of Medicine, 294(24), 1322–1328.

Jeon, S., Jeon, Y., Lim, J. Y., Kim, Y., Cha, B., & Kim, W. (2025). Emerging regulatory mechanisms and functions of biomolecular condensates: implications for therapeutic targets. In Signal Transduction and Targeted Therapy (Vol. 10, Issue 1). Springer US. https://doi.org/10.1038/s41392-024-02070-1

Jeselsohn R, Barry WT, Migliaccio I, Biagioni C, Zhao J, De Tribolet-Hardy J, Guarducci C, Bonechi M, Laing N, Winer EP, Brown M, Leo AD, Malorni L. TransCONFIRM: Identification of a Genetic Signature of Response to Fulvestrant in Advanced Hormone Receptor-Positive Breast Cancer. Clin Cancer Res. 2016 Dec 1;22(23):5755-5764. doi: 10.1158/1078-0432.CCR-16-0148.

Ji, D., Shao, C., Yu, J., Hou, Y., Gao, X., Wu, Y., Wang, L., & Chen, P. (2024). FOXA1 forms biomolecular condensates that unpack condensed chromatin to function as a pioneer factor. Molecular Cell, 84(2), 244-260.e7. https://doi.org/10.1016/j.molcel.2023.11.020

Jin, Y., Tam, O. H., Paniagua, E., & Hammell, M. (2015). TEtranscripts: A package for including transposable elements in differential expression analysis of RNA-seq datasets. Bioinformatics, 31(22), 3593–3599. https://doi.org/10.1093/bioinformatics/btv422

Juan, W. C., & Hong, W. (2016). Targeting the Hippo signaling pathway for tissue regeneration and cancer therapy. Genes, 7(9), 1–25. https://doi.org/10.3390/genes7090055

Justice, R. W., Zilian, O., Woods, D. F., Noll, M., & Bryant, P. J. (1995). The Drosophila tumor suppressor gene warts encodes a homolog of human myotonic dystrophy kinase and is required for the control of cell shape and proliferation. Genes and Development, 9(5), 534–546. https://doi.org/10.1101/gad.9.5.534

Kastan, N., Gnedeva, K., Alisch, T., Petelski, A. A., Huggins, D. J., Chiaravalli, J., Aharanov, A., Shakked, A., Tzahor, E., Nagiel, A., Segil, N., & Hudspeth, A. J. (2021). Small-molecule inhibition of Lats kinases may promote Yap-dependent proliferation in postmitotic mammalian tissues. Nature Communications, 12(1), 1–12. https://doi.org/10.1038/s41467-021-23395-3

Kato S, Endoh H, Masuhiro Y, Kitamoto T, Uchiyama S, Sasaki H, Masushige S, Gotoh Y, Nishida E, Kawashima H, Metzger D, Chambon P. Activation of the estrogen receptor through phosphorylation by mitogen-activated protein kinase. Science. 1995 Dec 1;270(5241):1491-4. doi: 10.1126/science.270.5241.1491. PMID: 7491495.

Kern, J. G., Tilston-Lunel, A. M., Federico, A., Ning, B., Mueller, A., Peppler, G. B., Stampouloglou, E., Cheng, N., Johnson, R. L., Lenburg, M. E., Beane, J. E., Monti, S., & Varelas, X. (2022). Inactivation of LATS1/2 drives luminal-basal plasticity to initiate basal-like mammary carcinomas. Nature Communications, 13(1). https://doi.org/10.1038/s41467-022-34864-8

Khan, J. A., Bellance, C., Guiochon-Mantel, A., Lombès, M., & Loosfelt, H. (2012). Differential Regulation of Breast Cancer-Associated Genes by Progesterone Receptor Isoforms PRA and PRB in a New Bi-Inducible Breast Cancer Cell Line. PLoS ONE, 7(9). https://doi.org/10.1371/journal.pone.0045993

Kim, D., Langmead, B., & Salzberg, S. L. (2015). HISAT: A fast spliced aligner with low memory requirements. Nature Methods, 12(4), 357–360. https://doi.org/10.1038/nmeth.3317

Kima, E., Kima, E., Kang, J. G., Kang, M. J., Park, J. H., Kim, Y. J., Kim, Y. J., Kweon, T. H., Kweon, T. H., Lee, H. W., Jho, E. H., Jho, E. H., Lee, Y. H., Kim, S. Il, Yi, E. C., Yi, E. C., Park, H. W., Yang, W. H., Yang, W. H., & Cho, J. W. (2020). O-GlcNAcylation on LATS2 disrupts the Hippo pathway by inhibiting its activity. Proceedings of the National Academy of Sciences of the United States of America, 117(25), 14259–14269. https://doi.org/10.1073/pnas.1913469117

Koo, J. H., & Guan, K. L. (2018). Interplay between YAP/TAZ and Metabolism. Cell Metabolism, 28(2), 196–206. https://doi.org/10.1016/j.cmet.2018.07.010

Kumar, Raj, Moure, C. M., Khan, S. H., Callaway, C., Grimm, S. L., Goswami, D., Griffin, P. R., & Edwards, D. P. (2013). Regulation of the structurally dynamic N-terminal domain of progesterone receptor by protein-induced folding. Journal of Biological Chemistry, 288(42), 30285–30299. https://doi.org/10.1074/jbc.M113.491787

Kumar, Ramesh, & Hong, W. (2024). Hippo Signaling at the Hallmarks of Cancer and Drug Resistance. Cells, 13(7). https://doi.org/10.3390/cells13070564

Kyriazoglou, A., Liontos, M., Zakopoulou, R., Kaparelou, M., Tsiara, A., Papatheodoridi, A. M., Georgakopoulou, R., & Zagouri, F. (2021). The Role of the Hippo Pathway in Breast Cancer Carcinogenesis, Prognosis, and Treatment: A Systematic Review. Breast Care, 16(1), 6–15. https://doi.org/10.1159/000507538

Lai, Z. C., Wei, X., Shimizu, T., Ramos, E., Rohrbaugh, M., Nikolaidis, N., Ho, L. L., & Li, Y. (2005). Control of cell proliferation and apoptosis by mob as tumor suppressor, mats. Cell, 120(5), 675–685. https://doi.org/10.1016/j.cell.2004.12.036

Lange, C. A., Shen, T., & Horwitz, K. B. (2000). Phosphorylation of human progesterone receptors at serine-294 by mitogen-activated protein kinase signals their degradation by the 26S proteasome. Proceedings of the National Academy of Sciences of the United States of America, 97(3), 1032–1037. https://doi.org/10.1073/pnas.97.3.1032

Langmead, B., & Salzberg, S. L. (2012). Fast gapped-read alignment with Bowtie 2. Nature Methods, 9(4), 357–359. https://doi.org/10.1038/nmeth.1923

Li, F. L., & Guan, K. L. (2022). The two sides of Hippo pathway in cancer. Seminars in Cancer Biology, 85(February 2021), 33–42. https://doi.org/10.1016/j.semcancer.2021.07.006

Li, H., Handsaker, B., Wysoker, A., Fennell, T., Ruan, J., Homer, N., Marth, G., Abecasis, G., & Durbin, R. (2009). The Sequence Alignment/Map format and SAMtools. Bioinformatics, 25(16), 2078–2079. https://doi.org/10.1093/bioinformatics/btp352

Li, K., Wu, R., Zhou, M., Tong, H., & Luo, K. Q. (2021). Desmosomal proteins of DSC2 and PKP1 promote cancer cells survival and metastasis by increasing cluster formation in circulatory system. Science Advances, 7(40), 1–20. https://doi.org/10.1126/sciadv.abg7265

Li, N., Lu, N., & Xie, C. (2019). The Hippo and Wnt signalling pathways: crosstalk during neoplastic progression in gastrointestinal tissue. FEBS Journal, 286(19), 3745–3756. https://doi.org/10.1111/febs.15017

Li, Xiaoxian, Lewis, M. T., Huang, J., Gutierrez, C., Osborne, C. K., Wu, M. F., Hilsenbeck, S. G., Pavlick, A., Zhang, X., Chamness, G. C., Wong, H., Rosen, J., & Chang, J. C. (2008). Intrinsic resistance of tumorigenic breast cancer cells to chemotherapy. Journal of the National Cancer Institute, 100(9), 672–679. https://doi.org/10.1093/jnci/djn123

Li, Xu, Zhuo, S., Cho, Y. S., Liu, Y., Yang, Y., Zhu, J., & Jiang, J. (2023). YAP antagonizes TEAD -mediated AR signaling and prostate cancer growth . The EMBO Journal, 42(4). https://doi.org/10.15252/embj.2022112184

Li, Xu, Zhuo, S., Zhuang, T., Cho, Y. S., Wu, G., Liu, Y., Mu, K., Zhang, K., Su, P., Yang, Y., Zhang, C. C., Zhu, J., & Jiang, J. (2022). YAP inhibits ERα and ER+ breast cancer growth by disrupting a TEAD-ERα signaling axis. Nature Communications, 13(1). https://doi.org/10.1038/s41467-022-30831-5

Li, Y. W., Shen, H., Frangou, C., Yang, N., Guo, J., Xu, B., Bshara, W., Shepherd, L., Zhu, Q., Wang, J., Hu, Q., Liu, S., Morrison, C. D., Sun, P., & Zhang, J. (2015). Characterization of TAZ domains important for the induction of breast cancer stem cell properties and tumorigenesis. Cell Cycle, 14(1), 146–156. https://doi.org/10.4161/15384101.2014.967106

Lin, K. C., Park, H. W., & Guan, K. L. (2017). Regulation of the Hippo Pathway Transcription Factor TEAD. Trends in Biochemical Sciences, 42(11), 862–872. https://doi.org/10.1016/j.tibs.2017.09.003

Liu, L., Graff, S. L., & Wang, Y. (2025). New Emerging Therapies Targeting PI3K/AKT/mTOR/PTEN Pathway in Hormonal Receptor-Positive and HER2-Negative Breast Cancer—Current State and Molecular Pathology Perspective. Cancers, 17(1), 1–12. https://doi.org/10.3390/cancers17010016

Liu, Y., Wu, W., Cai, C., Zhang, H., Shen, H., & Han, Y. (2023). Patient-derived xenograft models in cancer therapy: technologies and applications. Signal Transduction and Targeted Therapy, 8(1). https://doi.org/10.1038/s41392-023-01419-2

Li Z, Razavi P, Li Q, Toy W, Liu B, Ping C, Hsieh W, Sanchez-Vega F, Brown DN, Da Cruz Paula AF, Morris L, Selenica P, Eichenberger E, Shen R, Schultz N, Rosen N, Scaltriti M, Brogi E, Baselga J, Reis-Filho JS, Chandarlapaty S. Loss of the FAT1 Tumor Suppressor Promotes Resistance to CDK4/6 Inhibitors via the Hippo Pathway. Cancer Cell. 2018 Dec 10;34(6):893-905.e8. doi: 10.1016/j.ccell.2018.11.006.

Lonard DM, O'Malley BW. Nuclear receptor coregulators: modulators of pathology and therapeutic targets. Nature reviews Endocrinology. 2012;8(10):598-604. doi:10.1038/nrendo.2012.100

Love, M. I., Huber, W., & Anders, S. (2014). Moderated estimation of fold change and dispersion for RNA-seq data with DESeq2. Genome Biology, 15(12), 1–21. https://doi.org/10.1186/s13059-014-0550-8

Luo, J., & Li, P. (2022). Context-dependent transcriptional regulations of YAP/TAZ in stem cell and differentiation. Stem Cell Research and Therapy, 13(1), 1–11. https://doi.org/10.1186/s13287-021-02686-y

Manavathi, B., Samanthapudi, V. S. K., & Gajulapalli, V. N. R. (2014). Estrogen receptor coregulators and pioneer factors: The orchestrators of mammary gland cell fate and development. Frontiers in Cell and Developmental Biology, 2(AUG), 1–13. https://doi.org/10.3389/fcell.2014.00034

Martin, L. A., Ribas, R., Simigdala, N., Schuster, E., Pancholi, S., Tenev, T., Gellert, P., Buluwela, L., Harrod, A., Thornhill, A., Nikitorowicz-Buniak, J., Bhamra, A., Turgeon, M. O., Poulogiannis, G., Gao, Q., Martins, V., Hills, M., Garcia-Murillas, I., Fribbens, C., … Dowsett, M. (2017). Discovery of naturally occurring ESR1 mutations in breast cancer cell lines modelling endocrine resistance. Nature Communications, 8(1). https://doi.org/10.1038/s41467-017-01864-y

Mercogliano, M. F., Bruni, S., Mauro, F. L., & Schillaci, R. (2023). Emerging Targeted Therapies for HER2-Positive Breast Cancer. Cancers, 15(7). https://doi.org/10.3390/cancers15071987

Merenbakh-Lamin, K., Ben-Baruch, N., Yeheskel, A., Dvir, A., Soussan-Gutman, L., Jeselsohn, R., Yelensky, R., Brown, M., Miller, V. A., Sarid, D., Rizel, S., Klein, B., Rubinek, T., & Wolf, I. (2013). D538G mutation in estrogen receptor-α: A novel mechanism for acquired endocrine resistance in breast cancer. Cancer Research, 73(23), 6856–6864. https://doi.org/10.1158/0008-5472.CAN-13-1197

Messner, E. A., Steele, T. M., Tsamouri, M. M., Hejazi, N., Gao, A. C., Mudryj, M., & Ghosh, P. M. (2020). The androgen receptor in prostate cancer: Effect of structure, ligands and spliced variants on therapy. Biomedicines, 8(10), 1–19. https://doi.org/10.3390/biomedicines8100422

Migliaccio, A., Di Domenico, M., Castoria, G., De Falco, A., Bontempo, P., Nola, E., & Auricchio, F. (1996). Tyrosine kinase/p21ras/MAP-kinase pathway activation by estradiol-receptor complex in MCF-7 cells. EMBO Journal, 15(6), 1292–1300. https://doi.org/10.1002/j.1460-2075.1996.tb00471.x

Migliaccio, Antimo, Piccolo, D., Castoria, G., Domenico, M. Di, Bilancio, A., Lombardi, M., Gong, W., Beato, M., & Auricchio, F. (1998). Activation of the Src/p21(ras)/Erk pathway by progesterone receptor via cross-talk with estrogen receptor. EMBO Journal, 17(7), 2008–2018. https://doi.org/10.1093/emboj/17.7.2008

Montaser, R. Z., & Coley, H. M. (2018). Crosstalk between ERα and receptor tyrosine kinase signalling and implications for the development of anti-endocrine resistance. Cancers, 10(6). https://doi.org/10.3390/cancers10060209

Murayama, T., & Gotoh, N. (2019). Patient-derived xenograft models of breast cancer and their application. Cells, 8(6). https://doi.org/10.3390/cells8060621

Musgrove EA, Sutherland RL. Cell cycle control by steroid hormones. Semin Cancer Biol. 1994 Oct;5(5):381-9. PMID: 7849266.

Nacht, A Silvina, Ferrari, R., Zaurin, R., Scabia, V., Carbonell-Caballero, J., Le Dily, F., Quilez, J., Leopoldi, A., Brisken, C., Beato, M., & Vicent, G. P. (2019). C/EBPα mediates the growth inhibitory effect of progestins on breast cancer cells. The EMBO Journal, 38(18), 1–22. https://doi.org/10.15252/embj.2018101426

Nacht, Ana Silvina, Pohl, A., Zaurin, R., Soronellas, D., Quilez, J., Sharma, P., Wright, R. H., Beato, M., & Vicent, G. P. (2016). Hormone-induced repression of genes requires BRG 1-mediated H1.2 deposition at target promoters . The EMBO Journal, 35(16), 1822–1843. https://doi.org/10.15252/embj.201593260

Narayanan, R., Adigun, A. A., Edwards, D. P., & Weigel, N. L. (2005). Cyclin-Dependent Kinase Activity Is Required for Progesterone Receptor Function: Novel Role for Cyclin A/Cdk2 as a Progesterone Receptor Coactivator. Molecular and Cellular Biology, 25(1), 264–277. https://doi.org/10.1128/mcb.25.1.264-277.2005

Norman, A. W., Mizwicki, M. T., & Norman, D. P. G. (2004). Steroid-hormone rapid actions, membrane receptors and a conformational ensemble model. Nature Reviews Drug Discovery, 3(1), 27–41. https://doi.org/10.1038/nrd1283

Okimoto, T., Friedmann, T., & Miyanohara, A. (2001). VSV-G envelope glycoprotein forms complexes with plasmid DNA and MLV retrovirus-like particles in cell-free conditions and enhances DNA transfection. Molecular Therapy, 4(3), 232–238. https://doi.org/10.1006/mthe.2001.0443

Ou, Y., Wang, S. J., Li, D., Chu, B., & Gu, W. (2016). Activation of SAT1 engages polyamine metabolism with p53-mediated ferroptotic responses. Proceedings of the National Academy of Sciences of the United States of America, 113(44), E6806–E6812. https://doi.org/10.1073/pnas.1607152113

Patel, R., Klein, P., Tiersten, A., & Sparano, J. A. (2023). An emerging generation of endocrine therapies in breast cancer: a clinical perspective. Npj Breast Cancer, 9(1), 1–12. https://doi.org/10.1038/s41523-023-00523-4

Payvar, F., DeFranco, D., Firestone, G. L., Edgar, B., Wrange, Ö., Okret, S., Gustafsson, J. Å., & Yamamoto, K. R. (1983). Sequence-specific binding of glucocorticoid receptor to MTV DNA at sites within and upstream of the transcribed region. Cell, 35(2 PART 1), 381–392. https://doi.org/10.1016/0092-8674(83)90171-X

Pecci, A., Ogara, M. F., Sanz, R. T., & Vicent, G. P. (2022). Choosing the right partner in hormone-dependent gene regulation: Glucocorticoid and progesterone receptors crosstalk in breast cancer cells. Frontiers in Endocrinology, 13(November), 1–10. https://doi.org/10.3389/fendo.2022.1037177

Pedram, A., Razandi, M., Sainson, R. C. A., Kim, J. K., Hughes, C. C., & Levin, E. R. (2007). A conserved mechanism for steroid receptor translocation to the plasma membrane. Journal of Biological Chemistry, 282(31), 22278–22288. https://doi.org/10.1074/jbc.M611877200

Pedroza, D. A., Subramani, R., & Lakshmanaswamy, R. (2020). Classical and non-classical progesterone signaling in breast cancers. Cancers, 12(9), 1–16. https://doi.org/10.3390/cancers12092440

Pereira, B., Chin, S. F., Rueda, O. M., Vollan, H. K. M., Provenzano, E., Bardwell, H. A., Pugh, M., Jones, L., Russell, R., Sammut, S. J., Tsui, D. W. Y., Liu, B., Dawson, S. J., Abraham, J., Northen, H., Peden, J. F., Mukherjee, A., Turashvili, G., Green, A. R., … Caldas, C. (2016). The somatic mutation profiles of 2,433 breast cancers refines their genomic and transcriptomic landscapes. Nature Communications, 7(May). https://doi.org/10.1038/ncomms11479

Pratt, W. B., & Toft, D. O. (1997). Steroid receptor interactions with heat shock protein and immunophilin chaperones. Endocrine Reviews, 18(3), 306–360. https://doi.org/10.1210/er.18.3.306

Qian, X., He, L., Hao, M., Li, Y., Li, X., Liu, Y., Jiang, H., Xu, L., Li, C., Wu, W., Du, L., Yin, X., & Lu, Q. (2021). YAP mediates the interaction between the Hippo and PI3K/Akt pathways in mesangial cell proliferation in diabetic nephropathy. Acta Diabetologica, 58(1), 47–62. https://doi.org/10.1007/s00592-020-01582-w

Quinlan, A. R., & Hall, I. M. (2010). BEDTools: A flexible suite of utilities for comparing genomic features. Bioinformatics, 26(6), 841–842. https://doi.org/10.1093/bioinformatics/btq033

Ramírez-Cuéllar, J., Ferrari, R., Sanz, R. T., Valverde-Santiago, M., García-García, J., Nacht, A. S., Castillo, D., Le Dily, F., Neguembor, M. V., Malatesta, M., Bonnin, S., Marti-Renom, M. A., Beato, M., & Vicent, G. P. (2024). LATS1 controls CTCF chromatin occupancy and hormonal response of 3D-grown breast cancer cells. EMBO Journal, 43(9), 1770–1798. https://doi.org/10.1038/s44318-024-00080-x

Ramírez, F., Ryan, D. P., Grüning, B., Bhardwaj, V., Kilpert, F., Richter, A. S., Heyne, S., Dündar, F., & Manke, T. (2016). deepTools2: a next generation web server for deep-sequencing data analysis. Nucleic Acids Research, 44(W1), W160–W165. https://doi.org/10.1093/NAR/GKW257

Rayasam, G. V., Elbi, C., Walker, D. A., Wolford, R., Fletcher, T. M., Edwards, D. P., & Hager, G. L. (2005). Ligand-Specific Dynamics of the Progesterone Receptor in Living Cells and during Chromatin Remodeling In Vitro. Molecular and Cellular Biology, 25(6), 2406–2418. https://doi.org/10.1128/mcb.25.6.2406-2418.2005

Rayon T, Menchero S, Nieto A, Xenopoulos P, Crespo M, Cockburn K, Cañon S, Sasaki H, Hadjantonakis AK, de la Pompa JL, Rossant J, Manzanares M. Notch and hippo converge on Cdx2 to specify the trophectoderm lineage in the mouse blastocyst. Dev Cell. 2014 Aug 25;30(4):410-22. doi: 10.1016/j.devcel.2014.06.019.

Richer, J. K., Lange, C. A., Manning, N. G., Owen, G., Powell, R., & Horwitz, K. B. (1998). Convergence of progesterone with growth factor and cytokine signaling in breast cancer: Progesterone receptors regulate signal transducers and activators of transcription expression and activity. Journal of Biological Chemistry, 273(47), 31317–31326. https://doi.org/10.1074/jbc.273.47.31317

Robinson, J. L. L., & Carroll, J. S. (2012). FoxA1 is a key mediator of hormonal response in breast and prostate cancer. Frontiers in Endocrinology, 3(MAY), 1–6. https://doi.org/10.3389/fendo.2012.00068

Romagnolo, D. F., Zempleni, J., & Selmin, O. I. (2014). Nuclear receptors and epigenetic regulation: Opportunities for nutritional targeting and disease prevention. Advances in Nutrition, 5(4), 373–385. https://doi.org/10.3945/an.114.005868

Saadh, M. J., Ahmed, H. H., Kareem, R. A., Bishoyi, A. K., Roopashree, R., Shit, D., Arya, R., Sharma, A., Khaitov, K., Sameer, H. N., Yaseen, A., Athab, Z. H., & Adil, M. (2025). Molecular mechanisms of Hippo pathway in tumorigenesis: therapeutic implications. Molecular Biology Reports, 52(1), 1–17. https://doi.org/10.1007/s11033-025-10372-y

Saha, S., Dey, S., & Nath, S. (2021). Steroid Hormone Receptors: Links With Cell Cycle Machinery and Breast Cancer Progression. Frontiers in Oncology, 11(March), 1–11. https://doi.org/10.3389/fonc.2021.620214

Sancho, M., Diani, E., Beato, M., & Jordan, A. (2008). Depletion of human histone H1 variants uncovers specific roles in gene expression and cell growth. PLoS Genetics, 4(10). https://doi.org/10.1371/journal.pgen.1000227

Savkur, R. S., & Burris, T. P. (2004). The coactivator LXXLL nuclear receptor recognition motif. Journal of Peptide Research, 63(3), 207–212. https://doi.org/10.1111/j.1399-3011.2004.00126.x

Schindelin, J., Arganda-Carreras, I., Frise, E., Kaynig, V., Longair, M., Pietzsch, T., Preibisch, S., Rueden, C., Saalfeld, S., Schmid, B., Tinevez, J. Y., White, D. J., Hartenstein, V., Eliceiri, K., Tomancak, P., & Cardona, A. (2012). Fiji: An open-source platform for biological-image analysis. Nature Methods, 9(7), 676–682. https://doi.org/10.1038/nmeth.2019

Severson, T. M., Kim, Y., Joosten, S. E. P., Schuurman, K., Van Der Groep, P., Moelans, C. B., Ter Hoeve, N. D., Manson, Q. F., Martens, J. W., Van Deurzen, C. H. M., Barbe, E., Hedenfalk, I., Bult, P., Smit, V. T. H. B. M., Linn, S. C., Van Diest, P. J., Wessels, L., & Zwart, W. (2018). Characterizing steroid hormone receptor chromatin binding landscapes in male and female breast cancer. Nature Communications, 9(1), 1–12. https://doi.org/10.1038/s41467-018-02856-2

Sheikh, M. S., & Satti, S. A. (2021). The emerging CDK4/6 inhibitor for breast cancer treatment. Molecular and Cellular Pharmacology, 13(3), 9–12. https://doi.org/10.4255/mcpharmacol.21.01

Shen, K., Yu, H., Xie, B., Meng, Q., Dong, C., Shen, K., & Zhou, H. B. (2023). Anticancer or carcinogenic? The role of estrogen receptor β in breast cancer progression. Pharmacology and Therapeutics, 242, 108350. https://doi.org/10.1016/j.pharmthera.2023.108350

Shrinivas, K., Sabari, B. R., Coffey, E. L., Klein, I. A., Zamudio, A. V, Schuijers, J., Hannett, N. M., Sharp, P. A., Young, R. A., & Chakraborty, A. K. (2020). HHS Public Access. 75(3), 549–561. https://doi.org/10.1016/j.molcel.2019.07.009.Enhancer

Stallcup MR, Poulard C. Gene-Specific Actions of Transcriptional Coregulators Facilitate Physiological Plasticity: Evidence for a Physiological Coregulator Code. Trends Biochem Sci. 2020 Jun;45(6):497-510. doi: 10.1016/j.tibs.2020.02.006.

Stender, J. D., Kim, K., Charn, T. H., Komm, B., Chang, K. C. N., Kraus, W. L., Benner, C., Glass, C. K., & Katzenellenbogen, B. S. (2010). Genome-Wide Analysis of Estrogen Receptor α DNA Binding and Tethering Mechanisms Identifies Runx1 as a Novel Tethering Factor in Receptor-Mediated Transcriptional Activation. Molecular and Cellular Biology, 30(16), 3943–3955. https://doi.org/10.1128/mcb.00118-10

Strutt, H., Paro, R. (1999). Mapping DNA Target Sites of Chromatin Proteins In Vivo by Formaldehyde Crosslinking. In: Becker, P.B. (eds) Chromatin Protocols. Methods in Molecular Biology™, vol 119. Humana Press. https://doi.org/10.1385/1-59259-681-9:455

Takaku, M., Grimm, S. A., De Kumar, B., Bennett, B. D., & Wade, P. A. (2020). Cancer-specific mutation of GATA3 disrupts the transcriptional regulatory network governed by Estrogen Receptor alpha, FOXA1 and GATA3. Nucleic Acids Research, 48(9), 4756–4768. https://doi.org/10.1093/nar/gkaa179

Takaku, M., Grimm, S. A., & Wade, P. A. (2015). GATA3 in breast cancer: Tumor suppressor or oncogene? Gene Expression, 16(4), 163–168. https://doi.org/10.3727/105221615X14399878166113

Talukdar, P. D., & Chatterji, U. (2023). Transcriptional co-activators: emerging roles in signaling pathways and potential therapeutic targets for diseases. Signal Transduction and Targeted Therapy, 8(1). https://doi.org/10.1038/s41392-023-01651-w

Tao W, Zhang S, Turenchalk GS, Stewart RA, St John MA, Chen W, Xu T. Human homologue of the Drosophila melanogaster lats tumour suppressor modulates CDC2 activity. Nat Genet. 1999 Feb;21(2):177-81. doi: 10.1038/5960. PMID: 9988268.

Tapon, N., Harvey, K. F., Bell, D. W., Wahrer, D. C. R., Schiripo, T. A., Haber, D. A., & Hariharan, I. K. (2002). salvador promotes both cell cycle exit and apoptosis in Drosophila and is mutated in human cancer cell lines. Cell, 110(4), 467–478. https://doi.org/10.1016/S0092-8674(02)00824-3

Tetel, M. J., Auger, A. P., & Charlier, T. D. (2009). Who's in charge? Nuclear receptor coactivator and corepressor function in brain and behavior. Frontiers in Neuroendocrinology, 30(3), 328–342. https://doi.org/10.1016/j.yfrne.2009.04.008

Theodorou, V., Stark, R., Menon, S., & Carroll, J. S. (2013). GATA3 acts upstream of FOXA1 in mediating ESR1 binding by shaping enhancer accessibility. Genome Research, 23(1), 12–22. https://doi.org/10.1101/gr.139469.112

Thompson, B. J. (2020). YAP/TAZ: Drivers of Tumor Growth, Metastasis, and Resistance to Therapy. BioEssays, 42(5), 1–16. https://doi.org/10.1002/bies.201900162

Tian, J. M., Ran, B., Zhang, C. L., Yan, D. M., & Li, X. H. (2018). Estrogen and progesterone promote breast cancer cell proliferation by inducing cyclin G1 expression. Brazilian Journal of Medical and Biological Research, 51(3), 1–7. https://doi.org/10.1590/1414-431X20175612

Tian Xu, Weiyi Wang, Sheng Zhang, Rodney A. Stewart, Wan Yu; Identifying tumor suppressors in genetic mosaics: the Drosophila lats gene encodes a putative protein kinase. Development 1 April 1995; 121 (4): 1053–1063. doi: https://doi.org/10.1242/dev.121.4.1053

Varelas, X., Sakuma, R., Samavarchi-Tehrani, P., Peerani, R., Rao, B. M., Dembowy, J., Yaffe, M. B., Zandstra, P. W., & Wrana, J. L. (2008). TAZ controls Smad nucleocytoplasmic shuttling and regulates human embryonic stem-cell self-renewal. Nature Cell Biology, 10(7), 837–848. https://doi.org/10.1038/ncb1748

Varlakhanova, N., Snyder, C., Jose, S., Hahm, J. B., & Privalsky, M. L. (2010). Estrogen Receptors Recruit SMRT and N-CoR Corepressors through Newly Recognized Contacts between the Corepressor N Terminus and the Receptor DNA Binding Domain. Molecular and Cellular Biology, 30(6), 1434–1445. https://doi.org/10.1128/mcb.01002-09

Vicent, G. P., Ballaré, C., Nacht, A. S., Clausell, J., Subtil-Rodríguez, A., Quiles, I., Jordan, A., & Beato, M. (2006). Induction of Progesterone Target Genes Requires Activation of Erk and Msk Kinases and Phosphorylation of Histone H3. Molecular Cell, 24(3), 367–381. https://doi.org/10.1016/j.molcel.2006.10.011

Vicent, G. P., Ballaré, C., Nacht, A. S., Clausell, J., Subtil-Rodríguez, A., Quiles, I., Jordan, A., & Beato, M. (2008). Convergence on chromatin of non-genomic and genomic pathways of hormone signaling. Journal of Steroid Biochemistry and Molecular Biology, 109(3–5), 344–349. https://doi.org/10.1016/j.jsbmb.2008.03.015

Vicent, G. P., Nacht, A. S., Zaurín, R., Ballaré, C., Clausell, J., & Beato, M. (2010). Minireview: Role of kinases and chromatin remodeling in progesterone signaling to chromatin. Molecular Endocrinology, 24(11), 2088–2098. https://doi.org/10.1210/me.2010-0027

Vignali M, Hassan AH, Neely KE, Workman JL. ATP-dependent chromatin-remodeling complexes. Mol Cell Biol. 2000 Mar;20(6):1899-910. doi: 10.1128/MCB.20.6.1899-1910.2000.

Weikum, E. R., Liu, X., & Ortlund, E. A. (2018). The nuclear receptor superfamily: A structural perspective. Protein Science, 27(11), 1876–1892. https://doi.org/10.1002/pro.3496

Wiench, M., Miranda, T. B., & Hager, G. L. (2011). Control of nuclear receptor function by local chromatin structure. FEBS Journal, 278(13), 2211–2230. https://doi.org/10.1111/j.1742-4658.2011.08126.x

Won, S. J., Zhang, Y., Reinhardt, C. J., MacRae, N. S., DeMeester, K. E., Njomen, E., Hargis, L. M., Remsberg, J. R., Melillo, B., Cravatt, B. F., & Erb, M. A. (2024). Redirecting the pioneering function of FOXA1 with covalent small molecules. BioRxiv, 84(21), 2024.03.21.586158. https://doi.org/10.1016/j.molcel.2024.09.024

Xu T, Wang W, Zhang S, Stewart RA, Yu W. Identifying tumor suppressors in genetic mosaics: the Drosophila lats gene encodes a putative protein kinase. Development. 1995 Apr;121(4):1053-63. doi: 10.1242/dev.121.4.1053.

Yu, S., Cai, X., Wang, X., Lin, X., & Cai, S. (2024). Disease burden of breast cancer and risk factors in Europe 44 countries, 1990-2019: findings of the global burden of disease study 2019. Frontiers in Endocrinology, 15(May), 1–9. https://doi.org/10.3389/fendo.2024.1405204

Zanconato, F., Cordenonsi, M., & Piccolo, S. (2016). YAP/TAZ at the Roots of Cancer. Cancer Cell, 29(6), 783–803. https://doi.org/10.1016/j.ccell.2016.05.005

Zaurin, R., Ferrari, R., Nacht, A. S., Carbonell, J., Le Dily, F., Font-Mateu, J., Cucalon, L. I. de L., Vidal, E., Lioutas, A., Beato, M., & Vicent, G. P. (2021). A set of accessible enhancers enables the initial response of breast cancer cells to physiological progestin concentrations. Nucleic Acids Research, 49(22), 12716–12731. https://doi.org/10.1093/nar/gkab1125

Zeng, R., & Dong, J. (2021). The hippo signaling pathway in drug resistance in cancer. Cancers, 13(2), 1–23. https://doi.org/10.3390/cancers13020318

Zhang, Y., Liu, T., Meyer, C. A., Eeckhoute, J., Johnson, D. S., Bernstein, B. E., Nussbaum, C., Myers, R. M., Brown, M., Li, W., & Shirley, X. S. (2008). Model-based analysis of ChIP-Seq (MACS). Genome Biology, 9(9). https://doi.org/10.1186/gb-2008-9-9-r137

Zhao, B., Li, L., Tumaneng, K., Wang, C. Y., & Guan, K. L. (2010). A coordinated phosphorylation by Lats and CK1 regulates YAP stability through SCFβ-TRCP. Genes and Development, 24(1), 72–85. https://doi.org/10.1101/gad.1843810

Zhou, B. R., Feng, H., Huang, F., Zhu, I., Portillo-Ledesma, S., Shi, D., Zaret, K. S., Schlick, T., Landsman, D., Wang, Q., & Bai, Y. (2024). Structural insights into the cooperative nucleosome recognition and chromatin opening by FOXA1 and GATA4. Molecular Cell, 84(16), 3061-3079.e10. https://doi.org/10.1016/j.molcel.2024.07.016

Zhu, C., Li, L., Zhang, Z., Bi, M., Wang, H., Su, W., Hernandez, K., Liu, P., Chen, J., Chen, M., Huang, T. H. M., Chen, L., & Liu, Z. (2019). A Non-canonical Role of YAP/TEAD Is Required for Activation of Estrogen-Regulated Enhancers in Breast Cancer. Molecular Cell, 75(4), 791-806.e8. https://doi.org/10.1016/j.molcel.2019.06.010

Annex

Article

SOURCE DATA | TRANSPARENT PROCESS | OPEN ACCESS | CHECK FOR UPDATES

THE EMBO JOURNAL

LATS1 controls CTCF chromatin occupancy and hormonal response of 3D-grown breast cancer cells

Julieta Ramírez-Cuéllar[1,2,8], Roberto Ferrari[1,7,8], Rosario T Sanz[3], Marta Valverde-Santiago[3], Judith García-García[3], A Silvina Nacht[1], David Castillo[4], Francois Le Dily[1], Maria Victoria Neguembor[1], Marco Malatesta[5], Sarah Bonnin[1], Marc A Marti-Renom[1,2,4,6], Miguel Beato[1,2] & Guillermo P Vicent[1,3]✉

Abstract

The cancer epigenome has been studied in cells cultured in two-dimensional (2D) monolayers, but recent studies highlight the impact of the extracellular matrix and the three-dimensional (3D) environment on multiple cellular functions. Here, we report the physical, biochemical, and genomic differences between T47D breast cancer cells cultured in 2D and as 3D spheroids. Cells within 3D spheroids exhibit a rounder nucleus with less accessible, more compacted chromatin, as well as altered expression of ~2000 genes, the majority of which become repressed. Hi-C analysis reveals that cells in 3D are enriched for regions belonging to the B compartment, have decreased chromatin-bound CTCF and increased fusion of topologically associating domains (TADs). Upregulation of the Hippo pathway in 3D spheroids results in the activation of the LATS1 kinase, which promotes phosphorylation and displacement of CTCF from DNA, thereby likely causing the observed TAD fusions. 3D cells show higher chromatin binding of progesterone receptor (PR), leading to an increase in the number of hormone-regulated genes. This effect is in part mediated by LATS1 activation, which favors cytoplasmic retention of YAP and CTCF removal.

Keywords Three-dimensional Cell Growth; Breast Cancer; CTCF; LATS1 Kinase and Hormonal Response
Subject Categories Cancer; Signal Transduction
https://doi.org/10.1038/s44318-024-00080-x
Received 15 May 2023; Revised 5 February 2024; Accepted 27 February 2024
Published online: 2 April 2024

Introduction

Over the years, two-dimensional (2D) cultures have been used to improve our understanding of cellular signaling pathways and to decode the mechanisms deregulated in many diseases, including cancer. Yet, in recent years increasing evidence showed that 2D cultures do not fully reflect the complexity of the microenvironment encountered by cells as part of tissues or organs, endorsing the use of three-dimensional (3D) culture conditions generated by the presence of more physiological extracellular milieu (Kim et al, 2020). Within tissues, cells are exposed to a complex environment, including blood-circulating molecules, neighboring cells, and the extracellular matrix (ECM). 3D cell culture systems have been experimented for decades (Barcellos-Hoff et al, 1989) and the importance of the ECM in cell behavior and gene expression is now well accepted.

The Hippo pathway is one of the several routes that have been reported to respond to the cell's environment. In mammals, the core Hippo pathway is characterized by serine/threonine kinases; mammalian Sterile 20-related 1 and 2 kinases (MST1 and MST2), and Large Tumor Suppressor 1 and 2 kinases (LATS1 and LATS2). The transcriptional co-activators Yes-associated protein (YAP) and the Transcriptional coactivator with PDZ-binding motif (TAZ) act as nuclear relays of mechanical signals exerted by ECM rigidity and cell shape (Dupont et al, 2011). It has been previously described that on soft substrates, YAP is inactivated by LATS-dependent phosphorylation on serine 127 and later tagged for degradation in the cytoplasm (Meng et al, 2016). The unphosphorylated YAP translocates into the cell nucleus followed by the regulation of gene transcription (Zanconato et al, 2016). LATS1 and LATS2 (LATS) have emerged as central regulators of cell fate, and modulate the functions of numerous oncogenic or tumor suppressive effectors, including YAP/TAZ, the Aurora mitotic kinase family and the tumor suppressive transcription factor p53 (Furth and Aylon, 2017). Except for YAP, not many substrates have been described for LATS, however, it was recently reported that LATS can phosphorylate the architectural protein CTCF within its zinc finger (ZF) linkers, reducing their affinity for DNA (Luo et al, 2020).

In breast cancer cells, steroid hormones are key regulators of cell differentiation and proliferation. The steroid hormones estrogens and progesterone acting via their specific receptors (ERα and PR, respectively) control the proliferation of breast cancer cells in a very

[1]Center for Genomic Regulation (CRG), Barcelona Institute for Science and Technology (BIST) Barcelona, Barcelona, Spain. [2]Universitat Pompeu Fabra (UPF), Barcelona, Spain. [3]Molecular Biology Institute of Barcelona, Consejo Superior de Investigaciones Científicas (IBMB-CSIC), C/ Baldiri Reixac, 4-8, 08028 Barcelona, Spain. [4]CNAG-CRG, Centre for Genomic Regulation, The Barcelona Institute of Science and Technology, Baldiri Reixac 4, Barcelona 08028, Spain. [5]Department of Chemistry, Life Sciences and Environmental Sustainability, University of Parma, Parma, Italy. [6]ICREA, Barcelona, Spain. [7]Present address: Department of Chemistry, Life Sciences and Environmental Sustainability, University of Parma, Parma, Italy. [8]These authors contributed equally: Julieta Ramirez Cuellar, Roberto Ferrari. ✉E-mail: gvmbmc@ibmb.csic.es

different way. While estrogens are inducers of cell proliferation that activate cyclin D1 (Musgrove et al, 1994; Planas-Silva et al, 1999) and decrease the expression of CDK inhibitors (Prall et al, 1997), progestins promote a single-cell cycle followed by proliferation arrest at G1/S, that correlates with a delayed activation of CDK inhibitor $p21^{WAF1}$ (Owen et al, 1998).

The activated receptors of estrogens and progesterone regulate gene expression mainly by interacting with specific DNA sequences in chromatin and recruiting chromatin remodeling complexes and transcriptional coregulators (Beato et al, 1995). In addition, a minor fraction of ERα and PR is attached to the cell membrane via palmitoylation of a conserved cysteine. Binding of the hormone to this membrane-attached receptors can activate the Src/Erk/Msk1 and CyclinA/CDK2 signaling cascades (Migliaccio et al, 1996; Vicent et al, 2006; Vicent et al, 2011), leading to PR activation via phosphorylation at S294, binding to progesterone responsive elements, and modulation of chromatin structure as prerequisite for gene regulation (Beato and Vicent, 2011). One limitation of these results is that they were obtained from breast cancer cells cultured as monolayer ignoring other physiological signaling pathways, such as the Hippo pathway. Although progress has been made toward understanding the roles of LATS in tumorigenesis, the kinase substrates or downstream target proteins mediating LATS function remain largely unknown.

In this work, we try to overcome this limitation by cultivating T47D breast cancer cells as spheroids in Matrigel (3D) and compared the results with those obtained with the same cells grown in monolayer on plastic (2D). We found that compared to 2D-grown cells, the nucleus of the 3D cells is more rounded and exhibits a larger surface, a more compact chromatin and a distinctive set of 1700 downregulated genes. Using Hi-C assays, we did not detect strong differences at the genome structural level between cells grown in 3D and those gown in 2D, but only a modest increase in the B-compartment regions and a tendency to TAD fusions. However, we did observe an increase in LATS1 kinase activity in 3D-grown cells, which triggered the displacement of the architectural protein CTCF from 75% of its genomic binding regions, including the promoters of genes regulated in 3D. Despite less accessible chromatin in 3D, hormone regulation was more pronounced compared to 2D, with more responsive genes and more extensive PR binding.

Results

Characterization of T47D-derived spheroids

To explore how the extracellular matrix (ECM) and cell-cell contacts impact on the structure and function of the cell nucleus, we grew breast tubular epithelial cells on Matrigel, to enable the formation of three-dimensional (3D) structures. We cultured breast cancer cell lines MCF10A, T47D, MCF-7; BT-474, and ZR-75-1 on plastic (2D) or embedded on Matrigel (3D), for 10 days, the time required to form multicellular acini (Appendix Fig. S1A). While T47D cells formed spheroids containing proliferating cells, the non-tumorigenic MCF10A cells formed round structures with a polarized acinar internal pattern (Fig. 1A,B). The other tumorigenic cell lines (MCF-7 and BT-474) cultured on Matrigel also form spheroids, as previously reported (Lee et al, 2007) (Appendix Fig. S1A). In this study, we focused on PR + T47D cells as a model system. These cells are known for their robust responsiveness to the hormone progesterone, and their genomic structure, the PR cistrome, and the associated signaling pathway network have been extensively characterized (Ballare et al, 2013; Le Dily et al, 2014; Le Dily et al, 2019; Vicent et al, 2006; Vicent et al, 2010; Zaurin et al, 2021).

We performed a functional and phenotypic characterization of the T47D spheroids. First, we assessed the physical properties of the cell nuclei in the spheroids compared to 2D by implementing IMARIS and ImageJ tools (Martin et al, 2021). The nuclear volume of 3D cells, measured after DAPI staining, was significantly enlarged compared to the 2D cell nuclei (488.7 μm^3 vs. 408.5 μm^3, P value < 0.001, Appendix Fig. S1B, left panel) while the diameter of the 3D nuclei was smaller (9.17 µm vs.15.56 µm, p value < 0.001, Appendix Fig. S1B, middle panel). This translates into an increased sphericity coefficient of the 3D nuclei (0.74 vs. 0.57 in 2D, P value < 0.001, Appendix Fig. S1B, right panel) and a larger surface area (643.3 μm^2 vs. 381.6 μm^2, P value < 0.001, Appendix Fig. S1B, lower panel).

We also evaluated the proliferation capacity of T47D cells cultured in 3D compared to cells grown in 2D. We found that 3D cells proliferated at a rate 2.6 times faster than its 2D counterpart (Fig. 1C, left panel). Within 10 days of culture the 3D cells formed spheroids with an average diameter of 100 µm, typically comprising 119 ± 12 cells (Fig. 1C, right panel). The increased cell proliferation detected in 3D cells was in accordance to the high levels of Ki67-positive cells detected in the spheres, also evident by using a live/dead cell imaging Kit (Appendix Fig. S2A).

Next, we probed the signaling pathways known to be regulated in cells grown in 3D conditions, such as the Hippo and the Focal Adhesion Kinase (FAK/ PTK2) pathways. In 3D-cultured breast cancer cells, YAP displayed higher level of phosphorylation on S127 compared to 2D, while total YAP levels remained unchanged (Fig. 1D, left panel). YAP was also found largely in the cytoplasm of 3D-grown cells (Fig. 1D, right panels), as previously described (Zanconato et al, 2019). In contrast, in 2D cells, the Hippo pathway was switched off and YAP mainly found into the nucleus (Fig. 1D, top right panels). When probing the FAK/PTK2 pathways, we found p-FAK severely deregulated in 3D cells, as indicated by its significant reduction in FAK-Y397 phosphorylation, compared to the levels found in 2D cells (Fig. 1E), despite no changes in total FAK levels (Fig. 1E). Therefore, in 3D-grown cells the presence of a less stiff environment is sensed, integrated and transduced leading to both repression of focal adhesion and activation of the Hippo pathway.

Increased levels of phospho-LATS (part of the Hippo pathway) in response to 3D cell growth was also observed in ER^+ MCF-7 cells. However, this activation was less pronounced in comparison to T47D cells (Appendix Fig. S1C compared to Fig. 5B). Notably, there was no significant increase in pYAP or decrease in p-FAK in MCF-7 cells, where YAP expression notably remained low in comparison to other mammary cell lines (Appendix Fig. S1C, lower panel). This observation indicates a partial conservation of the cytosolic activation of the Hippo pathway in response to 3D in MCF-7 cells. (Appendix Fig. S1C). In addition, it is worth mentioning that reduced ER levels in MCF-7 3D cells (Appendix Fig. S1C) had an impact on their proliferative capacity.

To investigate whether these changes in signaling, shape, surface and volume of the 3D nucleus impact on gene activity, we performed

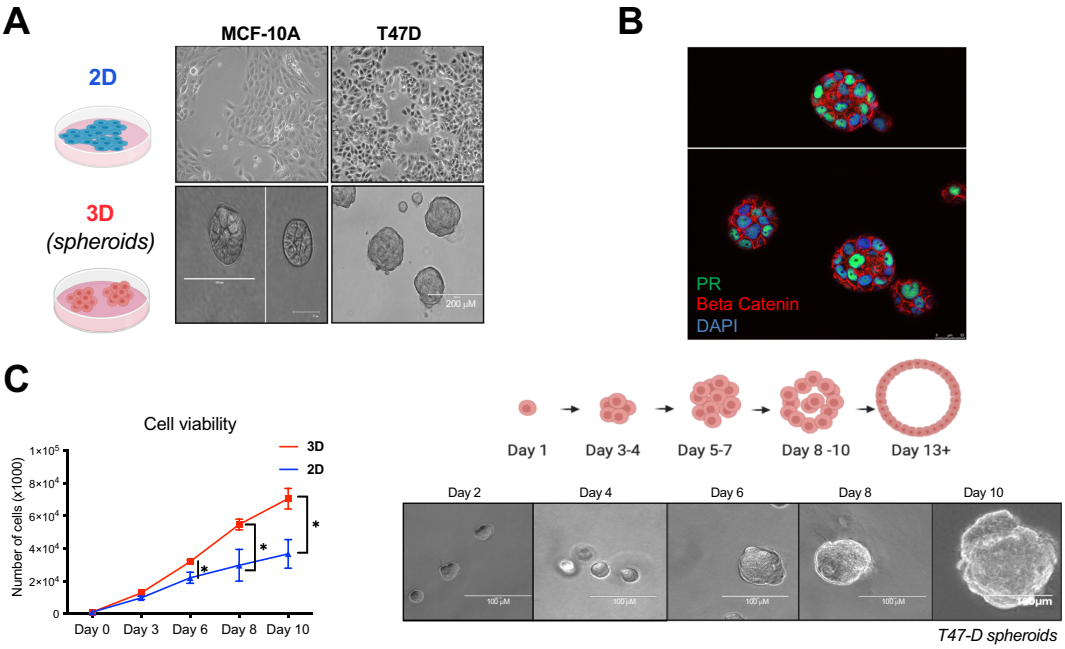
A
MCF-10A
T47D
2D
3D
(spheroids)
200 µM
B
PR
Beta Catenin
DAPI
C
Cell viability
Number of cells (x1000)
3D
2D
Day 0
Day 3
Day 6
Day 8
Day 10
Day 1
Day 3-4
Day 5-7
Day 8 -10
Day 13+
Day 2
Day 4
Day 6
Day 8
Day 10
T47-D spheroids
D
2D
3D
pYAP-S127
YAP
GAPDH
YAP
DAPI
Merge
nuclear YAP
cytoplasmic YAP
E
pFAK-Y397
FAK
GAPDH
F
Gene expression
2D vs 3D
up (619)
down (1758)
P-value < 0.05
FC=1.5
Log2 FC 3D vs 2D
Log2 P-value
Rep 1
Rep 2
Rep 3
Rep 4
Activated
Repressed
Log2 FC 3D vs 2D
Normalized Enrichment Score
Ribosome
Mineral absorption
Arginine and proline metabolism
Histidine metabolism
Phenylalanine metabolism
Salivary secretion
Hedgehog signaling pathway
Melanogenesis
Glycosphingolipid biosynthesis
Alcoholism
Legionellosis
Hypertrophic cardiomyopathy (HCM)
Hippo signaling pathway
Cardiac muscle contraction
Toxoplasmosis
Apelin signaling pathway
Th1 and Th2 cell differentiation
Cytokine-cytokine receptor interaction
Vascular smooth muscle contraction
Transcriptional misregulation in cancer
Activated
Repressed
Normalized Enrichment Score
Major Hippo Pathway targets

Figure 1. Evaluation of cell growth, signaling pathways, and differentially expressed genes in T47D cells grown in 3D and 2D conditions.

(A) Comparison of MCF10A and T47D breast cell lines grown on the plastic dish 2D and as 3D culture in Matrigel. **(B)** Immunofluorescence analysis showed that PR expression is conserved in 3D T47D cells. **(C)** Cell proliferation assays performed in 2D and 3D cells (left panel). The growth of 3D T47D cells over a period of 10 days to reach an estimated size of 100 µm is depicted (right panel). **(D)** Increased levels of YAP protein phosphorylation (pYAP-S127) in 3D was assessed by western blot (left panel). Immunostaining of Hippo pathway effector YAP in 2D and 3D T47D cells. When cells are grown in 3D conditions YAP is phosphorylated and re-localized to the cytoplasm (right panel). **(E)** T47D cells in grown in a 3D downregulate phosphorylation of FAK and its downstream pathways. **(F)** RNA-seq Differential Expression Analysis (DEA), performed in 2D and 3D T47D cells using [log2FC = 2 and *P* value < 0.05], the experiment reveals over 2300 genes deregulated when cells were grown in 3D (left panel). Using the DEA results 3D/2D, enriched signaling pathways (KEGG) are shown, FDR < 0.05 (right panel). Source data are available online for this figure.

RNA-seq analysis in T47D cells grown in 2D and 3D. The transcriptional profiles of 2D and 3D samples, yielded statistically significant changes for 2377 transcripts: 619 were upregulated and 1758 were downregulated in 3D-cultured cells compared to 2D cells [log2FC = 2 and *P* value < 0.05] (Fig. 1F). Gene Ontology analysis of biological processes and cellular compartments showed that cultivating cells in 3D lead to upregulation of genes enriched in terms associated to neurogenesis, nervous system development, axon genesis and neuronal projection. While 3D downregulated genes were overrepresented in cell and focal adhesion, cell junction and cell periphery (Appendix Fig. S3A). These results suggest that cells cultured in 3D possess a unique gene expression program that recapitulates neuronal growth and, additionally, decreases the expression of genes associated to adhesion, most likely due to the presence of a less stiff environment compared to 2D. The similarities between growth as 3D spheres and the nervous system has been previously proposed (Caswell and Zech, 2018). Further analysis of KEGG-exclusive 3D pathways showed terms related to *Ribosome*, *Mineral Absorption* and *Amino acid Metabolism* for 3D upgenes (Fig. 1F, right panel). The physical characteristics of the surrounding structure play a pivotal role in coordinating this regulatory interplay. Concerning *Amino acid Metabolism*, the stiffness of the extracellular matrix regulates the activation of the Hippo pathway and, consequently, the nuclear localization of YAP/TAZ. YAP/TAZ play a critical role in controlling genes involved in amino acid synthesis, transport and metabolism (Ge et al, 2021). Therefore, in response to the mechanical properties of their environment, cells adjust amino acid metabolism to acquire the energy necessary for specific cellular functions, such as enhanced cell proliferation, as illustrated in Fig. 1C.

Extracellular matrix stiffness also influences *Mineral Absorption*, as previously documented (Derricks et al, 2015). Cells on softer substrates (4 kPa) demonstrate increased responsiveness to VEGF, while cells on stiffer substrates (125 kPa) exhibit a diminished response.

The enrichment of genes related to *Ribosomes* suggests that protein synthesis is differentially regulated in 3D environments. This may be attributed to the unique demand for specialized proteins involved in cell-cell interactions, the integration of external signals, and mechano-transduction, especially in cells growing as spheres with low stiffness. In summary, the regulation of genes associated with *Amino acid Metabolism*, *Mineral Absorption*, and *Ribosomes* in 3D environments underscores the significant influence of extracellular matrix stiffness on various cellular processes. This intricate interplay allows cells to adapt to their mechanical surroundings, ultimately affecting crucial aspects of cell biology and physiology.

The 3D-repressed genes exhibit an enrichment in genes associated with *Transcriptional deregulation in Cancer*, the *Hippo* and *Apelin pathways*, among others. The Apelin pathway is not well-documented in breast cancer, with only one report associating high levels of Apelin with postmenopausal breast cancer (Salman et al, 2016). However, genes involved in vasodilation and *Muscle Contraction* are significantly repressed, which could be explained as an adaptation to the softer 3D environment. The suppression of these pathways could also be linked to the upregulation of *Mineral Absorption* pathway, as calcium ions (Ca2+) can regulate the contractility of vascular smooth muscle cells (Brozovich et al, 2016).

Next, we asked whether the changes in gene expression that we observed in 3D-grown cells (Fig. 1F) were due to changes in histone acetylation. To this end, cells grown in 2D and 3D were subjected to ChIP-seq of H3K27ac and H3K18ac, two marks strongly associated to gene expression (Ferrari et al, 2012; Wang et al, 2008). In general, a notable variation, ranging from 20% to 44%, was observed in the two marks when cells transitioned from 2D to 3D culture conditions (Appendix Fig. S4A,B). These alterations were particularly concentrated in genes influenced by the growth environment. Consequently, a substantial reduction in H3K27ac was detected for genes downregulated and upregulated in 3D (Appendix Fig. S4C), along with an increase in H3K18ac for genes upregulated in 3D (Appendix Fig. S4D, right panel), as compared to their 2D counterparts.

RNA polymerase 2 (pol2) which globally did not show drastic changes (Appendix Fig. S4E) was significantly reduced at the TSS and gene body of 3D downregulated genes (Appendix Fig. S4F, left panel) and increased in 3D upregulated genes (Fig. S4F, right panel) as visualized at the *HSPA8* and *CXCL12* loci, two representative genes of each category (Appendix Fig. S4G).

We then tested whether the levels of repressive marks such as H3K27me3 and H3K9me3 are affected on genes that change their expression with the culture condition. In 3D downregulated genes an increase in H3K27me3 was detected (Fig. EV1A) while H3K9me3 levels remained unchanged (Fig. EV1B). Surprisingly, a significant increase in H3K9me3 was found in 3D upgenes (Fig. EV1B).

Given that Polycomb operates through a digital mechanism with two opposing expression states signifying its presence or absence on target genes (Menon et al, 2021), assigning the modest increase in H3K27me3 detected in 3D downgenes directly to its final impact on transcription is challenging. Instead, it is likely a complex interplay of various histone modifications, along with other transcriptional and architectural factors, that contributes to this phenomenon.

We also evaluated whether the change in cell culture condition affects the presence and distribution of super-enhancers (SEs) (Hnisz et al, 2013). To date, 214 genomic regions were identified as SEs in T47D breast cancer cells (Jiang et al, 2019). The overlap

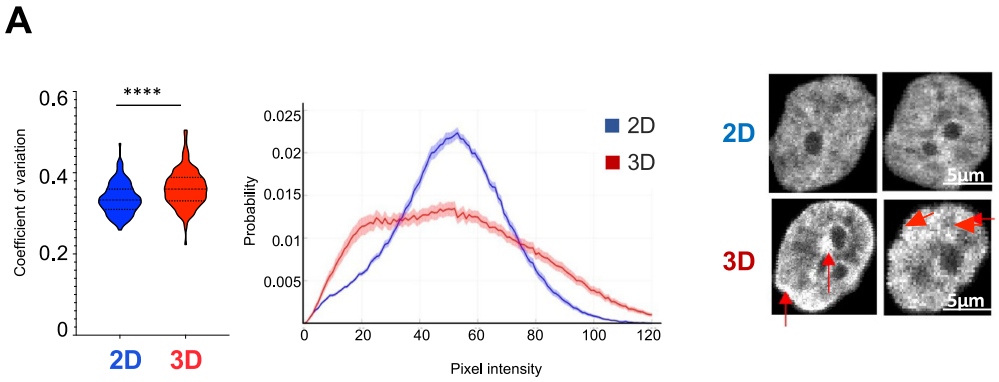
A
****
Coefficient of variation
0.6
0.4
0.2
0
2D
3D
Probability
0.025
0.02
0.015
0.01
0.005
0
20
40
60
80
100
120
Pixel intensity
2D
3D
2D
3D
5µm
5µm

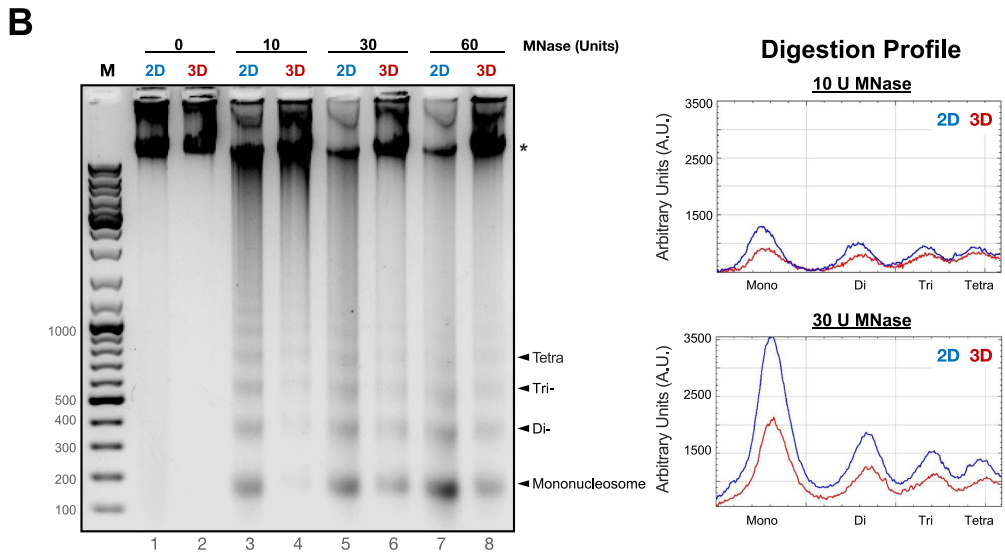
B
M
0
10
30
60
MNase (Units)
2D
3D
1000
500
400
300
200
100
*
Tetra
Tri-
Di-
Mononucleosome
1
2
3
4
5
6
7
8
Digestion Profile
10 U MNase
Arbitrary Units (A.U.)
3500
2500
1500
Mono
Di
Tri
Tetra
30 U MNase

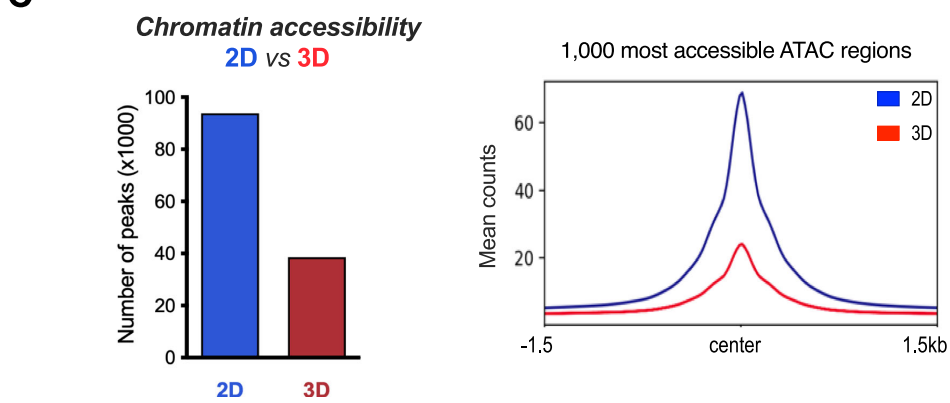
C
Chromatin accessibility
2D vs 3D
Number of peaks (x1000)
100
80
60
40
20
0
2D
3D
1,000 most accessible ATAC regions
Mean counts
60
40
20
-1.5
center
1.5kb

Figure 2. Chromatin organization and accessibility in 2D and 3D-grown cells.

(**A**) Coefficient of variation of DAPI staining distribution between T47D cells grown in 2D and in 3D, $n = 100$ cells per condition. Violin plot (left panel). Probability distribution of the pixel intensities obtained in 2D and 3D (middle panel). T47D nuclei stained with DAPI exhibiting a clearer pattern of condensed chromatin clusters in 3D-grown cells is shown (right panel, red arrows indicate highly compacted regions). Scale bar: 5 µm. (**B**) T47D cells grown in 2D and 3D conditions were isolated, nuclei were prepared and digested with different concentrations of MNase. Digestion products were resolved in 1.2% agarose gel electrophoresis (left panel) and the intensity of the bands was quantified by ImageJ software (right panel). (**C**) Number of peaks per sample of ATAC-seq experiments (up left panel). The 1000 peaks with the highest score for 2D and 3D condition were plotted (bottom left panel). The overlap between ATAC-seq replicates is shown (right panel). Source data are available online for this figure.

between the super-enhancers detected in 2D and 3D according to the H3K27ac signal (579 and 564, respectively) was close to 80% (Fig. EV1C). This observation would support that cells fundamentally maintain their regulatory gene network in both of these environments (Fig. EV1D). Nonetheless, it is essential to acknowledge that 20% of super-enhancers are exclusively activated in the 3D environment. The question of whether these variances have implications for the alteration of cell identity remains open.

To address this point, by using a proximity-based script (Hnisz et al, 2013), we found 129 and 95 genes associated to 2D and 3D SEs, respectively (Fig. EV2A). The 2D-exclusive genes are related to terms like abnormal embryo size, abnormal development, and hematopoiesis, which are closely linked to the Hippo pathway (as reported in (Yu et al, 2015)) (Fig. EV2C). Conversely, in the case of genes exclusively regulated in the 3D condition by SEs, many of them appear to be artifacts, as illustrated with the HSPA8 gene (Fig. EV2B). This hampers the identification of significant associated terms.

When attempting to establish a connection between super-enhancers and alterations in genome structure, such as the A to B transition, it becomes evident that the quantity of SEs is reduced, and this transformation exhibits subtler changes, predominantly shifting from A to less degree of A, or toward emerging B, and vice versa (Fig. EV2D). Snapshots from the genome browser illustrating these transitions for two 3D downregulated genes, SLC26A7 and RUNX1T1, and two 3D upregulated genes, PI15 and ITGAL are shown (Fig. EV2D).

Impact of 3D growth on nuclear structure

To explore how 3D culture impacts on nuclear structure, we measured the distribution of the chromatin throughout the nucleus by determining the coefficient of variation of DNA stained with DAPI (Martin et al, 2021). We found that the chromatin is organized differently, presenting a more heterogenous pattern in 3D-grown cells, with an increased coefficient of variation compared to cells grown in 2D (Fig. 2A, left panel), a broader distribution of DAPI signal intensity and the appearance of highly dense foci in 3D-grown cells (Fig. 2A, middle and right panels, respectively).

In order to assess chromatin accessibility within the cell nucleus of 2D and 3D-grown cells, we conducted a comprehensive approach that includes: (i) MNase experiments, which detect the compaction of chromatin fibers at a large scale, potentially indicating changes in the presence of linker histones and heterochromatin, and (ii) ATAC-seq experiments, which measure focal nucleosome depletion at sites where sequence-specific transcription factors, such as CTCF could bind, as well as the nucleosome-depleted region at transcription start sites (TSS).

To estimate the accessibility of the chromatin at large scale, we performed micrococcal nuclease (MNase) digestion assays. Isolated nuclei obtained from cells grown in 2D and 3D were treated with increasing concentrations of MNase, and the products of digestion were analyzed by gel electrophoresis (Fig. 2B). We found that the accessibility to MNase was compromised in 3D compared to its 2D counterpart at the range of MNase concentrations tested. (Fig. 2B). In addition, the amount of undigested DNA present in 3D was higher compared to 2D, even at 60U MNase (Fig. 2B, left panel). These results support that chromatin is less accessible in nuclei from 3D growing cells.

To assess whether the chromatin accessibility changed at nucleosome level with the growth conditions, we performed an Assay for Transposase-accessible chromatin followed by sequencing (ATAC-seq), which is a technique used to assess genome-wide chromatin accessibility (Buenrostro et al, 2013).

Nuclei obtained from cells grown in 2D and 3D conditions were incubated with 2.5 U of the tagmentase Tn5. The average number of ATAC peaks was significantly higher in 2D than in 3D growing cells (93,850 vs. 38,542 peaks for 2D and 3D, respectively) (Fig. 2C), pointing to a general decrease of accessibility in nuclei from 3D-grown cells. When comparing the 1000 most accessible ATAC regions detected in both 2D and 3D-grown cells, we observed that 3D peaks contained less reads/peak (Fig. 2C, right panel). Most of the peaks detected in 3D-grown cells also appeared in 2D (96.88%; 37,342). Only 547 new ATAC peaks were detected in 3D-grown cells, while 24,242 sites were lost when comparing all replicates. Hence, the chromatin structure in 3D-grown T47D cells exhibited a noticeably less accessible conformation, both at the level of larger fibers and at nucleosome resolution, in contrast to the 2D cells. These findings align with the results from gene expression analysis and imaging studies (Figs. 1F and 2A–C).

To characterize the regions that become more accessible in 2D and 3D we conducted a more in-depth analysis of the ATAC-seq data (Fig. EV3A,B). Our results suggest that the sites that become more accessible in 2D and 3D are enriched in the TF motifs of CTCF, TEAD, FOXA1, and PR motifs (Fig. EV3B). However, when we combined our analysis with ChIP-seq data (Zheng et al, 2019), word cloud plots indicated that open sites in 3D are enriched in the estrogen pathway through the ER itself, alongside pioneer factors FOXA1 and GATA3; the cofactor GREB1 and the coactivator P300 (Fig. EV4B,C, lower panels), which could explain the increased proliferation observed in 3D cells (Fig. 1C). In contrast, the sites that become closed in 3D (2D-exclusive) are enriched in CTCF, an architectural factor that we have shown to be displaced when we grow the cells as spheroids (Fig. 4A). This would imply that in 3D cells a more estrogenic program is turned on along with CTCF being displaced, if these two events are connected require further investigation.

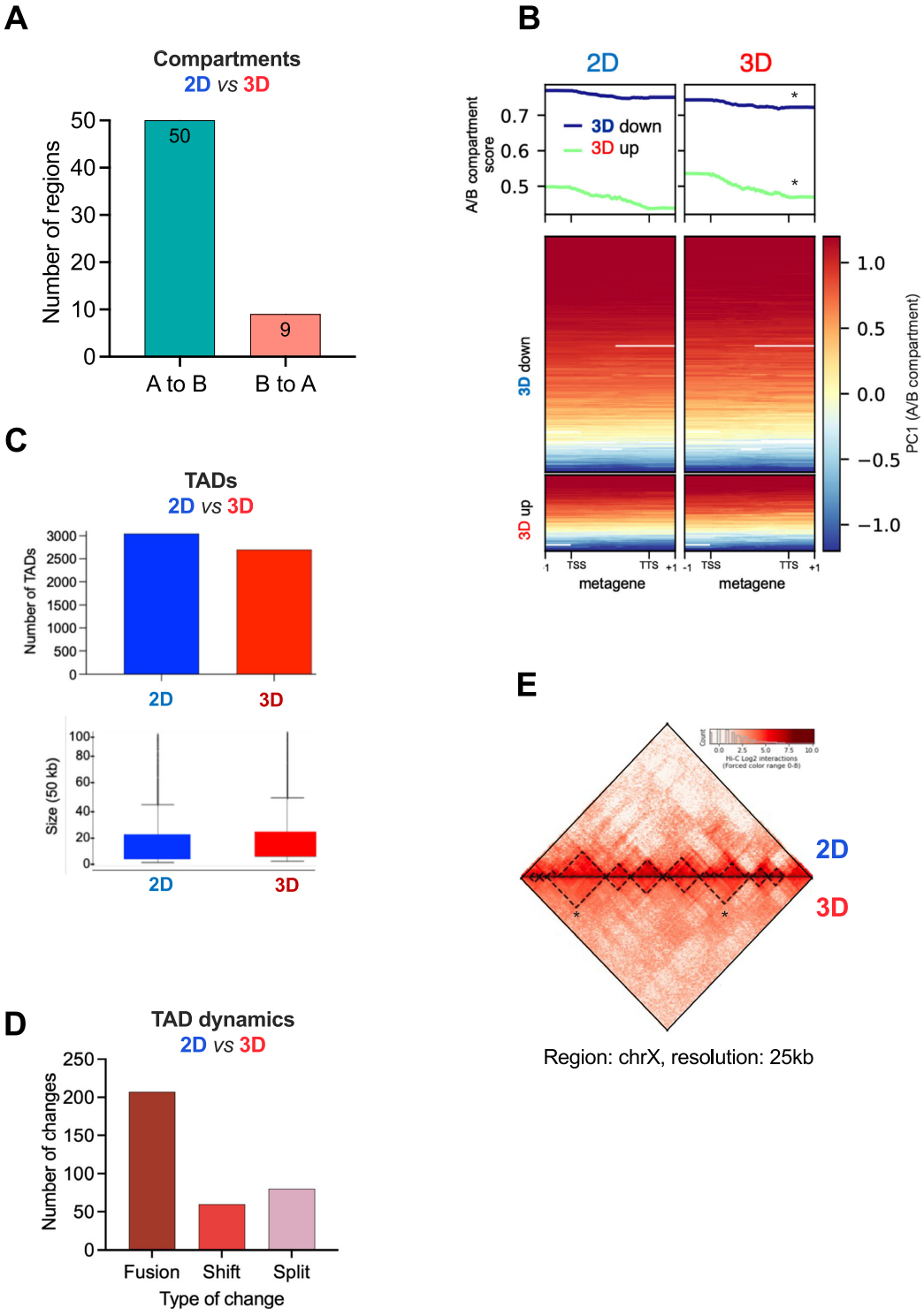
A
Compartments
2D vs 3D
Number of regions
50
9
A to B
B to A
B
2D
3D
A/B compartment score
3D down
3D up
3D down
3D up
TSS
TTS
metagene
PC1 (A/B compartment)
C
TADs
2D vs 3D
Number of TADs
Size (50 kb)
D
TAD dynamics
2D vs 3D
Number of changes
Fusion
Shift
Split
Type of change
E
2D
3D
Region: chrX, resolution: 25kb

Figure 3. Genome topology in 2D and 3D-grown cells.

(**A**) Total number of compartments changing from 2D to 3D cells (bin = 50 kb). (**B**) Metagene analysis of A/B compartments versus gene expression. Metagene profiling of A/B compartments for 3D down and 3D upgenes is shown both as average profile (top) and heatmap (bottom). Both sets of genes show significant changes in compartment score (* two-tailed *t* test *P* values < 0.001). (**C**) Changes in total number (top) and size of TADs (bottom) between 2D and 3D-grown cells. (**D**) Type of TAD changes detected in 3D-grown cells. (**E**) A Hi-C heatmap of a region located in the X chromosome illustrating TADs fusions in 3D.

Furthermore, the chromatin accessibility of 2D and 3D-exclusive genes was also assayed, and we detected changes. As expected, 2D-upgenes exhibit greater accessibility within the gene body in 2D condition compared to their 3D counterpart, whereas in 3D condition the expected inverse trend is not observed (Fig. EV3D). However, we found increased accessibility in distantly located regulatory regions (enhancers) associated to 166 genes upregulated in 3D. To illustrate this finding, the TN2Cx and PTPRD genes are shown (Fig. EV3E).

Effect of 3D growth on genome architecture

Next, we addressed the overall 3D genome organization performing Hi-C experiments with cells grown in 2D and 3D conditions.

First, we explored the chromosome compartments by analyzing the correlation between the eigenvectors obtained from the interaction of Hi-C matrices in 2D and 3D-cultured cells at 1 Mb resolution. This analysis showed no substantial changes in the genome structure at this resolution ($R = 0.99$). We next evaluated the genome compartmentalization at 100 kb resolution and found a limited number of changes between cells grown in 2D and in 3D. We identified 50 regions that changed from A (active) to B (inactive) compartment in 3D-grown cells, while only nine regions changed from B to A compartment (Fig. 3A). In fact, when the A/B-compartment transitions were evaluated by calculating an A/B score using Hi-C homer (Heinz et al, 2018), we observed a significant increase of 3D upgenes in A compartments and conversely, decrease in A and increase in B compartments for downregulated genes in 3D (Fig. 3B). These findings suggest that in the 3D condition, the changes detected in gene expression sustain gradual transitions between the A and B compartments.

Finally, we assessed the behavior of topologically associating domains (TADs). As depicted in Fig. 3C, in 3D-grown cells there is a decrease in total number of TADs (3041 and 2860 in 2D and 3D, respectively) accompanied by a small increase in their size. This is due to the prevalence of TAD fusions (200) over splitting (60) or shifting (50) (Fig. 3D). A Hi-C heatmap plot at chromosome X depicting two TAD fusions detected in 3D-grown cells is shown (Fig. 3E).

Since the discovery of TADs, it became clear that the boundary regions separating topological domains are enriched in CTCF along with the structural maintenance of chromosomes (SMC) cohesin complex, housekeeping genes, and SINE elements (Barutcu et al, 2018; Dixon et al, 2012; Nora et al, 2012).

CTCF is a highly conserved zinc finger protein and is best known as a transcription factor. It can function as a transcriptional activator, repressor or as an insulator protein, blocking the communication between enhancers and promoters (Kim and Wirtz, 2015). Thus, targeted degradation of CTCF can affect either enhancer-promoter looping or local insulation, promoting TAD fusions. To map the genome distribution of CTCF in both 2D and 3D conditions, we performed ChIP-seq experiments. Even though CTCF protein levels remain unchanged in 2D and 3D growing conditions (Fig. 4A, bottom right panel), we found a 75% loss of CTCF binding in 3D cells (Fig. 4A, top right panel).

To rule out that the antibody against CTCF might not be properly recognizing CTCF in 3D, we perform chromatin fractionation assays in 2D and 3D-grown cells. Our results showed that about half of the CTCF is bound to 3D chromatin fraction compared to the 2D condition (Appendix Fig. S5A).

This led us to hypothesize that the loss of CTCF binding could be responsible for the loss of TAD borders resulting in their fusion detected in 3D-grown cells (Fig. 3E).

We found regions where TAD fusions and CTCF displacement overlap in 3D (Fig. 4B). However, the loss of CTCF binding was global and distributed throughout the entire genome, impacting on all TADs, irrespective of whether they change or not in 3D (Appendix Fig. S5B–D). Similar loss of CTCF was found at fused, shifted or split TADs (Fig. 4C). In fact, we identified several regions where the loss of CTCF did not have impact on the TAD structure at all (Appendix Fig. S5E). Around 95% of the TAD borders were conserved in 2D and 3D conditions.

To assess whether changes in the 3D TADs could be assigned to differential loading of cohesin components in these regions, we conducted RAD21 ChIP-seq experiments under 2D and 3D growth conditions. Our findings indicate that there are no significant alterations in RAD21 occupancy within both fused and random TADs (Appendix Fig. S6).

Interestingly, HOMER motif analysis of the ATAC-seq peaks showed that the motif for CTCF tops the rank of enrichment in sites where accessibility is reduced in 3D (Appendix Fig. S5F). It is important to note that even though BORIS (CTCFL) is ranked second, this protein is not present in breast cancer cells. Several reports show that displacement of CTCF leads to a decrease in ATAC-seq signal and gene regulation (Franke et al, 2021; Xu et al, 2021). This would suggest that in 3D, CTCF displacement results in a more compact chromatin at those sites and could affect gene activity.

CTCF displacement and gene regulation in T47D 3D cells

Although the displacement of CTCF observed in the chromatin of 3D-grown T47D cells does not always lead to changes in TADs boundaries examined by Hi-C, we wanted to investigate whether the absence of CTCF is associated to changes in gene regulation.

Combined analyses of RNA-seq and ChIP-seq data showed that 3D up and downregulated genes showed a significant depletion in CTCF around the TSS compared to random genes (Fig. 4D). Therefore, the genes activated or repressed as a result of growing cells in 3D, present less CTCF around the transcription start site, which would imply a reduction of long-distance interactions ("looping") between regulatory regions (enhancers, silencers) and

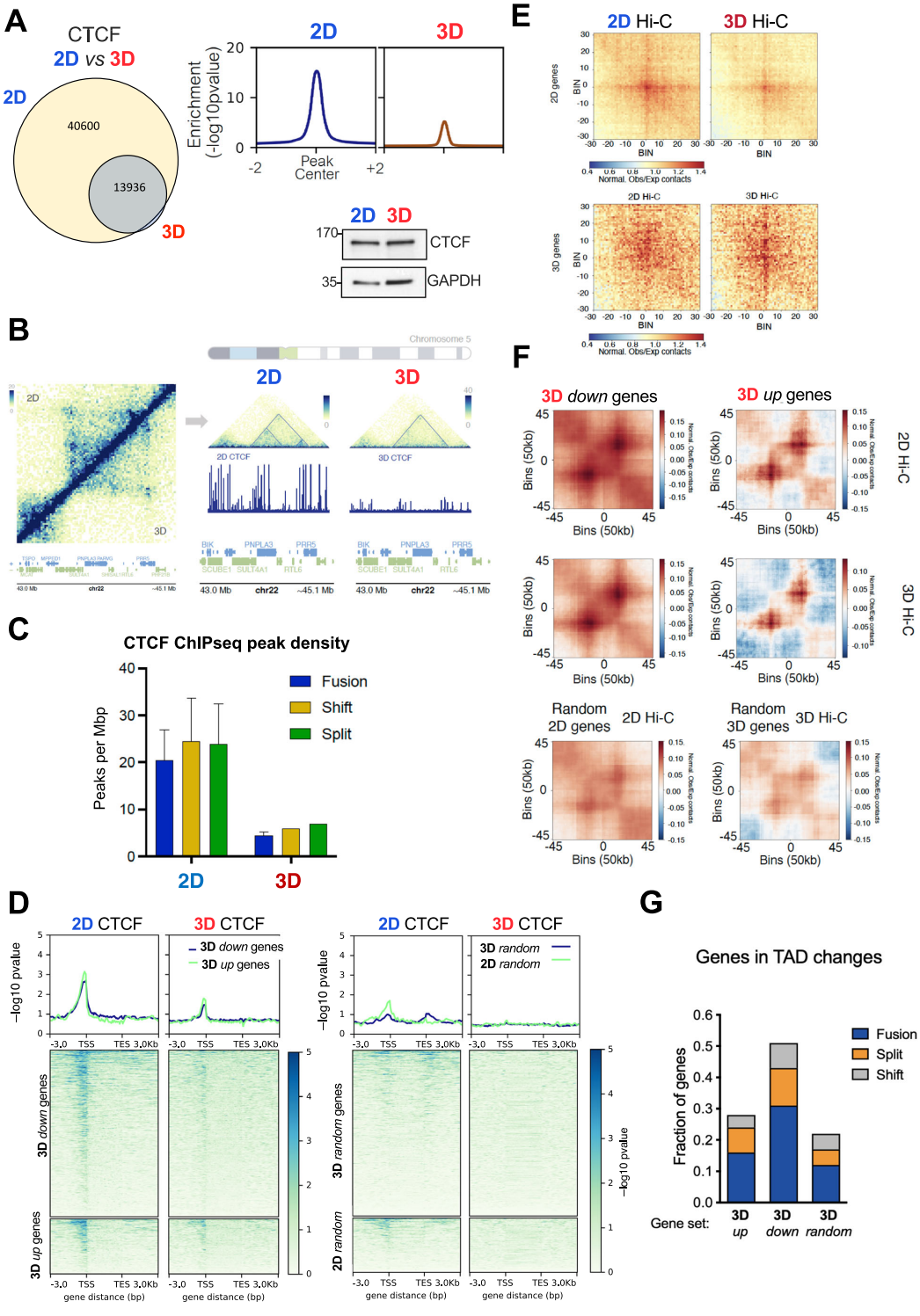
A
CTCF
2D vs 3D
2D
40600
13936
3D
Enrichment (-log10pvalue)
2D
3D
Peak Center
-2
+2
2D 3D
170
CTCF
35
GAPDH
B
Chromosome 5
2D
3D
2D CTCF
3D CTCF
C
CTCF ChIPseq peak density
Peaks per Mbp
Fusion
Shift
Split
2D
3D
D
2D CTCF
3D CTCF
3D down genes
3D up genes
3D random genes
2D random genes
-log10 pvalue
TSS
TES
3.0Kb
gene distance (bp)
E
2D Hi-C
3D Hi-C
2D genes
3D genes
BIN
Normal Obs/Exp contacts
F
3D down genes
3D up genes
2D Hi-C
3D Hi-C
Random 2D genes
Random 3D genes
Bins (50kb)
G
Genes in TAD changes
Fusion
Split
Shift
Fraction of genes
Gene set:
3D up
3D down
3D random

Figure 4. The architectural protein CTCF is displaced from target chromatin in 3D-grown cells.

(A) Cells grown in 2D and 3D were lysed and total extracts were analyzed by western blot using CTCF and GAPDH-specific antibodies (left panel). ChIP-seq of CTCF performed in 2D and 3D conditions showed differential CTCF binding regions genome-wide (middle and right panels). **(B)** Snapshot of a region presenting a 3D-exclusive TAD fusion event that overlaps with the loss of CTCF binding. **(C)** The density of CTCF peaks in 3D-exclusive fused, split and shifted TADs is shown. **(D)** The presence of CTCF in 3D up- and downgenes (left panels) and in random genes (right panels) are shown. **(E)** Hi-C explorer aggregate plots. Long-distance interactions among 3D down- and upregulated genes grown in 3D and 2D conditions. The genomic coordinates of the 3D down- and upregulated genes are centered between half the number of bins and the other half the number of bins. Plotted are the submatrices of the aggregated contact frequency for 20 bins (1.5 kb bin size, 35 kb in total) in both upstream and downstream directions. Color bar scale with increasing red shades of color stands for higher contact frequency. **(F)** Aggregate FAN-C plots depict a region that is three times the size of the TAD located in its center. TADs are selected on the basis of containing 3D up- or downgenes (upper panels) or random genes (lower panels). High signal is located in the center, especially at the TAD corner, where the corner loops are typically located. **(G)** CTCF displacement impacts in 3D-regulated genes, by changing their contact environment through TADs fusion. The percentages of up, down or random genes in 3D condition that fall into fused, split or shifted TADs are shown. Source data are available online for this figure.

their target genes. In fact, this loss in interactions detected in 3D resulted into a decrease of Hi-C contacts, particularly evident in 3D downregulated genes (P value <0.001) (Fig. 4E and S6G).

As mentioned above, CTCF is also enriched at TADs borders. We asked whether long range CTCF-interactions and therefore TADs structure as a whole, could be particularly affecting those TADs specifically enriched in 3D deregulated genes. To address this point, we used FAN-C aggregate plots using the TADs containing genes differentially expressed in 3D-grown cells and measure the levels of CTCF by ChIP-seq. Our results showed that for genes downregulated in 3D, the global interactions between two CTCF sites that formed a TAD corner were drastically reduced (P value <0.001) (Fig. 4F, left panels), whereas for genes activated in 3D cells we could detect a slight decrease, but not statistically significant (P value >0.001) (Fig. 4F, right panels). No difference was found for a random set of genes and TADs as a control (Fig. 4F, bottom panels). Therefore, CTCF displacement could be involved in the prevailing 3D-gene repression. This implies changes at the level of intra-TAD interactions as well as at the level of TAD borders, decreasing its ability to isolate and regulate genes.

We then assessed whether the observed differences in CTCF and TAD structure associated to 3D genes (Fig. 4E,F) could lead to any preferential change of TADs in 3D condition. We found that 17% of up and 30% of downgenes in 3D are included in 3D fused TADs, while the percentages were significantly lower in split and shift TADs (7 and 13% for split and 3.5 and 7% for shifted TADs, P <0.001) as well as in all categories for random genes (Fig. 4G). Thus, CTCF displacement particularly impacts in 3D genes, by changing their contact environment through TADs fusion as shown for the 3D down gene *DUSP1* whose expression is associated with an increased risk of metastasis and shorter overall survival in breast cancer (Candas et al, 2014) (Appendix Fig. S7A–C).

LATS activity and CTCF binding to chromatin in T47D grown in 3D cells

In 3D condition, we have shown that the Hippo pathway is activated, resulting in the phosphorylation of YAP at serine 127 by the LATS kinase (Fig. 1D).

A recent study reported that LATS can phosphorylate CTCF at T347 and S402 and disables its DNA-binding activity (Luo et al, 2020). In that system, loss of CTCF binding was able to disrupt local chromatin domains and downregulate genes located in the neighborhood (Luo et al, 2020). Therefore, we tested whether the displacement of CTCF found in 3D-grown cells could be due to increased LATS-dependent phosphorylation of CTCF.

As no commercial phos-CTCF antibody is available, we performed a Phos-tag gel, that would allow detection of phos-CTCF as slow-migrating bands depending on their state of phosphorylation. When extracts from 2D and 3D-grown cells were analyzed in Phos-tag gels, we detected a retarded band in 3D, which was not present in 2D extracts (Fig. 5A). To confirm that this band corresponded to a phosphorylated version of CTCF, we prepared 3D extracts by using a buffer lacking phosphatase inhibitors. Under this condition, the CTCF band ran faster in Phos-tag gel as a nonphosphorylated version of CTCF (compare lanes 2 and 3 in Fig. 5A), supporting that phosphorylated-CTCF is preferentially found in extracts from 3D-grown cells.

The direct impact of LATS on CTCF phosphorylation was tested using TRULI, a potent ATP-competitive inhibitor of LATS kinases (Kastan et al, 2021). Incubation for 24 h with 10 μM TRULI decreased the phosphorylated (activated) version of YAP at S127 (Fig. 5B, left panel).

To have a formal proof that LATS1 phosphorylates CTCF in 3D cells, we performed immunoprecipitation of CTCF in 3D-grown cells treated or not with TRULI and then probed with specific antibodies recognizing the phosphorylated RXXpS/T residues that match the changes observed in T374 and S402 as previously described (Luo et al, 2020). Our results showed that the phospho-CTCF signal in 3D is reduced by 40% in the presence of TRULI, confirming the raised hypothesis (Fig. EV4A).

To confirm that T374 and S402 of CTCF are the phosphorylation targets of LATS, and to assess their impact on chromatin binding in our experimental system, we transfected T47D cells with both wild-type and the phospho-mimetic T374E/S402E CTCF variant. Subsequently, we evaluated their chromatin binding abilities. The T374E/S402E mutant displayed a diminished capacity to bind to chromatin when compared to the wild-type CTCF (Fig. EV4B). In addition, we carried out chromatin fractionation and ChIP assays in T47D and HEK293 cells, treated or not with the LATS1 activator Latrunculin B, and transfected with the wild-type CTCF and the phospho-mutant. While the wild-type CTCF was displaced in the presence of LatB, the mutant remained bound regardless of LATS1 activation. However, these results should be taken with caution as these residues could also participate in the stability of CTCF, which makes the scenario more complex and challenges for definitive interpretations.

It has been reported that the overexpression of CTCF impedes the proliferation and metastasis of breast cancer cells by deactivating the nuclear factor-kappaB pathway in breast cancer cells (Wu et al, 2017). To elucidate the function T474 and S402, we conducted a functional assay by evaluating cell growth in T47D cells

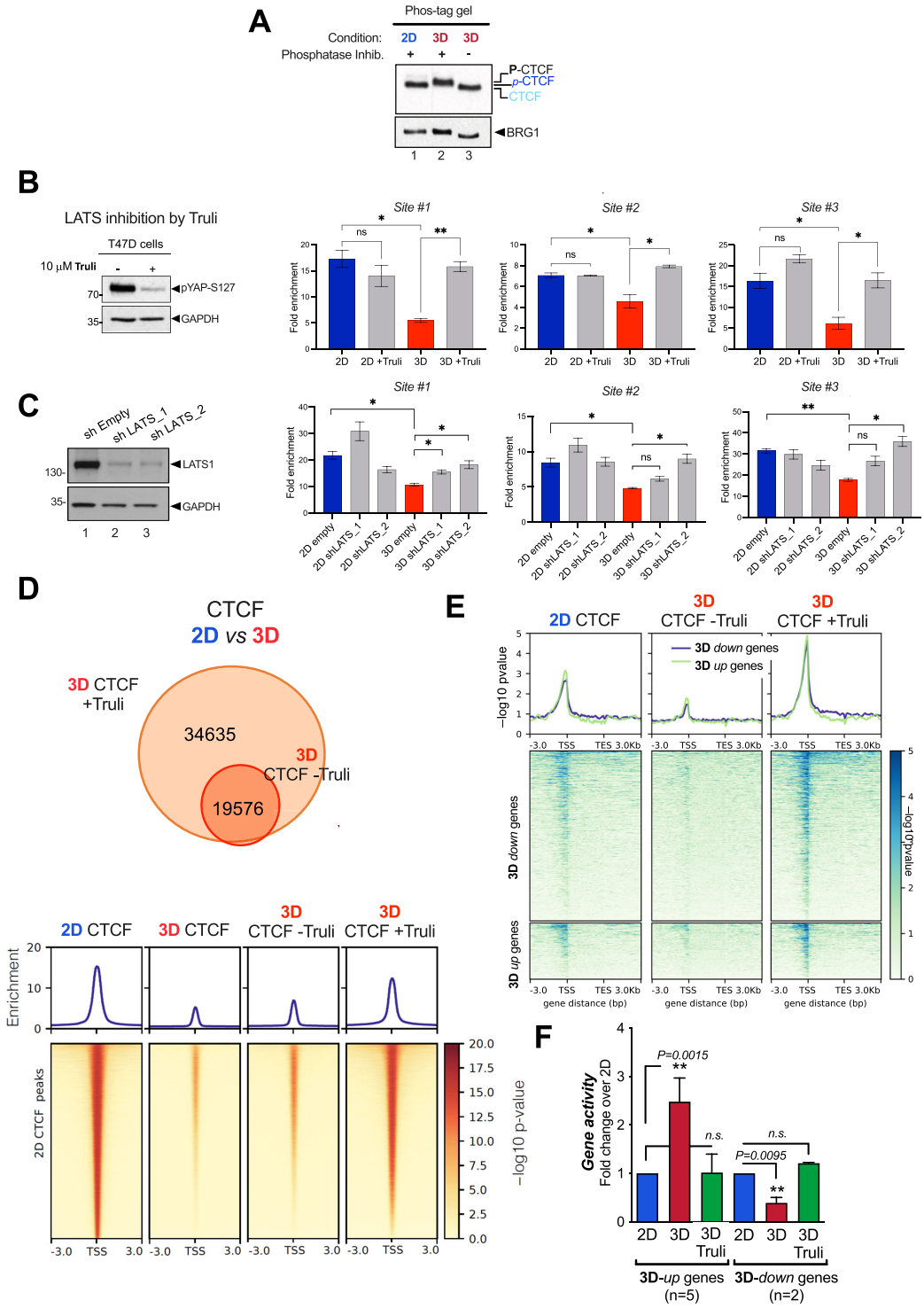
A
Phos-tag gel
Condition: 2D 3D 3D
Phosphatase Inhib. + + -
P-CTCF
p-CTCF
CTCF
BRG1
1 2 3
B
LATS inhibition by Truli
T47D cells
10 μM Truli - +
pYAP-S127
GAPDH
Site #1
Site #2
Site #3
Fold enrichment
2D 2D +Truli 3D 3D +Truli
C
sh Empty
sh LATS_1
sh LATS_2
LATS1
GAPDH
2D empty
2D shLATS_1
2D shLATS_2
3D empty
3D shLATS_1
3D shLATS_2
D
CTCF
2D vs 3D
3D CTCF +Truli
34635
3D CTCF -Truli
19576
2D CTCF
3D CTCF
3D CTCF -Truli
3D CTCF +Truli
Enrichment
2D CTCF peaks
-log10 p-value
-3.0 TSS 3.0
E
2D CTCF
3D CTCF -Truli
3D CTCF +Truli
3D down genes
3D up genes
−log10 pvalue
-3.0 TSS TES 3.0Kb
gene distance (bp)
F
Gene activity
Fold change over 2D
P=0.0015
n.s.
P=0.0095
2D 3D 3D Truli
3D-up genes (n=5)
3D-down genes (n=2)

Figure 5. Inhibition or depletion of the Hippo pathway LATS kinase compromises the loss of CTCF detected in 3D-grown cells.

(A) Cells grown in 2D and 3D were lysed and total extracts were analyzed by Phos-tag gel which identifies putative phosphorylated bands of CTCF exclusively in 3D. **(B)** Cells grown in 2D or 3D conditions and treated or not with the LATS inhibitor TRULI were subjected to ChIP-qPCR of CTCF in three regions where CTCF binding is lost in cells grown in 3D ($n = 2$, P value < 0.05) (right panel). T47D cells treated or not with TRULI were lysed and total extracts were analyzed by western blot using pYAP-S127 and GAPDH-specific antibodies (left panel). **(C)** Effect of LATS1 depletion on CTCF binding. Left panel: quantification of LATS1 by western blot. Right panel: ChIP-qPCR analysis of CTCF in extracts derived from control cells transfected with shEmpty and two distinct shLATS. **(D)** Cells grown in 3D conditions treated or not with the LATS inhibitor TRULI were subjected to CTCF ChIP-seq. Venn diagrams showed the overlapping in CTCF binding. **(E)** Cells grown in 3D conditions and treated or not with TRULI were subjected to CTCF ChIP-seq. The enrichment of CTCF in 3D up- and downgenes as well as in random genes is shown. The heatmaps, illustrating CTCF ChIP-seq results under both 2D and 3D untreated conditions, are the same as those previously presented in Fig. 4D, left panels. **(F)** Cells grown in 2D and 3D conditions and treated or not with TRULI as indicated, were submitted to gene activity assays. Several up and downregulated genes in 3D were tested. Results are represented as mean and SD from three experiments performed in duplicate. The P value was calculated using the Student's t test. Source data are available online for this figure.

expressing both wild-type (WT) and a phospho-mimetic variant of CTCF T374E/S402E (Fig. EV4C). The overexpression of WT CTCF in T47D cells inhibited cell growth compared to the control transfection (Fig. EV5C). Conversely, in the T374E/S402E mutant in which chromatin binding is compromised (see Fig. EV4B), this effect was not appreciated (compare WT vs. mutant in Fig. EV5C). This suggests that LATS1-dependent phosphorylation of CTCF induced its displacement and participates in 3D cell growth, as demonstrated in Fig. 1C.

Therefore, we performed qPCR-ChIP of CTCF in 2D and 3D-grown cells in the absence or in the presence of TRULI. As expected, a decrease in CTCF binding was detected in 3D compared to 2D in the three different genomic regions tested (Fig. 5B, right panels). In the presence of TRULI, CTCF binding was significantly recovered (Fig. 5B, right panels).

To support these findings and to discard indirect effects of TRULI, we performed similar ChIP experiments in cells deficient of LATS1 (Fig. 5C, left panel). As with TRULI, knockdown of LATS1 rescues CTCF binding in 3D cells (Fig. 5C, right panels). Interestingly, these results point to LATS1 as responsible for the observed effects.

The potential involvement of LATS2 was assessed using a specific antibody that recognizes phosphorylation at T1079 and T1041 present in both LATS1 and LATS2, in wild-type cells and LATS1-depleted cells. The dual phosphorylation signal in 3D cells decreased proportionally with the reduction of LATS1 (Fig. 5C), supporting that LATS1 is the Hippo kinase involved in our system (Fig. EV4D).

To extend our conclusions, we performed ChIP-seq of CTCF in 3D cells in the presence and absence of TRULI. We found that binding of CTCF was recovered across the genome in the presence of the LATS inhibitor (Fig. 5D). In fact, in this condition, we observed that CTCF binding was preferentially recovered at 3D-dependent genes (Fig. 5E).

The sensitivity of CTCF ChIP-seq experiments is notably influenced by the particular protocol employed. This results in varying outcomes regarding the detected 3D shift. Notably, using a stringent ChIP protocol, which includes multiple washes and the use of DNA purification columns (ChIP-IT, Active Motif), revealed a 75% displacement of CTCF when cells were cultured in a 3D environment, as depicted in Fig. 4A.

In contrast, using a standard protocol with gentler wash steps, as outlined by Vicent et al, 2014 (Vicent et al, 2014), and incorporating an internal Drosophila spike-in control, reduced this displacement to 40% (Appendix Fig. S8A–C). Notably, this reduction remained statistically significant when compared to cells cultured in a 2D monolayer setting. Moreover, in spike-in-controlled CTCF ChIP-seq experiments conducted in the presence of the LATS inhibitor TRULI, CTCF binding was restored (refer to Appendix Fig. S8C). These findings align with our earlier results; the average of all three CTCF ChIP-seq replicates obtained from 2D and 3D cells is depicted in Fig. S8D.

We next asked whether the activity of the LATS kinase and its effect on CTCF binding was required for the proper regulation of 3D genes. We tested 5 genes up and 2 genes down in 3D and we found that TRULI significantly changed their activity, approaching to that detected in 2D (Fig. 5F).

Moreover, we also evaluate the effect of TRULI on 3D growth. In the presence of TRULI, 3D cells grew less and the spheres were smaller compared to untreated 3D cells (Appendix Fig. S9A,B). In agreement with the gene activity, cell growth in the presence of TRULI turned out to be similar to that observed in 2D, coinciding with the presence of CTCF bound to the target genes and the activity exhibited in both conditions (Fig. 5E,F; Appendix Fig. S9).

Hormone-dependent gene regulation in 2D and 3D T47D cells

The exposure to progestins produces multiple effects in breast cancer cells which are mediated by the activation of the Progesterone Receptor (PR). The hormone-activated PR translocates to the nucleus where it actively regulates gene transcription. To explore the response to progestins of T47D cells grown in 3D, we measured the level of expression of different transcription factors known to be involved in PR activation in cells cultured in 2D conditions. The levels of PR, ERα and FOXA1 remained similar between 2D and 3D-grown cells (Appendix Fig. S10A). A slight increase in activated PR phosphorylated at S294 (pPRS294) levels was detected in 3D compared to 2D in the absence and in the presence of 10 nM R5020 (Appendix Fig. S10A,B). However, no differences either in the extent of pPRS294 signal induced by hormone or in the percentage of cells responding to the hormonal stimulus were found (Appendix Fig. S10B). The pPRS294 signal increased with hormone and its expression was detected homogeneously distributed throughout the cells of the spheroid (Appendix Fig. S10C, upper panels), similar to the pattern observed for total PR (Appendix Fig. S10D).

To globally evaluate the hormone-regulated genes in the spheroids and compare them to the 2D model, we performed RNA-seq experiments. Briefly, T47D cells grown in 2D or 3D were exposed to solvent or to 10 nM R5020 for 6 h, followed by RNA extraction, mRNA library preparation, and massive sequencing.

Almost twice as many genes were regulated by hormone in 3D-grown cells compared to 2D cells (7654 vs 4681, log2FC > 1, adj *P* value < 0.01). Upregulated genes increased by around 35%, while downregulated genes increased by 100% (Fig. 6A). Most of the genes regulated in 3D were not regulated in 2D (4749 vs 2961 genes, respectively) (Fig. 6B).

Interestingly, among the GO categories regulated by hormone exclusively in 3D we found terms such as *cytoskeleton, actin filament organization, cell growth*, and *cell–cell junction* (Appendix Fig. S11A,B). These terms were also overrepresented when the extracellular matrix was the only variable incorporated into the analysis (Appendix Fig. S3). Thus, when exposed to hormone, T47D breast cancer cells grown as spheroids responded differently to those grown as monolayers.

PR binding in 2D and 3D-grown T47D cells

To explore whether the environmental-dependent changes detected in gene expression are associated with changes on PR binding to the genome, we carried out ChIP-seq experiments of PR in 2D and 3D-grown cells exposed to 10 nM R5020.

In line with the increased number of genes regulated in 3D-grown cells, we also found more PR-binding sites (PRbs) in cells grown as spheroids. Almost all PRbs found in 2D were also present in 3D, but 10,226 new PRbs were exclusively found in 3D-grown cells (Fig. 6C). The genomic distribution of total PRbs in 3D turned out to be very similar to 2D (Appendix Fig. S12A). Compared to 2D-exclusive, the distribution slightly changed in the 3D-exclusive PRbs, with less PRbs found in introns and an increased number in promoter, UTR and exons (Appendix Fig. S12A).

The majority of the PRbs in 2D-grown cells are localized far from the target genes, in enhancers (Ballare et al, 2013). To map the hormone-dependent active enhancers we overlapped 3D-exclusive PRbs (10,226 regions) with H3K27ac peaks obtained from a ChIP-seq performed in 3D-grown cells. We measured the distances between these peaks to the nearest significantly regulated gene in 3D-grown cells or to random genes set. The 3D-exclusive genes were significantly closer to 3D PRbs enriched in H3K27ac (enhancers), compared to random genes (Fig. 6D). Thus, in 3D-grown cells a program is implemented aiming at the regulation of a distinct group of genes that involves the specific binding of PR to 3D-exclusive active enhancers.

Activation of the Hippo pathway in 3D-grown cells impacts in hormone-dependent PR binding

As YAP is a transcriptional coactivator that lacks DNA-binding activity, it could act on gene expression via interaction with other DNA-binding factors. Reported YAP binding partners include TEAD, p73, Runx2, and the ErbB4 cytoplasmic domain (Li et al, 2010). However, only TEAD has been demonstrated to be important for the growth-promoting function of YAP (Zhao et al, 2008). Interestingly, the 3D-exclusive PR-binding sites turned out to be enriched in the TEAD DNA-binding motif beyond the classical HRE DNA-binding motif (Appendix Fig. S12C). As in 3D-grown cells the Hippo pathway is activated and YAP is phosphorylated in S127 by LATS1 and tagged for degradation in the cytoplasm (Fig. 1D), we hypothesize that decreased levels of nuclear YAP would increase the proportion of free TEAD sites, thus, accounting for the enhanced PR binding detected upon hormone in 3D cells.

To address this point, we performed ChIP-seq of PR in siControl and siYAP T47D cells treated with hormone in 2D conditions. We found that 32.7% of PR-binding sites that appeared only when YAP is depleted in 2D (10,168 regions) overlap with 3D-exclusive PR-binding sites (3381 regions, *P* value < $2.2e^{-16}$) (Fig. 6E). These new sites could regulate a new set of genes associated to a "3D spheroid" condition. Interestingly, PR binding increased globally in the absence of YAP compared to control cells (Fig. 6F).

According to this model, YAP and PR would compete for binding to 3D-exclusive chromatin regions. As YAP does not bind to DNA directly, but rather via TEAD, the role of TEAD1, TEAD4 and TAZ in this proposed mechanism should be further elucidated.

Recently in our lab, a classification of PR-binding sites has been established according to their accessibility at various progestin concentrations. The lowest progestin concentration that allows detection of ligand-dependent PRbs was 50 pM. At this physiological concentration, 2848 PRbs, termed "Highly Accessible PR binding sites", (HAs) were identified (Zaurin et al, 2021) (Fig. EV5A).

As HAs constitute essential regulatory elements in hormone-dependent growth of breast cancer cells, we decided to evaluate whether the Hippo pathway also impacted on their function. First, we tested whether HAs-dependent genes required LATS1 activity in 3D-grown cells. Our results showed that hormone-dependent regulation of *EGFR*, *STAT5A*, *TIPARP, PGR, BCAS1*, and *IGFBP5* was compromised in the presence of TRULI (Fig. EV5B). Thus, LATS1 impacts in hormonal response affecting a significant proportion of 3D-exclusive and HAs-associated genes. Unveiling the molecular mechanism by which LATS participates in hormone-dependent gene regulation requires further research.

Therefore, the global impact of the Hippo pathway -through p-LATS activation- in 3D cells could be explained at least in two ways: (i) at basal conditions, via CTCF phosphorylation inducing its displacement and (ii) via YAP phosphorylation and inactivation, releasing "hidden" TEAD sites for PR binding allowing regulation of 3D unique genes (Appendix Fig. S13). In fact, silencing YAP in 2D partially recapitulate the pattern of PR binding in 3D conditions.

Discussion

By culturing tubular epithelial breast cancer cells as spheroids (3D), we aimed to explore novel cell signaling pathways, gene networks, transcription factors, chromatin remodelers that might have been overlooked in previous experiments performed in cells cultured as monolayer in plastic dishes (2D). The work reported here on the hormone-responsive T47D cell line is a first step in the description and characterization of a more appropriate and physiological in vitro model for breast cancer that should include various epithelial cell types, the supporting fibroblasts and blood cell environment.

Morphologically, T47D cells grown as spheroids in matrigel presented an increase in nuclear volume coupled with a reduction in nuclear diameter (Appendix Fig. S1B). These seemingly conflicting alterations might be attributed to the underlying physicochemical modifications that dictate the irregular shapes of

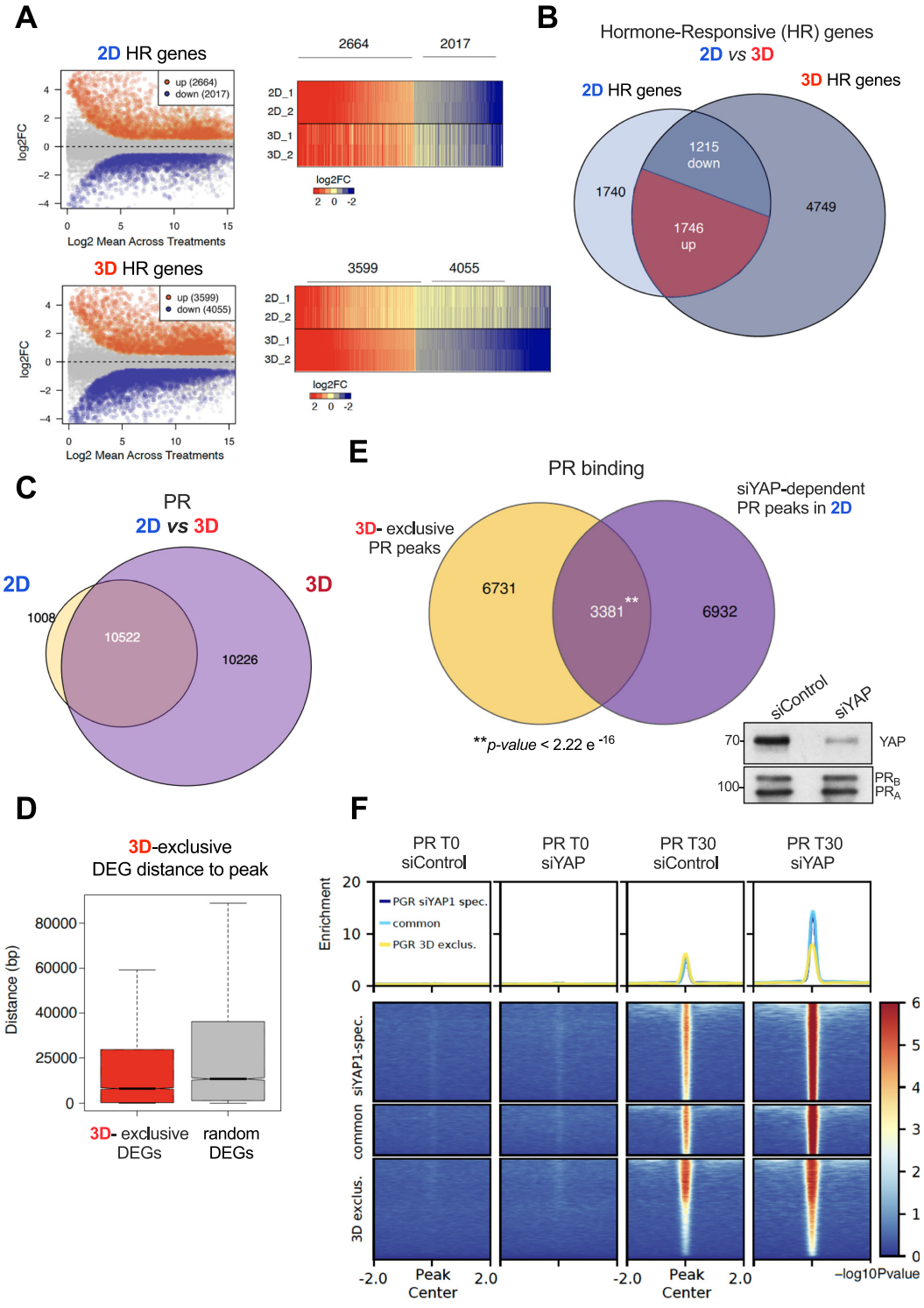
A
2D HR genes
up (2664)
down (2017)
log2FC
Log2 Mean Across Treatments
2664
2017
2D_1
2D_2
3D_1
3D_2
log2FC
3D HR genes
up (3599)
down (4055)
3599
4055
B
Hormone-Responsive (HR) genes
2D vs 3D
2D HR genes
3D HR genes
1740
1215
down
1746
up
4749
C
PR
2D vs 3D
2D
3D
1008
10522
10226
D
3D-exclusive
DEG distance to peak
Distance (bp)
3D- exclusive DEGs
random DEGs
E
PR binding
siYAP-dependent
PR peaks in 2D
3D- exclusive
PR peaks
6731
3381
**
6932
**p-value < 2.22 e -16
siControl
siYAP
70-
YAP
100-
PRB
PRA
F
PR T0
siControl
PR T0
siYAP
PR T30
siControl
PR T30
siYAP
Enrichment
PGR siYAP1 spec.
common
PGR 3D exclus.
siYAP1-spec.
common
3D exclus.
-2.0
Peak
Center
2.0
-log10Pvalue

Figure 6. 3D-grown cells showed an increased response to the hormone.

(A) T47D cells grown in 2D and 3D conditions in the presence or absence of 10 nM R5020 during 6 h were subjected to RNA-seq assays (log2FC > 1, *P* adj <0.01). The number of genes regulated by hormone in each condition is depicted (left panel). The volcano plot of the distribution of genes regulated in both conditions is shown (right panel). **(B)** Venn diagrams of up- and downregulated genes detected in 2D and 3D cells are shown. **(C)** T47D cells grown in 2D and 3D conditions in the presence or absence of 10 nM R5020 during 30 min were subjected to PR ChIP-seq. **(D)** Distance between enhancer-associated PRbs (those which overlapped with H3K27ac ChIP-seq signal) to the most proximal differentially expressed gene (3D-exclusive). The distance to random genes is used as control. **(E)** Venn diagram depicting the overlap of PR-binding sites from ChIP-seq experiments performed in siYAP cells treated with hormone and the subset of 3D-exclusive PR peaks. Thus, a total of 3381 PR-binding sites of 3D-exclusive PR peaks may be a result of YAP displacement detected in the 3D nucleus (*P* value < 2.2e-16). **(F)** Heatmap plots of the PR ChIP-seq experiments performed in siControl and siYAP T47D cells. Source data are available online for this figure.

the cell nucleus. These processes encompass mechanical forces acting through microtubules, actin filaments, and the osmotic pressure within the cytoplasm (Kim et al, 2015).

It has been widely reported that modifying the stiffness and composition of the used matrix can have an impact on cell growth, cell cycle, differentiation, and the activation of specific signaling pathways, such as the Hippo pathway (Garreta et al, 2019; Uroz et al, 2018). It is known that exposure of cells to a stiffer environment such as plastic implies a force transmission through focal adhesions leading to nuclear flattening and stretching of nuclear pores, reducing their mechanical resistance to molecular transport, increasing YAP nuclear import (Elosegui-Artola et al, 2017), and indirectly affecting gene expression. Conversely, on soft substrates, the nucleus is mechanically uncoupled from the matrix and not submitted to strong forces, inducing a balance between nuclear import and export of YAP through the nuclear pores (Elosegui-Artola et al, 2017).

Beyond this mechanical connection between the shape of the nucleus and YAP distribution, we found that 3D cells presented an increased LATS kinase activity which preferentially phosphorylates YAP, reducing its presence in the 3D nucleus (Figs. 1D and 5B).

Impact of 3D growth on chromatin structure and gene regulation

The differential distribution of DAPI nuclear staining in 2D and 3D-grown cells pointed to an increased and more structured heterochromatin in 3D-grown cells. MNase and ATAC-cleavage experiments provided confirmation that chromatin in 3D-cultured cells is characterized by increased compaction, affecting both the larger chromatin fibers and the localized regions where transcription factors interact with nucleosomes. This heightened compaction results in reduced accessibility (Fig. 2B,C). In line with these results, we found an increased number of downregulated genes in 3D-grown cells (Fig. 1F) and terms related to neurogenesis, lamellipodia, and axon guidance are enriched, suggesting higher mobility to migrate in matrigel. In 3D-grown cells, we detected protrusions emerging from the cell membrane (pseudopodia) and filopodia extending out from lamellipodia, both clear indicators of cell–matrix interactions. These protrusions are associated with cellular sensing mechanisms, involving cell adhesion and cytoskeleton organization strategies (Caswell and Zech, 2018), as supported by the GO terms of the regulated genes.

As T47D cells exhibit an upregulation of genes related to neurogenesis (Appendix Fig. S3A), we sought to determine whether this phenomenon was exclusive to breast cancer cells. To address this, we conducted a comparative analysis using non-tumorigenic MCF10A cells cultured as monolayers and in 3D spheres (Maguire et al, 2016). When we examined the genes upregulated in the 3D environment in both cell lines and categorized them by tissue-associated genes, we consistently found an enrichment of brain-associated genes, followed by those associated with the lung, mammary gland, and blood (see Appendix Fig. S14A). This suggests that culture conditions have a significant influence on gene expression patterns, rather than being solely dependent on the tumor type itself.

However, upon closer examination of the expression of upregulated genes in the 3D environment and their clustering, distinctive differences emerged. Notably, in cluster 2, we identified an exclusive overexpression of the term "nervous system development" in T47D cells compared to MCF10A cells (see Appendix Fig. S14B). Additionally, we observed significant variations in the expression of genes related to cell and focal adhesion, particularly in cluster 3, which turned out to be distinct between tumor and non-tumoral cells cultured in the 3D environment (see Appendix Fig. S14B). Therefore, the distinct expression of neurogenesis-related genes in a 3D environment appears to be associated with a more cancerous behavior. However, further investigations involving a broader range of both tumor and normal cells are required to confirm this observation.

Our results suggest that 3D-gene repression program is driven by a reduction of H3K27ac signal and a concomitant increase in its trimethylation, while gene activation is led by an increase in H3K18ac, surprisingly, accompanied by H3K9me3 (Appendix Fig. S4; EV1). In this regard, it has been previously reported that H3K9me3 can be found in promoters of repressed genes, as well as at some active genes (Barski et al, 2007).

In addition, T47D cells grown in 3D exhibit a higher overlap of the nuclear lamina with H3K9me3 and H3K27me3 heterochromatin marks compared to 2D-grown cells. A tempting hypothesis is that the presence of a more consistent heterochromatin at the Lamina Associated Domains (LADs) might be responsible for the increased gene repression detected in 3D condition. This would imply a 3D-dependent repositioning of genes close to the nuclear lamina, as previously shown in other systems (Reddy et al, 2008). However, more research is required to find the mechanistic and functional basis that support this hypothesis.

The hippo kinase LATS promotes CTCF displacement from chromatin in 3D-grown cells

Despite the changes in chromatin compaction detected by microscopy and nuclease accessibility (Fig. 2B,C), when the topology of the genome was assessed through Hi-C experiments, no significant differences in the contact matrices were found at 1 Mb resolution (Fig. 3A). However, at higher resolution we detected changes between cells grown in 2D and in 3D at the level

of compartments and TAD structure. We found subtle differences indicative of changes in gene repression (more transitions from A to B compartment) (Fig. 3B,C). These results along with the identification of the active SEs (Fig. EV1D) suggest that the cell identity is maintained in cells grown in 3D (Flyamer et al, 2017; Stadhouders et al, 2019; Vilarrasa-Blasi et al, 2021).

However, we detected moderate changes in genome structure. Compared to cells grown on plastic, cells grown in 3D cells exhibit a higher number of TAD fusions over splits or shifts. Even though the levels of architectural CTCF protein are similar in 2D and 3D-grown cells, we detected by ChIP-seq less CTCF bound to chromatin in 3D-grown cells (Fig. 4A). A possible explanation of this finding could be associated to the increased Hippo pathway activity detected in 3D-grown cells, which is translated into a more active p-LATS1 (Fig. 5B).

It has been reported that activated p-LATS can phosphorylate CTCF resulting in reduced binding to a subset of genomic binding sites (Luo et al, 2020). In our system CTCF is phosphorylated in 3D-grown cells and inhibition or depletion of LATS restores CTCF binding to target regions. Therefore, the Hippo pathway is turned on in 3D-grown cells impacting on the cell nucleus through the reduction of CTCF binding, and thus promoting TAD fusions and changes in gene regulation of the neighboring genes. As the dissociation of CTCF we observed in 3D is more global -and not limited to fused TADs-, than previously reported (Luo et al, 2020), the role of p-LATS would be critical and CTCF binding would be more dependent on the Hippo pathway in 3D-grown cells. In fact, inhibition of p-LATS by TRULI compromised 3D cell proliferation and reduced the size of the spheroids (Appendix Fig. S9A,B).

It is worth to mention, that given the high molecular weight of the CTCF protein (140 KDa) along with the few LATS-dependent phosphorylation sites found (Luo et al, 2020), the effect of TRULI on CTCF phosphorylation could not be detected in Phos-tag gels, even though different conditions were assayed.

It has been reported in breast tissue that LATS activity modulates estrogen receptor (ERα) activity (Lit et al, 2013). More recently, LATS1/2 kinases have been shown to restrict the activity of ERα by binding and promoting its degradation (Britschgi et al, 2017). These studies implicate a nuclear function of LATS kinases in cell lineage commitment and in the malignant progression of breast and prostate cancers (Britschgi et al, 2017; Powzaniuk et al, 2004).

Although limited at the level of genome structure, the effect of CTCF depletion detected in 3D had consequences on the activity of 3D-specific genes. Thus, the role of CTCF as a general transcription factor involved in enhancer-promoter looping rather than its function as insulator at TAD borders, would be more relevant in 3D culture cells.

Regarding the uncoupling between displacement of CTCF detected in 3D-grown cells and changes in genome architecture, previous work carried out in different systems has shown that CTCF may not be as essential in establishing genome structure/TADs (Barutcu et al, 2018), at least in the mammalian genome, but this is still a matter of debate. In fact, collectively, our findings suggest that the 70% of CTCF displacement detected in 3D chromatin is either not sufficient to change the arrangement of TADs or other factors may be involved and minimize the effect of such substantial depletion. As we previously mentioned, the association of housekeeping genes with boundary regions extends previous studies in yeast and insects (Duan et al, 2010; Ulianov et al, 2016) and suggests that non-CTCF factors may also be involved in insulator/barrier functions in mammalian cells. Although it is a debatable topic, it has been recently reported that very strong loss of CTCF is required (>99%) to detect changes in TADs (Cummings and Rowley, 2022). In fact, additional experiments carried out on compatible systems are needed in order to reach more precise conclusions.

A more sensitive response to hormone is achieved in 3D cells

Cells grown as spheroids are surrounded by other cells, interact differentially with the ECM and receive nutrients and growth factors in a very heterogeneous manner.

However, in response to hormone, the number of hormone-regulated genes is increased twofold in 3D-grown cells compared to 2D, particularly in repressed genes (2017 vs 4055 downregulated, and 2664 vs 3599 upregulated, in 2D and 3D, respectively). In cells grown in 3D, progestins regulate a group of breast cancer-associated genes that are also regulated in 2D including *CDH10, PGR, CHEK2, LSP1, TERT, SDPR*, but also a new set of 3D-exclusive genes, associated to the ECM including members of the integrin family, Laminins, and *AKT3*.

The response to progestins is more sensitive in 3D-grown cells than in cells grown in 2D, as more genes are regulated by hormone. Moreover, the increase in the number of hormone-regulated genes in 3D was accompanied by an increase in the number of PR-binding sites detected by ChIP-seq and many of the 3D-exclusive genes are closer to 3D-exclusive PR peaks (Fig. 6D). Most of these PR-binding sites correspond to enhancers, as determined by H3K27 acetylation.

Moreover, LATS1 activity turned out to be essential for high accessible PR-binding sites (HAs) (Zaurin et al, 2021) function, as the presence of TRULI compromised hormone-dependent response of HA-associated genes (Fig. EV5B). How LATS1 participates in hormonal gene regulation requires further investigation.

Our data support that in 3D-grown cells the chromatin is organized differently compared to monolayer cultured 2D cells. DAPI staining, MNase digestion and ATAC-seq assays confirm that the genome is less accessible in 3D (Fig. 2), which seems somewhat paradoxical to the increased response to hormone (Fig. 6). We found that 3D-activated signals such as the Hippo pathway LATS kinase, impact on the cell nucleus in at least two ways: the LATS kinase phosphorylates both CTCF and YAP promoting the displacement of the first and cytoplasmic retention of the latter. The absence of these two proteins in the 3D nucleus determines the activity of a subset of genes specifically regulated in 3D and in turn, enhances and assures the proper response to hormone (Appendix Fig. S13).

In summary, mechanical and chemical signals in 3D-grown cells "protect" the nucleus by making it more compact, restricting accessibility to certain regions in the genome and facilitating access to others, thus creating a more sensitive platform for the response to external hormonal cues.

3D spheroids: a system that recapitulates the physiological environment of the tumor cell

Cancer cells grown in 3D culture systems exhibit physiologically relevant cell-cell and cell–matrix interactions, gene expression and signaling pathway profiles, heterogeneity and structural complexity

that reflect *in vivo* tumors (Nath and Devi, 2016). Actually, the non-cellular components of the tumor microenvironment (TME), those that are preserved in spheroids, as the extracellular matrix (ECM), growth factors, cytokines, and chemokines, play a significant role in cancer progression (Paszek et al, 2005). We found that breast cancer 3D spheroids showed high expression of key genes involved in tumor growth, as well as LATS1-dependent nuclear receptor binding features shared with PDXs but absent in 2D cells (Appendix Figs. S3 and S12B). In line with this, LATS1 has been linked to cancer cell plasticity and increased resistance to hormone therapy in breast tumors (Furth and Aylon, 2017).

To assess whether our 3D system recapitulate the resistance of breast cancer cells to CDK4/6 inhibitors and endocrine therapy, which is associated with low FAT1 levels and Hippo pathway activation, we conducted a comparative analysis of gene expression data. Specifically, we compared the gene expression profiles of our 3D breast cancer cell model with those from a previous study (Li et al, 2018). Our analysis revealed that cells resistant to CDK4/6 inhibitors and endocrine therapy exhibited reduced levels of FAT1 and demonstrated activation of the Hippo pathway, which matched the characteristics observed in our 3D-grown cells (as depicted in Appendix Fig. S15). However, the resistant cells had lower progesterone receptor (PR) status (Appendix Fig. S15A), leading to decreased expression of genes controlled by progestin, both in terms of activation and repression (Appendix Fig. S15D). Thus, although our 3D model partially replicated the characteristics of resistant cells, it did not entirely reproduce the diminished hormonal response observed in cells lacking FAT1 expression (Appendix Fig. S15E). In fact, in our 3D model, this response was enhanced (Fig. 6A).

Regarding the heterogeneity, gene expression analysis showed that 3D spheroids are enriched in terms associated to nervous system development compared to 2D cells (Fig. 1F; Appendix Fig. S3A). In fact, increasing evidence suggests that the nervous system itself, as well as neurotransmitters and neuropeptides present in the tumor microenvironment, play a role in orchestrating tumor progression (Fernandez-Nogueira et al, 2016). Thus, 3D cells accurately recapitulate the intratumor heterogeneity facilitating tumor progression and fostering the adaptation and survival of the different tumor cells to the different microenvironments in which a tumor resides.

Our results highlight the importance of the 3D system as a reliable model lacking cross-species incompatibilities for breast cancer studies.

Methods

Cell culture and hormone treatments

T47D breast cancer cells were routinely grown in RPMI 1640 medium supplemented with 10% FBS, 2 mM L-glutamine, 100 U/ml penicillin, and 100 µg/ml streptomycin. BT-474, ZR-75, and MCF10A cells were obtained from ATCC and cultured in 2D and 3D in the recommended medium.

For the experiments, cells were plated in RPMI medium without phenol red supplemented with 10% dextran-coated charcoal-treated FBS (DCC/FBS) and 48 h later medium was replaced by fresh medium without serum. After 24 h in serum-free conditions, cells were incubated with 10 nM R5020 for different times at 37 °C.

MCF10A cells were routinely grown in DMEM/F12 medium with 5% horse serum, 20 ng/ml EGF, 100 U/ml penicillin and 100 mg/ml streptomycin, 0.5 mg/mL hydrocortisone, 100 ng/ml cholera toxin, and 10 mg/ml insulin.

3D cell culture on Matrigel

Prechilled p60 plates were coated with a thin layer of Matrigel (Corning Life Sciences) and then incubated for 20–30 min at 37 °C to allow polymerization without over-drying. In total, 200,00 cells trypsinized cells were resuspended and plated on top of the Matrigel without disrupting the capsule. Culture was maintained for 10 days changing the medium every 2–3 days. For hormonal induction on the 3D spheroids, T47D cells were plated on top of phenol red-free Matrigel and after 7 days of culture medium was replaced by RPMI medium without phenol red supplemented with 10% dextran-coated charcoal-treated FBS (DCC/FBS) and 48 h later medium was replaced by fresh medium without serum. After 24 h in serum-free conditions, cells were incubated with 10 nM R5020 for different times at 37 °C.

Spheroids extraction from 3D matrix

Dishes containing the spheroids grown for 10 days were rinsed twice with PBS, followed by the addition of 3 ml ice-cold PBS-EDTA. Matrigel, including the 3D spheroids, was carefully detached with a plastic scraper and left on ice for 30 min to allow complete depolymerization of the gel. The liquid solution was transferred to a conical tube, centrifuged for 5 min at 112 × *g*, and rinsed twice with 0.5 volume of PBS-EDTA. The cell pellet was then ready for further processing.

Chromatin immunoprecipitation (ChIP) in 2D- and 3D-cultured cells

ChIP assays were performed as described (Strutt and Paro, 1999) using anti-PR (H190 SC-7208, Santa Cruz,); anti-RNApol II (#2629, Cell Signaling); anti-CTCF (07-729, Merck); anti-H3K27ac (ab4729, Abcam); anti-H3K18ac (#39693, Active Motif). Quantification of chromatin immunoprecipitation was performed by real-time PCR using Roche Lightcycler (Roche). The fold enrichment of target sequence in the immunoprecipitated (IP) compared to input (Ref) fractions was calculated using the comparative Ct (the number of cycles required to reach a threshold concentration) method with the Eq. (2) $^{Ct(IP)-Ct(Ref)}$. Each of these values was corrected by the human β-globin gene and referred as relative abundance over time zero. Primers sequences for target regions are available on request.

RNA interference experiments

Stable LATS-depleted T47D cells were generated by using lentiviral shRNAs obtained from Sigma (MISSION) shRNA Lentiviral Transduction Particles: TRCN0000001777_LATS and TRCN0000001779_LATS.

Cell proliferation

T47D cells (1×10^3) were plated in a non-transparent-walled 96-well plate in RPMI medium or in charcolized medium in the presence or absence of 10 nM R5020. The TiterGlo reagent

(Promega) was added, and cells were then incubated for 2 min at RT with agitation, followed by 10 min incubation at RT. Bioluminescence was detected in a Barthold luminometer system allowing 0.25 s per well. The experiments were performed in quintuplicate.

Flow cytometry

T47D cells were plated into duplicate wells of six-well plastic dishes and preincubated as described. After 24 h 10 nM R5020 was added. Cells were harvested at the start of treatment (control, zero time) and after 24 h of hormone addition. The cell suspension was pelleted, stained with propidium iodide and treated with ribonuclease (RNase). Samples were cooled to 4 °C, and 10,000 cells were analyzed on a BD FACSCanto analyser flow cytometer.

Live/dead assay

To visualize the number of viable cells in a 3D spheroid the LIVE/DEAD™ Cell Imaging Kit was used according to the manufacturer protocol.

Immunofluorescence

For immunostaining, 1×10^3 cells per well were seeded on Matrigel precoated eight-well LabTek (10 mm). 2D and 3D cells grown for 3 and 10 days, respectively, were washed two times with PBS and fixed for 10 min with 4% fresh Paraformaldehyde (PFA), before being permeabilized during 30 min with 0.5% Triton X-100 in PBS. Samples were then blocked during 1.5 h with 5% BSA solution. Then, the cells were incubated o/n at 4 °C with the corresponding antibody diluted in the IF solution.

The following day, cells were washed three consecutive times with IF solution during 10 min each. The samples were then incubated during 1 h at 4 °C with the secondary antibody in a humid dark chamber.

The secondary antibodies used were: AlexaFluor 488 anti-rabbit IgG (1:1000; raised in donkey) and AlexaFluor 546 anti-mouse (1:1000; raised in goat). After the incubation with the secondary antibody, cells were washed once with IF solution, incubated during 10 min with 0.1 mg/ml DAPI in PBS, and then washed with PBS three times, before mounting in Mowiol 4-88 Mounting Medium for imaging. Images were collected sequentially on a Leica SP8-STED confocal laser-scanning microscope using the software Leica Application Suite X. All collected images conserved an optical thickness of 0.25 µm. Image analysis for marker distribution, quantification, and colocalization were performed using ImageJ (Schindelin et al, 2012).

Preparation of cell extracts and western blot

Matrigel-free cell pellets were collected and washed two times with PBS-EDTA and lysed with RIPA buffer followed by incubation at 95 °C for 10 min. For western blotting, pellets were centrifuged and quantified by Bradford before being loaded and run in SDS-acrylamide gels. The following antibodies were used: CTCF (07-729, Millipore); ERα (H20, Santa Cruz); PR (H190, Santa Cruz); FAK (PTK2) (3285, Cell Signaling); LATS (3477, Cell Signaling); LATS-S909(9157, Cell Signaling); pFAKT397 (ab81298, Abcam); pPRs294 (ab61785, Abcam); pYAP127 (4911, Cell Signaling) and YAP (sc-101199, Santa Cruz).

Phos-tag gels

Whole-cell lysates were separated on a 5% SDS/PAGE containing 20 µM Phos-tag (NARD Institute), followed by western blotting with anti-CTCF antibody.

MNase digestion

2D and 3D-grown T47D cells were washed once with PBS, collected in 2 ml cold PBS + PIC, and centrifuged 5 min at 900 × *g* at 4 °C. The cell pellet was then gently resuspended in 50 µl RBS buffer (10 mM Tris-HCl pH 7.4, 10 mM NaCl, 3 mM CaCl2.) followed by the addition of 1.3 ml RBS buffer + 0.1% NP40. Cells were centrifuged again for 10 min at 500 × *g* at 4 °C and the nuclei were then resuspended in RBS buffer for counting. An amount of 600,000 nuclei obtained from 2D and 3D-grown cells were treated with 0, 30, 45, 90 Units of MNase to obtain differential digestion patterns. The MNase reaction was carried out in 500 µl final volume reaction. The nuclei were then incubated for 2 min at 37 °C. The reaction was stopped with 40 mM EDTA 0.5 M and then treated with RNAseA 10 mg/ ml for 30 min at 37 °C and Proteinase K (1.2 µg/µl) for 1 h at 45 °C. The DNA was purified with Phenol/Chloroform, and 600 ng of material was loaded in a 1.2% agarose gel.

RNA-seq

RNA was extracted from T47D cells grown in 2D and 3D conditions in RPMI 1640 medium. To evaluate the effect of the hormone, 2D and 3D T47D cells were treated or not for 6 h with 10 nM R5020 and submitted to massive sequencing using the Solexa Genome Analyzer. The protocol followed to analyze the RNA-seq data can be found in the Supplementary Methods section.

ChIP-seq

ChIP-DNA was purified and subjected to deep sequencing using the Solexa Genome Analyzer (Illumina, San Diego, CA). The protocol followed to analyze the ChIP-seq data can be found in the Supplementary Methods section.

ATAC-seq

ATAC experiments were performed as described (Buenrostro et al, 2013) using nuclei obtained from 2D or 3D-grown T47D cells. Extended bioinformatics methods can be found in the Supplementary information.

Hi-C experiments

Hi-C libraries were generated from 2D and 3D-grown T47D cells treated or not with R5020 for 60 min according to the previously published Hi-C protocol with minor adaptations (Lieberman-Aiden et al, 2009). Hi-C libraries were generated independently in both conditions using HindIII and NcoI restriction enzymes. Hi-C libraries were controlled for quality and sequenced on an Illumina

Hiseq2000 sequencer. The Illumina Hi-seq paired-end reads were processed by aligning to the reference human genome (GRCh37/hg19) using BWA.

Data availability

The raw sequencing data from this study (ChIP- seq, ATAC-seq, RNA-seq, and Hi-C) were submitted to the NCBI Gene Expression Omnibus (GEO; http://www.ncbi.nlm.nih.gov/geo/) repository, and the accession number is GSE247777.

Expanded view data, supplementary information, appendices are available for this paper at https://doi.org/10.1038/s44318-024-00080-x.

Peer review information

A peer review file is available at https://doi.org/10.1038/s44318-024-00080-x

References

Ballare C, Castellano G, Gaveglia L, Althammer S, Gonzalez-Vallinas J, Eyras E, Le Dily F, Zaurin R, Soronellas D, Vicent GP et al (2013) Nucleosome-driven transcription factor binding and gene regulation. Mol Cell 49:67–79

Barcellos-Hoff MH, Aggeler J, Ram TG, Bissell MJ (1989) Functional differentiation and alveolar morphogenesis of primary mammary cultures on reconstituted basement membrane. Development 105:223–235

Barski A, Cuddapah S, Cui K, Roh TY, Schones DE, Wang Z, Wei G, Chepelev I, Zhao K (2007) High-resolution profiling of histone methylations in the human genome. Cell 129:823–837

Barutcu AR, Maass PG, Lewandowski JP, Weiner CL, Rinn JL (2018) A TAD boundary is preserved upon deletion of the CTCF-rich Firre locus. Nat Commun 9:1444

Beato M, Herrlich P, Schutz G (1995) Steroid hormone receptors: many actors in search of a plot. Cell 83:851–857

Beato M, Vicent GP (2011) When every minute counts: the enzymatic complexity associated with the activation of hormone-dependent genes. Cell Cycle 10:2407–2409

Britschgi A, Duss S, Kim S, Couto JP, Brinkhaus H, Koren S, De Silva D, Mertz KD, Kaup D, Varga Z et al (2017) The Hippo kinases LATS1 and 2 control human breast cell fate via crosstalk with ERalpha. Nature 541:541–545

Brozovich FV, Nicholson CJ, Degen CV, Gao YZ, Aggarwal M, Morgan KG (2016) Mechanisms of vascular smooth muscle contraction and the basis for pharmacologic treatment of smooth muscle disorders. Pharmacol Rev 68:476–532

Buenrostro JD, Giresi PG, Zaba LC, Chang HY, Greenleaf WJ (2013) Transposition of native chromatin for fast and sensitive epigenomic profiling of open chromatin, DNA-binding proteins and nucleosome position. Nat Methods 10:1213–1218

Candas D, Lu CL, Fan M, Chuang FY, Sweeney C, Borowsky AD, Li JJ (2014) Mitochondrial MKP1 is a target for therapy-resistant HER2-positive breast cancer cells. Cancer Res 74:7498–7509

Caswell PT, Zech T (2018) Actin-based cell protrusion in a 3D matrix. Trends Cell Biol 28:823–834

Cummings CT, Rowley MJ (2022) Implications of dosage deficiencies in CTCF and cohesin on genome organization, gene expression, and human neurodevelopment. Genes 13:583

Derricks KE, Trinkaus-Randall V, Nugent MA (2015) Extracellular matrix stiffness modulates VEGF calcium signaling in endothelial cells: individual cell and population analysis. Integr Biol 7:1011–1025

Dixon JR, Selvaraj S, Yue F, Kim A, Li Y, Shen Y, Hu M, Liu JS, Ren B (2012) Topological domains in mammalian genomes identified by analysis of chromatin interactions. Nature 485:376–380

Duan Z, Andronescu M, Schutz K, McIlwain S, Kim YJ, Lee C, Shendure J, Fields S, Blau CA, Noble WS (2010) A three-dimensional model of the yeast genome. Nature 465:363–367

Dupont S, Morsut L, Aragona M, Enzo E, Giulitti S, Cordenonsi M, Zanconato F, Le Digabel J, Forcato M, Bicciato S et al (2011) Role of YAP/TAZ in mechanotransduction. Nature 474:179–183

Elosegui-Artola A, Andreu I, Beedle AEM, Lezamiz A, Uroz M, Kosmalska AJ, Oria R, Kechagia JZ, Rico-Lastres P, Le Roux AL et al (2017) Force triggers YAP nuclear entry by regulating transport across nuclear pores. Cell 171:1397–1410.e1314.

Fernandez-Nogueira P, Bragado P, Almendro V, Ametller E, Rios J, Choudhury S, Mancino M, Gascon P (2016) Differential expression of neurogenes among breast cancer subtypes identifies high risk patients. Oncotarget 7:5313–5326

Ferrari R, Su T, Li B, Bonora G, Oberai A, Chan Y, Sasidharan R, Berk AJ, Pellegrini M, Kurdistani SK (2012) Reorganization of the host epigenome by a viral oncogene. Genome Res 22:1212–1221

Flyamer IM, Gassler J, Imakaev M, Brandao HB, Ulianov SV, Abdennur N, Razin SV, Mirny LA, Tachibana-Konwalski K (2017) Single-nucleus Hi-C reveals unique chromatin reorganization at oocyte-to-zygote transition. Nature 544:110–114

Franke M, De la Calle-Mustienes E, Neto A, Almuedo-Castillo M, Irastorza-Azcarate I, Acemel RD, Tena JJ, Santos-Pereira JM, Gomez-Skarmeta JL (2021) CTCF knockout in zebrafish induces alterations in regulatory landscapes and developmental gene expression. Nat Commun 12:5415

Furth N, Aylon Y (2017) The LATS1 and LATS2 tumor suppressors: beyond the Hippo pathway. Cell Death Differ 24:1488–1501

Garreta E, Prado P, Tarantino C, Oria R, Fanlo L, Marti E, Zalvidea D, Trepat X, Roca-Cusachs P, Gavalda-Navarro A et al (2019) Fine tuning the extracellular environment accelerates the derivation of kidney organoids from human pluripotent stem cells. Nat Mater 18:397–405

Ge H, Tian M, Pei Q, Tan F, Pei H (2021) Extracellular matrix stiffness: new areas affecting cell metabolism. Front Oncol 11:631991

Heinz S, Texari L, Hayes MGB, Urbanowski M, Chang MW, Givarkes N, Rialdi A, White KM, Albrecht RA, Pache L et al (2018) Transcription elongation can affect genome 3D structure. Cell 174:1522–1536.e1522

Hnisz D, Abraham BJ, Lee TI, Lau A, Saint-Andre V, Sigova AA, Hoke HA, Young RA (2013) Super-enhancers in the control of cell identity and disease. Cell 155:934–947

Jiang Y, Qian F, Bai X, Liu Y, Wang Q, Ai B, Han X, Shi S, Zhang J, Li X et al (2019) SEdb: a comprehensive human super-enhancer database. Nucleic Acids Res 47:D235–D243

Kastan N, Gnedeva K, Alisch T, Petelski AA, Huggins DJ, Chiaravalli J, Aharanov A, Shakked A, Tzahor E, Nagiel A et al (2021) Small-molecule inhibition of Lats kinases may promote Yap-dependent proliferation in postmitotic mammalian tissues. Nat Commun 12:3100

Kim DH, Li B, Si F, Phillip JM, Wirtz D, Sun SX (2015) Volume regulation and shape bifurcation in the cell nucleus. J Cell Sci 128:3375–3385

Kim DH, Wirtz D (2015) Cytoskeletal tension induces the polarized architecture of the nucleus. Biomaterials 48:161–172

Kim J, Koo BK, Knoblich JA (2020) Human organoids: model systems for human biology and medicine. Nat Rev Mol Cell Biol 21:571–584

Le Dily F, Bau D, Pohl A, Vicent GP, Serra F, Soronellas D, Castellano G, Wright RH, Ballare C, Filion G et al (2014) Distinct structural transitions of chromatin

topological domains correlate with coordinated hormone-induced gene regulation. Genes Dev 28:2151–2162

Le Dily F, Vidal E, Cuartero Y, Quilez J, Nacht AS, Vicent GP, Carbonell-Caballero J, Sharma P, Villanueva-Canas JL, Ferrari R et al (2019) Hormone-control regions mediate steroid receptor-dependent genome organization. Genome Res 29:29–39

Lee GY, Kenny PA, Lee EH, Bissell MJ (2007) Three-dimensional culture models of normal and malignant breast epithelial cells. Nat Methods 4:359–365

Li Z, Razavi P, Li Q, Toy W, Liu B, Ping C, Hsieh W, Sanchez-Vega F, Brown DN, Da Cruz Paula AF et al (2018) Loss of the FAT1 tumor suppressor promotes resistance to CDK4/6 inhibitors via the hippo pathway. Cancer Cell 34:893–905.e898

Li Z, Zhao B, Wang P, Chen F, Dong Z, Yang H, Guan KL, Xu Y (2010) Structural insights into the YAP and TEAD complex. Genes Dev 24:235–240

Lieberman-Aiden E, van Berkum NL, Williams L, Imakaev M, Ragoczy T, Telling A, Amit I, Lajoie BR, Sabo PJ, Dorschner MO et al (2009) Comprehensive mapping of long-range interactions reveals folding principles of the human genome. Science 326:289–293

Lit LC, Scott S, Zhang H, Stebbing J, Photiou A, Giamas G (2013) LATS2 is a modulator of estrogen receptor alpha. Anticancer Res 33:53–63

Luo H, Yu Q, Liu Y, Tang M, Liang M, Zhang D, Xiao TS, Wu L, Tan M, Ruan Y et al (2020) LATS kinase-mediated CTCF phosphorylation and selective loss of genomic binding. Sci Adv 6:eaaw4651

Maguire SL, Peck B, Wai PT, Campbell J, Barker H, Gulati A, Daley F, Vyse S, Huang P, Lord CJ et al (2016) Three-dimensional modelling identifies novel genetic dependencies associated with breast cancer progression in the isogenic MCF10 model. J Pathol 240:315–328

Martin L, Vicario C, Castells-Garcia A, Lakadamyali M, Neguembor MV, Cosma MP (2021) A protocol to quantify chromatin compaction with confocal and super-resolution microscopy in cultured cells. STAR Protoc 2:100865

Meng Z, Moroishi T, Guan KL (2016) Mechanisms of Hippo pathway regulation. Genes Dev 30:1–17

Menon G, Schulten A, Dean C, Howard M (2021) Digital paradigm for Polycomb epigenetic switching and memory. Curr Opin Plant Biol 61:102012

Migliaccio A, Di Domenico M, Castoria G, de Falco A, Bontempo P, Nola E, Auricchio F (1996) Tyrosine kinase/p21ras/MAP-kinase pathway activation by estradiol-receptor complex in MCF-7 cells. EMBO J 15:1292–1300

Musgrove EA, Lee CS, Buckley MF, Sutherland RL (1994) Cyclin D1 induction in breast cancer cells shortens G1 and is sufficient for cells arrested in G1 to complete the cell cycle. Proc Natl Acad Sci USA 91:8022–8026

Nath S, Devi GR (2016) Three-dimensional culture systems in cancer research: focus on tumor spheroid model. Pharmacol Ther 163:94–108

Nora EP, Lajoie BR, Schulz EG, Giorgetti L, Okamoto I, Servant N, Piolot T, van Berkum NL, Meisig J, Sedat J et al (2012) Spatial partitioning of the regulatory landscape of the X-inactivation centre. Nature 485:381–385

Owen GI, Richer JK, Tung L, Takimoto G, Horwitz KB (1998) Progesterone regulates transcription of the p21(WAF1) cyclin-dependent kinase inhibitor gene through Sp1 and CBP/p300. J Biol Chem 273:10696–10701

Paszek MJ, Zahir N, Johnson KR, Lakins JN, Rozenberg GI, Gefen A, Reinhart-King CA, Margulies SS, Dembo M, Boettiger D et al (2005) Tensional homeostasis and the malignant phenotype. Cancer Cell 8:241–254

Planas-Silva MD, Donaher JL, Weinberg RA (1999) Functional activity of ectopically expressed estrogen receptor is not sufficient for estrogen-mediated cyclin D1 expression. Cancer Res 59:4788–4792

Powzaniuk M, McElwee-Witmer S, Vogel RL, Hayami T, Rutledge SJ, Chen F, Harada S, Schmidt A, Rodan GA, Freedman LP et al (2004) The LATS2/KPM tumor suppressor is a negative regulator of the androgen receptor. Mol Endocrinol 18:2011–2023

Prall OW, Sarcevic B, Musgrove EA, Watts CK, Sutherland RL (1997) Estrogen-induced activation of Cdk4 and Cdk2 during G1-S phase progression is accompanied by increased cyclin D1 expression and decreased cyclin-dependent kinase inhibitor association with cyclin E-Cdk2. J Biol Chem 272:10882–10894

Reddy KL, Zullo JM, Bertolino E, Singh H (2008) Transcriptional repression mediated by repositioning of genes to the nuclear lamina. Nature 452:243–247

Salman T, Demir L, Varol U, Akyol M, Oflazoglu U, Yildiz Y, Taskaynatan H, Cengiz H, Guvendi G, Kucukzeybek Y et al (2016) Serum apelin levels and body composition changes in breast cancer patients treated with an aromatase inhibitor. J BUON 21:1419–1424

Schindelin J, Arganda-Carreras I, Frise E, Kaynig V, Longair M, Pietzsch T, Preibisch S, Rueden C, Saalfeld S, Schmid B, Tinevez JY, White DJ, Hartenstein V, Eliceiri K, Tomancak P, Cardona A (2012) Fiji: an open-source platform for biological-image analysis. Nat Methods. 9:676–682.

Stadhouders R, Filion GJ, Graf T (2019) Transcription factors and 3D genome conformation in cell-fate decisions. Nature 569:345–354

Strutt H, Paro R (1999) Mapping DNA target sites of chromatin proteins in vivo by formaldehyde crosslinking. Methods Mol Biol 119:455–467

Ulianov SV, Khrameeva EE, Gavrilov AA, Flyamer IM, Kos P, Mikhaleva EA, Penin AA, Logacheva MD, Imakaev MV, Chertovich A et al (2016) Active chromatin and transcription play a key role in chromosome partitioning into topologically associating domains. Genome Res 26:70–84

Uroz M, Wistorf S, Serra-Picamal X, Conte V, Sales-Pardo M, Roca-Cusachs P, Guimera R, Trepat X (2018) Regulation of cell cycle progression by cell-cell and cell-matrix forces. Nat Cell Biol 20:646–654

Vicent GP, Ballare C, Nacht AS, Clausell J, Subtil-Rodriguez A, Quiles I, Jordan A, Beato M (2006) Induction of progesterone target genes requires activation of Erk and Msk kinases and phosphorylation of histone H3. Mol Cell 24:367–381

Vicent GP, Nacht AS, Ballare C, Zaurin R, Soronellas D, Beato M (2014) Progesterone receptor interaction with chromatin. Methods Mol Biol 1204:1–14

Vicent GP, Nacht AS, Font-Mateu J, Castellano G, Gaveglia L, Ballare C, Beato M (2011) Four enzymes cooperate to displace histone H1 during the first minute of hormonal gene activation. Genes Dev 25:845–862

Vicent GP, Nacht AS, Zaurin R, Ballare C, Clausell J, Beato M (2010) Minireview: role of kinases and chromatin remodeling in progesterone signaling to chromatin. Mol Endocrinol 24:2088–2098

Vilarrasa-Blasi R, Soler-Vila P, Verdaguer-Dot N, Russinol N, Di Stefano M, Chapaprieta V, Clot G, Farabella I, Cusco P, Kulis M et al (2021) Dynamics of genome architecture and chromatin function during human B cell differentiation and neoplastic transformation. Nat Commun 12:651

Wang Z, Zang C, Rosenfeld JA, Schones DE, Barski A, Cuddapah S, Cui K, Roh TY, Peng W, Zhang MQ et al (2008) Combinatorial patterns of histone acetylations and methylations in the human genome. Nat Genet 40:897–903

Wu J, Li PC, Pang JY, Liu GY, Xie XM, Li JY, Yin YC, Han JH, Guo XZ, Qiu L (2017) CCCTC-binding factor inhibits breast cancer cell proliferation and metastasis via inactivation of the nuclear factor-kappaB pathway. Oncotarget 8:93516–93529

Xu B, Wang H, Wright S, Hyle J, Zhang Y, Shao Y, Niu M, Fan Y, Rosikiewicz W, Djekidel MN et al (2021) Acute depletion of CTCF rewires genome-wide chromatin accessibility. Genome Biol 22:244

Yu FX, Zhao B, Guan KL (2015) Hippo pathway in organ size control, tissue homeostasis, and cancer. Cell 163:811–828

Zanconato F, Battilana G, Cordenonsi M, Piccolo S (2016) YAP/TAZ as therapeutic targets in cancer. Curr Opin Pharmacol 29:26–33

Zanconato F, Cordenonsi M, Piccolo S (2019) YAP and TAZ: a signalling hub of the tumour microenvironment. Nat Rev Cancer 19:454–464

Zaurin R, Ferrari R, Nacht AS, Carbonell J, Le Dily F, Font-Mateu J, de Llobet Cucalon LI, Vidal E, Lioutas A, Beato M et al (2021) A set of accessible enhancers enables the initial response of breast cancer cells to physiological progestin concentrations. Nucleic Acids Res 49:12716–12731

Zhao B, Ye X, Yu J, Li L, Li W, Li S, Yu J, Lin JD, Wang CY, Chinnaiyan AM et al (2008) TEAD mediates YAP-dependent gene induction and growth control. Genes Dev 22:1962–1971

Zheng R, Wan C, Mei S, Qin Q, Wu Q, Sun H, Chen CH, Brown M, Zhang X, Meyer CA et al (2019) Cistrome Data Browser: expanded datasets and new tools for gene regulatory analysis. Nucleic Acids Res 47:D729–D735

Acknowledgements

The authors would like to thank Jianrong Lu (University of Florida College of Medicine, USA) for generously sharing the CTCF constructs. Additionally, we also would like to thank Dr. Julia Ponomarenko (Bioinformatics Unit, CRG) for their valuable advice, technical assistance and involvement in processing the RNA-seq, ChIP-seq, and ATAC-seq data. The experimental work was supported by grants from the Departament d'Innovació Universitat i Empresa (DIUiE), the Spanish Ministry of Economy and Competitiveness (SAF2016-75006-P, PID2019-105173RB-I00, and PID2022-137045OB-I00) and Consejo Superior de Investigaciones Científicas (Ref# 2018201131), 'Centro de Excelencia Severo Ochoa 2013-2017', SEV-2012-2018 and ERC Synergy Grant "4DGenome" nr: 609989. MAM-R acknowledges support by the Spanish Ministerio de Ciencia e Innovación (PID2020-115696RB-I00). This work has benefited from the equipment and framework of the COMP-HUB and COMP-R Initiatives, funded by the 'Departments of Excellence' program of the Italian Ministry for University and Research (MIUR, 2018-2022 and MUR, 2023-2027) and from the HPC (High-Performance Computing) facility of the University of Parma, Italy.

Author contributions

Julieta Ramirez Cuellar: Investigation; Methodology. **Roberto Ferrari**: Formal analysis; Investigation. **Rosario T Sanz**: Investigation; Methodology. **Marta Valverde-Santiago**: Investigation; Methodology. **Judith García García**: Formal analysis; Investigation; Methodology. **A Silvina Nacht**: Investigation; Methodology. **David Castillo**: Formal analysis; Investigation; Methodology. **Francois Le Dily**: Formal analysis; Investigation. **Maria Victoria Neguembor**: Formal analysis; Investigation; Methodology. **Marco Malatesta**: Formal analysis; Investigation; Writing—review and editing. **Sarah Bonnin**: Formal analysis; Supervision; Investigation; Methodology; Writing—original draft; Writing—review and editing. **Marc A Marti-Renom**: Formal analysis; Investigation; Methodology. **Miguel Beato**: Investigation; Methodology; Writing—review and editing. **Guillermo P Vicent**: Formal analysis; Supervision; Investigation; Methodology; Writing—original draft; Writing—review and editing.

Disclosure and competing interests statement

The authors declare no competing interests.

Expanded View Figures

Figure EV1. Profiles of H3K27me3, H3K9me3 and super-enhancers detected in 2D and 3D T47D breast cancer cells.

(**A**) The H3K27me3 profiles in 3D-repressed and activated genes (blue and green lines, respectively) obtained in both conditions (first and second panels, from the left) is shown. Third and fourth panel from the left: profiles of H3K27me3 in 2D and 3D random genes. Right panel: Genome browser view of H3K27me3 ChIP-seq data in the NRCAM gene. (**B**) The H3K9me3 profiles in 3D-repressed and activated genes (blue and green lines, respectively) obtained in both conditions (first and second panels, from the left) is depicted. Third and fourth panels from the left: profiles of H3K9me3 in 2D and 3D random genes. (**C**) The enrichment of the H3K27ac signal in super-enhancers obtained from 2D and 3D cells is shown. (**D**) Venn diagram corresponding to the super-enhancers detected in T47D cells grown in 2D and 3D conditions.

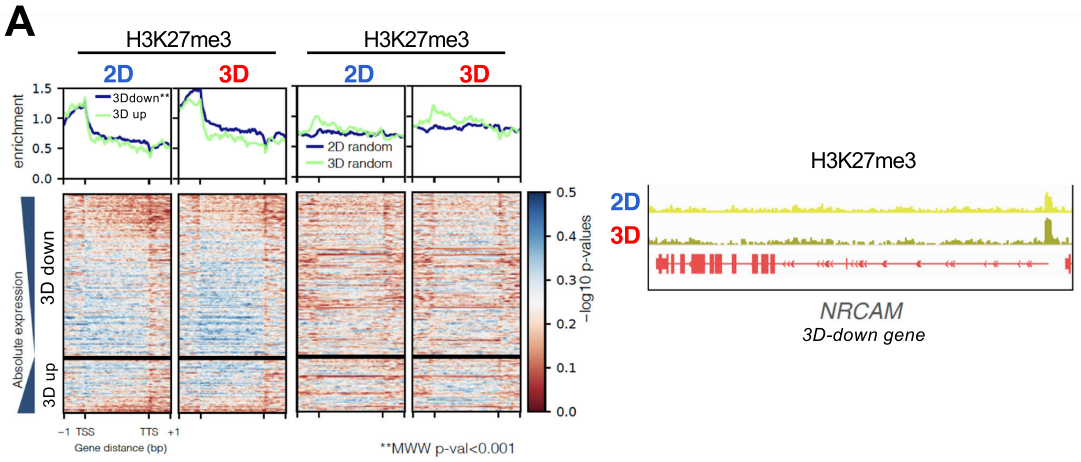
A
H3K27me3
H3K27me3
2D
3D
2D
3D
enrichment
3Ddown**
3D up
2D random
3D random
3D down
3D up
Absolute expression
−log10 p-values
−1 TSS
TTS +1
Gene distance (bp)
**MWW p-val<0.001
H3K27me3
2D
3D
NRCAM
3D-down gene

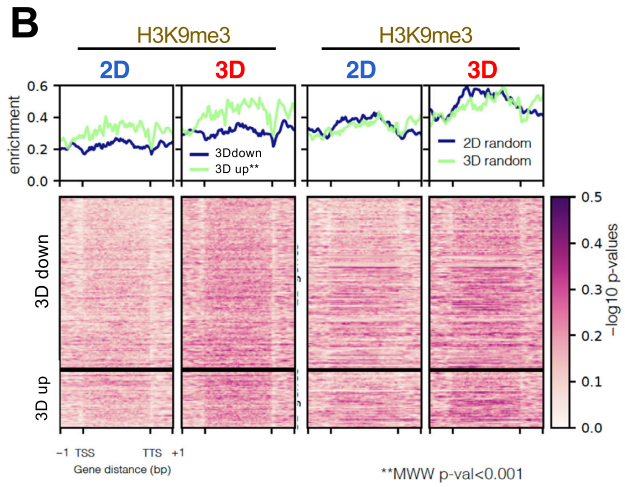
B
H3K9me3
H3K9me3
2D
3D
2D
3D
enrichment
3Ddown
3D up**
2D random
3D random
3D down
3D up
−log10 p-values
−1 TSS
TTS +1
Gene distance (bp)
**MWW p-val<0.001

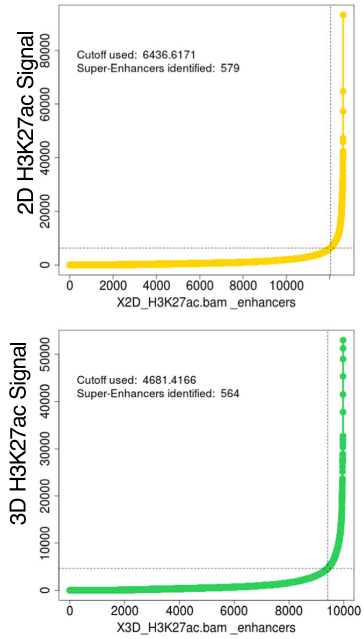
C
2D H3K27ac Signal
Cutoff used: 6436.6171
Super-Enhancers identified: 579
X2D_H3K27ac.bam _enhancers
3D H3K27ac Signal
Cutoff used: 4681.4166
Super-Enhancers identified: 564
X3D_H3K27ac.bam _enhancers

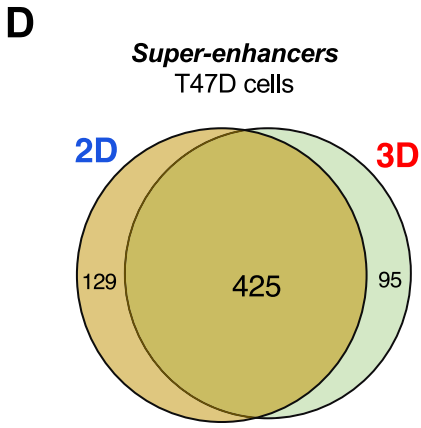
D
Super-enhancers
T47D cells
2D
3D
129
425
95

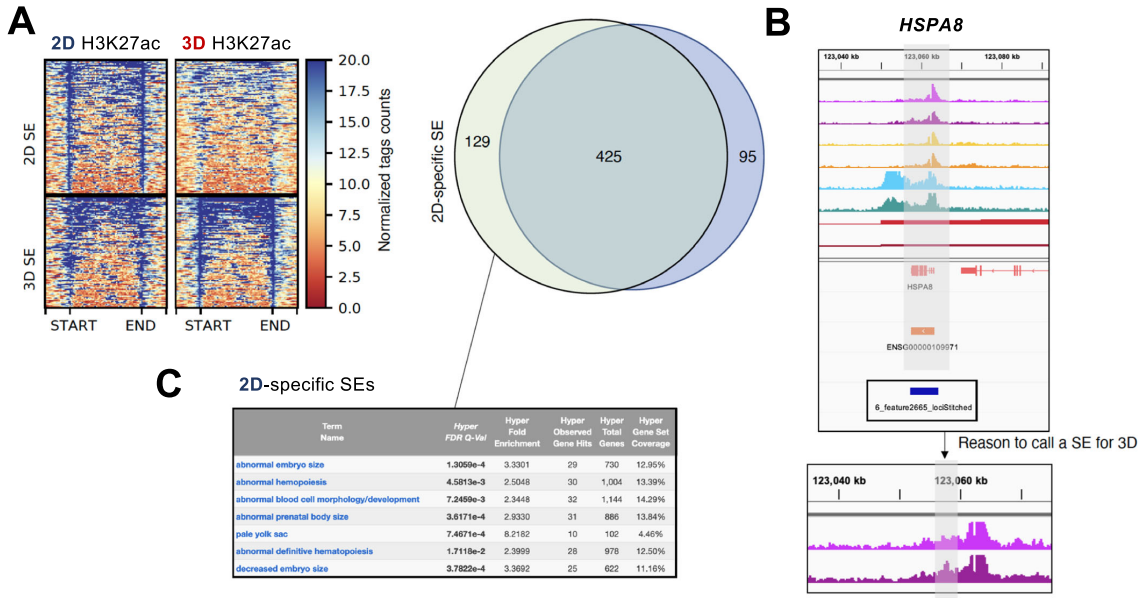

Term Name	Hyper FDR Q-Val	Hyper Fold Enrichment	Hyper Observed Gene Hits	Hyper Total Genes	Hyper Gene Set Coverage
abnormal embryo size	1.3059e-4	3.3301	29	730	12.95%
abnormal hemopoiesis	4.5813e-3	2.5048	30	1,004	13.39%
abnormal blood cell morphology/development	7.2459e-3	2.3448	32	1,144	14.29%
abnormal prenatal body size	3.6171e-4	2.9330	31	886	13.84%
pale yolk sac	7.4671e-4	8.2182	10	102	4.46%
abnormal definitive hematopoiesis	1.7118e-2	2.3999	28	978	12.50%
decreased embryo size	3.7822e-4	3.3692	25	622	11.16%

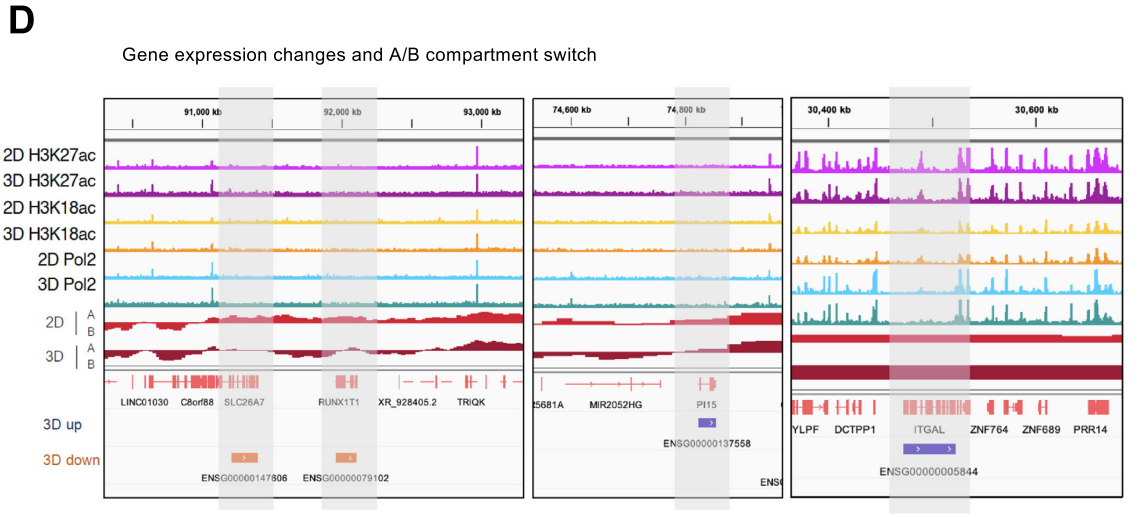

Figure EV2. Characterization of super-enhancers identified in 2D and 3D cells.

(A) The enrichment of the H3K27ac signal in super-enhancers obtained from 2D and 3D cells is shown. Venn diagram corresponding to the super-enhancers detected in T47D cells grown in 2D and 3D conditions. By using a proximity-based script (Hnisz et al, 2013), we found 129 and 95 genes associated to 2D and 3D SEs, respectively (right panel). In the case of genes exclusively regulated in the 3D condition by SEs, many of them appear to be artifacts, as illustrated with the HSPA8 gene (**B**). (**C**) The 2D-exclusive genes are related to terms like abnormal embryo size, abnormal development, and hematopoiesis. (**D**) Snapshots from the genome browser illustrating the transitions for two 3D downregulated genes, SLC26A7 and RUNX1T1, and two 3D upregulated genes, PI15 and ITGAL are shown.

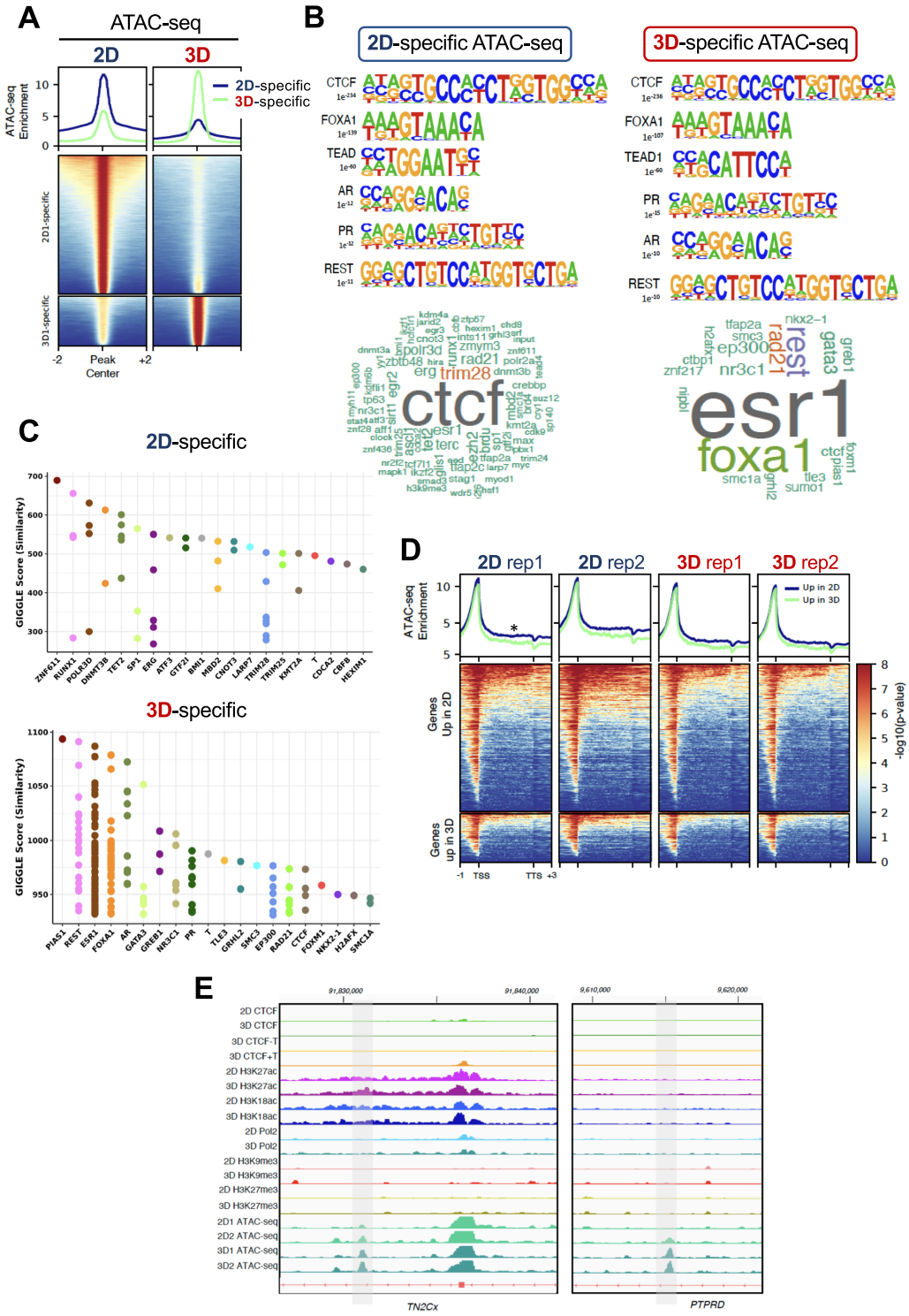
A
ATAC-seq
2D
3D
2D-specific
3D-specific
ATAC-seq Enrichment
2D1-specific
3D1-specific
-2
Peak Center
+2
B
2D-specific ATAC-seq
3D-specific ATAC-seq
CTCF
FOXA1
TEAD
TEAD1
AR
PR
REST
C
2D-specific
3D-specific
GIGGLE Score (Similarity)
D
2D rep1
2D rep2
3D rep1
3D rep2
Up in 2D
Up in 3D
Genes Up in 2D
Genes up in 3D
-log10(pvalue)
TSS
TTS
E
2D CTCF
3D CTCF
3D CTCF-T
3D CTCF+T
2D H3K27ac
3D H3K27ac
2D H3K18ac
3D H3K18ac
2D Pol2
3D Pol2
2D H3K9me3
3D H3K9me3
2D H3K27me3
3D H3K27me3
2D1 ATAC-seq
2D2 ATAC-seq
3D1 ATAC-seq
3D2 ATAC-seq
TN2Cx
PTPRD

Figure EV3. Regions more accessible in 3D are enriched in estrogenic signaling.

(**A**) Heatmaps of ATAC-seq data performed in 2D and 3D T47D cells. The exclusive regions belonging to each condition is highlighted. (**B**) Homer motif analysis of 2D and 3D-exclusive ATAC-seq regions (upper panel). When the same regions are contrasted with available ChIP-seq data, the CTCF and ESR1 terms appear enriched (bottom panels). (**C**) Giggle score of the data presented in (**B**). (**D**) Heatmaps of the ATAC-seq signal around 2D and 3D upgenes. (**E**) Snapshot of the genome browser around TN2Cx and PTPRD genes showing the profiles of H3K27ac, RNAPol2, H3K9me3, H3K27me3 and ATAC-seq.

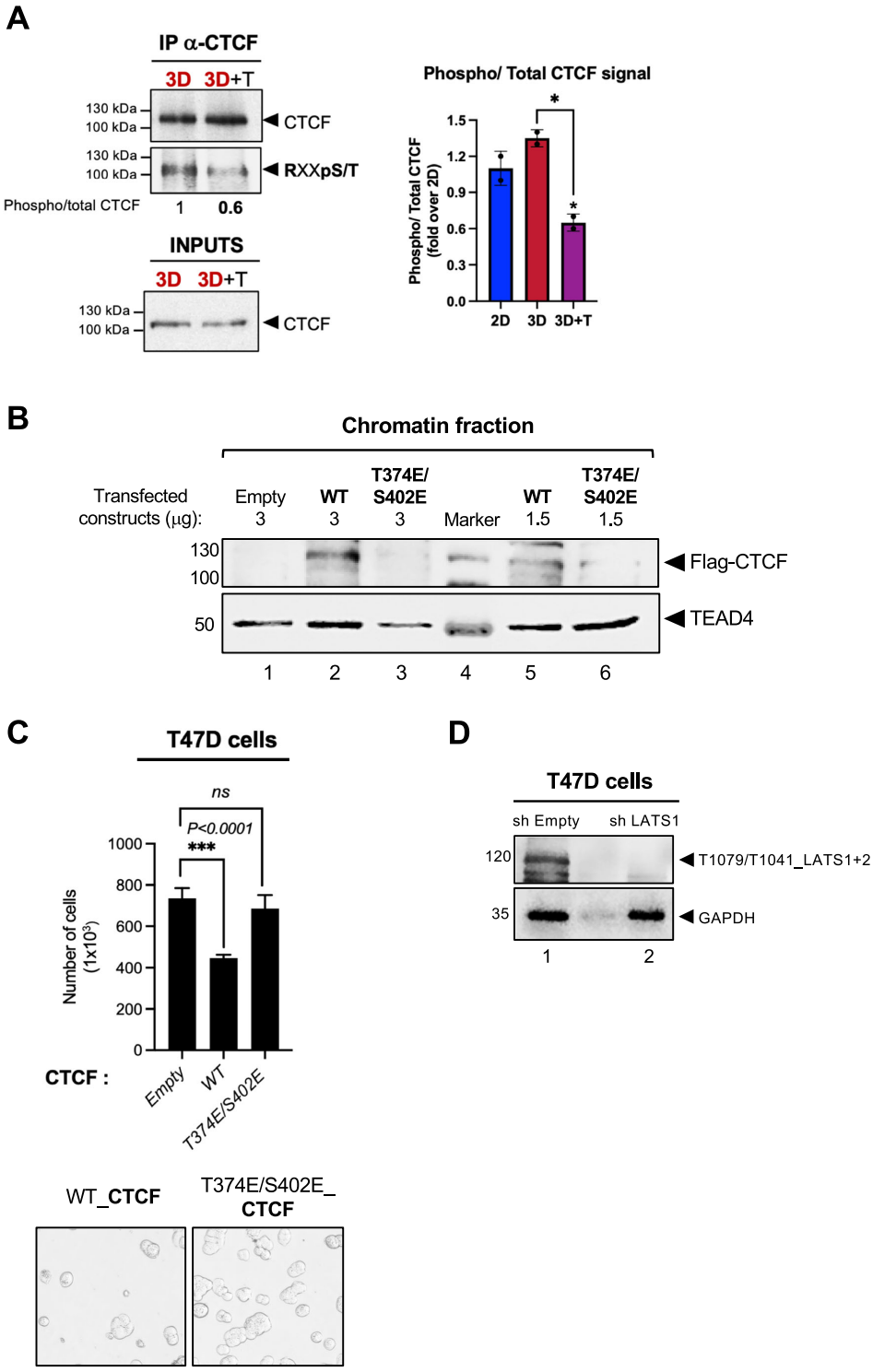
A
IP α-CTCF
3D 3D+T
130 kDa
100 kDa
CTCF
RXXpS/T
Phospho/total CTCF 1 0.6
INPUTS
3D 3D+T
CTCF
Phospho/ Total CTCF signal
Phospho/ Total CTCF (fold over 2D)
2D 3D 3D+T
B
Chromatin fraction
Transfected constructs (μg):
Empty 3
WT 3
T374E/ S402E 3
Marker
WT 1.5
T374E/ S402E 1.5
130
100
50
Flag-CTCF
TEAD4
1 2 3 4 5 6
C
T47D cells
ns
P<0.0001
***
Number of cells (1x10³)
CTCF :
Empty
WT
T374E/S402E
WT_CTCF
T374E/S402E_ CTCF
D
T47D cells
sh Empty
sh LATS1
120
35
T1079/T1041_LATS1+2
GAPDH
1 2

Figure EV4. CTCF phosphorylation is reduced in the presence of LATS inhibitor.

(**A**) 2D, 3D and 3D treated with TRULI T47D cells were cultured and subjected to immunoprecipitation with anti-CTCF antibodies and the immunoblotting for phospho-RxxS/T was performed. For quantification, the intensity of phospho-CTCF versus total CTCF signal in control samples is shown (right panel). (**B**) T47D cells were transiently transfected with wild-type (WT) and T374E/S402E (phospho-mimetic) CTCF flag-tagged constructs. Subsequently, cells were lysed, and the chromatin fraction was isolated to display the presence of flag-CTCF bound to the chromatin fraction. (**C**) Cell growth assays performed in T47D cells expressing both wild-type (WT) and a phospho-mimetic variant of CTCF T374E/S402E. (**D**) The levels of T1079/T1041p LATS1 + 2 signal in both shEmpty (control) and shLATS1 cells is shown. The noticeable decrease in the phospho T1079/T1041 signal and LATS1 (Fig. 5C) suggests that the predominant portion of detected p-LATS corresponds to LATS1 in the 3D model. GAPDH is used as loading control. Source data are available online for this figure.

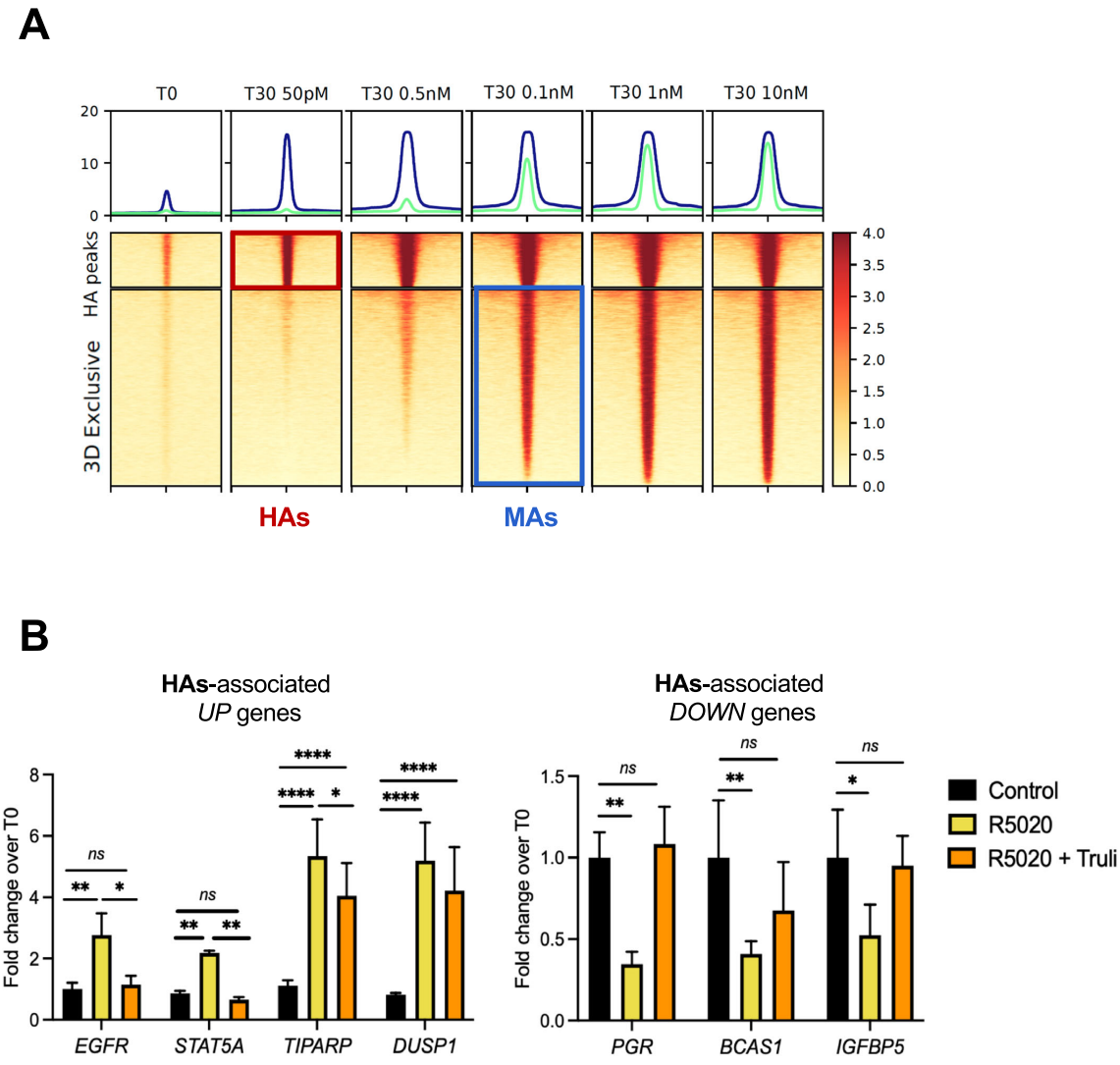

Figure EV5. Hormone-dependent CTCF recruitment to High accessible PR binding sites (HAs) requires LATS1 activity.

(**A**) Heatmaps of PR ChIP-seq signal obtained at different concentrations of R5020 and corresponding to HAs and 3D-exclusive PR-binding sites are shown. (**B**) Cells grown in 3D conditions and treated or not with R5020 and TRULI as indicated, were submitted to gene activity assays. Four up and three down-HAs-associated genes were tested. Results are represented as mean and SD from two experiments performed in duplicate. The *P* value was calculated using the Student's *t* test.

frontiers | Frontiers in Endocrinology

TYPE Mini Review
PUBLISHED 04 November 2022
DOI 10.3389/fendo.2022.1037177

OPEN ACCESS

EDITED BY
Anton M. Jetten,
National Institute of Environmental Health Sciences (NIH), United States

REVIEWED BY
Filipp Frank,
Emory University, United States
Xu Liu,
Emory University, United States

*CORRESPONDENCE
Adali Pecci
apecci@qb.fcen.uba.ar
Guillermo Pablo Vicent
gvmbmc@ibmb.csic.es

SPECIALTY SECTION
This article was submitted to Molecular and Structural Endocrinology, a section of the journal Frontiers in Endocrinology

RECEIVED 05 September 2022
ACCEPTED 06 October 2022
PUBLISHED 04 November 2022

CITATION
Pecci A, Ogara MF, Sanz RT and Vicent GP (2022) Choosing the right partner in hormone-dependent gene regulation: Glucocorticoid and progesterone receptors crosstalk in breast cancer cells.
Front. Endocrinol. 13:1037177.
doi: 10.3389/fendo.2022.1037177

Choosing the right partner in hormone-dependent gene regulation: Glucocorticoid and progesterone receptors crosstalk in breast cancer cells

Adali Pecci[1,2*], María Florencia Ogara[2], Rosario T. Sanz[3] and Guillermo Pablo Vicent[3*]

[1]Departamento de Química Biológica, Facultad de Ciencias Exactas y Naturales, Universidad de Buenos Aires, Ciudad Universitaria, Buenos Aires, Argentina, [2]Instituto de Fisiología, Biología Molecular y Neurociencias (IFIBYNE), Consejo Nacional de Investigaciones Científicas y Técnicas (CONICET)-Universidad de Buenos Aires, Ciudad Universitaria, Buenos Aires, Argentina, [3]Molecular Biology Institute of Barcelona, Consejo Superior de Investigaciones Científicas (IBMB-CSIC), Barcelona, Spain

Steroid hormone receptors (SHRs) belong to a large family of ligand-activated nuclear receptors that share certain characteristics and possess others that make them unique. It was thought for many years that the specificity of hormone response lay in the ligand. Although this may be true for pure agonists, the natural ligands as progesterone, corticosterone and cortisol present a broader effect by simultaneous activation of several SHRs. Moreover, SHRs share structural and functional characteristics that range from similarities between ligand-binding pockets to recognition of specific DNA sequences. These properties are clearly evident in progesterone (PR) and glucocorticoid receptors (GR); however, the biological responses triggered by each receptor in the presence of its ligand are different, and in some cases, even opposite. Thus, what confers the specificity of response to a given receptor is a long-standing topic of discussion that has not yet been unveiled. The levels of expression of each receptor, the differential interaction with coregulators, the chromatin accessibility as well as the DNA sequence of the target regions in the genome, are reliable sources of variability in hormone action that could explain the results obtained so far. Yet, to add further complexity to this scenario, it has been described that receptors can form heterocomplexes which can either compromise or potentiate the respective hormone-activated pathways with its possible impact on the pathological condition. In the present review, we summarized the state of the art of the functional cross-talk between PR and GR in breast cancer cells and we also discussed new paradigms of specificity in hormone action.

KEYWORDS

glucocorticoid receptor, progesterone receptor, mammary epithelial cell proliferation, chromatin, gene expression-regulation

Introduction

Steroid hormones play diverse roles in the regulation of biological functions such as pregnancy, sex organ development, inflammation and immune responses, cholesterol distribution and brain function (1, 2). These effects are mediated by the members of the highly conserved Steroid Hormone receptor (SHR) sub-family that includes receptors for estrogens (ER), progestins (PR), androgens (AR), glucocorticoids (GR) and mineralocorticoids (MR) (3) (Figure 1A i). In fact, a general structural organization is common to all nuclear receptor family members, although the regulation of their quaternary structure may differ (5).

The SHR´s structure has been extensively discussed in excellent reviews (11–13). Briefly, SHRs are composed of three different domains: an N-terminal ligand-independent activation function 1 domain composed of an intrinsically disordered region (AF-1), a central DNA-binding domain (DBD), which links to the C-terminal ligand-binding and the activation function 2 domain (LBD/AF-2) through a hinge region. Particularly, the AF-2 domain is a primarily hydrophobic groove formed by residues from helices H3, H4 and H12 of the LBD/AF-2 domain, where the H12 position plays a critical role in the AF-2 spatial conformation and SHRs function. In fact, AF-2 interacts with specific residues present in particular coregulators' amino acid motifs (LxxLL and I/LxxII for coactivators and corepressors families, respectively) arranged on one side of their amphipathic helix (7). Here we will focus on PR and GR, two receptors that shared several features ranging from several aspects of ligand-binding to the DNA sequences to which the receptor binds (Figure 1A ii). In the absence of ligands, these receptors are part of a protein complex associated with chaperones and co-chaperones, which increase the affinity of SHRs to their ligands *in vivo* (14). Early reconstitution experiments with GR (15) and with PR established that the central proteins in the activation pathway include Hsp40, Hsp70, Hsp90, HOP, and p23 (16, 17). Recently, has been shown that coordinated chaperone interactions enhance stability, function and regulation of GR (18).

Activation occurs when the ligand interacts with the receptor and initiates a signal transduction cascade which ultimately leads to changes in gene expression, whose canonical pathway is depicted in Figure 1B i. PR and GR present a heterogeneous distribution concentrated in liquid condensates or foci (Figure 1B ii). The formation of these discrete foci (19–29), containing ~40-80 receptor molecules have been reported (30). This nuclear compartmentalization would modulate the kinetics of biochemical reactions and thus would actively participate the transcription process (reviewed in (4)).

SHR´s mechanism of action involves genomic and nongenomic processes. Genomic actions result from the direct binding of ligand-activated receptor complexes to specific hormone responsive DNA elements located at the enhancers and promoters of target genes; and/or the ligand-receptor recruitment to other regions in the genome, relying on additional transcription factors such as FOXA1, GATA-3, STAT5, NFκ-B, and AP-1, among others (31, 32).

Several families of co-activators interact directly with ligand-receptor complexes. Some of them do so through the AF-1 domain (33, 34), while others by means of the LBD/AF-2 (35). In this way, the regulation of gene transcription by these receptors is closely associated with the reorganization of chromatin at target genes.

In addition to these direct genomic effects, steroid hormones induce rapid nongenomic responses similar to those initiated by peptide growth factors (36, 37). For example, progestins can activate Src/p21ras/Erk and the PI3K/Akt pathways, either *via* an interaction of the PR with ERα, which itself activates c-Src and PI3K, or by direct interaction of PR with the SH3 domain of c-Src (38–40). A growing body of evidence suggests that GR may also act *via* nongenomic mechanisms. Glucocorticoid activation of a membrane associated GR regulates gap junction intercellular communication and neural progenitor cell proliferation by a mechanism that requires c-Src activity and rapid MAPK-dependent phosphorylation of connexin-43 (41).

Traditionally, the genomic and nongenomic actions of steroid hormones have been considered as two independent pathways, but we found that both pathways converge in the modification of structural components of the target chromatin (42).

The breast develops predominantly after birth: a poorly developed ductal system initially begins to unfold during puberty and gains in complexity during adulthood (43). From pregnancy to lactation, lobuloalveolar growth is followed by the complete differentiation of the mammary epithelium and at weaning, a dramatic switch from survival to death signaling occurs, leading to mammary gland involution. During these periods experienced throughout a woman's life, hormones promote first mammary gland development resulting in ductal elongation, then in adulthood, through recurrent estrous cycles trigger side branching and upon each pregnancy they control cyclical periods of cellular proliferation, differentiation and regression of the mammary epithelium (44). While ER is required at an earlier stage to induce ductal elongation, PR is needed later for side branching and alveologenesis (44–46). Progestins were described to be involved in driving cell proliferation, thus favoring breast cancer development but also to inhibit ER-dependent breast tumorigenesis (7, 47). Moreover, progestins also inhibit the production and secretion of milk and stimulate the proliferation of epithelial cells during late pregnancy (48). On the other hand, glucocorticoids (GCs) play a key role at puberty and pregnancy (49, 50); they promote lactation and the synthesis of milk proteins, maintaining the differentiation stage of the mammary epithelium (51–53). GR is expressed in all stages from normal to cancerous breast tissue (54, 55).

10.3389/fendo.2022.1037177

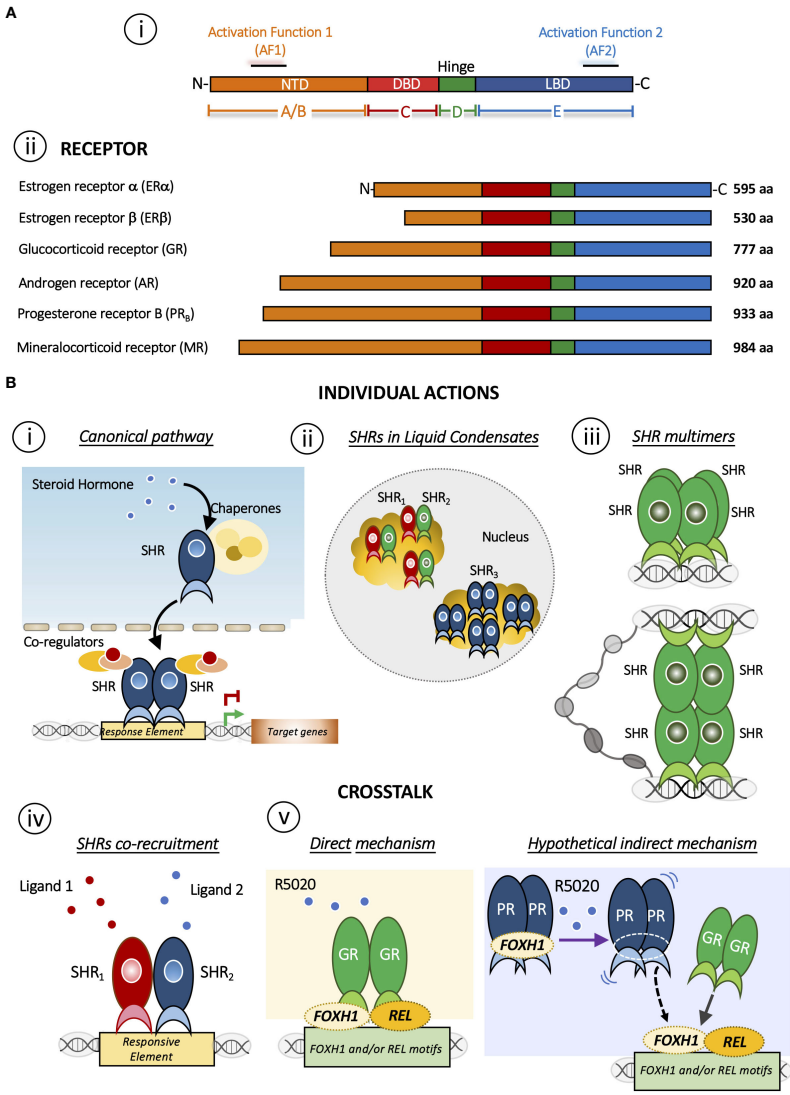

FIGURE 1
(A) Domain structure of SHRs. **i)** Basic domain structure of SHRs is composed of an unstructured N-terminal domain (NTD) that contains the Activation Function 1 (AF-1) surface, a zinc finger DNA-binding domain (DBD), a flexible hinge region, and a LBD that binds to ligands and interacts with co-regulator proteins through the Activation Function 2 (AF-2) surface. **ii)** Domain size and amino acid length of different members of the SHRs sub-family. The DBD and LBDs are the most conserved regions whereas the other domains are more variable in length and sequence composition. **(B)** Mechanisms of action of SHRs. Individual action **i)** The canonical pathway is shown. Steroid hormone binding to the steroid hormone receptor (SHR), often in the cytoplasm, causes the receptor to undergo a conformational change and translocate to the nucleus, where it interacts with specific DNA sequences to regulate transcription of target genes. **ii)** Distribution of SHRs in liquid condensates or foci in the nucleus [Reviewed in (4)]. **iii)** Steroid hormone receptor could form multimers or quaternary structure after DNA binding (5, 6). Interesting, this mechanism brings together regions that may be distant in the linear genome. Crosstalk between SHRs. **iv)** The SHRs co-recruitment to DNA response elements occurs in presence of both ligands. As a result, this crosstalk triggers a specific gene program. SHRs= ERα/PR (7); SHRs= GR/PR (8); SHRs= ERα/GR (9). **v)** Redirection mechanism in which the presence of R5050 in GC-free medium leads to the binding of GR to REL and FHOX1 motifs and repress the expression genes required for PR function (8). On one hand, it has been described that R5020 can directly activate and could drive GR binding (10) but R5020 activated PR could also participate indirectly stabilizing REL and/or FOXH1, increasing GR binding. This possibility, although feasible, requires further investigation.

PR in mammary epithelial cells: Different mechanisms engaged depending on the cell type and clinical status

PR is expressed from a single gene as two main isoforms, PR_A (94 kDa) and PR_B (116 kDa) (56, 57), both are transcribed from two distinct promoters and exhibit different transcriptional and biological activities as ligand-activated transcription factors. PR_B is a full-length receptor; PR_A is a truncated form of PR_B lacking the N-terminal 164 amino acids (56, 58). Both isoforms are usually co-expressed at similar levels in normal breast while a significant increase in PR_A or PR_B was detected in breast cancer that correlates with lesion progression, from the normal state to malignancy. In this regard, the PR_A/PR_B ratio has been proposed as a prognostic and predictive factor for antiprogestin responsiveness in breast cancer (59). Some reports indicated that a high ratio of PR_A/PR_B is associated with worse prognosis, and recurrence after tamoxifen (60, 61), yet other studies concluded that higher PR_A/PR_B are related with biomarkers of better prognosis (59, 62). These contradictory results speak clearly that the mechanism of action of PR is more complex than we originally thought and requires further investigation. Moreover, PR_A and PR_B can form homodimers or heterodimers that exhibit distinct transcriptional regulatory functions by targeting different subsets of genes (63–66).

In the mammary gland, the luminal epithelium forms the inner layer of the ducts and the basal epithelium harbors myoepithelial cells that form the outer layer of the mature mammary ducts as well as stem and progenitor cells. The mammary ducts also comprise fibrous connective tissue, and variable amounts of adipose tissue (43, 67). In the adult mouse mammary gland, PR is expressed only in a fraction of the luminal epithelial cells, where progesterone promotes alveolar growth by a paracrine mechanism. In PR^+ breast luminal cells progesterone upregulates RANKL expression. Then, RANKL binds to RANK expressed on the surface of neighboring PR^- luminal cells or basal cells, activating downstream pathways of cell proliferation, expansion, and survival. Progesterone can also induce adjacent PR^+ cell proliferation by a cell-autonomous, CCND1-dependent mechanism. Moreover, progesterone also elicits the proliferation of PR^- luminal epithelial cells by a paracrine mechanism involving RANK and the NFκB signaling pathway (68).

Most of the research performed so far has been carried out in breast cancer cell lines, with very few studies conducted in normal human breast. Therefore, the role of PR in mammary physiology is underrepresented. This is justified by the loss of receptors detected in normal mammary cells once in culture. However, some steps have already been taken to overcome this issue. In 2009 Graham et al. reported the development and validation of a physiologically relevant model of matrix-embedded normal human breast cells, which was appropriate for studying hormone action in the normal breast (69). Moreover, Clarke et al. performed genome wide PR binding studies in breast cancer cells and in immortalized normal breast cells (70). Although PR binding was correlated with transcriptional outcome in both cell lines, there was a remarkably low overlap between the PR cistromes and in transcriptional targets. Moreover, distinct patterns of enrichment of known cofactor binding motifs were detected, with FOXA1 sites over-represented in breast cancer binding regions and NF1 and AP-1 motifs uniquely enriched in normal cells (70). What determines this difference? The expression levels and/or activation of the cofactors that participate in PR signaling could explain these variations. Hence, the pioneer factor FOXA1 would be a tumoral cofactor of PR. Conversely, NF1 and AP-1 would be the transcription factors chosen by PR in the normal context. An in-depth analysis of the differences in gene expression and PR binding in systems that adequately recapitulate both normal and breast cancer systems, may provide clinically valuable information on hormonal action. Thus, cofactor levels may modulate PR specificity (70).

Functional studies, performed in human breast, support that PR^+/ER^+ cells do not proliferate in direct response to hormone signals, but rather exert a paracrine effect on the surrounding PR^-/ER^- cells (71, 72). In contrast, almost 70% of breast cancers express ER and PR and require their ligands during breast cancer progression, suggesting that these cells switch from paracrine to autocrine mechanisms, as they acquire the ability to proliferate during the tumorigenic process. However, the mechanisms that drive this "switch" are not known. In this regard, the presence of tumoral cofactors such as FOXA1 or the availability of other receptors could help to redirect PR and/or ER binding towards an oncogenic program. Indeed, as it has been described for ER and PR, the formation of receptor heterocomplexes in the presence of both ligands could regulate the process towards malignancy in PR^+/ER^+ cells (7).

GR in mammary epithelial cells: Its dual role in cell proliferation/differentiation depending on the cellular context

It is well known that GR mediates the effects of stress hormones, and of synthetic derivatives that are widely used in the clinic as anti-inflammatory and immunosuppressive agents (73). In the mammary gland, GR was found strongly localized in the nuclei of myoepithelial cells surrounding lobular and duct units and occasionally localized in the nuclei of stromal and endothelial cells (74). The GR nuclear localization indicates that

the receptor is transcriptionally active, since the inactive GR resides mainly in the cytoplasm bound to heat shock proteins and immunophilins (14, 75).

In mammary development, GR was shown to be essential for cell proliferation during lobulo-alveolar development and to contribute to mammary lobular unit spatial formation (50). Of note, GCs also exert anti-proliferative and anti-apoptotic activity in mammary epithelial breast cancer cell lines (76, 77). These steroids are used in the treatment of metastatic breast cancer to reduce the side effects produced by the chemotherapy, and to treat symptoms related to advanced cancer. However, despite the fact that GR expression in mammary tissue declines from normal to precancerous lesions and to invasive breast carcinoma (54, 78), the increment in stress hormones during breast cancer progression results in GR activation even at distant metastatic sites. This, in turn, increases intra-tumor heterogeneity and colonization, therefore reducing cell survival. These observations suggest that caution is needed when including GCs in the treatment of breast cancer patients (79).

Activated GR undergoes phosphorylation, oligomerization and nuclear translocation (80). In the nucleus, the receptor is predominantly recruited to pre-accessible sites along with chromatin remodeling enzymes (81). Interestingly, GR is also able to initiate DNAse hypersensitive sites as a pioneer factor (82–84).

Like PR, chromatin remodeling factors regulate GR binding to DNA and thus, are involved in the overall function of GR. This points out the chromatin landscape as a major contributing factor to the GR-regulated cell-type specific gene expression (84–90). In fact, Johnson et al. reported that all GR binding events involving the SWI/SNF remodeling complex are either pre-recruited by other factors or recruited by the receptor itself (88).

In mouse mammary epithelial cells, 51% of pre-programmed GR binding sites are enriched in the pioneer transcription factor AP-1 (89), which along with GR triggers the recruitment of several remodelers such as Brg1, Chd4, and Snf2h (91). Nevertheless, activated GR induces *de novo* remodeling of chromatin at a minority (~15%) of GR binding sites in a highly tissue-specific manner (85, 89, 90, 92, 93). The current evidence suggests that in mammary epithelial cells this pioneering capacity of AP-1 would be relevant for regulating chromatin accessibility not only at GR target enhancers but also at other genomic regions (89).

The oligomeric status of the GR has also been considered to play a key role in the mechanism of action of the activated receptor. Moreover, in the late 1990s the oligomerization state was proposed as a parameter in the search for synthetic ligands with dissociate GC effects (6). In this sense, we have reported that hormone-activated GR adopts a dimer configuration in the nucleus of living murine mammary adenocarcinoma cells (94) and upon binding to a specific DNA binding site the GR dimer becomes a tetramer (Figure 1B iii) (5, 6). Of note, tetrameric configuration was also detected in activated PR complexes in the same cells (5). The influence of DNA binding on the quaternary structure of the GR proposes a similarity to an allosteric structural transition of the receptor once bound to its target DNA region (95–97).

Functional crosstalk between SHRs: Complexity comes to the forefront

Although at different concentrations, various hormones are present simultaneously in the bloodstream or locally at their target cells. For instance, estrogens that are governed by the menstrual cycle coincide at any time with high levels of GCs, which are regulated by stress and circadian cycles. These multiple signals converge to the same cell and, together, they participate in the cellular response. In this sense, the mechanisms of hormonal action need to be studied in an integrated manner, where different receptors could be activated simultaneously by their cognate ligands.

GCs exert an antagonistic effect on estrogen-dependent cell growth in ER^+/GR^+ breast carcinoma cells and reduce their cell proliferation through a functional crosstalk between both receptors (Figure 1B iv) (9, 32, 98–100). On the other hand, also in breast cancer models, it has been proposed that PR redirects ERα chromatin binding events. ERα and PR form a complex in the presence of both ligands, resulting in a unique gene expression program that is associated with good clinical outcome (Figure 1B iv) (7). In this case, it has been proposed that PR functions as a molecular rheostat to control ERα chromatin binding and transcriptional activity.

Furthermore, it was recently reported the generation of metastasis-competent circulating tumor cells (CTCs) in patients with breast cancer occur during sleep, in the rest phase; while CTCs generated during the active phase are devoid of metastatic ability. The authors found that key circadian rhythm hormones such as melatonin, testosterone and GCs dictate CTC generation dynamics (101). Treatment with the synthetic GC dexamethasone (DEX) or testosterone did not affect primary tumor size but resulted in a marked reduction in single CTCs and CTC clusters (101). These key effects of hormones that determine the metastatic capacity of cancer cells are likely to occur in the presence of both GCs and androgens, thus, a putative crosstalk between both activated receptors could be directly operating in this process.

Unlike the functional connections between ERα with PR and GR, or AR with ERα and GR, few studies have addressed the influence of GR on the transcriptional activity of PR and *vice versa*. Similarities in protein structure as well as in the DNA sequences to which the receptors bind are readily evident for PR and GR (>90% sequence identity between their DNA binding domains (DBD). However, the resulting biological response

10.3389/fendo.2022.1037177

differs markedly. For example, the association of progestins with breast cancer incidence and progression contrasts with the growth suppressive action of GCs on ER^+/PR^+ breast tumor cells (102, 103). In fact, in those cell types, increased circulating levels of progestins and estrogens and/or overexpression of their receptors lead to uncontrolled cell division (47, 104). On the other hand, previous works suggested that GR would act as a suppressor of proliferation (52, 105) as well as a cell death inducer in tumoral mammary epithelium (106).

To address the existence of a potential crosstalk between PR and GR, we used PR^+/GR^+ breast cancer cell lines (107, 108) where we found that GC-free or DEX-activated GR inhibits PR-dependent cell proliferation and dedifferentiation through the modulation of certain PR-target genes, i.e. *GREB1, STAT5A, ELF5* and *SNAI1* (8). In the presence of DEX, the antagonistic effect increases and involves the formation of GR-PR protein complexes. By ChIP-seq and sequential ChIP analyses, we detected overlapped binding of GR and PR at key enhancer sites and confirmed co-recruitment of both receptors to shared sites (Figure 1B iv). Moreover, GC-free GR upon stimulation with the PR-agonist R5020, can bind to REL and FOXH1 motifs and repress the expression of nearby genes encoding for SWI/SNF and other chromatin remodeler complexes such as SMARCD2, ARID1A and INO80C (Figure 1B v). Thus, in the presence of the synthetic progestin R5020, relocated GR are bound to a subset of genes required for PR function, reinforcing the anti-progestational effect of GCs in ER^+/PR^+ breast cancer cells (8).

The mechanism behind the R5020-dependent GR binding to approximately 600 unique sites could be due at least by two non-mutually exclusive mechanisms: 1) a direct effect of R5020 on the GR or 2) an indirect mechanism whereby activated PR would stabilize GR binding to other transcription factors (i.e. REL or FOXH1) genomic regions (Figure 1B v).

Regarding the direct effect, although R5020 is considered a PR specific agonist, it has been reported that R5020 can also activate GR (10). Thus, R5020 binding to GR would induce a unique conformational change to the receptor leading to its recruitment to REL and/or FOXH1-enriched regions. However, we can also speculate that R5020-activated PR could favor GR recruitment to REL and/or FOXH1 regions throughout an indirect mechanism. Accordingly, it has been reported that FOXH1 can act as a hormone-independent corepressor of AR in prostate cancer cells; indeed, a protein-protein interaction was identified between the AR AF-1 domain and FOXH1 independently of the presence of dihydrotestosterone (109). In this model, R5020-activated PR could release FOXH1/REL, which in turn would bind to their sites in the genome favoring GR loading (Figure 1B v, right panel). Whether GR and PR physically interact with FOXH1 and/or REL in mammary cells is unknown and more research is required to support this second hypothetical mechanism.

Conclusions and perspectives

Given the concentration of different steroid hormones varies considerably over a wide range of time (from hours, days and even weeks), several receptors might be coexisting and simultaneously activated by their ligands. Thus, the mechanism of control of one receptor over the other/s could be very frequent and could be involved in relevant receptor-mediated functions. This brings up a complex scenario in which several activated hormone receptors could be interacting reciprocally, regulating the final transcriptional output and their function in the target cell. This crosstalk between receptors could be positive, implying synergism between hormone pathways, or on the contrary, negative, through competition for pathways, for co-regulators and for binding sites in the genome.

Thus, it will be key to elucidate the causes that establish this hierarchy between receptors. What determines which receptor leads and regulates the activity over the other/s? The circulating levels of ligands, receptor levels, and the cellular identity of the target cell (more adapted to respond to one stimulus than to another) are factors that could be involved in this complex scenario. Also, under these circumstances, heterologous complexes, composed of different activated receptors and with different stoichiometry, could be formed and reciprocally regulate the hormonal pathways involved.

We propose that the prevalence of one or the other mechanism is dependent upon which ligand and/or combination of ligands bind to each receptor. Under this hypothesis, new questions arise regarding GR and PR functional crosstalk. How does the ligand-dependent conformation acquired by each receptor influence the control of gene expression? Do the GR-PR heterocomplexes display the same activity as homo-PR or homo-GR complexes? Do the GR-PR heterocomplexes recruit the same set of co-regulators? Do they have similar intranuclear dynamics compared to homodimers? Recruitment of the GR to non-canonical sites requires the presence of the transcription factor that directly recognizes that site, or does it do so by a different mechanism?

To address these questions, state-of-the-art techniques that allow us to monitor simultaneously homo- and heterocomplexes populations of PR and GR in the same cell, are required. For this purpose, it is necessary to engineered cell lines through mutations targeting the interacting regions involved in the formation of homo- and heterodimers. Moreover, mass spectrometry will enable to identify the protein interactome of each receptor population; Next Generation Sequencing (NGS) including ChIP-seq and RNA-seq will help to decipher the defined cistromes for each receptor population; and high-resolution microscopy will allow to visualize the nuclear dynamics of homo- or hetero-complexes in response to hormone, including the formation of condensates. This will shed light on the complex mechanism by which SHRs act upon simultaneous activation. Therefore, and from a

pharmacological point of view, understanding PR-GR crosstalk could contribute to the design of new endocrine combined therapies that minimize tumor resistance, colonization, and metastasis and thus, provide tumorigenesis vulnerability for therapeutic improvement in patients.

Author contributions

GV and AP wrote the manuscript. MO and RS searched for references and built the Figure. All authors contributed to the article and approved the submitted version.

Funding

Grants from the Agencia Estatal de Investigación AEI/10.13039/501100011033 [PID2019-105173RBI00]; Agencia Nacional de Programación Científica y Tecnológica, [Préstamo BID-PICT2019-0158] and University of Buenos Aires [20820180100745BA], Argentina. MO and AP are members of the CONICET-Argentina. GV is Researcher of the Spanish National Research Council (CSIC), Spain.

Acknowledgments

Authors thanks Dr. Diego M. Presman (IFIBYNE, University of Buenos Aires-CONICET) for advice on the manuscript.

Conflict of interest

The authors declare that the research was conducted in the absence of any commercial or financial relationships that could be construed as a potential conflict of interest.

Publisher's note

References

1. Zhao L, Hu H, Gustafsson JA, Zhou S. Nuclear receptors in cancer inflammation and immunity. *Trends Immunol* (2020) 41:172–85. doi: 10.1124/pr.112.006833

2. Burris TP, Solt LA, Wang Y, Crumbley C, Banerjee S, Griffett K, et al. Nuclear receptors and their selective pharmacologic modulators. *Pharmacol Rev* (2013) 65:710–78. doi: 10.1038/nrd1551

3. Gronemeyer H, Gustafsson JA, Laudet V. Principles for modulation of the nuclear receptor superfamily. *Nat Rev Drug Discov* (2004) 3:950–64. doi: 10.1042/BCJ20200883

4. Stortz M, Presman DM, Pecci A, Levi V. Phasing the intranuclear organization of steroid hormone receptors. *Biochem J* (2021) 478:443–61. doi: 10.1073/pnas.1606774113

5. Presman DM, Ganguly S, Schiltz RL, Johnson TA, Karpova TS, Hager GL. DNA Binding triggers tetramerization of the glucocorticoid receptor in live cells. *Proc Natl Acad Sci USA* (2016) 113:8236–41. doi: 10.1080/21541264.2016.1249045

6. Presman DM, Hager GL. More than meets the dimer: What is the quaternary structure of the glucocorticoid receptor? *Transcription* (2017) 8:32–9. doi: 10.1038/nature14583

7. Mohammed H, Russell IA, Stark R, Rueda OM, Hickey TE, Tarulli GA, et al. Progesterone receptor modulates ERalpha action in breast cancer. *Nature* (2015) 523:313–7. doi: 10.1093/nar/gkz857

8. Ogara MF, Rodriguez-Segui SA, Marini M, Nacht AS, Stortz M, Levi V, et al. The glucocorticoid receptor interferes with progesterone receptor-dependent genomic regulation in breast cancer cells. *Nucleic Acids Res* (2019) 47:10645–61. doi: 10.1074/jbc.M113.473819

9. Karmakar S, Jin Y, Nagaich AK. Interaction of glucocorticoid receptor (GR) with estrogen receptor (ER) alpha and activator protein 1 (AP1) in dexamethasone-mediated interference of ERalpha activity. *J Biol Chem* (2013) 288:24020–34. doi: 10.1210/endo-107-2-566

10. Svec F, Yeakley J, Harrison RW. 3rd, progesterone enhances glucocorticoid dissociation from the AtT-20 cell glucocorticoid receptor. *Endocrinology* (1980) 107:566–72. doi: 10.1042/BST20210419

11. Frank F, Ortlund EA, Liu X. Structural insights into glucocorticoid receptor function. *Biochem Soc Trans* (2021) 49:2333–43. doi: 10.1002/pro.3496

12. Weikum ER, Liu X, Ortlund EA. The nuclear receptor superfamily: A structural perspective. *Protein Sci Publ Protein Soc* (2018) 27:1876–92. doi: 10.1146/annurev-physiol-021909-135917

13. Huang P, Chandra V, Rastinejad F. Structural overview of the nuclear receptor superfamily: insights into physiology and therapeutics. *Annu Rev Physiol* (2010) 72:247–72. doi: 10.1016/j.celrep.2022.111039

14. Backe SJ, Sager RA, Regan BR, Sit J, Major LA, Bratslavsky G, et al. A specialized Hsp90 co-chaperone network regulates steroid hormone receptor response to ligand. *Cell Rep* (2022) 40:111039. doi: 10.1007/3-540-29717-0_5

15. Pratt WB, Morishima Y, Murphy M, Harrell M. Chaperoning of glucocorticoid receptors. *Handb Exp Pharmacol* (2006), 172:111–38. doi: 10.1074/jbc.271.22.12833

16. Dittmar KD, Hutchison KA, Owens-Grillo JK, Pratt WB. Reconstitution of the steroid receptor hsp90 heterocomplex assembly system of rabbit reticulocyte lysate. *J Biol Chem* (1996) 271:12833–9. doi: 10.1074/jbc.273.49.32973

17. Kosano H, Stensgard B, Charlesworth MC, McMahon N, Toft D. The assembly of progesterone receptor-hsp90 complexes using purified proteins. *J Biol Chem* (1998) 273:32973–9. doi: 10.1016/j.cell.2014.04.038

18. Kirschke E, Goswami D, Southworth D, Griffin PR, Agard DA. Glucocorticoid receptor function regulated by coordinated action of the Hsp90 and Hsp70 chaperone cycles. *Cell* (2014) 157:1685–97. doi: 10.1016/0014-4827(91)90057-2

19. Vazquez-Nin GH, Echeverria OM, Fakan S, Traish AM, Wotiz HH, Martin TE. Immunoelectron microscopic localization of estrogen receptor on pre-mRNA containing constituents of rat uterine cell nuclei. *Exp Cell Res* (1991) 192:396–404. doi: 10.1083/jcb.102.4.1191

20. Perrot-Applanat M, Groyer-Picard MT, Logeat F, Milgrom E. Ultrastructural localization of the progesterone receptor by an immunogold method: Effect of hormone administration. *J Cell Biol* (1986) 102:1191–9. doi: 10.1007/BF00215514

21. Isola JJ. The effect of progesterone on the localization of progesterone receptors in the nuclei of chick oviduct cells. *Cell Tissue Res* (1987) 249:317–23. doi: 10.1210/mend-5-2-217

22. Martins VR, Pratt WB, Terracio L, Hirst MA, Ringold GM, Housley PR. Demonstration by confocal microscopy that unliganded overexpressed glucocorticoid receptors are distributed in a nonrandom manner throughout all planes of the nucleus. *Mol Endocrinol* (1991) 5:217–25. doi: 10.1210/mend-5-2-217

23. Yang J, DeFranco DB. Differential roles of heat shock protein 70 in the *in vitro* nuclear import of glucocorticoid receptor and simian virus 40 large tumor antigen. *Mol Cell Biol* (1994) 14:5088–98. doi: 10.1073/pnas.95.6.2973

24. Fejes-Toth G, Pearce D, Naray-Fejes-Toth A. Subcellular localization of mineralocorticoid receptors in living cells: effects of receptor agonists and antagonists. *Proc Natl Acad Sci United States America* (1998) 95:2973–8. doi: 10.1074/jbc.M101755200

25. Tomura A, Goto K, Morinaga H, Nomura M, Okabe T, Yanase T, et al. The subnuclear three-dimensional image analysis of androgen receptor fused to green fluorescence protein. *J Biol Chem* (2001) 276:28395–401. doi: 10.1210/me.2002-0110

26. Matsuda K, Ochiai I, Nishi M, Kawata M. Colocalization and ligand-dependent discrete distribution of the estrogen receptor (ER)alpha and ERbeta. *Mol Endocrinol* (2002) 16:2215–30. doi: 10.1074/jbc.M105966200

27. Pearce D, Naray-Fejes-Toth A, Fejes-Toth G. Determinants of subnuclear organization of mineralocorticoid receptor characterized through analysis of wild type and mutant receptors. *J Biol Chem* (2002) 277:1451–6. doi: 10.1210/me.2005-0050

28. Schaaf MJ, Lewis-Tuffin LJ, Cidlowski JA. Ligand-selective targeting of the glucocorticoid receptor to nuclear subdomains is associated with decreased receptor mobility. *Mol Endocrinol* (2005) 19:1501–15. doi: 10.1210/me.2006-0041

29. Arnett-Mansfield RL, Graham JD, Hanson AR, Mote PA, Gompel A, Scurr LL, et al. Focal subnuclear distribution of progesterone receptor is ligand dependent and associated with transcriptional activity. *Mol Endocrinol* (2007) 21:14–29. doi: 10.1038/s41598-017-06676-0

30. Stortz M, Presman DM, Bruno L, Annibale P, Dansey MV, Burton G, et al. Mapping the dynamics of the glucocorticoid receptor within the nuclear landscape. *Sci Rep* (2017) 7:6219. doi: 10.1016/0039-128X(96)00030-X

31. Beato M, Chavez S, Truss M. Transcriptional regulation by steroid hormones. *Steroids* (1996) 61:240–51. doi: 10.1016/j.mce.2013.03.002

32. Miranda TB, Morris SA, Hager GL. Complex genomic interactions in the dynamic regulation of transcription by the glucocorticoid receptor. *Mol Cell Endocrinol* (2013) 380:16–24. doi: 10.1126/science.1093686

33. Verdel A, Jia S, Gerber S, Sugiyama T, Gygi S, Grewal SI, et al. RNAi-mediated targeting of heterochromatin by the RITS complex. *Science* (2004) 303:672–6. doi: 10.1038/nature02269

34. Bastow R, Mylne JS, Lister C, Lippman Z, Martienssen RA, Dean C. Vernalization requires epigenetic silencing of FLC by histone methylation. *Nature* (2004) 427:164–7. doi: 10.1210/me.2003-0116

35. Xu J, Li Q. Review of the *in vivo* functions of the p160 steroid receptor coactivator family. *Mol Endocrinol* (2003) 17:1681–92. doi: 10.1038/nrm1009

36. Losel R, Wehling M. Nongenomic actions of steroid hormones. *Nat Rev Mol Cell Biol* (2003) 4:46–56. doi: 10.1016/j.mce.2021.111453

37. Thiebaut C, Vlaeminck-Guillem V, Tredan O, Poulard C, Le Romancer M. Non-genomic signaling of steroid receptors in cancer. *Mol Cell Endocrinol* (2021) 538:111453. doi: 10.1128/MCB.23.6.1994-2008.2003

38. Ballare C, Uhrig M, Bechtold T, Sancho E, Di Domenico M, Migliaccio A, et al. Two domains of the progesterone receptor interact with the estrogen receptor and are required for progesterone activation of the c-Src/Erk pathway in mammalian cells. *Mol Cell Biol* (2003) 23:1994–2008. doi: 10.1016/S1097-2765(01)00304-5

39. Boonyaratanakornkit V, Scott MP, Ribon V, Sherman L, Anderson SM, Maller JL, et al. Progesterone receptor contains a proline-rich motif that directly interacts with SH3 domains and activates c-src family tyrosine kinases. *Mol Cell* (2001) 8:269–80. doi: 10.1093/emboj/17.7.2008

40. Migliaccio A, Piccolo D, Castoria G, Di Domenico M, Bilancio A, Lombardi M, et al. Activation of the Src/p21ras/Erk pathway by progesterone receptor *via* cross-talk with estrogen receptor. *EMBO J* (1998) 17:2008–18. doi: 10.1073/pnas.1102821108

41. Samarasinghe RA, Di Maio R, Volonte D, Galbiati F, Lewis M, Romero G, et al. Nongenomic glucocorticoid receptor action regulates gap junction intercellular communication and neural progenitor cell proliferation. *Proc Natl Acad Sci USA* (2011) 108:16657–62. doi: 10.1016/j.molcel.2006.10.011

42. Vicent GP, Ballare C, Nacht AS, Clausell J, Subtil-Rodriguez A, Quiles I, et al. Induction of progesterone target genes requires activation of erk and msk kinases and phosphorylation of histone H3. *Mol Cell* (2006) 24:367–81. doi: 10.1152/physrev.00040.2018

43. Fu NY, Nolan E, Lindeman GJ, Visvader JE. Stem cells and the differentiation hierarchy in mammary gland development. *Physiol Rev* (2020) 100:489–523. doi: 10.1101/cshperspect.a003178

44. Brisken C, O'Malley B. Hormone action in the mammary gland. *Cold Spring Harbor Perspect Biol 2* (2010), l12:a003178. doi: 10.1002/dvdy.1179

45. Hovey RC, Trott JF, Ginsburg E, Goldhar A, Sasaki MM, Fountain SJ, et al. Transcriptional and spatiotemporal regulation of prolactin receptor mRNA and cooperativity with progesterone receptor function during ductal branch growth in the mammary gland. *Dev Dynamics an Off Publ Am Assoc Anat* (2001) 222:192–205. doi: 10.1007/s10911-021-09496-1

46. Chen W, Wei W, Yu L, Ye Z, Huang F, Zhang L, et al. Mammary development and breast cancer: A notch perspective. *J Mammary Gland Biol Neoplasia* (2021) 26:309–20. doi: 10.1038/nrc.2016.116

47. Carroll JS, Hickey TE, Tarulli GA, Williams M, Tilley WD. Deciphering the divergent roles of progestogens in breast cancer. *Nat Rev Cancer* (2017) 17:54–64. doi: 10.1038/nrc.2016.116

48. Graham JD, Clarke CL. Physiological action of progesterone in target tissues. *Endo Rev* (1997) 18:502–19. doi: 10.1210/me.2004-0068

49. Wintermantel TM, Bock D, Fleig V, Greiner EF, Schutz G. The epithelial glucocorticoid receptor is required for the normal timing of cell proliferation during mammary lobuloalveolar development but is dispensable for milk production. *Mol Endocrinol* (2005) 19:340–9. doi: 10.1083/jcb.200403020

50. Murtagh J, McArdle E, Gilligan E, Thornton L, Furlong F, Martin F. Organization of mammary epithelial cells into 3D acinar structures requires glucocorticoid and JNK signaling. *J Cell Biol* (2004) 166:133–43. doi: 10.1016/0303-7207(94)90288-7

51. Groner B, Altiok S, Meier V. Hormonal regulation of transcription factor activity in mammary epithelial cells. *Mol Cell Endocrinol* (1994) 100:109–14. doi: 10.1002/jcp.22896

52. Hoijman E, Rocha-Viegas L, Kalko SG, Rubinstein N, Morales-Ruiz M, Joffe EB, et al. Glucocorticoid alternative effects on proliferating and differentiated mammary epithelium are associated to opposite regulation of cell-cycle inhibitor expression. *J Cell Physiol* (2012) 227:1721–30. doi: 10.1210/en.2010-0517

53. Bertucci PY, Quaglino A, Pozzi AG, Kordon EC, Pecci A. Glucocorticoid-induced impairment of mammary gland involution is associated with STAT5 and STAT3 signaling modulation. *Endocrinology* (2010) 151:5730–40. doi: 10.1093/nar/gkt327

54. Allegra JC, Lippman ME, Thompson EB, Simon R, Barlock A, Green L, et al. Distribution, frequency, and quantitative analysis of estrogen, progesterone, androgen, and glucocorticoid receptors in human breast cancer. *Cancer Res* (1979) 39:1447–54. doi: 10.1155/2017/1403054

55. Alyusuf R, Wazir JF, Brahmi UP, Fakhro AR, Bakhiet M. The immunoexpression of glucocorticoid receptors in breast carcinomas, lactational change, and normal breast epithelium and its possible role in mammary carcinogenesis. *Int J Breast Cancer* (2017) 2017:1403054. doi: 10.1002/j.1460-2075.1990.tb08280.x

56. Kastner P, Krust A, Turcotte B, Stropp U, Tora L, Gronemeyer H, et al. Two distinct estrogen-regulated promoters generate transcripts encoding the two functionally different human progesterone receptor forms a and b. *EMBO J* (1990) 9:1603–14. doi: 10.1002/j.1460-2075.1990.tb08280.x

57. Giulianelli S, Riggio M, Guillardoy T, Perez Pinero C, Gorostiaga MA, Sequeira G, et al. FGF2 induces breast cancer growth through ligand-independent activation and recruitment of ERalpha and PRBDelta4 isoform to MYC regulatory sequences. *Int J Cancer* (2019) 145:1874–88. doi: 10.1186/bcr2097

58. Cork DM, Lennard TW, Tyson-Capper AJ. Alternative splicing and the progesterone receptor in breast cancer. *Breast Cancer Res BCR* (2008) 10:207. doi: 10.1093/jnci/djw317

59. Rojas PA, May M, Sequeira GR, Elia A, Alvarez M, Martinez P, et al. Progesterone receptor isoform ratio: A breast cancer prognostic and predictive factor for antiprogestin responsiveness. *J Natl Cancer Institute 109* (2017) 7:1–9. doi: 10.1016/j.jsbmb.2019.105560

60. Pateetin P, Pisitkun T, McGowan E, Boonyaratanakornkit V. Differential quantitative proteomics reveals key proteins related to phenotypic changes of breast cancer cells expressing progesterone receptor a. *J Steroid Biochem Mol Biol* (2020) 198:105560. doi: 10.1158/1078-0432.CCR-03-0141

61. Hopp TA, Weiss HL, Hilsenbeck SG, Cui Y, Allred DC, Horwitz KB, et al. Breast cancer patients with progesterone receptor PR-a-rich tumors have poorer disease-free survival rates. *Clin Cancer Res an Off J Am Assoc Cancer Res* (2004) 10:2751–60. doi: 10.1158/1078-0432.CCR-10-2950

62. Pathiraja TN, Shetty PB, Jelinek J, He R, Hartmaier R, Margossian AL, et al. Progesterone receptor isoform-specific promoter methylation: association of PRA promoter methylation with worse outcome in breast cancer patients. *Clin Cancer Res an Off J Am Assoc Cancer Res* (2011) 17:4177–86. doi: 10.1210/me.2005-0126

63. Graham JD, Yager ML, Hill HD, Byth K, O'Neill GM, Clarke CL. Altered progesterone receptor isoform expression remodels progestin responsiveness of breast cancer cells. *Mol Endocrinol* (2005) 19:2713–35. doi: 10.1210/me.2004-0287

64. Jacobsen BM, Schittone SA, Richer JK, Horwitz KB. Progesterone-independent effects of human progesterone receptors (PRs) in estrogen receptor-positive breast cancer: PR isoform-specific gene regulation and tumor biology. *Mol Endocrinol* (2005) 19:574–87. doi: 10.1002/ijc.21186

65. Leo JC, Wang SM, Guo CH, Aw SE, Zhao Y, Li JM, et al. Gene regulation profile reveals consistent anticancer properties of progesterone in hormone-independent breast cancer cells transfected with progesterone receptor. *Int J Cancer* (2005) 117:561–8. doi: 10.1371/journal.pone.0045993

66. Khan JA, Bellance C, Guiochon-Mantel A, Lombes M, Loosfelt H. Differential regulation of breast cancer-associated genes by progesterone receptor isoforms PRA and PRB in a new bi-inducible breast cancer cell line. *PloS One* (2012) 7:e45993. doi: 10.1002/wdev.35

67. Macias H, Hinck L. Mammary gland development. *Wiley Interdiscip Rev Dev Biol* (2012) 1:533–57. doi: 10.1186/bcr3166

68. Tanos T, Rojo L, Echeverria P, Brisken C. ER and PR signaling nodes during mammary gland development. *Breast Cancer Res BCR* (2012) 14:210. doi: 10.1007/s10911-009-9160-6

69. Graham JD, Mote PA, Salagame U, Balleine RL, Huschtscha LI, Clarke CL. Hormone-responsive model of primary human breast epithelium. *J Mammary Gland Biol Neoplasia* (2009) 14:367–79. doi: 10.1371/journal.pone.0035859

70. Clarke CL, Graham JD. Non-overlapping progesterone receptor cistromes contribute to cell-specific transcriptional outcomes. *PloS One* (2012) 7:e35859. doi: 10.1073/pnas.95.9.5076

71. Brisken C, Park S, Vass T, Lydon JP, O'Malley BW, Weinberg RA. A paracrine role for the epithelial progesterone receptor in mammary gland development. *Proc Natl Acad Sci USA* (1998) 95:5076–81. doi: 10.1023/A:1005805831460

72. Clarke RB, Howell A, Anderson E. Estrogen sensitivity of normal human breast tissue *in vivo* and implanted into athymic nude mice: analysis of the relationship between estrogen-induced proliferation and progesterone receptor expression. *Breast Cancer Res Treat* (1997) 45:121–33. doi: 10.1016/j.jaci.2013.09.007

73. Oakley RH, Cidlowski JA. The biology of the glucocorticoid receptor: new signaling mechanisms in health and disease. *J Allergy Clin Immunol* (2013) 132:1033–44. doi: 10.1002/path.1982

74. Lien HC, Lu YS, Cheng AL, Chang WC, Jeng YM, Kuo YH, et al. Differential expression of glucocorticoid receptor in human breast tissues and related neoplasms. *J Pathol* (2006) 209:317–27. doi: 10.1016/j.tem.2021.07.005

75. Mazaira GI, Piwien Pilipuk G, Galigniana MD. Corticosteroid receptors as a model for the Hsp90*immunophilin-based transport machinery. *Trends Endocrinol Metab: TEM* (2021) 32:827–38. doi: 10.1002/j.1460-2075.1990.tb08280.x

76. Moran TJ, Gray S, Mikosz CA, Conzen SD. The glucocorticoid receptor mediates a survival signal in human mammary epithelial cells. *Cancer Res* (2000) 60:867–72. doi: 10.1038/bjc.1995.343

77. Harris RA, Hiles ID, Page MJ, O'Hare MJ. The induction of apoptosis in human mammary luminal epithelial cells by expression of activated c-neu and its abrogation by glucocorticoids. *Br J Cancer* (1995) 72:386–92. doi: 10.1007/s10549-011-1689-6

78. Vilasco M, Communal L, Mourra N, Courtin A, Forgez P, Gompel A. Glucocorticoid receptor and breast cancer. *Breast Cancer Res Treat* (2011) 130:1–10. doi: 10.1038/s41586-019-1019-4

79. Obradovic MMS, Hamelin B, Manevski N, Couto JP, Sethi A, Coissieux MM, et al. Glucocorticoids promote breast cancer metastasis. *Nature* (2019) 567:540–4. doi: 10.3389/fimmu.2019.01545

80. Timmermans S, Souffriau J, Libert C. A general introduction to glucocorticoid biology. *Front Immunol* (2019) 10:1545. doi: 10.1080/10253890802506409

81. Biddie SC, Hager GL. Glucocorticoid receptor dynamics and gene regulation. *Stress* (2009) 12:193–205. doi: 10.1016/0092-8674(84)90523-3

82. Zaret KS, Yamamoto KR. Reversible and persistent changes in chromatin structure accompany activation of a glucocorticoid-dependent enhancer element. *Cell* (1984) 38:29–38. doi: 10.1002/j.1460-2075.1987.tb02507.x

83. Richard-Foy H, Hager GL. Sequence-specific positioning of nucleosomes over the steroid-inducible MMTV promoter. *EMBO J* (1987) 6:2321–8. doi: 10.1016/j.molcel.2008.02.010

84. John S, Sabo PJ, Johnson TA, Sung MH, Biddie SC, Lightman SL, et al. Interaction of the glucocorticoid receptor with the chromatin landscape. *Mol Cell* (2008) 29:611–24. doi: 10.1038/ng.759

85. John S, Sabo PJ, Thurman RE, Sung MH, Biddie SC, Johnson TA, et al. Chromatin accessibility pre-determines glucocorticoid receptor binding patterns. *Nat Genet* (2011) 43:264–8. doi: 10.1093/nar/gkw1163

86. Love MI, Huska MR, Jurk M, Schopflin R, Starick SR, Schwahn K, et al. Role of the chromatin landscape and sequence in determining cell type-specific genomic glucocorticoid receptor binding and gene regulation. *Nucleic Acids Res* (2017) 45:1805–19. doi: 10.1016/j.cels.2018.06.007

87. D'Ippolito AM, McDowell IC, Barrera A, Hong LK, Leichter SM, Bartelt LC, et al. Pre-established chromatin interactions mediate the genomic response to glucocorticoids. *Cell Syst* (2018) 7:146–160.e7. doi: 10.1093/nar/gkx1044

88. Johnson TA, Chereji RV, Stavreva DA, Morris SA, Hager GL, Clark DJ. Conventional and pioneer modes of glucocorticoid receptor interaction with enhancer chromatin in vivo. *Nucleic Acids Res* (2018) 46:203–14. doi: 10.1016/j.molcel.2011.06.016

89. Biddie SC, John S, Sabo PJ, Thurman RE, Johnson TA, Schiltz RL, et al. Transcription factor AP1 potentiates chromatin accessibility and glucocorticoid receptor binding. *Mol Cell* (2011) 43:145–55. doi: 10.1038/emboj.2013.106

90. Grontved L, John S, Baek S, Liu Y, Buckley JR, Vinson C, et al. C/EBP maintains chromatin accessibility in liver and facilitates glucocorticoid receptor recruitment to steroid response elements. *EMBO J* (2013) 32:1568–83. doi: 10.1038/nsmb.2718

91. Morris SA, Baek S, Sung MH, John S, Wiench M, Johnson TA, et al. Overlapping chromatin-remodeling systems collaborate genome wide at dynamic chromatin transitions. *Nat Struct Mol Biol* (2014) 21:73–81. doi: 10.1002/bies.201600137

92. Swinstead EE, Paakinaho V, Presman DM, Hager GL. Pioneer factors and ATP-dependent chromatin remodeling factors interact dynamically: A new perspective: Multiple transcription factors can effect chromatin pioneer functions through dynamic interactions with ATP-dependent chromatin remodeling factors. *BioEssays News Rev molecular Cell Dev Biol* (2016) 38:1150–7. doi: 10.1007/s00709-016-1063-y

93. Grbesa I, Hakim O. Genomic effects of glucocorticoids. *Protoplasma* (2017) 254:1175–85. doi: 10.1371/journal.pbio.1001813

94. Presman DM, Ogara MF, Stortz M, Alvarez LD, Pooley JR, Schiltz RL, et al. Live cell imaging unveils multiple domain requirements for *in vivo* dimerization of the glucocorticoid receptor. *PloS Biol* (2014) 12:e1001813. doi: 10.1126/science.1164265

95. Meijsing SH, Pufall MA, So AY, Bates DL, Chen L, Yamamoto KR. DNA Binding site sequence directs glucocorticoid receptor structure and activity. *Science* (2009) 324:407–10. doi: 10.1038/nsmb.2595

96. Watson LC, Kuchenbecker KM, Schiller BJ, Gross JD, Pufall MA, Yamamoto KR. The glucocorticoid receptor dimer interface allosterically transmits sequence-specific DNA signals. *Nat Struct Mol Biol* (2013) 20:876–83. doi: 10.1101/gr.244814.118

97. Paakinaho V, Johnson TA, Presman DM, Hager GL. Glucocorticoid receptor quaternary structure drives chromatin occupancy and transcriptional outcome. *Genome Res* (2019) 29:1223–34. doi: 10.1007/s11010-016-2810-2

98. Hegde SM, Kumar MN, Kavya K, Kumar KM, Nagesh R, Patil RH, et al. Interplay of nuclear receptors (ER, PR, and GR) and their steroid hormones in MCF-7 cells. *Mol Cell Biochem* (2016) 422:109–20. doi: 10.1158/1541-7786.MCR-15-0433

99. West DC, Pan D, Tonsing-Carter EY, Hernandez KM, Pierce CF, Styke SC, et al. GR and ER coactivation alters the expression of differentiation genes and associates with improved ER+ breast cancer outcome. *Mol Cancer Res MCR* (2016) 14:707–19. doi: 10.1093/nar/gkt100

100. Bolt MJ, Stossi F, Newberg JY, Orjalo A, Johansson HE, Mancini MA. Coactivators enable glucocorticoid receptor recruitment to fine-tune estrogen receptor transcriptional responses. *Nucleic Acids Res* (2013) 41:4036–48. doi: 10.1038/s41586-022-04875-y

101. Diamantopoulou Z, Castro-Giner F, Schwab FD, Foerster C, Saini M, Budinjas S, et al. The metastatic spread of breast cancer accelerates during sleep. *Nature* (2022) 607:156–62. doi: 10.1210/er.13.2.146

102. Horwitz KB. The molecular biology of RU486 is there a role for antiprogestins in the treatment of breast cancer? *Endo Rev* (1992) 13:146–63. doi: 10.1210/mend.16.6.0848

103. Wan Y, Nordeen SK. Overlapping but distinct gene regulation profiles by glucocorticoids and progestins in human breast cancer cells. *Mol Endocrinol* (2002) 16:1204–14. doi: 10.1007/978-0-387-78818-0_7

104. Lange CA, Sartorius CA, Abdel-Hafiz H, Spillman MA, Horwitz KB, Jacobsen BM. Progesterone receptor action: translating studies in breast cancer models to clinical insights. *Adv Exp Med Biol* (2008) 630:94–111.

105. Goya L, Maiyar AC, Ge Y, Firestone GL. Glucocorticoids induce a G1/G0 cell cycle arrest of Con8 rat mammary tumor cells that is synchronously reversed

by steroid withdrawal or addition of transforming growth factor-alpha. *Mol Endocrinol* (1993) 7:1121–32. doi: 10.1016/j.bcp.2014.04.006

106. Orqueda AJ, Dansey MV, Espanol A, Veleiro AS, Bal de Kier Joffe E, Sales ME, et al. The rigid steroid 21-hydroxy-6,19-epoxyprogesterone (21OH-6,19OP) is a dissociated glucocorticoid receptor modulator potentially useful as a novel coadjuvant in breast cancer chemotherapy. *Biochem Pharmacol* (2014) 89:526–35. doi: 10.1210/mend-3-8-1270

107. Nordeen SK, Kuhnel B, Lawler-Heavner J, Barber DA, Edwards DP. A quantitative comparison of dual control of a hormone response element by progestins and glucocorticoids in the same cell line. *Mol Endocrinol* (1989) 3:1270–8. doi: 10.1210/mend-2-11-1064

108. Arteaga CL, Coronado E, Osborne CK. Blockade of the epidermal growth factor receptor inhibits transforming growth factor alpha-induced but not estrogen-induced growth of hormone-dependent human breast cancer. *Mol Endocrinol* (1988) 2:1064–9. doi: 10.1074/jbc.M506147200

109. Chen G, Nomura M, Morinaga H, Matsubara E, Okabe T, Goto K, et al. Modulation of androgen receptor transactivation by FoxH1. *A newly identified androgen receptor corepressor. J Biol Chem* (2005) 280:36355–63. doi: 10.1016/j.it.2019.12.006